REPUBLIQUE DU CAMEROUN
Paix – Travail – Patrie

UNIVERSITE DE YAOUNDE I

CENTRE DE RECHERCHE ET DE FORMATION DOCTORALE EN SCIENCE, TECHNOLOGIES, ET GEOSCIENCES

UNITE DE RECHERCHE ET DE FORMATION DOCTORALE EN PHYSIQUE ET APPLICATIONS

BP 812 Yaoundé

Email : crfd_stg@uy1.uninet.cm

REPUBLIC OF CAMEROON
Peace – Work – Fatherland

THE UNIVERSITY OF YAOUNDE I

POSTGRADUATE SCHOOL OF SCIENCES, TECHNOLOGY AND GEOSCIENCES

RESEARCH AND POSTGRADUATE TRAINING UNIT FOR PHYSICS AND APPLICATIONS

P.O. Box 812 Yaoundé

Email : crfd_stg@uy1.uninet.cm

Laboratoire de Mécanique, Matériaux et Structures
Laboratory of mechanics, Materials and structures

TRANSITIONS TO CHAOS IN THE DYNAMICS OF A BOSE-EINSTEIN CONDENSATE LOADED INTO A MOVING OPTICAL FOURIER-SYNTHESIZED LATTICE

Thesis submitted in partial fulfillment of the requirements for the award of the degree of Doctor of Philosophy/PhD in Physics

Speciality: Fundamental Mechanics and Complex Systems

By

TCHATCHUENG Sylvin

Registration number: **99S293**

Holder of D.E.A in Physics

Examination panel

PRESIDENT: -- **NDJAKA Jean-Marie Bienvenu,** Professor, University of Yaoundé 1

SUPERVISORS: -- **TCHAWOUA Clément,** Professor, University of Yaoundé 1

-- **MOUKAM KAKMENI François Marie**, Associate Professor, University of Buea

EXAMINERS: -- **BEN-BOLIE Germain Hubert,** Professor, University of Yaoundé 1

-- **ZEKENG Serge**, Associate Professor, University of Yaoundé 1

-- **NANA Laurent,** Associate Professor, University of Douala

-- **NANA NBENDJO Blaise Roméo**, Associate Professor, University of Yaoundé 1

Year 2020

UNIVERSITE DE YAOUNDE I
UNIVERSITY OF YAOUNDE I

FACULTE DES SCIENCES
FACULTY OF SCIENCE

DEPARTEMENT DE PHYSIQUE
DEPARTMENT OF PHYSICS

ATTESTATION DE CORRECTION DE LA THESE DE DOCTORAT/Ph.D

Nous, Professeur **NANA NBENDJO Blaise Roméo** et Professeur **NDJAKA Jean-Marie Bienvenu**, respectivement Examinateur et Président du jury de la Thèse de Doctorat/Ph.D de Monsieur **TCHATCHUENG Sylvin**, Matricule **99S293,** préparée sous la direction du Professeur **TCHAWOUA Clément** et du Professeur **MOUKAM KAKMENI François Marie,** intitulée : « **Transitions to chaos in the dynamics of a Bose-Einstein condensate loaded into a moving optical Fourier-synthesized lattice**», soutenue le **Mardi 14 Juillet 2020**, en vue de l'obtention du grade de Docteur/Ph.D en Physique, Spécialité **Mécanique, Matériaux et Structures** option **Mécanique Fondamentale et Systèmes Complexes,** attestons que toutes les corrections demandées par le jury de soutenance ont été effectuées.

En foi de quoi, la présente attestation lui est délivrée pour servir et valoir ce que de droit.

Fait à Yaoundé, le 05 AUG 2020

Examinateur

NANA NBENDJO Blaise Roméo
Maître de Conférences

Le Président du jury

NDJAKA Jean-Marie Bienvenu
Professeur

Le Chef de Département de Physique

UNIVERSITE DE YAOUNDE I ★ FACULTE DES SCIENCES ★ DEPARTEMENT DE PHYSIQUE
Le Chef de Département

Ndjaka Jean-Marie Bienvenu
Professeur

UNIVERSITY OF YAOUNDE I

FACULTY OF SCIENCES

DEPARTMENT OF PHYSICS

TRANSITIONS TO CHAOS IN THE DYNAMICS OF A BOSE-EINSTEIN CONDENSATE LOADED INTO A MOVING OPTICAL FOURIER-SYNTHESIZED LATTICE

Thesis submitted in partial fulfillment of the requirements for the award of the degree of Doctor of Philosophy/PhD in Physics

Speciality: Fundamental Mechanics and Complex Systems

By

TCHATCHUENG Sylvin

Registration number: 99S293

Holder of D.E.A in Physics

Director

MOUKAM KAKMENI François Marie

Associate Professor

University of Buea

Supervisor

TCHAWOUA Clément

Professor

University of Yaoundé 1

Laboratory of mechanics, Materials and structures

DEDICATION

To my late parents

ACKNOWLEDGEMENTS

It is a great pleasure for me through this opportunity I have today, to say some personal words.
I would like first and foremost to express my sincere gratitude to Professor **Clément TCHAWOUA** for the opportunity he gave me to work with him as supervisor. This thesis is the outcome of his guidance, fruitful discussions and constant support. It was very exciting to work with him.
I would like to thank Professor **François Marie MOUKAM KAKMENI** whose guidance, useful discussions and encouragements have made this long road as enjoyable and rewarding. As my director, his warm and caring personality, enthusiasm and skills made it a joy to work on this project.
I also owe much gratitude to Professor **Martin SIEWE SIEWE** for his consistent support and encouragements in the middle of many failures and sometimes slow progress in the research activity, contributing thus enormously to make this adventure possible and enjoyable.
I would like to express all my recognition to Professor **Timoléon Crépin KOFANE**, who has been an outstanding teacher during my first encounter with nonlinear dynamics and chaos theory, concepts in which I fell in love during my second year in my Masters courses, and which are at the base of this thesis.
I would like to thank the Professor **Jean-Marie Bienvenu NDJAKA**, Head of Department of Physics, for his understanding, and especially for the promptness with which his staff manages our administrative problems.
For all teachers of the department of physics in the university of Yaoundé 1, and mainly those of the laboratory of mechanics, I say thank you for all sacrifices you have made to make the scientist I am today.
To the jury made up of: Prof. **Jean-Marie Bienvenu NDJAKA**, Prof. **Clément TCHAWOUA**, Prof. **Germain Hubert BEN-BOLIE**, Prof. **Serge Sylvain ZEKENG**, Prof. **Laurent NANA**, Prof. **Blaise Roméo NANA NBENDJO**, Prof. **François Marie MOUKAM KAKMENI** responsible for evaluating this work I say thank you in advance.
I owe much gratitude to my friend **Manase CHI** for proof-reading and editing my manuscripts, and for all the effort and enthusiasm he put into understanding my work and discussing it with me, even though physics is not even close to his field.
It would be ungrateful for me to end this acknowledgements without saying a great thank you to my family, mainly my wife **Judith NGASSA**, in spite of daily difficulties of life, difficulties which sometimes tend to discouragement and abandonment of my research activities, has never ceased to encourage me.

LIST OF ABBREVIATIONS

NLSE: Nonlinear Schrödinger Equation

BEC: Bose-Einstein Condensate

GPE: Gross-Pitaevskii Equation

GPGE: Gross-Pitaevskii-Ginzburg Equation

1D: One Dimensional

2D: Two Dimensional

3D: Three Dimensional

WIDBG: Weakly Interacting Dilute Bose Gas

MM: Melnikov Method

NIST: National Institute of Standards and Technology

JILA: Joint Institute for Lab Astrophysics

MIT: Massachusetts Institute of Technology

ENS: Ecole Normale Supérieure

TFA: Thomas-Fermi Approximation

rf: radio-frequency

OGY: Ott-Grebogi-York

Contents

List of Figures

ABSTRACT

This thesis deals with the study of global bifurcations, and transition routes to chaos in the dynamical behaviour of a one-dimensional Bose-Einstein condensate with two-and three-body elastic and inelastic collisions between the atoms loaded into a moving optical Fourier synthesized lattice. The analytical tool for the prediction of chaos is the Melnikov method, whereas the fourth-order Runge-Kutta and Euler-Cromer schemes are used in Fortran 90 and Matlab codes to determine the bifurcation points and the transition routes to chaos in the dynamics of the condensate.
In the first part of this thesis, we consider a condensate with repulsive two-body and attractive three-body elastic collisions between atoms. Under such conditions, only homoclinic bifurcations can occur, and the condition for the occurrence of chaos deduced from Melnikov's method reveals that the depth and the parameter shape of the optical lattice enhance a chaotic behaviour of the condensate, while the velocity of the optical lattice and parameters related to dissipations and three-body elastic collisions annihilate the instability and chaos in the dynamics of the condensate. These results are in accordance with numerical simulations which reveal in addition that the transition routes to homoclinic chaos is the period-doubling scenario with the bifurcation points which sometime obey the Feigenbaum formula, thus proving the universality of chaos in this physical system.
In the second part of this thesis, a condensate with attractive two-body and repulsive three-body elastic collisions between atoms is considered. Under certain conditions, homoclinic and heteroclinic bifurcations can occur. In this context, the conditions for the occurrence of chaos obtained with Melnikov's method reveal that the depth and the velocity of the optical lattice enhance the homoclinic and heteroclinic chaos, while the other parameters reduce the chaotic behaviour of the condensate. From this analytical study, it also emerges that homoclinic chaos is obtained when the parameter related to atomic feeding is about one order of magnitude larger than the parameter related to three-body inelastic collisions. These results are confirmed by numerical simulations which in addition reveal that the transition route to chaos is the quasi-periodicity through the Hopf bifurcations.

Keywords: Bose-Einstein condensation, bifurcations theory, homoclinic orbit, heteroclinic orbit, Melnikov theory, bifurcation diagram, Poincaré section, phase portrait, basin of attraction, Lyapunov exponent, elastic collisions, inelastic collisions.

RESUME

Cette thèse porte sur l'étude des bifurcations globales, et la transition vers le chaos dans le comportement dynamique d'un condensat de Bose-Einstein unidimensionnel avec des collisions élastiques et inélastiques à deux et à trois corps entre les atomes piégés par un réseau optique mobile. La méthode analytique utilisée est celle de Melnikov qui prédit le seuil d'apparition du chaos, tandis que les schémas d'Euler-Cromer et de Runge-Kutta d'ordre 4 utilisés dans les programmes Fortran 90 et Matlab permettent de déterminer les points de bifurcation et les routes de transition vers le chaos.
La première partie de cette thèse est consacrée au cas des collisions élastiques à deux corps répulsives, et à trois corps attractives. Dans ces conditions, seules les bifurcations homoclines peuvent apparaître, et le seuil d'apparition du chaos révèle que la profondeur et le paramètre de forme(module de la fonction élliptique de Jacobi) du réseau optique amplifient le chaos, tandis que la vitesse du réseau optique, le coefficient de dissipation, et le paramètre relatif aux collisions élastique à trois corps annihilent le comportement chaotic du condensat. Ces résultats sont en accord avec les simulations numériques qui révèlent en outre que la transition vers le chaos s'effectue via le scénario de bifurcations par dédoublement de période, avec des points de bifurcation qui parfois obeïssent à la formule de Feigenbaum(Les nombres de Feigenbaum), provant ainsi l'universalité du chaos dans ce systeme physique.
Dans la deuxième partie de cette thèse, un condensat avec des collisions élastiques à deux corps attractives, et à trois corps répulsives est considéré. Sous certaines conditions, des bifurcations homoclines et hétéroclines peuvent être obtenues. Dans cette optique, les conditions d'apparition du chaos révèlent que la profondeur et la vitesse du réseau optique amplifient le chaos homocline et hétérocline, tandis que les autres paramètres réduisent le comportement chaotique du condensat. De cette étude analytique, il ressort également que le chaos homocline est obtenue lorsque le paramètre lié au pompage optique est environ dix fois le paramètre lié aux collisions inélastiques à trois corps. Ces résultats sont confirmés par les simulations numériques qui révèlent en plus que la route de transition vers le chaos est la quasi-périodicité, via les bifurcations de Hopf.

Mots clés: Condensation de Bose-Einstein, théorie des bifurcations, orbite homocline, orbite heterocline, théorie de Melnikov, diagramme de bifurcation, sections de Poincaré, bassin d'attraction, exposant de Lyapunov, collisions élastiques et inélastiques.

GENERAL INTRODUCTION

In 1924, Einstein received a draft article written by a young Indian physicist Satyendra Nath Bose who demonstrated Planck's law for black body radiation, by treating light as a gas of identical particles(photons). Strongly interested, Einstein translated the manuscript from English to German, and made sure of its publication [1]. Latter on, Einstein extended and generalized this Bose's idea to a gas of material particles, and predicted in articles [2, 3, 4] published in 1924 and 1925 that for a monoatomic ideal gas, at sufficiently low but finite temperatures, a large fraction of the atoms would go into the lowest energy quantum state of the system, becoming indistinguishable, and consequently the system would behave like a giant matter wave in which particles can have the same energy state and share a single quantum state. This new state of matter is today known as Bose-Einstein condensation. At that time, the required conditions for its realization being too difficult, this phenomenon will remain a theoretical fact until 1938 with the discovery of the superfluidity of liquid helium(^{4}He) by Kapitsa[5], and independently by Allen and Misener[6]. By comparing the transition temperature(2,17K) to the superfluid state of helium 4 with the transition temperature(3,1K) of helium 4 atoms at the Bose-Einstein condensate state, London[7, 8], suggested a certain connection between these two phenomena, giving rise to a renewed interest in the Bose-Einstein condensation phenomenon. To capture the dynamics of particles involved in this phenomenon, particles with a spin which is an integer multiple of reduced Planck's constant $\hbar$, called bosons, numerous theoretical studies were made throughout the world, culminating in 1961 to the Gross-Pitaevskii-equation(**GPE**). This famous nonlinear Schrödinger equation(**NLSE**) derived by Pitaevskii [9] and independently by Gross [10], describes well the low temperature properties of the trapped Bose gases such as its size, shape and energy.

The **GPE** was derived for a weakly-interacting dilute Bose gas(**WIDBG**) at temperatures close to absolute zero, in the framework of lowest-order mean-field theory. The requirement for a gas to be dilute is that the average distance between atoms is much larger than the range of potential. Consequently, third and higher order interaction terms can be neglected, and only the elastic

two-body interaction between atoms is taken into account. Although the condensate state is surrounded by non-condensed atoms(thermal cloud) responsible for thermal and quantum fluctuations, in the **GPE**, the condensate is assumed to be isolated.

This multi-context equation which describes well the dynamics of condensates, is also used in nonlinear optics and fluid mechanics. In the context of Bose-Einstein condensation, this Gross-Pitaevskii equation is given by

$$\imath\hbar\frac{\partial\psi(r,t)}{\partial t} = -\frac{\hbar^2}{2m}\Delta\psi(r,t) + V(r,t)\psi(r,t) + \frac{4\pi\hbar^2 a_s(r,t)}{m}|\psi(r,t)|^2\psi(r,t). \quad (1)$$

$\psi(\vec{r},t)$ is the macroscopic wave function, Δ the **3D** Laplacian, V(r,t) the trapping potential, $g = \frac{4\pi\hbar^2 a_s(r,t)}{m}$ the so-called coupling constant characterizing the elastic atom-atom collisions, m the atomic mass, and $a_s(r,t)$ the s-scattering length.

If the external potential is time-independent and the gas is in thermal equilibrium, then the **GPE** becomes

$$\imath\hbar\frac{\partial\psi(r,t)}{\partial t} = \left(-\frac{\hbar^2}{2m}\Delta + V(r) + g|\psi(r,t)|^2\right)\psi(r,t), \quad (2)$$

with g a real constant, which can be negative in the case of attractive interactions or positive in the case of repulsive interactions. Today, one has the possibility through the Feshbach resonance techniques to control the scattering length, varying it from positive to negative values as recently shown in the Bose-Einstein condensation of ^{85}Rb.

After this theoretical achievement obtained in 1961, the efforts in the realization of a Bose-Einstein condensate(**BEC**) started in 1976 at the Massachusetts Institute of Technology (**MIT**) with the Bose-Einstein condensation of spin-polarized hydrogen. The quest for temperatures close to absolute zero became a new challenge in physics. During about twenty five years, the appropriate experimental techniques needed to reach the necessary ultra-low temperatures will be progressively improved, culminating in 1995 at the first observation of a Bose-Einstein condensate of ^{87}Rb, produced around 170nK by Carl E. Wieman and Eric A. Cornell at the **NIST-JILA** laboratory at the university of Colorado at Boulder. Three months latter at **MIT**, a group led by Wolfgang Ketterle independently produced a **BEC** of sodium (^{23}Na), with about 200.000 atoms. For these remarkable achievements, these three physicists were awarded the 2001 Nobel prize in Physics.

Shortly after the experimental realization of Bose-Einstein condensation of ^{87}Rb and ^{23}Na prov-

ing that Einstein's prediction was true, interest in this phenomenon was revived in the scientific community. In the first days following the first realization of a **BEC**, the researches was focused on its properties, like the interference between two coupled Bose-Einstein condensates as reported in references [11, 12], Josephson effects, π oscillations, atomic population oscillations, and macroscopic quantum self-trapping as reported in [13, 14].

During these theoretical and experimental explorations to understand this newly observed state of matter, it was observed that the Bose-Einstein condensation of certain species was realized at high temperatures with very strong interactions between atoms, and with high densities of condensed atoms. It was the case of helium 4 (^{4}He) in which strong interactions restrict the condensed atoms only at about ten per cent of initial atoms even at temperatures very close to absolute zero. The high density in helium condensates implies that multi-body interactions and non-condensed fractions cannot be ignored or treated as perturbations, making helium condensates very difficult to describe theoretically. The dynamics of such condensates which takes into account the thermal cloud and higher order interactions is described within the framework of Hartree-Fock-Bogoliubov equations, which are essentially more cumbersome than the relatively simple **GPE**.

In the framework of condensates subjected to multi-body interactions, the presence of inelastic collisions was demonstrated with the Feshbach resonance techniques in references [15, 16, 17] and proven experimentally by Jean Dalibard in reference [18]. It comes from these references that the relevant inelastic two-body loss mechanism is the dipolar spin relaxation, and the relevant three-body loss mechanism is the three-body recombination. Considering these losses phenomena, in references [19, 20, 21, 22, 23, 24, 25, 26] a group of Brazilian researchers has studied successfully through this extended Gross-Pitaevskii formalism known as Gross-Pitaevskii-Ginzburg equation(**GPGE**), the stability of condensates magnetically trapped in a harmonic potential, with elastic three-body collisions between atoms taken into account. These studies reveal chaotic dynamics as well as solitonic solutions, due to the presence of nonlinearities in the equation modeling the dynamics of the condensate. The importance of studying stability and chaos in the dynamics of condensed atoms resides in its probable use in technological devices.

However, During the long quest for the realization of the first condensate, around the 1970s, the introduction of new methods of trapping and cooling with laser beams was introduced. Today, it is well known that Laser beams have played a key role in the final realization of early

condensates, and the advent of optical lattices in Physics as trapping potential has contributed enormously to the realization of the condensation of many species. In the framework of condensates in the mean-field approach with an optical lattice as trapping potential, numerous studies have been done, chaotic behaviours and solitonic solutions have been observed in the dynamics of such condensates governed by the simple Gross-Pitaevskii equation, as reported in references [27, 28].

Motivated by results of the Brazilian team mentioned above, and especially due to the fact that in the scientific literature there is no substantial research works on the Bose-Einstein condensation beyond the mean-field approach concerning the study of stability and chaos in the dynamical behaviour of condensed atoms governed by a complex Gross-Pitaevski-Ginzburg equation and trapped into optical lattices, particularly a moving optical Fourier-synthesized lattice, our research team invested himself in this arduous task, crowned in 2014 and 2017 by the following publications[29, 30]. The aim of this thesis is to present in detail, the relevant results obtained during these investigations, mainly the role played by parameters of the optical lattice and parameters related to inelastic collisions between atoms in the transition route to chaos.

The outline of this thesis is as follows:

The chapter I is devoted to the literature review on the Bose-Einstein condensation and chaos theory.

The chapter II deals with the model and the different methods used in this thesis to capture the dynamical behaviour of condensed atoms in the framework of the complex Gross-Pitaevskii-Ginzburg equation. In the first section, a brief introduction is given. In the second section, are presented different methods used in the analytical and numerical studies. In the third section, the model is presented, and the general equation governing the dynamics of condensed atoms is derived. Subsequently, the analytical method is applied to the amplitude equation to determine the conditions for the occurrence of chaotic oscillations of condensed atoms.

The chapter III is devoted to results and discussion. In the first section, a brief introduction is given. The second section deals with a comparative study between analytical and numerical investigations in the case of a condensate with repulsive two-body interactions and attractive three-body interactions. In the third section, a comparative study between analytical and numerical investigations in the case of a condensate with attractive two-body interactions and repulsive three-body interactions is presented.

CHAPTER I

LITERATURE REVIEW ON THE BOSE-EINSTEIN CONDENSATION AND CHAOS THEORY

I.1 History of Bose-Einstein condensation

I.1.1 Einstein's prediction and response from liquid helium

The starting point of the Bose-Einstein condensation phenomenon was the draft article written by the Indian physicist Satyendra Nath Bose in 1924, paper in which he used a statistical argument to derive the Planck law for black-body radiation, by treating the light as a gas of identical particles. Unable to publish his work, he sent it to Einstein who found the manuscript interesting enough, so that he decided to translate it from English to German, and got it published in Zeitschrift für Physik [1]. Inspired by Bose's ideas, Einstein saw that Bose's mathematics later known as Bose-Einstein statistics could be applied to atoms as well as light, and he published in years 1924 and 1925 his own articles [2, 3, 4] describing the Bose statistical model and its implications, culminating into the concept of Bose gas. He generalized Bose's theory to an ideal gas of identical atoms or molecules for which the number of particles is conserved, and predicted that at sufficiently low but finite temperatures, a large fraction of the atoms would cluster together in the lowest quantum state of the system, becoming indistinguishable, and the system would behave like a giant matter wave in which particles can have the same energy state and share a single quantum state. This phenomenon is now known as Bose-Einstein condensation. Roughly speaking, the Bose-Einstein condensation would be what happens to a dilute gas when it is made very cold near absolute zero. The condition for Bose-Einstein condensation to happen is that the phase space density must be greater than approximately unity, in natural units. Another way to express this condition is that the De Broglie wavelength of each atoms given by

$$\lambda_{dB} = \frac{h}{\sqrt{2\pi m k_B T}}, \tag{3}$$

must be large enough to overlap with its neighbours. In this expression, T represents the temperature, m the mass of the particle, k_B the Boltzmann constant, and h the Planck constant. More precisely, the phase-space density $n\lambda_{dB}^3$ which represents the number of particles con-

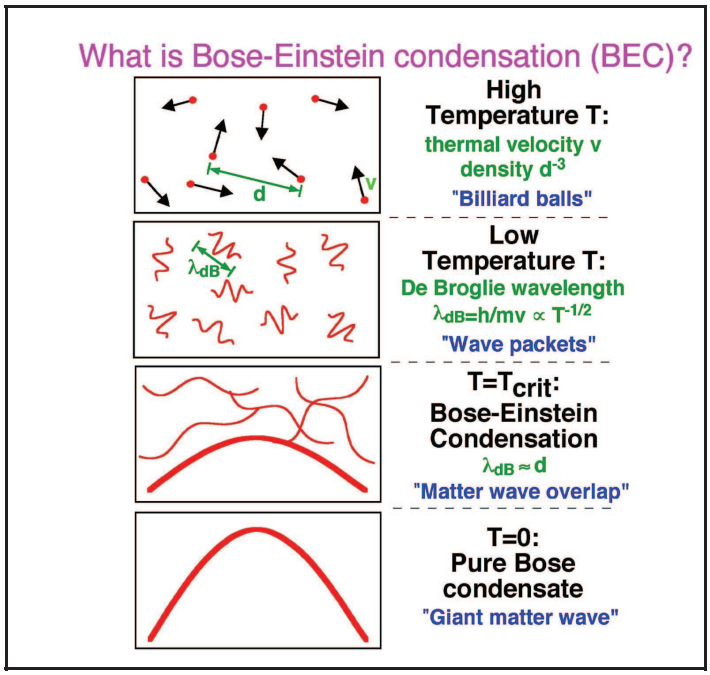

Figure 1: Criterion for Bose-Einstein condensation. At high temperatures, a weakly interacting gas can be treated as a system of "billiard balls". In a simplified quantum description, the atoms can be regarded as wave packets with an extension of their De Broglie wavelength. At the **BEC** transition temperature, λ_{dB} becomes comparable to the distance between atoms, and a Bose condensate forms. As the temperature approaches zero, the thermal cloud disappears, leaving a pure Bose condensate.

Pictures from Nobel lecture for 2001 physics Nobel prize published in reference [79]

tained in a volume equal to the cube of the thermal De Broglie wavelength must be greater than $\zeta(3/2) \simeq 2.61$. That is to say

$$n\lambda_{dB}^3 \geq 2.61. \tag{4}$$

n denotes the density of atoms, $\zeta(\alpha) = \sum_{k=1}^{+\infty} \frac{1}{k^\alpha}$ represents the Riemann zeta function, and $\zeta(3/2)$ represents this Riemann zeta function calculated at the value $3/2$. In fact, atoms at temperature T and with mass m can be regarded as quantum-mechanical wave packets that have a

spatial extent on the order of a thermal De Broglie wavelength. The value of λ_{dB} is the position uncertainty associated with the thermal momentum distribution and increases with decreasing temperature. When atoms are cooled to the point where De Broglie wavelength is comparable to the interatomic separation, the atomic wave packets overlap and the gas starts to become a quantum system of indistinguishable particles. Bosonic atoms undergo a quantum-mechanical phase transition and form a Bose-Einstein condensate, a cloud of atoms all occupying the same quantum-mechanical state at a precise temperature. That is well summarized in Fig.1.

From these aforementioned Einstein's papers, it also turns out that this phenomenon would happens only for particles with gregarious behaviour named bosons to pay homage to Bose. These types of particles, with a total spin that is an integer multiple of reduced Planck's constant $\hbar$, obey Bose-Einstein statistics. As opposed to bosons, the fermions are particles with half-integer spin (in units of reduced Plank's constant $\hbar$) which obey Fermi-Dirac statistics and the Pauli exclusion principle which forbids two Fermionic particles to be in the same quantum state. Atoms consist of protons, neutrons and electrons which are all fermions. Atoms will be bosons if the total number of electrons, protons and neutrons add up to be an even number, and fermions if the total number of electrons, protons and neutrons add up to be an odd number. For instance, ^{4}He is a bosonic particle(2 electrons, 2 protons and 2 neutrons), while ^{3}He is a fermionic particle(2 electrons, 2 protons and 1 neutrons). At high temperatures, the effects of quantum statistics can be neglected, and the distinction between fermions and bosons is not relevant. The mean occupation number in each quantum energy level is in fact much less than one, and the particles behave according to the classical Boltzmann distribution. However, when the temperature is lowered to a critical value (which depends on the thermodynamic parameters of the system), the wavelengths become comparable to the interatomic distance, and begin to overlap. When this occurs, the particles become indistinguishable, roughly speaking they lose their identity, and exhibit a wave-like behaviour. In a bosonic gas this leads to the onset of a macroscopic occupation of a single quantum state.

After Einstein's prediction, the Bose-Einstein condensation was considered to be unrealistic by the assumption of ideal gas, and had not attracted much interest until the discovery in 1938 of the superfluidity of liquid helium(^{4}He) below the transition temperature $T_\lambda = 2.17K$ by Kapitsa [5] and independently by Allen and Misener [6]. They found that the fluid flowed without any apparent viscosity below the transition temperature T_λ. Soon after the discovery of the super-

fluid nature of ^{4}He, and noting that the phase transition temperature $T_{BEC} = 3.1K$ deriving from Einstein's formula given by

$$T_c(n) = \frac{h^2}{2\pi m k_B}\left(\frac{n}{\zeta(3/2)}\right)^{2/3} \tag{5}$$

is very close to the transition temperature $(T_\lambda = 2.17K)$ of the superfluid state, London in references [7, 8] suggested that this new phase of matter might have some connection with the phenomenon of Bose-Einstein condensation. From this London conjecture, it seemed clear that the Bose-Einstein condensation is related to two remarkable low-temperature phenomena: superfluidity, in which the helium isotope ^{4}He forms a liquid that flows with zero friction, and superconductivity in which electrons move through a material with zero electrical resistance.

I.1.2 Theoretical investigations leading to the famous Gross-Pitaevskii equation

Extending London's work, Tisza in [31, 32] phenomenologically introduced the two-fluid model which describes the character of liquid helium by two interpenetrating fluids, a normal fluid and superfluid, and interpreted the superfluid component as Bose condensed helium atoms. Landau in reference [33] presented a theory of superfluidity based on the idea of quasi particles. He developed a theory of quantum hydrodynamics without any assumption on the statistics of atoms consisting the liquid, and strongly opposed London and Tisza idea. After the long controversy on the connection between Bose-Einstein condensation and superfluidity, the idea of London and Tisza was supported by most physicists. However, the relevance of Bose-Einstein condensation and superfluidity was still unclear due to the lack of a microscopic theory of liquid helium(^{4}He), because the perturbation theory was not applicable to strongly interacting helium atoms. On the other hand, theories for a weakly interacting dilute Bose gas (**WIDBG**) were developed without any real experimental system. In 1947, Bogoliubov in reference [34] reported the first microscopic theory of **WIDBG** based on the treatment of the condensate annihilation operators as complex numbers. This amounts to the assumption that the condensate can be described by a coherent state and corresponds to a description of Bose-Einstein condensation in terms of spontaneous symmetry breaking. He calculated the excitation spectrum and showed that it has a phonon spectrum for small momentum, which ensures the stability of superfluidity. Beliaev in reference [35] developed and generalized the methods of quantum field theory for **WIDBG**, with an approach based on Green's functions of quantum field theory at zero temper-

ature. Beliaev's approach at zero temperature will be pursued by Hugenholtz and Pines [36], who calculated higher order contributions to the ground state energy, and derived the result now known as the Hugenholtz-Pines theorem. This theorem states that the energy spectrum of a Bose gas is gapless. That is to say that the energy of an excitation tends to zero as its momentum becomes zero. Pitaevskii in reference [9] developed Bogoliubov's theory to an inhomogeneous case to study vortex lines in a Bose condensate. He introduced a concept of macroscopic wave function $\phi(\vec{r},t)$ and derived the famous Gross-Pitaevskii equation(**GPE**)

$$i\hbar\frac{\partial\phi(r,t)}{\partial t} = -\frac{\hbar^2}{2m}\Delta\phi(r,t) + V(r,t)\phi(r,t) + \frac{4\pi\hbar^2 a_s(r,t)}{m}|\phi(r,t)|^2\phi(r,t), \tag{6}$$

where Δ stands for the **3D** Laplacian, $V(r,t)$ is the trapping potential, $g = \dfrac{4\pi\hbar^2 a_s(r,t)}{m}$ is the so-called coupling constant characterizing the elastic atom-atom collisions, m is the atomic mass, and $a_s(r,t)$ the s-scattering length. The negative values of a_s corresponds to attractive interactions as in the cases of ^{7}Li, ^{85}Rb and the positive values of a_s corresponds to repulsive interactions between atoms of the condensate as in the ^{87}Rb, ^{23}Na and ^{1}H species. The sign and magnitude of the scattering length can be tuned by external fields with Feshbach resonance techniques, making the scattering length a tunable parameter for systems of condensates. This equation which describes well the low temperature properties of the trapped Bose gases such as its size, shape and energy was also derived independently by Gross in [10]. If the external potential is time-independent and the gas is in thermal equilibrium, then the **GPE** becomes

$$i\hbar\frac{\partial\phi(r,t)}{\partial t} = \left(-\frac{\hbar^2}{2m}\Delta + V(r) + g|\phi(r,t)|^2\right)\phi(r,t), \tag{7}$$

with g a real constant. That is to say a_s is a real constant.

The importance of this equation in the field of quantum mechanics requires a particular attention to its derivation. The effective interaction between atoms in a **BEC** is due to s-wave scattering process. The effective two-body interaction may be written as a short range interaction potential $U(r-r') = g\delta(r-r')$. g is the interaction strength mentioned above and δ is the Dirac function. The starting point for the treatment of a real gas of interacting particles is the respective many-body Hamiltonian in second quantization, given by

$$\hat{H} = \int d^3r\hat{\Phi}^\dagger(r)\left(-\frac{\hbar^2}{2m}\Delta + V(r)\right)\hat{\Phi}(r) + \frac{1}{2}\int d^3r\int d^3r'\hat{\Phi}^\dagger(r)\hat{\Phi}^\dagger(r')U(r-r')\hat{\Phi}(r)\hat{\Phi}(r'). \tag{8}$$

$\hat{\Phi}^{\dagger}(r)$ and $\hat{\Phi}(r)$ represent the creation and annihilation of a boson at position r, and V(r) represents the external trapping potential. According to the bosonic character of the system, the field operators must fulfilled the following bosonic commutation relations: $[\hat{\Phi}(r), \hat{\Phi}^{\dagger}(r')] = \delta(r - r')$ and $[\hat{\Phi}(r), \hat{\Phi}(r')] = [\hat{\Phi}^{\dagger}(r), \hat{\Phi}^{\dagger}(r')] = 0$. These commutation relations characterize the algebraic counterpart of the symmetry properties of bosonic wave functions. Using the Heisenberg equation given by

$$\imath\hbar\frac{\partial\hat{\Phi}(r,t)}{\partial t} = [\hat{\Phi}(r,t), \hat{H}] \tag{9}$$

and the two commutation relations mentioned above, the equation of motion is then given by

$$i\hbar\frac{\partial\hat{\Phi}(r,t)}{\partial t} = \left(-\frac{\hbar^2}{2m}\Delta + V(r) + \int d^3r'\hat{\Phi}^{\dagger}(r',t)U(r-r')\hat{\Phi}(r',t)\right)\hat{\Phi}(r,t). \tag{10}$$

When the temperature T is close to the critical temperature T_c, the number of atoms in the ground state is macroscopic, and the field operator can be separated into two parts. One for the condensate part and the other for the excited state part. The excited state part of the field operator is small compared to the condensate part and can be treated as a perturbation term. Thus, the Bose field operator is decomposed as $\hat{\Phi}(r,t) = \phi(r,t) + \hat{\Psi}(r,t)$. The first term $\phi(r,t) = \langle\hat{\Phi}(r,t)\rangle$ represents the expectation value of $\hat{\Phi}(r,t)$ and the second term $\hat{\Psi}(r,t)$ represents thermal fluctuations about this value. Assuming the limit of zero temperature, such that the thermal component of the system is non-existent, and considering the weakly-interacting nature ($a_s \ll \lambda_{dB}$) of the condensate, quantum depletion at zero temperature is expected to be minimal. It is then reasonable to neglect the non-condensed atoms($\hat{\Psi}(r,t) \to 0$) and consider only the classical field $\hat{\Phi}(r,t) \to \phi(r,t)$. It is also to note that the assumption of zero temperature is generally satisfied in reality for temperatures much less than the transition temperature for condensation given by the Einstein formula eq.(5), or for temperatures T leading to the phase density larger than 2.61 as defined in eq.(4). Inserting $U(r-r')$ expressed above into eq.(10) allows to derive an important equation for the condensate wave function $\phi(r,t)$, called Gross-Pitaevskii equation, as defined in eq.(7).

The time-independent **GPE** is obtained by searching the solutions of eq.(7) which are only time-dependent through a global phase. Writing such solutions as $\phi(r,t) = \phi(r)\exp\left(\frac{-i\mu t}{\hbar}\right)$ one obtains

$$\left[-\frac{\hbar^2}{2m}\Delta + V(r) + g|\phi(r)|^2\right]\phi(r) = \mu\phi(r), \tag{11}$$

which is a time-independent **GPE**. μ denotes the chemical energy which represents the energy required to add an-other particle to the condensate.
When the kinetic energy term $\left(-\frac{\hbar^2}{2m}\Delta\right)$ in the **GPE** is negligible in front of potential energy V(r) due to the trapping potential, one obtains the Thomas-Fermi approximation(**TFA**) given in the case of relatively strong repulsive interactions $(g > 0)$ by

$$n(r) = \begin{cases} \dfrac{\mu - V(r)}{g}, & \mu \geq V(r) \\ 0 & otherwise. \end{cases} \tag{12}$$

$n(r) = |\phi(r)|^2$ represents the condensate density.
After the theoretical investigations about the Bose-Einstein condensation, the main problem to test Einstein's prediction was to know how to cool a sample of atoms at very low temperature? From then on, the quest for temperatures very close to absolute zero has become a new challenge in modern physics.

I.1.3 The quest for low temperatures close to absolute zero and the first observation of a Bose-Einstein Condensate (BEC)

To test Einstein's prediction, the quest for temperatures very close to absolute zero $(-273°C)$ became a new challenge in ultracold Physics. In 1959, Hecht [37] suggested that spin-polarised hydrogen could be the ideal candidate for the first experimental realisation of **BEC**, since the characteristic interactions were estimated to be weak, even at very low temperatures. This idea was later confirmed by Stwalley and Nosanow in their paper [38] published in 1976. They argued that spin-polarized hydrogen had no bound states and hence would remain a gas down to zero temperature, and so it would be a good candidate for a Bose-Einstein condensate. This result motivated a number of experimental groups [39, 40] in the late 1970s and early 1980s to begin pursuing this idea using traditional cryogenics to cool a sample of polarized hydrogen. Spin-polarized hydrogen was first stabilized by Silvera and Walraven [39] in Amsterdam in 1980. However, it became increasingly clear that the walls of the cell cause severe limitations to the lifetime of the gas. In fact, as the temperature is lowered, the density of atoms absorbed on the surface increases to the point where the three-body rate on the surface becomes exorbitant. To circumvent this surface problem, Hess from the **MIT** hydrogen group realized that magnetic trapping of atoms [41] would be an improvement over a cell. In fact, atoms in a magnetic trap

have no contact with a physical surface, and thus, the surface-recombination problem could be avoided. By using low-field seeking states of hydrogen atoms, it was possible to trap atoms at a local minimum of the magnetic field. Moreover, thermally isolated atoms in a magnetic trap were the perfect candidate for evaporative cooling. Most energetic atoms simply leave the trap from the edge, effectively cooling what remains in the trap. The only disadvantage, was the heating due to the dipolar relaxation of low-field seeking states, which limits the maximum density at the trap center to a modest value, not sufficient to observe the transition to the Bose-Einstein condensed phase. In 1988, the **MIT** and Amsterdam groups had implemented these ideas and the power of evaporative cooling demonstrated. In 1991, according to reference [42], they obtained at a temperature of 100μK, a density only factor of five, too low for **BEC**.

At roughly the same time, but independent of the hydrogen work, an entirely different type of cold-atom physics and technology was developed: Laser cooling and trapping. The idea that Laser light could be used to cool atoms was suggested in early papers from Wineland and Dehmelt [43], from H*ä*nsch and Schawlow [44], and from Letokhov's group [45]. The starting point of the Laser cooling and trapping of atoms was Ashkin's work in late 1970s. His dream was to slow down an atomic beam using the radiation pressure of a Laser beam, and then to trap them using a dipole force from focused Laser beam(s), and he has proposed several schemes and done some proof-of principle experiments with atomic beams [46, 47]. Thenceforth, at the Heidelberg university [48] and at the National Bureau of Standards in Boulder (Colorado) now known as **NIST**, the trapped ions were laser-cooled [49]. Atomic beams were deflected and slowed in the early 1980s [50, 51, 52]. The mid 1980s saw the heyday of laser-cooling and trapping. In 1985, at the Bell labs, the atoms were cooled to very low temperatures by six perpendicular intersecting laser beams leading to optical molasses [53]. Measured temperatures in the early molasses experiments were consistent with the so-called Doppler limit, which amounts to a few hundred microkelvin in most alkalis. One year later, Chu and Ashkin [54] used the light to trap atoms using the dipole force exerted by a strongly focused Laser beam. The years 1987 and 1988 saw a major breakthrough in the quest for very low temperatures necessary for the creation of condensates. Firstly, a practical spontaneous-force trap, the Magneto-Optical Trap (**MOT**) was demonstrated [55], and secondly it was observed that under certain conditions, the temperatures in optical molasses are in fact much colder than the Doppler limit [56, 57, 58]. Ashkin's dreams were realized one after another. Scattering force from Laser beams were used to cool both atomic

beams and vapor, and atom traps were realized using a dipole force or magnetic field potential. Roughly speaking, the most important advance in this period was the invention of the magneto-optical trap (**MOT**), which became the workhorse of the ultracold atom community.

The realization of **MOT** was financially too expensive. During the mid 1980s Carl E. Wieman began investigating how useful the technology of Laser trapping and cooling could become for general use in atomic Physics. He replaced in the original **MOT** the expensive Lasers with vastly cheaper semiconductor Lasers, and then searched for ways to allow atom trapping with these low cost but also low power lasers[59, 60]. He used the demonstration of the **MOT** and sub-Doppler molasses to study what Physics was limiting the coldness and denseness of these trapped atoms, with the hope of extending the limits further. Carl and his colleagues discovered that several atomic processes were responsible for these limits. Light assisted collisions were found to be the major loss process from the **MOT** as the density increased [61]. However, even before that became a serious problem, the light pressure from reradiated photons limited the density [62, 63]. At about the same time, the sub-Doppler temperatures of molasses found by American Physicists William D. Phillips, Steven Chu, and the French Physicist Claude Cohen-Tannoudji were shown to be due to a combination of light-shifts and optical pumping that became known as Sisyphus cooling [64]. They were rewarded by the 1997 Physics Nobel prize, for development of methods to cool and trap atoms with Laser light [65, 66, 67]. The efforts in technology development of Carl's group culminated in the creation of a useful **MOT** in a simple glass vapor cell [68]. In spite of the improvement of Laser cooling and trapping of atoms, the phase-space density remains always small, around 10^{-5}. Investigating about this problem, Carl E. Wieman and his student Chris Monroe had the idea to load the cold **MOT** atoms into a magnetic trap. In other words, they decided to combine the two types of trapping and cooling. This successful approach known today as the hybrid approach, was to use Laser cooling only as pre-cooling for magnetic trapping and evaporative cooling. There were several important advances towards achieving efficient evaporation. The Dark-SPOT trap was invented at **MIT** to enhance the density of atoms in **MOT** [69], and **rf**-induced evaporation was proposed and successfully implemented in magnetic traps. Physicist's long quest to observe the Bose-Einstein condensate in its pure form ended in 1995. The world first **BEC** was achieved at 10:54 AM on June 5, 1995 in a laboratory at **JILA**, a joint institute of the university of Colorado Boulder and **NIST**. The **BEC** was formed inside a carrot sized glass cell, and made visible by a video camera. It mea-

sured only about 20 microns in diameter, or about one fifth the thickness of a sheet of paper. This remarkable accomplishment realized by a group of Physicists led by Carl E. Wieman and Eric A. Cornell produced around 170nK the first **BEC** in a gas of 2000 rubidium atoms (^{87}Rb) at the **NIST-JILA** laboratory at the university of Colorado at Boulder(see Fig.2(a)). Just about one month later, at the Rice university in Houston, Texas, the **BEC** of a dilute gas of ^{7}Li was obtained by R. Hulet et al. By September 1995 at **MIT**, a group led by Wolfgang Ketterle independently produced a **BEC** with about 200.000 sodium atoms (^{23}Na)(see Fig.2(b)). For their accomplishments, Eric A. Cornell, Carl E. Wieman and Wolfgang Ketterle received the 2001 Nobel prize in Physics [76, 77, 78, 79].

After the first realization of the Bose-Einstein condensate, the next major goal was to prove its

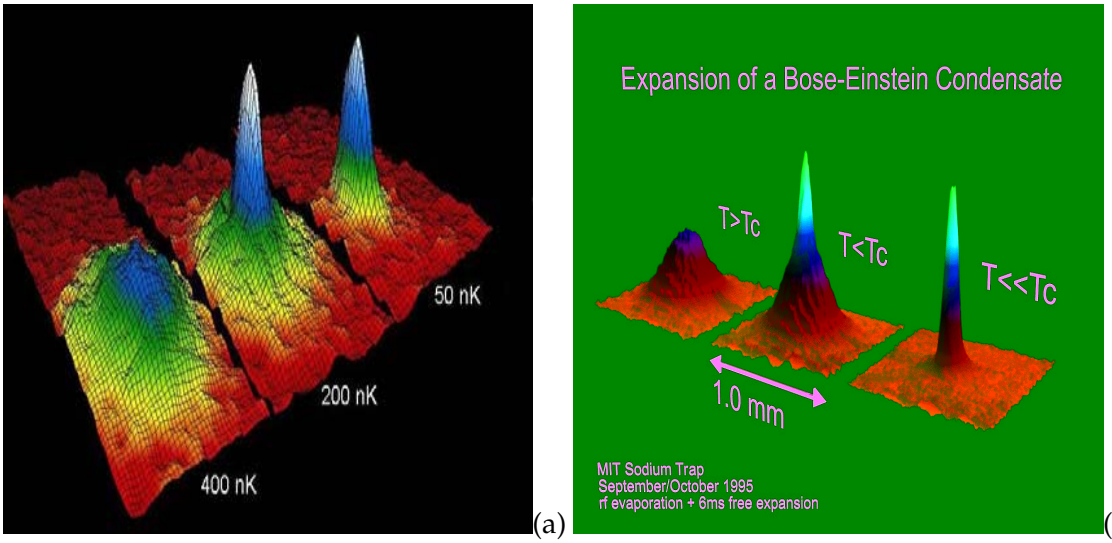

(a) (b)

Figure 2: Pictures provided by the cameras after the production of first Bose-Einstein condensates, proving that Einstein's prediction is true. a) Condensate of rubidium atoms (^{87}Rb) produced at the **NIST-JILA** laboratory at the university of Colorado at Boulder. b) Condensate of sodium atoms(^{23}Na) produced at **MIT**.

Pictures from Nobel lecture for 2001 physics Nobel prize published in references [78, 79]

wave nature. In this respect, Wolfgang Ketterle and his team observed striking interference(see Fig.3(a)) patterns between two Bose-Einstein condensates [11, 70] in November 1996, and in 1997 they developed an atom Laser based on Bose-Einstein condensates that was able to drip single atoms downward from a micro spout, and the coherence(see Fig.3(b)) of the condensate was remarkably observed. In February 1999, the Danish physicist Lene Hau of Harvard university and her colleagues slowed light traveling through a **BEC** from its speed in vacuum of 3.10^{8} meters per second to a mere 17 meters per second. Two years later the team announced that it had

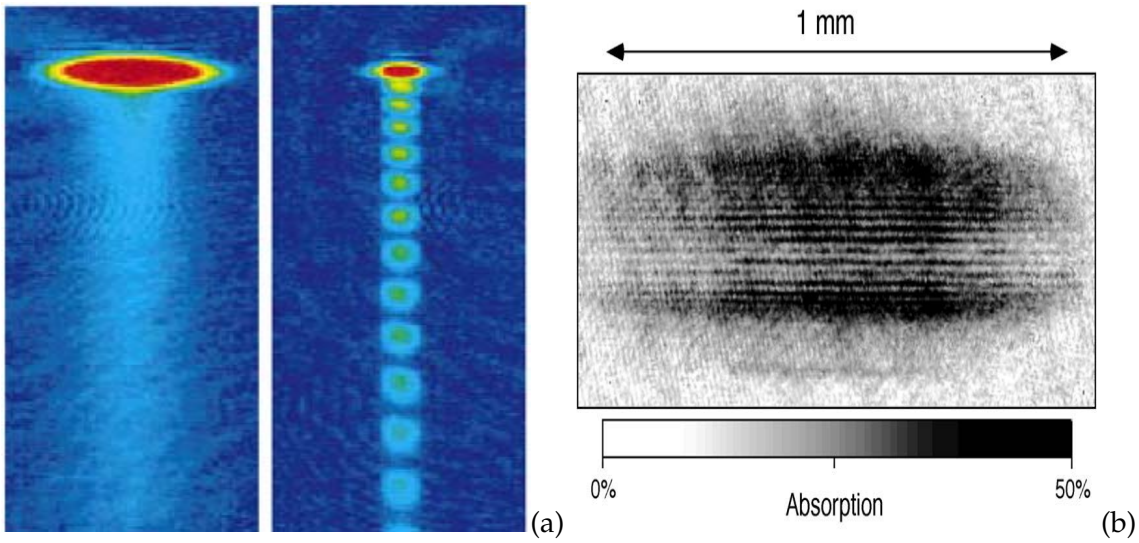

Figure 3: a) Interference between two jets of atoms falling from an atomic cloud. On the left, the cloud is not cold enough to be condensed and there is no interference between the two atomic jets. On the right, with a Bose-Einstein condensate one observes destructive interferences in some points and constructive interferences in others. b) Interference pattern of two expanding condensates demonstrating the coherence of Bose-Einstein condensates. This absorption image was observed after 40 ms time of flight. The interference fringes have a spacing of $15\mu m$, a huge length for matter waves.

Pictures from Nobel lecture for 2001 physics Nobel prize published in reference [79]

briefly brought light to a complete stop. On June 18, 1999, **JILA** researchers used this technique to achieve the first Fermi degenerate gas of atoms. A group of German researchers demonstrated in 2001 that condensates can be created and manipulated using so-called atom chips, an achievement that could form the basis of integrated atom circuit based on the motion of atoms rather than electrons. The challenging aim of creating a **BEC** in the gas of spin-polarized hydrogen atoms has been finally achieved in June 1998 at **MIT** by D. Kleppner et al, concluding two decades of efforts to observe the Bose-Einstein condensation in that system. The Bose-Einstein condensates of ^{85}Rb atoms were produced in 2000 [71] based on a new tool established by condensate Physics, the Feshbach resonance techniques [15]. Feshbach's resonances have originally been a phenomenon in the field of nuclear reactions and have been described theoretically by Herman Feshbach [72, 73]. Such resonances have been predicted in collisions of alkali atoms for the first time by Tiesinga et al. [74, 75] and are now studied and applied in many experiments. In February 2001, Alain Aspect, Chris Westbrook, and colleagues at the Institut d'Optique in Orsay (France) reported the observation of **BEC** in a gas of metastable helium $(He^{\star})$. Eight days later, a team led by Claude Cohen-Tannoudji and Michèle Leduc at Ecole Normale Supérieure (ENS)

in Paris also announced condensation of helium 4.

In December 2002, physicists at Innsbruck in Austria created the first **BEC** of cesium atoms, which is the basis of atomic clocks and also plays a key role in certain metrological applications, including measurements of the electric dipole moment of the electron. In 2003, Deborah Jin and her colleagues at **JILA** used paired fermions to create the first atomic fermionic condensate. The first molecular condensates were created in November 2003 by the team of Rudolf Grimm at the University of Innsbruck in Austria. In November, 2010, the first photon Bose-Einstein Condensate was observed. The techniques for creating Bose-Einstein condensates are progressively improved, as indicates the reference [80] in which the rubidium 87 atoms are Bose-Einstein Condensed with a simple evaporative cooling method.

The realization of Bose-Einstein condensation in dilute atomic gases in 1995 triggered the exploration of quantum phenomena in a macroscopic scale. This technological prowess has provided new systems for studying Bose-Einstein condensates as well as, superfluidity, superconductivity, and many other phenomena concerning basic concepts of quantum Physics. It has opened a new area of physics called cold atoms, which is still growing rapidly and attracting interest from all areas of Physics. In this thesis our attention is focused mainly on the case of a **BEC** loaded into a moving optical lattice.

I.2 Bose-Einstein condensates in optical lattices

In the **BEC** history, Laser beams have played a key role in its final realization in 1995. An optical lattice is an artificial crystal of light, consisting of hundreds of thousands of optical micro-traps, obtained by interfering optical Laser beams. Its spatially periodic potential, works on the principle of the ac Stark shift. When an atom is placed in a light field, the oscillating electric field of the latter induces an electric dipole moment in the atom, and the interaction between this induced dipole and the electric field leads to an energy shift ΔE of an atomic energy level. These optical lattices are powerful model systems of quantum many-body systems in periodic potentials for probing nonlinear wave dynamics and strongly correlated quantum phases. Optical lattices for atomic condensates raised enormous interest, as they mirror features known from solid state physics to the field of atom optics. By interfering more Laser beams, one can obtain one(**1D**), two(**2D**), and three-dimensional(**3D**) periodic potentials. One advantage not negligible in the use of an optical lattice in condensed matter physics is the possibility to control the geometry

and the depth of the optical potential by the experimentalist. The geometry can be changed for example in the creation of a one dimensional optical lattice by interfering two Laser beams at an angle less than 180°, and the depth can be changed by simply increasing or decreasing the intensity of the Laser light. Interfering Laser beams under a different angle can lead to complex lattice configurations such as Kagomé and Toda lattices. One major difference between atoms in optical lattices and most systems in condensed matter physics is their excellent isolation from their environment, which leads to coherent dynamics on long timescales. The ultracold bosonic and fermionic quantum gases combined to optical lattices have enhanced research activities in the field of condensed-matter physics, as well as finding applications in quantum optics and quantum information processing, and understanding atomic and molecular physics.

In this thesis, we consider a particular case of optical lattices, the Fourier-synthesized optical lattice. According to reference [81], this kind of optical lattice is obtained as follows. A conventional lattice with sinusoidal shape and spatial periodicity $\lambda/2$ is generated by overlapping two counterpropagating off-resonant Laser beams with frequency ω forming a standing wave. Due to a spatial varying ac-Stark shift, atoms experience a dipole force depending on the sign of the polarizability, which attracts the atoms to the nodes (for $\omega > \omega_0$) or the anti-nodes(for $\omega < \omega_0$) of the Laser intensity, where ω_0 is an atomic resonance frequency. The effective potential for an atom exposed to a standing optical wave may also be described in a quantum picture by the exchange of photons changing the atoms momentum. The atoms here undergo virtual two-photon processes of absorption of one photon from one Laser beam and stimulated emission of an-other photon into a counterpropagating beam. An atom undergoing such a two photon process exchanges a momentum amount of $2\hbar k$ with the lattice.

The multi-photon Raman technique is used to generate a lattice potential of periodicity $\lambda/4$, as the first harmonic for a Fourier-synthesis of lattice potentials. The scheme uses three-level atoms with two stable ground states and one electronically excited state. The atoms are irradiated by two optical beams of frequencies $\omega + \Delta\omega$ and $\omega - \Delta\omega$ from the left and by a beam of frequency ω from the right. Momentum is transferred to the atoms in units of $4\hbar k$ during an induced virtual four-photon processes, being a factor two above the corresponding process in a standing wave. This suggests a spatial periodicity of $\lambda/4$ for the adiabatic light shift potential. This scheme can be extended to generate lattice potentials with higher periodicities $\lambda/2n$ by a 2n-th photon process. The high resolution of Raman spectroscopy between two stable ground states over an

excited state allows to clearly separate in frequency space the desired 2n-th order process from lower order contributions.

By combining lattice potentials of different spatial periodicities, variable periodic potentials can be synthesized, and are called Fourier-synthesized optical lattices. As example, by superimposing two one-dimensional lattice potentials of spatial periodicities $\lambda/2$ and $\lambda/4$ one obtains a Fourier-synthesized atom potential given by

$$V(z) = \frac{V_1}{2}\cos(2kz) + \frac{V_2}{2}\cos(4kz + \varphi). \tag{13}$$

where V_1 and V_2 denote the potential depths of the two lattice harmonics respectively, φ the relative phase, and k the wave vector.

In the following lines, we emphasize with only relevant results related to condensate trapped or loaded into optical lattices. It has been argued in references [82, 83, 84] that ultracold quantum gases loaded into an optical lattice can be use as a quantum simulator, as Richard Feynman originally conceived for a quantum computer. This new physical system can be used to simulate the dynamical behaviour of another complex quantum system. The first experiment of Bose condensates in an optical lattice was reported in 1998 by Anderson and Kasevich [85], and they observed interference of atomic wave tunneling from a condensate confined in a vertically oriented one dimensional optical lattice, in analogy with a pulsed mode-locked photon Laser. From this experiment, Bloch oscillations, number squeezing, and Landau-Zener tunneling between different energy bands in an optical lattice were observed. Moreover, coupled condensates acting as Josephson junction was realized and the Josephson effect was observed. Latter on, the Josephson oscillations will be observed and reported in reference [86]. The theoretical analysis of the superfluid-Mott insulator transition in the strongly interacting atomic regime was discussed in [87], and later accomplished by Greiner et al, and reported in reference [88]. Biao Wu and Qian Niu in reference [89] investigated the superfluidity of Bose-Einstein condensates in optical lattices, and as result, they have shown that apart from the usual Landau instability, which occurs when a **BEC** flows faster than the speed of sound, the **BEC** can also suffer a dynamical instability, resulting in period-doubling and other sorts of symmetry breaking of the system. This result will be also obtained by Smerzi et al in reference [90]. This phenomenon takes place when the spectrum of the excitations of the system exhibits complex frequencies. Later on, this dynamical instability will be observed and reported in reference [91]. From then on, the dynamics of

Bose-Einstein condensates in optical lattices aroused lots of interest. As relevant results, the shift of the oscillation frequency in the presence of the optical lattice was observed and reported in reference [92]. The experimental results have shown a good agreement with the prediction of the renormalized mass theory of Krömer et al [93]. It is experimentally proven in reference [94] that the thermal cloud stays locked at the center of the trap due to its incoherent nature in the presence of the optical lattice, while the condensate moves and oscillates with frictions through the lattice. In reference [95], the Bragg spectroscopy for a condensate in an optical lattice was suggested to investigate the excitation spectrum, and used in experiments to study the behaviour of a condensate prepared in a three-dimensional optical lattice by Störfle et al in reference [96]. In references [97, 98, 99], the properties of the condensate band structure called swallow tail were reported. The stability of superfluid currents in a system of ultracold bosons is studied using a moving optical lattice in [100], and the authors have proven that superfluid currents in a very weak lattice become unstable when their momentum exceeds half the recoil momentum. The authors of reference [101] have studied the magnetic solitons in spinor Bose-Einstein condensates confined in a one-dimensional optical lattice by the Holstein-Primakoff transformation method. They arrived to the conclusion that, due to the long-range light-induced and static magnetic dipole-dipole interactions, there exists different types of magnetic solitary excitations in different parameter regions.

I.3 Brief overview of chaos

I.3.1 What is chaos?

The history of chaos began at the end of the twentieth century with Henri-Poincaré working on the famous 3-body problem reported in reference [102]. Historically, the first specific three-body problem to receive extended study was the one involving the moon, the earth and the sun. In his research on this problem, Poincaré became the first person to discover a chaotic deterministic system which will be later considered as the foundation of modern chaos theory. Approximately at the beginning of 1960, the meteorologist Edward Lorenz of **MIT** was experimenting with early computer models of weather, and wished to rerun a simulation he had completed earlier in the day. He reentered the numbers as his machine had printed them, not realizing that the computer internal memory carried three more significant figures than did the printout. While

the new simulation closely followed the old for a brief time, it quickly diverged wildly until it was unrecognizable. What Lorenz did, after much investigation, was finally to codify the effect he had observed into the modern conception of *sensitive dependence on initial conditions* [103]. It will be latter shown that many nonlinear physical systems exhibit the same exponential growth of the distance between two trajectories for tiny difference in the two initial conditions as the meteorological system. Although no universally accepted mathematical definition of chaos exists, according to the chaos theory, a nonlinear dynamical system is said to be chaotic if it has a sensitivity to initial conditions. This sensitivity to initial conditions for nonlinear systems is popularly known as the "butterfly effect", so-called because of the title of a paper given by Edward Lorenz in 1972 to the American association for the advancement of science in Washington D.C, entitled *predictability*: Does the flap of a butterfly's wings in Brazil set off a tornado in Texas? The flapping wing represents a small change in the initial condition of the system, which causes a chain of events leading to large-scale phenomena. The orbits of such dynamical systems are confined to a bounded region, but behave unpredictably. This happens even though these systems are deterministic, meaning that their future behaviour is fully determined by their initial conditions, with no random elements involved. Roughly speaking, the unpredictability must be seen as a hallmark of a chaotic dynamics, due to the presence of nonlinear terms in the differential equation or the map governing the system. The study of the dynamics of such systems is called nonlinear dynamics. Although in general the differential equations or maps of such systems are very difficult to solve analytically (sometimes that is possible), scientists have developed some tools to determine the properties of unknown solutions.

I.3.2 Qualitative tools used in this thesis for the study of dynamical systems

I.3.2.1. Bifurcation diagram and Poincaré section

Poincaré introduced the bifurcation theory and the Poincaré section in the study of nonlinear dynamics. The French word "bifurcation" is used to indicate a qualitative change in the features of a system, such as the number and type of solutions, under the variation of one or more parameters on which the considered system depends. By the terminology local bifurcation, we mean a qualitative change occurring in the neighborhood of a fixed point or a periodic solution of the system. One considers any other qualitative change to be a global bifurcation. In bifurcation theory, one usually considers the state-control space to plot the state variable versus control pa-

rameter(s). The figure obtained, called bifurcation diagram is very useful in the understanding of the behaviour of the nonlinear system. In this space, positions at which bifurcations occur are called bifurcation points. A codimension-m bifurcation is a bifurcation which requires at least m control parameters to occur.

The second tool introduced by Poincaré was the poincaré section, a powerful method for examining the motion of dynamical systems. Let S be an n-1 dimensional surface transverse to the trajectories of a n-dimensional dynamical system. Consider a point X_0 on S at time t=0. As the trajectory starting at X_0 evolves it will eventually return to S at X_1 after a certain period. If we consider all initial points on S we can define a mapping P from S to itself such that $X_1 = P(X_0)$, and after k+1 iterations $X_{k+1} = P(X_k)$. The mapping P is called the return map or Poincaré map of the dynamical system. S is called Poincaré section. After the transient regime of the dynamical system has disappeared, the Poincaré section exhibiting a point attractor characterizes periodic oscillations, and period-n oscillations when the Poincaré section exhibits n points attractors. The Poincaré section of quasi-periodic oscillations exhibits closed curve(s). The chaotic regime of a dynamical system exhibits a set of points bounded in a finite region, called strange attractor.

I.3.2.2. The Lyapunov exponent

The Lyapunov exponent or Lyapunov characteristic exponent of a dynamical system introduced by the Soviet physicist Aleksandr Lyapunov is a quantity that characterizes the rate of separation of infinitesimally close trajectories. Let's consider in phase space two trajectories with a tiny initial separation ΔX_0. As the time evolves, the separation ΔX_t of the above two trajectories can be expressed as $|\Delta X_t| = e^{\lambda t}|\Delta X_0|$. The corresponding value of λ is called Lyapunov exponent. The positive Lyapunov exponent characterizes the sensitive dependence to initial conditions in the dynamical system, in other words the existence of chaotic dynamics. Conversely, the negative Lyapunov exponent implies a stable dynamical system.

I.3.2.3. Basin of attraction

To understand the notion of basin of attraction, let us begin by defining the concept of "attractor" of a dynamical system. Roughly speaking, an attractor of a dynamical system is a subset of the state space to which orbits originating from typical initial conditions tend as time increases. An attractor can be a point, a finite set of points, a curve, a manifold, or even a complicated set

with a fractal structure known as a strange attractor, hallmark of a chaotic motion. It is very common for dynamical systems to have more than one attractor. For each such attractor, its basin of attraction is the set of initial conditions leading to long-time behavior that approaches that attractor. Thus the qualitative behaviour of the long-time motion of a given system can be fundamentally different depending on which basin of attraction the initial condition lies in. Regarding a basin of attraction as a region in the state space, it has been found that the basic topological structure of such regions can vary greatly from system to system. If one plots the basin of attraction in phase space, the chaotic dynamics will be recognizable by its fractality. It is to note that there can be basin boundaries of qualitatively different types. As in the case of attractors, bifurcations can occur in which basin boundaries undergo qualitative changes as a system parameter passes through a critical bifurcation value. Such basin boundary bifurcations are called metamorphoses.

Due to the presence of nonlinearities into equations modeling the dynamics of Bose-Einstein condensates, the study of chaos therein has attracted many researchers. In reference [104], the authors have performed a careful analysis on a **BEC** governed by a generalized version of the Gross-Pitaevskii equation. The system is investigated considering several sets of values for the three body dissipation and linear feeding parameters.They observed that, for a certain range of the space of parameters, the equation presents unstable solutions that can lead to a chaotic behaviour, since the equation presents an exponential increase of the trajectory separation, in similar way found earlier for the complex Ginzburg-Landau equation. In reference [105], the authors present a theoretical study of a hybrid optomechanical system consisting of a Bose-Einstein condensate trapped inside a single-mode optical cavity with a moving end mirror. They investigate the dynamics in a regime where the intracavity optical field, the mirror, and the side-mode excitation all display bistable behaviour. In this regime they find that the dynamics of the system exhibits Hamiltonian chaos for appropriate initial conditions.

For a Bose-Einstein condensate confined in a double lattice consisting of two weak laser standing waves, authors in reference [106] have found the Melnikov chaotic solutions and chaotic regions of parameter space by using the direct perturbation method. Moreover, they have obtained in the chaotic region, spatial evolutions of chaotic solutions and the corresponding distribution of particle number density which is bounded, but unpredictable between their superior and inferior limits.

I.3.3 The control of chaos

The idea of chaos control was enunciated at the beginning of 1990s at the university of Maryland according to reference [107]. In this article, the ideas for controlling chaos were outlined and a method for stabilizing an unstable periodic orbit was suggested, as a proof of principle. The main idea consisted in waiting for a natural passage of the chaotic orbit close to the desired periodic behaviour, and then applying a small judiciously chosen perturbation, in order to stabilize such periodic dynamics. From then on, the control of chaos in dynamical systems became an important topic in scientific research today. Broadly speaking, there are two kinds of chaos control, the **OGY** method and the adaptive method.

The **OGY** method was introduced in 1990 by Ott et al. [107, 108], and the basic idea is that besides the occurrence of chaos in a large variety of natural processes, chaos may also occur because one may wish to design a physical, biological or chemical experiment, or to project an industrial plant to behave in a chaotic manner. The idea of Ott, Grebogi, and Yorke (**OGY**) is that chaos may indeed be desirable since it can be controlled by using small perturbation to some accessible parameter [109], or to some dynamical variable of the system [110]. The major key ingredient for the control of chaos is the observation that a chaotic set, on which the trajectory of the chaotic process lives, has embedded within it a large number of unstable low-period periodic orbits. In addition, because of ergodicity, the trajectory visits or accesses the neighborhood of each one of these periodic orbits. Some of these periodic orbits may correspond to a desired system's performance according to some criterion. The second ingredient is the realization that chaos, while signifying sensitive dependence on small changes to the current state and henceforth rendering unpredictable the system state in the long time, also implies that the system's behaviour can be altered by using small perturbations. Then, the accessibility of the chaotic systems to many different periodic orbits combined with its sensitivity to small perturbations allows for the control and the manipulation of the chaotic process. Specifically, the **OGY** approach is then as follows. One first determines some of the unstable low-period periodic orbits that are embedded in the chaotic set. One then examines the location and the stability of these orbits and chooses one which yields the desired system performance. Finally, one applies small control to stabilize this desired periodic orbit. However, all this can be done from data by using nonlinear time series analysis for the observation, understanding and control of the system. This is particularly important since chaotic systems are rather complicated and the detailed knowledge of the equations

of the process is often unknown.

The basic idea of the adaptive method for control of chaos in dynamical systems is that many alternative approaches to the **OGY** method have been proposed for the stabilization of the unstable periodic orbits of a chaotic dynamics. In general the strategies for the control of chaos can be classified into two main classes, namely: closed loop or feedback methods and open loop or non feedback methods.

The first class includes those methods which select the perturbation based upon a knowledge of the state of the system, and oriented to control a prescribed dynamics. Among them, we here recall (besides **OGY**) the so called occasional proportional feedback, simultaneously introduced by Hunt [111] and Showalter [112], the method of Huebler [113], and the method introduced by Pyragas [114], which apply a delayed feedback on one of the system variables. All these methods are model independent, in the sense that the knowledge on the system necessary to select the perturbation can be done by simply observing the system for a suitable learning time.

The second class includes those strategies which consider the effect of external perturbations (independent on the knowledge of the actual dynamical state) on the evolution of the system. Periodic [115] or stochastic [116] perturbations have been seen to produce drastic changes in the dynamics of chaotic systems, leading eventually to the stabilization of some periodic behaviour. These approaches, however, are in general limited by the fact that their action is not goal oriented, i.e; the final periodic state cannot be decided by the operator.

Both kinds of chaos control are still in development. As a matter of fact, chaos control may have a dual function: to generate chaos or to suppress it.

I.4 Applications of Bose-Einstein condensates

The primary application of atomic **BEC** systems is in basic research areas at the moment, and will probably remain so for the foreseeable future.

After the proof of the wave nature of condensates and the Laser effect with atoms realized at **MIT** in 1997 by Ketterle's team, the realization of atoms Laser, that is to say instruments able to deliver a beam of atoms all in the same quantum state, like the photons of a Laser beam, remains the major application of condensates. This would be of great interest to atomic optics, to interferometry and to chemistry (study of chemical reactions between two atomic beams under very well defined and controlled conditions, condensations of molecules, and so on). In fact, the

atoms Laser is based on the Laser effect with atoms, which consists to form a condensate and extract by a suitable means a portion of the condensed atoms. But there is still a long way to go before arriving at atomic fluxes of appreciable intensity and duration.

One sometimes hears people talk about condensates as a tool for lithography, but that is not likely to be a real commercial application any time soon, because the throughput is just too low. Nobody has a method for generating Bose-Einstein condensates at the sort of rate one would need to make interesting devices in a reasonable amount of time. As a result, most **BEC** applications will be confined to the laboratory.

One of the hottest areas in **BEC** at the moment is the use of Bose condensates (and the related phenomenon of degenerate Fermi gases) to simulate condensed matter systems. It is easy to make an optical lattice from an interference pattern of multiple Laser beams that looks to the atoms rather like a crystal lattice in a solid looks to electrons: a regular array of sites where the particles could be trapped, with all the sites interconnected by tunneling. The big advantage **BEC**/optical lattice systems have over real condensed matter systems is that they are more easily tunable. It is easy to vary the lattice spacing, the strength of the interaction between atoms, and the number density of atoms in the lattice, which allows the experimentalist to explore a range of different parameters with essentially the same sample, which is very difficult to do with condensed matter systems where one needs to grow all new samples for every new set of values you want to explore. As a result, there is a great deal of work in using **BEC** systems to explore condensed matter physics, essentially making cold atoms look like electrons.

There is also a good deal of interest in Bose-Einstein condensate for possible applications in precision measurement. At the moment, some of the most sensitive detectors ever made for things like rotation, acceleration, and gravity gradients come from atom interferometry, using the wavelike properties of atoms to do interference experiments that measure small shifts induced by these effects. **BEC** systems may provide an improvement beyond what one can do with thermal beams of atoms in these sorts of systems. There are a number of issues to be worked out in this relating to interatomic interactions, but it's a promising area.

The other really hot area of **BEC** research is in looking for ways to use **BEC** systems for quantum information processing. If you want to build a quantum computer, you need a way to start with a bunch of qubits that are all in the same state, and a **BEC** could be a good way to get there, because it consists of a macroscopic number of atoms occupying the same quantum state. There

are a bunch of groups working on ways to start with a **BEC**, and separate the atoms in some way, then manipulate them to do simple quantum computing operations.

There is a lot of overlap between these sub-sub fields. One of the best ways to separate the qubits for quantum information processing is to use an optical lattice for example. But those are probably the biggest current applications of **BEC** research. None of these are likely to provide a commercial product in the immediate future, but they are all providing useful information about the behaviour of matter on very small scales, which helps feed into other, more applied lines of research.

CHAPTER II

METHODOLOGY: MODELING AND MATHEMATICAL METHODS

II.1 Introduction

The equation generally considered to describe the dynamics of a Bose-Einstein condensate assumed to be a weakly-interacting dilute Bose gas is the well known Gross-Pitaevskii equation, obtained within the framework of lowest-order mean-field approximation. This equation rigorously valid at zero temperature(T=0K), is generally used in literature for temperatures much less than the transition temperature for condensation T_c, given by the Einstein formula defined in eq.(5). The assumption of a Bose gas to be dilute compels to neglect the higher order interaction terms, and to consider only the two-body elastic atom-atom collisions, characterized by the s-wave scattering length a_s. Furthermore, the impact of the uncondensed fraction of a Bose gas responsible of thermal and quantum fluctuations is not taken into account in the dynamical behaviour of such a condensate. Due to the fact that some atomic species have been Bose-condensed at very high transition temperatures with strong interatomic interactions and high density of atoms as in the cases of helium 4(^{4}He) and rubidium 85(^{85}Rb), it was clear that the **GPE** obtained in the mean-field approach can not describe accurately the dynamical behaviour of such condensates. All these observations compel to consider higher order interatomic interactions and thermal fluctuations in the dynamics of such condensates. Moreover, remembering that in the **BEC** history the two-and three-body recombination responsible for the formation of molecules(dimer) and losses of atoms from trapping potential were a major problem in its final achievement, these inelastic collisions proven experimentally with the Feshbach resonance techniques, were recently introduced into the **GPE** in references [19, 20, 21, 22, 23, 24, 25, 26] as a complex terms to describe the dynamics of certain condensates. It is also well known that all improvements in the cooling techniques in the achievement of Bose-Einstein condensation were

mainly to circumvent this phenomenon of losses of atoms and increase the density of atoms of the condensate. Therefore, one can understand the complex Gross-Pitaevskii-Ginzburg equation (**GPGE**) sometime used to describe the dynamical behaviour of atoms of certain condensates.
In this thesis we consider the dynamics of a condensate in the framework of this **GPGE**, with an external potential which is a moving optical Fourier-synthesized lattice. This choice of potential give the possibility to the experimentalist to control externally its geometry. The next sections of this chapter will be to present the different methods used, and the model considered in this thesis.

II.2 Methods used in this thesis

II.2.1 Analytical method

The analytical tool used in this thesis to predict the onset of chaos in the dynamical behaviour of the condensate is the Melnikov method (**MM**). The generalized Melnikov method, first introduced by Melnikov [147] and developed by Wiggins[148, 149], consists of studying a system in which the unperturbed problem is an integrable Hamiltonian system having a normally hyperbolic invariant set whose stable and unstable manifold intersect non-transversally. When a system is perturbed by external excitations and dissipative forces, the homoclinic motions can break into homoclinic tangles, providing the conditions for chaotic motions. Roughly speaking, the Melnikov theory defines the condition for the appearance of the so-called transverse intersection points between the perturbed and the unperturbed separatrices, or the appearance of the fractality on the basin of attraction. Although Melnikov's method is merely approximative, it is one of a few methods allowing analytical prediction of the occurrence of chaos. Moreover, it can be applied to a relatively large class of dynamical systems. The Smale-Birkhoff theorem states that a necessary condition for the occurrence of chaos is that the Melnikov function induced by the perturbation should have simple zeros. That is to say $M(t_0)$=0 and $\frac{dM(t_0)}{dt_0} \neq 0$ at $t = t_0$, where t_0 represents the cross-section time of the Poincaré map.
This method was successfully used in reference [150] to study the Melnikov chaos in a periodically driven Rayleigh-Duffing oscillator and in references [151, 152] to study the active control delay and the horseshoes chaos in a single and double well Duffing oscillators. In reference [153], this method was used to predict the onsets for apparition of homoclinic or heteroclinic bifurca-

tions in a parametrically excited mechanical system.

Before expressing the Melnikov function, let's define these few useful concepts.

A separatrix is a boundary separating two modes of behaviour in a differential equation. If the orbit of a point P in phase space of a mapping or a flow approaches an invariant set I as t approaches $\pm\infty$ then the orbit of P is said to be homoclinic to I. On the other hand, if the orbit of a point P in phase space of a mapping or a flow approaches an invariant set I as t approaches $+\infty$ and approaches another invariant set J as t approaches $-\infty$, then the orbit of P is said to be heteroclinic to I and J.

Let's consider the time periodic dynamical system

$$\dot{X} = f(X) + \epsilon g(X, t), \tag{14}$$

where $X = \begin{bmatrix} u \\ v \end{bmatrix}$ represents the state vector, $f(X)$ is a planar Hamiltonian vector field, $\epsilon g(X, t)$ is a small perturbation which need not to be Hamiltonian itself. $g(X, t)$ is a periodic function in time, that is to say there exists a real T such that $g(X, t + T) = g(X)$. Let's consider the unperturbed system corresponding at $\epsilon = 0$. This integrable Hamiltonian system can be written as a function of the Hamiltonian H as specified below

$$\begin{cases} \dot{u} = \dfrac{\partial H}{\partial v} \\ \dot{v} = -\dfrac{\partial H}{\partial u}. \end{cases} \tag{15}$$

From this system, the Hamiltonian is determined. On a separatrix, this Hamiltonian is constant. With this assumption, in phase space the velocity can be expressed as a function of the position. The family of curves subsequently obtained is called integral curves. With the remark that the saddle point(s) of the system belong(s) to the separatrix, the constant of the integral curves is then determined. Integrating this particular integral curve leads to a vector essential to the determination of the Melnikov function. Let $X_0(t) = \begin{bmatrix} u_0(t) \\ v_0(t) \end{bmatrix}$ be the solution of this particular integral curve, generating the separatrix. Thus, the Melnikov function which measure the distance between stable and unstable manifolds is given by

$$M(t_0) = \int_{-\infty}^{+\infty} f[X_0(t)] \wedge g[X_0(t), t + t_0]\, dt. \tag{16}$$

This formula giving the Melnikov function will be used in this thesis to predict analytically the onset of horseshoes chaos, which in fact represents the beginning or the end of the instability in the dynamics of the condensate.

II.2.2 Numerical methods

In this thesis, we use two numerical schemes: The fourth-order Runge-Kutta method and the Euler-Cromer method.

II.2.2.1. The fourth-order Runge-Kutta method

Developed around 1900 by the German mathematicians Carl Runge and Martin Kutta, the Runge-Kutta methods which include the Euler scheme, are a family of implicit and explicit iterative methods used in temporal discretization for the approximate solutions of ordinary differential equations. In this thesis, we use the fourth-order Runge-Kutta method, the most widely known member of the Runge-Kutta family. Let an initial value problem be specified as follows

$$\begin{cases} \dot{y} = f(t, y) \\ y(t_0) = y_0 \end{cases} \tag{17}$$

y is an unknown function (scalar or vector) of time t, which we would like to approximate. At the initial time t_0 the corresponding y value is y_0. The function f, t_0, and y_0 are given. Now picking a step-size the positive number h, the fourth-order Runge-Kutta scheme is given by

$$\begin{cases} y_{n+1} = y_n + \dfrac{1}{6}(k_1 + 2k_2 + 2k_3 + k_4) \\ t_{n+1} = t_n + h, \end{cases} \tag{18}$$

with n=0,1,2,3,..., and k_1, k_2, k_3, k_4 given by

$$\begin{cases} k_1 = hf(t_n, y_n) \\ k_2 = hf(t_n + \frac{h}{2}, y_n + \frac{k_1}{2}) \\ k_3 = hf(t_n + \frac{h}{2}, y_n + \frac{k_2}{2}) \\ k_4 = hf(t_n + h, y_n + k_3). \end{cases} \tag{19}$$

y_{n+1} is the fourth-order Runge-Kutta approximation of $y(t_{n+1})$, and is determined by the present value of y_n. The fourth-order in the denomination of the Runge-Kutta method means that the local truncation error is on the order of $O(h^5)$, while the total accumulated error is on the order of $O(h^4)$.

In this thesis, this fourth-order Runge-Kutta method is directly used to plot the Lyapunov exponents, the basins of attraction and some bifurcation diagrams in Fortran 90 codes. It is also indirectly used in ode45 Matlab solver to plot some phase portraits, some Poincaré sections and spatiotemporal evolutions of the condensate.

II.2.2.2. The Euler-Cromer method

Let's consider a second-order differential equation which can be written as a first-order system as follows.

$$\begin{cases} \dfrac{dx}{dt} = y \\ \dfrac{dy}{dt} = f(t, x, y). \end{cases} \tag{20}$$

This method was introduced to solve the amplitude growth problem of a damped oscillator with the Euler method. The Euler-Cromer algorithm, a modified Euler scheme is given by

$$\begin{cases} y_{n+1} = y_n + f(t_n, x_n, y_n)\Delta t \\ x_{n+1} = x_n + y_{n+1}\Delta t \\ t_{n+1} = t_n + \Delta t. \end{cases} \tag{21}$$

n=1,2,3,..., and f, t_0, x_0 and Δt are given. This method was used to plot some bifurcations diagrams and Poincaré sections.

II.3 The Model

II.3.1 From Gross-Pitaevskii equation to Gross-Pitaevskii-Ginzburg equation

At low enough temperatures, the mean-field approximation usually considered to describe the dynamics of a Bose-Einstein condensate(**BEC**) of dilute bosonic gases is a nonlinear Shrödinger equation(**NLSE**), the so-called Gross-Piteavskii equation(**GPE**). In this formalism, the atom-atom interactions are restricted only to elastic two-body collisions, and the thermal cloud responsible of thermal and quantum fluctuations neglected. According to nonlinear science, it is well

known that the key element for the possible existence of a chaotic behaviour in a dynamical system is the nonlinearity. Taking into account the two-body interactions (nonlinear term) between atoms in the Schrödinger equation to describe the dynamics of Bose-Einstein condensates can be considered as the required condition for the possible appearance of temporal[117, 118], spatial [119, 120], and spatiotemporal [27, 28, 121] chaos in the dynamical behaviour of condensates. This Gross-Pitaevskii equation based on the lowest-order mean-field theory, describes accurately the static and dynamical properties of the condensate of a dilute Bose gas. The first realization of a condensate in 1995 triggered enormous research works on its properties. Owing to the presence of a nonlinear term in the **GPE** modeled by the s-wave scattering length, and especially because of a probable use of condensates in technology as the atom Laser project initiated at **MIT** in 1997 and so on, there has been an avalanche of studies on the chaos therein as illustrated by the following examples.

As part of **GPE** with bosonic atoms trapped by a magnetic field, authors in reference [122] have shown that Bose-Einstein condensates with attractive interatomic interactions undergo collective collapse beyond a critical number. Moreover, they have shown theoretically that if the low-lying collective modes of the condensate are excited, the radial breathing mode further destabilizes the condensate. In reference [123] the authors investigated the possibility of quantum chaos for the Bogoliubov excitations of a Bose-Einstein condensate in billiards. As results, they found that because of the mean-field interaction in the condensate, the Bogoliubov excitations are very different from the single particle excitations in a noninteracting system. The spatial chaos in the dynamics of thin cigar-shape condensates is studied in reference [124]. As theoretical tool, the Melnikov approach is used to predict the onset of chaos, and the numerical simulations show the existence of chaotic dynamics in accordance with analytical results.

To combine cooled atoms and optical lattices has given opportunities to investigate a new regime of strongly correlated quantum systems in which interactions between particles dominate the properties of the system. Due to the periodic nature of these trapping potentials, such systems are closely related to those in condensed matter physics, but offer new possibilities to vary internal parameters of the system which cannot be influenced in a real solid state system. Within the framework of the study of stability and chaos in the dynamics of condensates trapped in optical lattices, authors of reference [89] have investigated the superfluidity of Bose-Einstein condensates, and as results, they observed that apart from the usual Landau instability, which occurs

when a condensate flows faster than the speed of sound, the condensate can also suffer a dynamical instability, resulting in period doubling and other sorts of symmetry breaking of the system. In reference [27] the authors have studied the chaotic properties of steady-state traveling-wave solutions of the particle number density of a Bose-Einstein condensate with an attractive interatomic interaction loaded into a moving optical Fourier-synthesized lattice. As results, they demonstrated theoretically and numerically that chaotic traveling steady states can be reliably suppressed by small changes of the traveling optical lattice shape while keeping the remaining parameters constant. In addition, they found that the regularization route as the optical lattice shape is continuously varied is fairly rich, including crisis phenomena and period-doubling bifurcations. In reference [125], the synchronization between two coupled Bose-Einstein condensates in their chaotic states based on a technique derived from nonlinear control theory is investigated. The nonlinear control is obtained using the active control and the controller is chosen such that a single control input is sufficient to guarantee global stability of the synchronized state. Furthermore, the effectiveness and feasibility of this technique is theoretically and numerically demonstrated

Beyond the mean-field approximation, quantum fluctuations and interactions of the condensate with the thermal component of the gas are described within the framework of the Hartree-Fock-Bogoliubov equations, which are essentially more cumbersome than the relatively simple **GPE**. In reference [21], the elastic three-body collisions between atoms in the dynamics of a condensate have been established theoretically. Although the experimental proof of this phenomenon remains an open question, it was introduced in the Gross-Pitaevskii formalism in references [19, 20, 126, 127, 128, 129] to stabilize the dynamics of condensed atoms with a negative s-wave atom-atom scattering length which is unstable for a large number of atoms according to reference [130]. However, it is to note that in these articles, the condensate is governed by the real time-dependant Gross-Pitaevskii-Ginzburg equation(**GPGE**). In reference [19], the stability of a trapped condensate, with two-body and three-body collisions is studied, and the validity of the stability criterion suggested by Vakhitov and Kolokolov is discussed. From this study, the maximum initial chirp that can lead a stable condensate to collapse even before the number of atoms reaches its critical limit is obtained for several specific cases. Moreover, considering two-body and three-body nonlinear terms, with negative cubic and positive quintic terms, the conditions for the existence of two phases in the condensate are established. Authors of reference [20] have

shown that, the addition of a positive three-body interaction allows stable solutions beyond the critical number, and a dynamical analysis of conditions for the collapse is introduced. The stability of a Bose-Einstein condensed state of trapped ultra-cold atoms is investigated in reference [21] under the assumption of an attractive two-body and a repulsive three-body interaction. The lowest collective mode excitations are determined and their dependence on the number of atoms and on the strength of the three-body force are studied. As another result, the addition of three-body dynamics can allow the number of condensed atoms to increase considerably, even when the strength of the three-body force is very small compared with the strength of the two-body force.

It is well known in the **BEC** history that these two-body and three-body losses related to inelastic collisions between atoms were a crucial problem for its achievement. The improvement in the technology of cooling samples was to circumvent these inelastic processes. Furthermore, it was proved with the Feshbach resonance techniques [15, 16, 17] the existence of these losses phenomena in the dynamics of certain condensates. These dissipation phenomena were clearly observed in the Bose-Einstein condensation of ^{85}Rb. Moreover, the studies reveal that the two kinds of inelastic processes which can contribute significantly to the decay of a Bose-Einstein condensate are the two-body dipolar spin relaxation and the three-body recombination. These inelastic collisions eject the atoms from the confining trap, and to keep constant the number of atoms in the trap, an atomic pumping process is required, taking atoms from uncondensed state and injecting them into the condensate. This process called atomic feeding or atomic pumping leads to a permanent non-reversible dynamics, induced by the coupling between condensed atoms and their environment. In this context, the dynamics of the condensate is governed by the complex Gross-Pitaevski-Ginzburg equation given by

$$i\hbar\frac{\partial\psi}{\partial t} = -\frac{\hbar^2}{2m}\Delta\psi + (V(r) + i\gamma_0)\psi + \left(\frac{4\pi\hbar^2 a_s(r,t)}{m} - i\gamma_1\right)|\psi|^2\psi + (g_1 - i\gamma_2)|\psi|^4\psi. \tag{22}$$

$\psi(\vec{r},t)$ represents the macroscopic wave function, m is the atomic mass, V(r) is the trapping potential, a_s is the s-wave scattering length, g_1 is the parameter related to the elastic three-body collisions, and $\gamma_0, \gamma_1, \gamma_2$ the parameters related respectively to feeding process, dipolar relation, and three-body recombination.

Considering this extended Gross-Pitaevskii mean-field approximation with a magnetic trapping potential, the stability of atomic condensed systems when the two-body interaction is attrac-

tive is studied in reference [22, 23]. The interesting dynamics leading to chaotic behaviour of the condensate, or to stable solitonic-like solutions resulting from the balance between feeding and dissipation were obtained. This chaotic behaviour is observed mainly when the feeding parameter is about one or two orders of magnitude larger than the dissipation parameters. Also observed were weak and strong instabilities causing collapses and growth-collapse cycles. Authors of [24] have analyzed the experimental results of ^{85}Rb Bose-Einstein condensation within the mean-field approximation with time-dependent two-body interaction and dissipation due to the three-body recombination. They found that the magnitude of the dissipation is consistent with the three-body theory for longer rise times. However, for shorter rise times, there is an enhancement of this parameter, consistent with a coherent dimer formation. In reference [25], the dynamics of a nonconservative Gross-Pitaevskii equation for trapped atomic systems with attractive two-body interaction is numerically investigated, considering wide variations of nonconservative parameters, related to atomic feeding and dissipation. Some stability zones are plotted in parameter space, and the results of references [22, 23] are confirmed. In reference [26] are discussed the conditions of existence of autosolitons in trapped Bose-Einstein condensates with attractive atomic interactions. Theoretically, the variational approach is employed to estimate the stationary solutions for the three-dimensional Gross-Pitaevskii equation. Linear atomic feeding from the thermal cloud, and two-and three-body inelastic collisions are considered. Using exact numerical calculations, they shown that the variational approach gives reliable analytical results, and also discussed, the possible observation of autosolitons in experiments with ^{7}Li. Always beyond the mean-field theory, in reference [131] the dynamics of Bose-Einstein condensates in a double-well trap is discussed, the two-mode model is used to describe the symmetry breaking and self-trapping bifurcations in the reversible and quasi-reversible cases. As results, they shown that the condensate can experience a transition to a chaotic behaviour described by the Lorenz equations. Furthermore, they used the one-dimensional **NLSE** to describe the self-trapping, and with numerical experiments as well as the reduction to amplitude equations they shown that Lorenz-like chaotic behaviour can be observed. In reference [132], the modulational instability of a Bose-Einstein condensate with both two-and three-body interatomic interactions and trapped in an external parabolic potential is investigated analytically and numerically. Analytical investigations performed lead them to establish an explicit time-dependent criterion for the modulational instability of the condensate, and subsequently, the effects of the potential as

well as of the quintic nonlinear interaction are studied. In reference [133], the author construct, through a further extension of the tanh-function method, the matter-wave solutions of Bose-Einstein condensates with a three-body interaction. The condensates are trapped in a potential comprising the linear magnetic and the time-dependent laser fields. As result, they realize that exact solutions obtained include soliton solutions, such as kink and antikink as well as bright, dark, multisolitonic modulated waves. In addition they realize that the motion and the shape of the solitary wave can be manipulated by controlling the strengths of the fields. Bose-Einstein condensates with time varying two-body and three-body interatomic interactions confined in a linear potential and exchanging atoms with the thermal cloud are investigated in [134]. Using the extended tanh-function method with an auxiliary equation(the Lenard equation), many exact solutions describing the dynamics of matter-wave condensates are derived. In addition, adjusting the strength of the linear potential, the rate of exchange of atoms, and many other free parameters allow to control many features of the condensate such as its height, width, position, velocity, acceleration, and its direction. Full numerical solutions corroborate the analytical predictions. In reference [135], a modified version of the **GPE** is used to describe the dynamics of condensates. The analytical study shows that the three-body interactions destabilize more the condensate system while the external potential alleviates the instability. This result obtained theoretically is confirmed by numerical simulations. Moreover, further numerical investigations of the behaviour of solitons reveal that the three-body interactions enhance the appearance of solitons, increase the number of solitons generated, and deeply change the lifetime of these solitons. In reference [136], the modulational instability of BoseEinstein condensates based on a modified Gross-Pitaevskii equation which takes into account quantum fluctuations and a shape-dependent term, trapped in an external time-dependent complex potential is investigated. The theoretical analysis uses a modified lens-type transformation which converts the modified **GPE** into a modified form without an explicit spatial dependence. Their numerical results reveal that the gravitational field has three effects on the modulational instability. (i) the deviation backward or forward of solitons trains, (ii) the enhancement of the appearance of the modulational instability, and (iii) the reduction of the lifetime of pulses. Moreover, their numerical simulations prove that it is possible to control the propagation of the generated solitons trains by a proper choice of parameters characterizing both the loss or feeding of atoms and the gravitational field, respectively.

These studies about the stability of condensates beyond the mean-field approach were made within the framework of bosonic atoms trapped by a magnetic field. Finding that in the literature there is no substantial research works about the stability and chaos for condensates governed by the **GPGE** with a trapping potential of type optical lattice, that motivated our research team to look in that direction. Interested in finding out what would be the dynamics of a damped condensate with repulsive two-body and attractive three-body elastic collisions and governed by the real time-dependent **GPGE**, with an external trapping potential which is a moving optical Fourier-synthesized lattice, we obtain as results in reference [29] that the depth and the variable shape of the optical lattice may help to enhance chaos while the strength of the effective three-body interactions, the velocity of the optical lattice, and the damping coefficients annihilate or reduce the chaotic behaviour of the condensate. Moreover, the numerical simulations reveal that for all control parameters, the route leading to chaotic oscillations or to regular oscillations is the period-doubling scenario. In reference [30], we study the dynamics of a condensate with attractive two-body and repulsive three-body elastic collisions and governed by the complex **GPGE**. As theoretical results, we discover that coupling the optical depth and parameters related to atomic feeding and atomic losses (dissipation) can help to reduce or annihilate the chaotic behaviour of the condensate, and within the framework of homoclinic bifurcations, the chaotic behaviour of the condensate occurs when the feeding parameter is about one order of magnitude larger than the three-body recombination parameter. This results was already obtained in the case of condensates trapped by a magnetic field [22, 23]. Furthermore, the numerical simulations reveal that the transition route to chaos is the quasi-periodicity.

The following lines of this thesis will be devoted to the details of these two articles aforementioned. We consider a thin cigar-shaped condensate resulting from a cylindrical **3D BEC** with a strong radial confinement, so that the transversal dynamics can be neglected. It was shown in references [137, 138, 139, 140] that, condensates as observed experimentally are weakly dissipative and decay over time. That can be interpreted as the result of nonzero temperature in the Bose-Einstein condensation, because the quantum fluid obtained will be weakly viscous, implying small frictions between the bosonic atoms. Henceforth, we consider this friction phenomenon between the atoms in the dynamics of the condensate. Moreover, we admit elastic and inelastic two-body and three-body collisions between atoms as it was proved in reference [15, 16, 17]. To maintain constant the number of atom into the condensate, a pumping process

is considered, taking atoms from thermal cloud for the condensed atoms. As trapping potential, we choose a moving optical Fourier-synthesized lattice, well described in the previous chapter. This trapping potential gives the possibility to control its depth and its velocity, roughly speaking, the possibility to change with external parameters its geometry. Thus, this thin cigar-shaped condensate is governed by the following quasi-one-dimensional (**1D**) time-dependent Gross-Pitaevskii-Ginzburg equation(**GPGE**)

$$(i+\gamma)\hbar\frac{\partial\psi}{\partial t} = -\frac{\hbar^2}{2m_a}\frac{\partial^2\psi}{\partial x^2} + \left(\tilde{V}_0 sn^2(\eta\xi;m) + \tilde{g}_0|\psi|^2 + \tilde{g}_1|\psi|^4\right)\psi + i\left(\tilde{\gamma}_0 - \tilde{\gamma}_1|\psi|^2 - \tilde{\gamma}_2|\psi|^4\right)\psi, \quad (23)$$

where $\psi(x,t)$ is the wave function of the condensate, $\xi = x + v_L t$ is the space-time variable, $v_L = \dfrac{\Delta f}{2k}$ the velocity of the traveling lattice, with Δf the frequency difference between the two Fourier-synthesized counter-propagating laser beams. $k = \dfrac{2\pi}{\lambda}$ is the laser wave vector, m_a is the atomic mass. The real number $\tilde{g}_0 = \dfrac{4\pi\hbar^2 a_s}{m_a}$ is the interatomic two-body interaction strength, with a_s the s-wave scattering length. The real number $\tilde{g}_1$ is the strength of the effective three-body interactions. η=$\dfrac{2K(m)k}{\pi}$, with K(m) the complete elliptic integral of the first kind. $\tilde{V}_{trap} = \tilde{V}_0 sn^2(\eta\xi;m)$ is the periodic moving optical lattice, where sn(.;m) is the Jacobian sine elliptic function of parameter m($0 \leq m \leq 1$). The choice of this form of trap potential compared with the classical form generally used, is that it will be very helpful in experiments, due to the possibility to change(with the variable shape m) the geometry of the optical lattice.

$\tilde{\gamma}_0$ represents the rate of the pumping process, $\tilde{\gamma}_1$ and $\tilde{\gamma}_2$ are parameters related to atomic losses. In fact, $\tilde{\gamma}_1$ and $\tilde{\gamma}_2$ are respectively related to the dipolar relaxation and to the three-body recombination. The sign(-) preceding the positive parameters $\tilde{\gamma}_1$ and $\tilde{\gamma}_2$ displayed in eq.(23) is to indicate that these two terms are related to dissipations. The parameter γ is related to the damping, due to the fact that the condensate is not really in the superfluidity form, implying a very small viscosity in the quantum fluid.

II.3.2 System transformation

The optical trapping potentials being generally periodic functions, we consider the traveling-wave solutions of eq.(23) in the form of Bloch-like waves [141, 142, 143]

$$\psi(x,t) = \varphi(\xi)e^{i(\tilde{\alpha}x+\tilde{\beta}t)}, \quad (24)$$

where $\varphi(\xi)$ is a complex function, modeling the amplitude of the traveling wave. The parameters $\tilde{\alpha}$ and $\tilde{\beta}$ are two real constants to be determined with boundary conditions on the wave function. With this form of wave function, according to reference [144] it is probable to have solitonic solutions. We note that this choice of $\psi(x,t)$ implies that the traveling wave $\varphi(\xi)$ and the elliptic optical lattice move with the same velocity. Inserting the partial derivatives of the wave function $\psi(x,t)$ given by the following expressions

$$\left\{\begin{array}{l} \dfrac{\partial\psi}{\partial t} = \left(\upsilon_L \dfrac{d\varphi}{d\xi} + i\tilde{\beta}\varphi\right) e^{i(\tilde{\alpha}x+\tilde{\beta}t)} \\ \dfrac{\partial\psi}{\partial x} = \left(\dfrac{d\varphi}{d\xi} + i\tilde{\alpha}\varphi\right) e^{i(\tilde{\alpha}x+\tilde{\beta}t)} \\ \dfrac{\partial^2\psi}{\partial x^2} = \left(\dfrac{d^2\varphi}{d\xi^2} + 2i\tilde{\alpha}\dfrac{d\varphi}{d\xi} - \tilde{\alpha}^2\varphi\right) e^{i(\tilde{\alpha}x+\tilde{\beta}t)}, \end{array}\right. \tag{25}$$

into eq.(23), and rescaling the complex amplitude φ by $k^{\frac{3}{2}}$ and the spatiotemporal variable ξ by $\dfrac{2K(m)}{\pi} = \dfrac{\eta}{k}$, we obtain

$$\begin{aligned} (i+\gamma)\hbar\left(\frac{\upsilon_L k^{\frac{3}{2}}}{\frac{2K(m)}{\pi}}\frac{d\varphi}{d\xi} + i\tilde{\beta}k^{\frac{3}{2}}\varphi\right) &= -\frac{\hbar^2}{2m_a}\left(\frac{k^{\frac{3}{2}}}{\left(\frac{2K(m)}{\pi}\right)^2}\frac{d^2\varphi}{d\xi^2} + \frac{2i\tilde{\alpha}k^{\frac{3}{2}}}{\frac{2K(m)}{\pi}}\frac{d\varphi}{d\xi} - \tilde{\alpha}^2 k^{\frac{3}{2}}\varphi\right) \\ &\quad + \left(\tilde{V}_0 sn^2\left(\frac{2K(m)}{\pi}\eta\xi, m\right) + \tilde{g}_0 k^3|\varphi|^2 + \tilde{g}_1 k^6|\varphi|^4\right) k^{\frac{3}{2}}\varphi \\ &\quad + i\left(\tilde{\gamma}_0 - \tilde{\gamma}_1 k^3|\varphi|^2 - \tilde{\gamma}_2 k^6|\varphi|^4\right) k^{\frac{3}{2}}\varphi. \end{aligned} \tag{26}$$

Simplifying this equation by $k^{\frac{3}{2}}$, and considering as new spatiotemporal variable the quantity $\tau = \eta\xi$, we obtain the following complex differential equation

$$\begin{aligned} \frac{\hbar^2k^2}{2m_a}\frac{d^2\varphi}{d\tau^2} + \hbar k\gamma\upsilon_L\frac{d\varphi}{d\tau} - \left(\frac{\hbar^2\tilde{\alpha}^2}{2m_a} + \hbar\tilde{\beta}\right)\varphi - \tilde{V}_0 sn^2\left(\frac{2K(m)}{\pi}\tau; m\right)\varphi - \left(\tilde{g}_0 k^3|\varphi|^2 + \tilde{g}_1 k^6|\varphi|^4\right)\varphi = \\ i\left[-\left(\hbar k\upsilon_L + \frac{\hbar^2 k\tilde{\alpha}}{m_a}\right)\frac{d\varphi}{d\tau} + \left(\tilde{\gamma}_0 - \tilde{\gamma}_1 k^3|\varphi|^2 - \tilde{\gamma}_2 k^6|\varphi|^4\right)\varphi - \hbar\tilde{\beta}\gamma\varphi\right]. \end{aligned} \tag{27}$$

Dividing this equation by the recoil energy $E_r = \dfrac{\hbar^2k^2}{2m_a}$, one obtains

$$\begin{aligned} \frac{d^2\varphi}{d\tau^2} + \gamma\upsilon\frac{d\varphi}{d\tau} - \left(\alpha^2 + \beta + V_0 sn^2\left(\frac{2K(m)\tau}{\pi}; m\right)\right)\varphi - g_0|\varphi|^2\varphi - g_1|\varphi|^4\varphi = \\ i\left[-(\upsilon + 2\alpha)\frac{d\varphi}{d\tau} + \left(\gamma_0 - \gamma\beta - \gamma_1|\varphi|^2 - \gamma_2|\varphi|^4\right)\varphi\right]. \end{aligned} \tag{28}$$

This nonlinear differential equation governs the complex amplitude of the condensate, where the dimensionless parameters appearing inside are given by:
$\alpha = \frac{\tilde{\alpha}}{k}, \beta = \frac{\hbar\tilde{\beta}}{E_r}, g_0 = \frac{\tilde{g_0}k^3}{E_r}, g_1 = \frac{\tilde{g_1}k^6}{E_r}, \gamma_0 = \frac{\tilde{\gamma}_0}{E_r}, \gamma_1 = \frac{\tilde{\gamma}_1 k^3}{E_r}, \gamma_2 = \frac{\tilde{\gamma}_2 k^6}{E_r}, V_0 = \frac{\tilde{V}_0}{E_r}$, and $\upsilon = \frac{2m_a \upsilon_L}{\hbar k}$.
The traveling wave amplitude $\varphi(\tau)$ being a complex function, can be expressed in Euler form as,

$$\varphi(\tau) = R(\tau)e^{i\theta(\tau)}. \tag{29}$$

$R(\tau)$ and $\theta(\tau)$ represent the real amplitude and the phase of the condensate respectively. From this equation, we obtain the following derivatives of the traveling amplitude $\varphi(\tau)$.

$$\begin{cases} \dfrac{d\varphi}{d\tau} = \left(\dfrac{dR}{d\tau} + iR\dfrac{d\theta}{d\tau}\right)e^{i\theta} \\ \dfrac{d^2\varphi}{d\tau^2} = \left(\dfrac{d^2R}{d\tau^2} - R\left(\dfrac{d\theta}{d\tau}\right)^2 + i\left(R\dfrac{d^2\theta}{d\tau^2} + 2\dfrac{dR}{d\tau}\dfrac{d\theta}{d\tau}\right)\right)e^{i\theta}. \end{cases} \tag{30}$$

Inserting eq.(30) into eq.(28), the real amplitude and the phase of the condensate are governed by the following nonlinear differential system

$$\begin{cases} \dfrac{d^2R}{d\tau^2} + \gamma\upsilon\dfrac{dR}{d\tau} - R\left(\dfrac{d\theta}{d\tau}\right)^2 - (\upsilon + 2\alpha)R\dfrac{d\theta}{d\tau} - \left[\alpha^2 + \beta + V_0 sn^2\left(\dfrac{2K(m)\tau}{\pi}; m\right)\right]R - g_0R^3 - g_1R^5 = 0 \\ R\dfrac{d^2\theta}{d\tau^2} + 2\dfrac{dR}{d\tau}\dfrac{d\theta}{d\tau} + \gamma\upsilon R\dfrac{d\theta}{d\tau} + (\upsilon + 2\alpha)\dfrac{dR}{d\tau} - (\gamma_0 - \beta\gamma)R + \gamma_1R^3 + \gamma_2R^5 = 0. \end{cases} \tag{31}$$

To keep the analysis close to a possible experimental realization, we expand the trapping potential in Fourier series. Thus, according to the table of integrals and series [145] we obtain the following expression of the Jacobi sine function

$$sn^2(\tau) = \sum_{j=1}^{+\infty} b_{j-1}\sin^2\left(\frac{j\pi\tau}{2K(m)}\right). \tag{32}$$

Henceforth, the trapping optical potential has the following trigonometric form

$$V_{trap}(\tau) = V_0 sn^2\left(\frac{2K(m)\tau}{\pi}; m\right) = V_0\sum_{j=1}^{+\infty} b_{j-1}\sin^2(j\tau), \tag{33}$$

more easy to use in analytical calculations. Always in reference [145], the Fourier coefficients b_{j-1} can be deduced from the Jacobi sine function series given by

$$sn^2\left(\frac{2K(m)}{\pi}\tau; m\right) = \frac{4\pi^2}{mK^2(m)}\sum_{n=0}^{+\infty}\sum_{l=0}^{+\infty} a_n(m)a_l(m)\sin((2n+1)\tau)\sin((2l+1)\tau), \tag{34}$$

with $a_n(m) = \dfrac{q^{n+\frac{1}{2}}}{1-q^{2n+1}}$, $q = q(m) = exp\left(-\dfrac{\pi K(1-m)}{K(m)}\right)$, and $0 \leq m \leq 1$.
Expanding the right-hand side of eq.(34) leads to

$$sn^2\left(\frac{2K(m)}{\pi}\tau, m\right) = \frac{4\pi^2}{mK^2(m)}(-2\,a_0a_1 + {a_0}^2 - 2\,a_1a_2)sin^2(\tau)$$
$$+\frac{4\pi^2}{mK^2(m)}(-2\,a_0a_2 + 2\,a_0a_1)sin^2(2\tau) + \frac{4\pi^2}{mK^2(m)}(2\,a_0a_2 + {a_1}^2)sin^2(3\tau) + ..., \tag{35}$$

with $a_0(m) = \dfrac{\sqrt{q}}{1-q}$, $a_1(m) = \dfrac{q^{3/2}}{1-q^3}$ and $a_2(m) = \dfrac{q^{5/2}}{1-q^5}$.
From eq.(35), one can deduce the expressions of three first Fourier coefficients $b_0(m)$, $b_1(m)$, and $b_2(m)$ of the trapping potential, given by

$$\begin{cases} b_0(m) = \dfrac{4\pi^2 q\left(1-q+q^2-q^3+q^4\right)}{m\left(K\left(m\right)\right)^2\left(1-q-q^5+q^6\right)} \\ b_1(m) = \dfrac{8\pi^2 q^2\left(1+q^4\right)}{m\left(K\left(m\right)\right)^2\left(1-q^3-q^5+q^8\right)} \\ b_2(m) = \dfrac{4\pi^2 q^3}{m(K(m))^2(1-q^3)^2}\left[1+\dfrac{2(1-q^3)^2}{(1-q)(1-q^5)}\right]. \end{cases} \tag{36}$$

The advantage of using this kind of optical trapping potential instead of the classical form usually considered is the large opportunity of the experimentalist to change its geometry, by acting on the shape parameter m. It is important to mention that this technique has been successfully used to control the quantum transport in a condensate, as reported in reference [146].
Finally, the real amplitude and the phase of the condensate are governed by the following parametrically driven nonlinear differential system

$$\begin{cases} \dfrac{d^2R}{d\tau^2} - \left[\alpha^2+\beta+\dfrac{V_0}{2}\left(b_0(m)+b_1(m)+b_2(m)-b_0(m)\cos(2\tau)-b_1(m)\cos(4\tau)-b_2(m)\cos(6\tau)\right)\right]R \\ +\gamma\upsilon\dfrac{dR}{d\tau} - R\left(\dfrac{d\theta}{d\tau}\right)^2 - (\upsilon+2\alpha)R\dfrac{d\theta}{d\tau} - g_0R^3 - g_1R^5 = 0 \\ R\dfrac{d^2\theta}{d\tau^2} + 2\dfrac{dR}{d\tau}\dfrac{d\theta}{d\tau} + \gamma\upsilon R\dfrac{d\theta}{d\tau} + (\upsilon+2\alpha)\dfrac{dR}{d\tau} - (\gamma_0-\beta\gamma)R + \gamma_1R^3 + \gamma_2R^5 = 0. \end{cases} \tag{37}$$

Wishing to have a global overview on the dynamics of such condensates, we consider the two possible cases of the sign of scattering length(positive and negative), corresponding to repulsive and attractive two-body interactions respectively. In this context, From eq.(37), the following questions emerge from our mind:

1. How the parameters of the optical lattice(depth, variable shape, velocity) affect the dynamical behaviour of such a condensate?

2. In the case of instabilities leading to chaotic behaviour of the condensate, which route to chaos uses each control parameter?

3. Is there solitonic-like solutions in the case of a stable regime of the condensate? If yes, which is the nature of the corresponding solitary wave?

4. How parameters related to two-body and three-body elastic and inelastic collisions affect the dynamical behaviour of such a condensate?

5. By coupling analytical and numerical studies, can we control the chaos in the dynamical behaviour of such a condensate?

II.4 Analytical study of a BEC with repulsive two-body and attractive three-body interactions loaded into a moving optical Fourier-synthesized lattice

In this section, we assume the elastic two-body atom-atom interaction repulsive and the elastic three-body atom-atom interaction attractive. Thus, g_0 is a positive number and g_1 is a negative number.

II.4.1 Case of a damped condensate not subjected to inelastic collisions

In this subsection, in order to study the impact of physical parameters of the optical lattice(depth, velocity, shape) on the dynamics of the condensate, we neglect the inelastic collisions. Thus, we assume $\gamma_0 = \gamma_1 = \gamma_2 = 0$. Under such conditions, the nonlinear system modeling the dynamical behaviour of the condensate is restricted at

$$\begin{cases} \dfrac{d^2R}{d\tau^2} - \left[\alpha^2 + \beta + \dfrac{V_0}{2}\left(b_0(m) + b_1(m) + b_2(m) - b_0(m)\cos(2\tau) - b_1(m)\cos(4\tau) - b_2(m)\cos(6\tau)\right)\right] R \\ +\gamma\upsilon\dfrac{dR}{d\tau} - R\left(\dfrac{d\theta}{d\tau}\right)^2 - (\upsilon + 2\alpha)R\dfrac{d\theta}{d\tau} - g_0R^3 - g_1R^5 = 0 \\ R\dfrac{d^2\theta}{d\tau^2} + 2\dfrac{dR}{d\tau}\dfrac{d\theta}{d\tau} + \gamma\upsilon R\dfrac{d\theta}{d\tau} + (\upsilon + 2\alpha)\dfrac{dR}{d\tau} + \beta\gamma R = 0. \end{cases} \tag{38}$$

If one multiplies the second equation of eq.(38) by the real amplitude R, then one obtains after some algebraic manipulations the following equation

$$\frac{d}{d\tau}\left[R^2\left(\frac{d\theta}{d\tau} + \left(\frac{\upsilon}{2} + \alpha\right)\right)\right] + \gamma R^2\left(\upsilon\frac{d\theta}{d\tau} + \beta\right) = 0. \tag{39}$$

It is obvious to observe that

$$\frac{d\theta}{d\tau} = -(\frac{\upsilon}{2} + \alpha) = -\frac{\beta}{\upsilon} \tag{40}$$

is a solution of eq.(39). This solution implies that the phase of the condensate varies linearly with the spatiotemporal variable τ. In this subsection, we focalize our attention on this obvious case. Inserting eq.(40) into the remaining equation of eq.(38), the nonlinear differential equation governing the dynamics of the real amplitude of the condensate is given by

$$\frac{d^2R}{d\tau^2} + \gamma\upsilon\frac{dR}{d\tau} - \left[\frac{\upsilon^2}{4} + \frac{V_0}{2}\left(b_0(m) + b_1(m) + b_2(m) - b_0(m)\cos(2\tau) - b_1(m)\cos(4\tau) - b_2(m)\cos(6\tau)\right)\right] R$$
$$-g_0R^3 - g_1R^5 = 0. \tag{41}$$

It is to note that $R(\tau)$ being the real amplitude of the wave function of the condensate, will be null for the spatiotemporal variable τ approaching $-\infty$ and $+\infty$. As initial conditions for $\tau = 0$, we consider the condensate at a stable fixed point.

Next, to approach the realistic case, we assume that the dissipation parameter γ and the optical lattice depth V_0 are of small amplitudes. Thus, we introduce the following scale transformations: $\gamma \to \epsilon\gamma$, $V_0 \to \epsilon V_0$. Hence, the differential equation eq.(41) can be rewritten as a first order parametrically driven system in the form

$$\begin{cases} \dot{R} = X \\ \dot{X} = \dfrac{v^2}{4}R + g_0R^3 + g_1R^5 + \epsilon[-\gamma v X + \dfrac{V_0}{2}(b_0 + b_1 + b_2 - b_0\cos(2\tau) - b_1\cos(4\tau) - b_2\cos(6\tau))R]. \end{cases} \tag{42}$$

ϵ is a small parameter($\epsilon \ll 1$) which characterizes the smallness of the dissipation and the depth of the optical lattice.

The unperturbed system obtained when $\epsilon = 0$ is a Hamiltonian system, and can be expressed as

$$\begin{cases} \dot{R} = X \\ \dot{X} = -\dfrac{dU}{dR} = \dfrac{v^2}{4}R + g_0R^3 + g_1R^5, \end{cases} \tag{43}$$

where U(R) represents the potential energy of the system. One can straightforwardly deduce from eq.(43) that

$$U(R) = -\frac{v^2}{8}R^2 - \frac{g_0}{4}R^4 - \frac{g_1}{6}R^6. \tag{44}$$

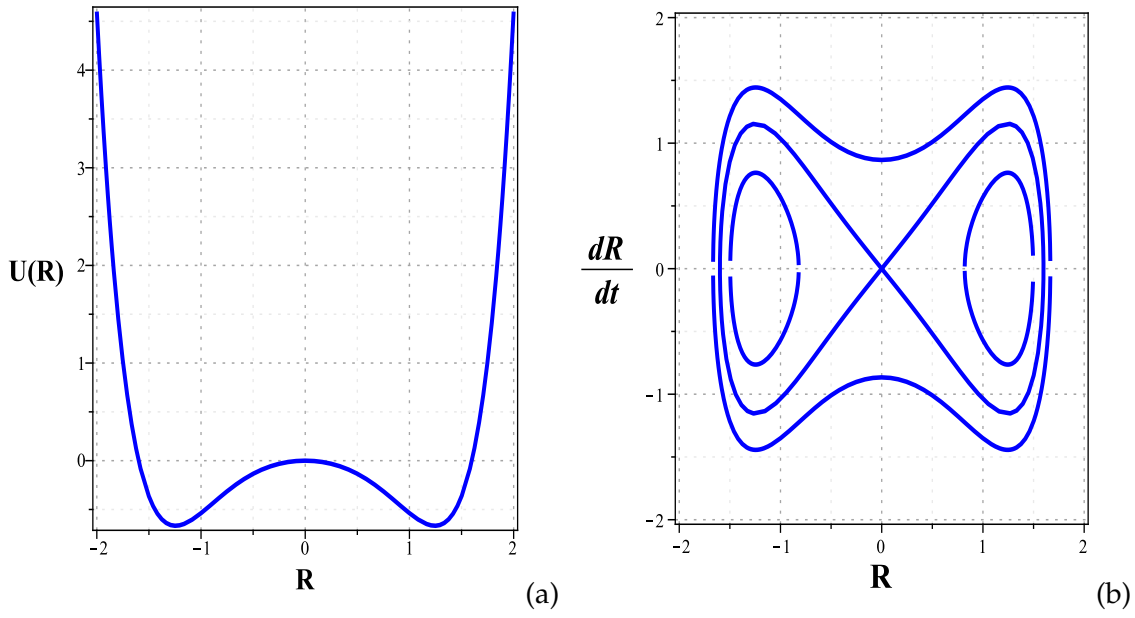

(a) (b)

Figure 4: (a) A configuration of the ϕ^6 potential with two wells (b) local bifurcation near the fixed points of the corresponding potential. The other parameters used are : $v = 2$, $g_0 = 0.75$, $g_1 = -0.9$

In general, depending on the set of parameters, three physically interesting situations can be considered where the potential is : (i) single-well, (ii) double-well or (iii) triple-well. The unperturbed system has a homoclinic or heteroclinic orbits or both of them, depending on the type of potential well. In this section, working with the hypotheses $g_0 > 0$ and $g_1 < 0$, one obtains a bounded double well potential, and the system eq.(43) exhibits only homoclinic orbits.

II.4.1.1. Fixed points of the unperturbed system and their stabilities

The fixed points of eq.(43) are solutions of $\dot{R} = 0$ and $\dot{X} = 0$. These equilibrium points are solution of the algebraic equation

$$\frac{\upsilon^2}{4}R + g_0R^3 + g_1R^5 = 0. \tag{45}$$

This equation leads to R = 0 or $g_1R^4 + g_0R^2 + \frac{\upsilon^2}{4} = 0$. The discriminant of the above equation, $\Delta = g_0^2 - \upsilon^2 g_1$ is a positive number according to signs of g_0 and g_1 mentioned above. Hence, the unperturbed system has three fixed points given by $S_1(0,0)$, $S_2(-R_1,0)$ and $S_3(+R_1,0)$, with

$$R_1 = \sqrt{-\frac{g_0}{2g_1}\left(1 + \sqrt{1 - \frac{g_1\upsilon^2}{g_0^2}}\right)}. \tag{46}$$

Now, let's study the stability of each fixed point. The Jacobian matrix of the unperturbed system is given by

$$J = \begin{bmatrix} 0 & 1 \\ \frac{\upsilon^2}{4} + 3\,g_0R^2 + 5\,g_1R^4 & 0 \end{bmatrix}. \tag{47}$$

For the fixed point $S_1(0,0)$, the eigenvalues of the corresponding Jacobian matrix are two real numbers, one positive and the other negative, given by $\lambda_1 = -\frac{\upsilon}{2}$ and $\lambda_2 = +\frac{\upsilon}{2}$. This unstable hyperbolic fixed point is a saddle point.
The fixed points $S_2(-R_1,0)$ and $S_3(+R_1,0)$ are associated with the same eigenvalues. The corresponding Jacobian matrix has as eigenvalues two imaginary complex conjugate numbers $\lambda_1 = -i\sqrt{-\frac{{g_0}^2}{g_1}\sqrt{1 - \frac{g_1\upsilon^2}{{g_0}^2}}\left(1 + \sqrt{1 - \frac{g_1\upsilon^2}{{g_0}^2}}\right)}$ and $\lambda_2 = +i\sqrt{-\frac{{g_0}^2}{g_1}\sqrt{1 - \frac{g_1\upsilon^2}{{g_0}^2}}\left(1 + \sqrt{1 - \frac{g_1\upsilon^2}{{g_0}^2}}\right)}$.
It is clear that these two stable nonhyperbolic fixed points are centers.

II.4.1.2. Derivation of state vectors generating the two homoclinic separatrices

As function of Hamiltonian H, the unperturbed system eq.(43) can be rewritten as

$$\begin{cases} \dfrac{\partial H}{\partial X} = X \\ \dfrac{\partial H}{\partial R} = -\left(\dfrac{\upsilon^2}{4}R + g_0R^3 + g_1R^5\right) \end{cases} \tag{48}$$

The integration of the first equation of eq.(48) yields $H(R,X) = \dfrac{X^2}{2} + C(R)$. Inserting this expression of the Hamiltonian H into the second equation of eq.(48) leads to $\dfrac{dC}{dR} = -\left(\dfrac{\upsilon^2}{4}R + g_0R^3 + g_1R^5\right)$. That is to say $C(R) = -\dfrac{\upsilon^2}{8}R^2 - \dfrac{g_0}{4}R^4 - \dfrac{g_1}{6}R^6 + H_0$
Finally the Hamiltonian of the unperturbed system eq.(43) is given by

$$H(R,X) = \frac{X^2}{2} - \frac{\upsilon^2}{8}R^2 - \frac{g_0}{4}R^4 - \frac{g_1}{6}R^6 + H_0. \tag{49}$$

Where H_0 is a real constant. On a separatrix, the Hamiltonian of the unperturbed system is constant. That implies $\dfrac{X^2}{2} - \dfrac{\upsilon^2}{8}R^2 - \dfrac{g_0}{4}R^4 - \dfrac{g_1}{6}R^6 + H_0$ = cste.
From this expression, one derives the integral curves given by

$$X^2 = \frac{\upsilon^2}{4}R^2 + \frac{g_0}{2}R^4 + \frac{g_1}{3}R^6 + C_0, \tag{50}$$

where C_0 is a real constant. The saddle point $S_1(0,0)$ belonging to both homoclinic separatrices, the integral curve characterizing these homoclinic separatrices is then given by the following equation

$$X_0^2 = \frac{\upsilon^2}{4}R_0^2 + \frac{g_0}{2}R_0^4 + \frac{g_1}{3}R_0^6. \tag{51}$$

From eq.(51), one obtains $\dfrac{dR_0}{d\tau} = \pm|R_0|\sqrt{\dfrac{\upsilon^2}{4} + \dfrac{g_0}{2}R_0^2 + \dfrac{g_1}{3}R_0^4}$. This integrable nonlinear differential equation can be carried out as $\displaystyle\int \frac{dR_0}{R_0\sqrt{\dfrac{\upsilon^2}{4} + \dfrac{g_0}{2}R_0^2 + \dfrac{g_1}{3}R_0^4}} = \pm\tau$.
Let's continue the integration by the change of variable $R_0^2 = u$. That is to say $2R_0dR_0 = du$. Inserting this new variable into the above integral, one obtains

$$\int \frac{du}{u\sqrt{\dfrac{\upsilon^2}{4} + \dfrac{g_0}{2}u + \dfrac{g_1}{3}u^2}} = \pm 2\tau \tag{52}$$

The integration of the left-hand side of eq.(52) can be made through the formula

$$\int \frac{dx}{x\sqrt{a+bx+cx^2}} = \frac{1}{\sqrt{a}}arc\cosh\left(\frac{2a+bx}{x\sqrt{-\Delta}}\right), with\left[a>0, \Delta<0, \Delta = 4ac-b^2\right],$$

published in page **97** of reference [145].

The outcome of this formula applied to eq.(52) is $\dfrac{1}{\sqrt{\dfrac{\upsilon^2}{4}}}arc\cosh\left(\dfrac{\dfrac{\upsilon^2}{2} + \dfrac{g_0}{2}u}{u\sqrt{\dfrac{3g_0^2 - 4\upsilon^2 g_1}{12}}}\right) = \pm 2\tau$,

which can be rewritten as $arc\cosh\left(\dfrac{\upsilon^2 + g_0u}{g_0u\sqrt{1 - \dfrac{4\upsilon^2 g_1}{3g_0^2}}}\right) = \pm\upsilon\tau$.

Let's solve this equation with $u(\tau)$ as unknown variable. Thus, we obtain $1+\frac{\upsilon^2}{g_0 u} = \sqrt{1-\frac{4\upsilon^2 g_1}{3g_0^2}}\cosh(\upsilon\tau)$.

Finally, the unknown variable u is given by $u(\tau) = \dfrac{\upsilon^2}{g_0\left(-1+\sqrt{1-\frac{4\upsilon^2 g_1}{3g_0^2}}\cosh(\upsilon\tau)\right)}$.

Remembering that $R_0^2 = u$, one obtains finally

$$R_0 = \pm\frac{\upsilon}{\sqrt{g_0\left(-1+\sqrt{1-\frac{4g_1\upsilon^2}{3g_0^2}}\cosh(\upsilon\tau)\right)}}.$$

The second component of the state vector defined as $X_0 = \dfrac{dR_0}{d\tau}$ is given by

$$X_0 = \pm\frac{\upsilon^2 g_0\sqrt{1-\frac{4\upsilon^2 g_1}{3g_0^2}}\sinh(\upsilon\tau)}{2\left(\sqrt{g_0\left(-1+\sqrt{1-\frac{4g_1\upsilon^2}{3g_0^2}}\cosh(\upsilon\tau)\right)}\right)^3}.$$

Hence, the expressions of the state vectors generating the two homoclinic separatrices are given by the following system

$$\begin{cases} R_0^{\pm}(\tau) = \pm\dfrac{\upsilon}{\sqrt{g_0\Big(-1+\sigma\cosh(\upsilon\tau)\Big)}} \\ X_0^{\pm}(\tau) = \pm\dfrac{\upsilon^2\sigma\sinh(\upsilon\tau)}{2\sqrt{g_0}\Big(-1+\sigma\cosh(\upsilon\tau)\Big)^{3/2}}, \end{cases} \tag{53}$$

with $\sigma = \sqrt{1-\frac{4g_1\upsilon^2}{3g_0^2}}$. g_1 being a negative number implies that $\sigma > 1$. The plus (minus) sign corresponds to the right (left) homoclinic orbit of this unperturbed system. It is important to note that R_0^+ corresponds to X_0^-, and R_0^- corresponds to X_0^+.

The maximum value R_{0max}^2 of the particle number density of the condensate deduced from the unperturbed system eq.(43) is obtained for τ = 0. R_{0max}^2 is then given by the expression

$$R_{0max}^2 = \frac{\upsilon^2}{g_0(-1+\sigma)}. \tag{54}$$

The width of the condensate at the mid-height $\Delta\tau$ for the unperturbed system is obtained by solving the equation $R_0^2(\tau) = \dfrac{R_{0max}^2}{2}$. This value of $\Delta\tau$ characterizing the spatiotemporal extension of the condensate is given by the expression

$$\Delta\tau = \frac{2}{\upsilon} arc\cosh(2-\frac{1}{\sigma}). \tag{55}$$

It comes from eq.(55) that, by regulating increasingly the scattering length a_s while the parameter g_1 related to three-body elastic collisions is kept constant, tends to increase the density, and decrease the spatiotemporal extension of the condensate. The same behaviour is observed when the parameter g_1 related to three-body elastic collisions is increasingly varied while the scattering length a_s is kept constant. These homoclinic separatrices obtained with eq.(53) is in perfect

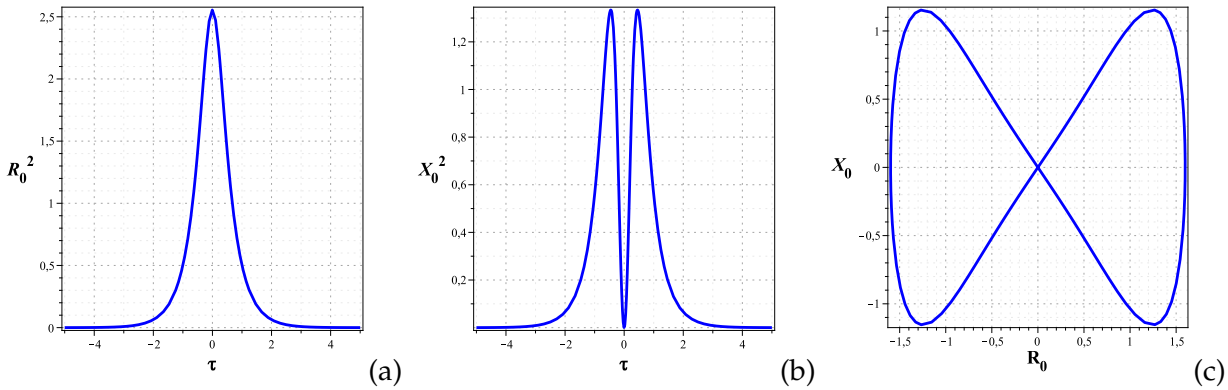

Figure 5: (a) Spatiotemporal evolution of the particle number density of condensate (bright solitons). (b) Spatiotemporal evolution of the first excited state of condensate (black solitons) (c) The homoclinic separatrices deduced from eq(53). The other parameters used are: $\upsilon = 2$, $g_0 = 0.75$, $g_1 = -0.9$

accord with the one obtained directly via a numerical integration, and displayed in Fig.4(b). In addition, one recognizes for this undamped condensate without trapping potential, solitonic solutions as bright solitons for $R_0(\tau)$ and black solitons for $X_0(\tau)$. These solitary waves can be interpreted as a balance between the both parts of the nonlinearity.

II.4.1.3. The Melnikov approach

Now, we consider the perturbed system eq.(42) which can be rewritten in term of state vector as

$$\frac{d}{d\tau}\begin{bmatrix} R \\ X \end{bmatrix} = \begin{bmatrix} X \\ \frac{\upsilon^2}{4}R + g_0R^3 + g_1R^5 \end{bmatrix} + \epsilon\begin{bmatrix} 0 \\ \left(\frac{V_0}{2}\Big(b_0 + b_1 + b_2 - b_0\cos(2\tau) - b_1\cos(4\tau) - b_2\cos(6\tau)\Big)R - \gamma\upsilon X\right) \end{bmatrix} \tag{56}$$

In the vector form, this equation can be merely rewritten as

$$\dot{S} = F\left(S\left(\tau\right)\right) + \epsilon G\left(S\left(\tau\right), \tau + \tau_0\right), \tag{57}$$

where $S = \begin{bmatrix} R \\ X \end{bmatrix}$ is a state vector. $F = \begin{bmatrix} X \\ \frac{\upsilon^2}{4}R + g_0R^3 + g_1R^5 \end{bmatrix}$ and $G\left(S\left(\tau\right), \tau + \tau_0\right) = \begin{bmatrix} 0 \\ G(\tau) \end{bmatrix}$ are two vector fields useful for the determination of the Melnikov function, with $G(\tau) = \left[\frac{V_0}{2}\Big(b_0 + b_1 + b_2 - b_0\cos\left(2\tau + 2\tau_0\right) - b_1\cos\left(4\tau + 4\tau_0\right) - b_2\cos\left(6\tau + 6\tau_0\right)\Big)R - \gamma\upsilon X\right]$.
According to eq.(16), the Melnikov function of this unperturbed system is given by

$$\overrightarrow{M}\left(\tau_0\right) = \int_{-\infty}^{+\infty} F\left[S_0\left(\tau\right)\right] \wedge G\left[S_0\left(\tau\right), \tau + \tau_0\right] d\tau, \tag{58}$$

where $S_0(\tau) = \begin{bmatrix} R_0(\tau) \\ X_0(\tau) \end{bmatrix}$ is a state vector taken on a homoclinic separatrix. Finally, the algebraic expression of the Melnikov function of the system eq.(42) is given by

$$M\left(\tau_0\right) = \int_{-\infty}^{+\infty} X_0\left(\tau\right) G_0\left(\tau\right) d\tau. \tag{59}$$

$G_0(\tau) = \left[\frac{V_0}{2}\Big(b_0 + b_1 + b_2 - b_0\cos\left(2\tau + 2\tau_0\right) - b_1\cos\left(4\tau + 4\tau_0\right) - b_2\cos\left(6\tau + 6\tau_0\right)\Big)R_0 - \gamma\upsilon X_0\right]$
Inserting this expression of $G_0(\tau)$ in eq.(59), one obtains

$$M\left(\tau_0\right) = \frac{V_0}{2}\left[b_0(m) + b_1(m) + b_2(m)\right] I_1 - \frac{V_0}{2} I_2 - \gamma\upsilon I_3, \tag{60}$$

with integrals I_1, I_2 and I_3 defined as follows

$$I_1 = \int_{-\infty}^{+\infty} R_0(\tau) X_0(\tau) d\tau, \tag{61}$$

$$I_2 = \int_{-\infty}^{+\infty} \left[b_0(m)\cos(2\tau + 2\tau_0) + b_1(m)\cos\left(4\tau + 4\tau_0\right) + b_2(m)\cos\left(6\tau + 6\tau_0\right)\right] R_0\left(\tau\right) X_0\left(\tau\right) d\tau, \tag{62}$$

$$I_3 = \int_{-\infty}^{+\infty} X_0^2\left(\tau\right) d\tau. \tag{63}$$

To evaluate these integrals, let's start by the calculation of $R_0(\tau)X_0(\tau)$ expressed below.

$$R_0(\tau)X_0(\tau) = -\frac{\upsilon^3\sigma\,\sinh\left(\upsilon\,\tau\right)}{2g_0\left(-1 + \sigma\,\cosh\left(\upsilon\,\tau\right)\right)^2}.$$

The sign (-) of the result is due to the fact that R_0^+ corresponds to X_0^- and R_0^- corresponds to X_0^+. This product being an odd function, one can therefore conclude that $I_1 = 0$.
To evaluate I_2, we expand the term preceding the product $R_0(\tau)X_0(\tau)$ and we retain only the

odd part of the expansion. Thus, this integral can be rewritten as

$$I_2 = \frac{b_0 \upsilon^3 \sigma \sin(2\tau_0)}{g_0} \int_0^{+\infty} \frac{\sinh(\upsilon\tau)\sin(2\tau)d\tau}{(-1+\sigma\cosh(\upsilon\tau))^2} + \frac{b_1 \upsilon^3 \sigma \sin(4\tau_0)}{g_0} \int_0^{+\infty} \frac{\sinh(\upsilon\tau)\sin(4\tau)d\tau}{(-1+\sigma\cosh(\upsilon\tau))^2} + \frac{b_2 \upsilon^3 \sigma \sin(6\tau_0)}{g_0} \int_0^{+\infty} \frac{\sinh(\upsilon\tau)\sin(6\tau)d\tau}{(-1+\sigma\cosh(\upsilon\tau))^2} \quad (64)$$

Each integral of eq.(64) can be simplified by the integration by part method. Thus, we have

$$\int_0^{+\infty} \frac{\sinh(\upsilon\tau)\sin(2\tau)d\tau}{(-1+\sigma\cosh(\upsilon\tau))^2} = \left[-\frac{\sin(2\,\tau)}{\sigma\,\upsilon\,(-1+\sigma\,\cosh(\upsilon\,\tau))}\right]_0^{+\infty} + 2\int_0^{+\infty} \frac{\cos(2\,\tau)\,d\tau}{\sigma\,\upsilon\,(-1+\sigma\,\cosh(\upsilon\,\tau))}$$
$$= \left(0 + 2\int_0^{+\infty} \frac{\cos(2\,\tau)\,d\tau}{\sigma\,\upsilon\,(-1+\sigma\,\cosh(\upsilon\,\tau))}\right) = \frac{2}{\upsilon\sigma}\int_0^{+\infty} \frac{\cos(2\,\tau)\,d\tau}{(-1+\sigma\,\cosh(\upsilon\,\tau))}$$

Continuing this reasoning on the other integrals, one obtains

$$\int_0^{+\infty} \frac{\sinh(\upsilon\tau)\sin(4\tau)d\tau}{(-1+\sigma\cosh(\upsilon\tau))^2} = \frac{4}{\upsilon\sigma}\int_0^{+\infty} \frac{\cos(4\,\tau)\,d\tau}{(-1+\sigma\,\cosh(\upsilon\,\tau))},$$

and

$$\int_0^{+\infty} \frac{\sinh(\upsilon\tau)\sin(6\tau)d\tau}{(-1+\sigma\cosh(\upsilon\tau))^2} = \frac{6}{\upsilon\sigma}\int_0^{+\infty} \frac{\cos(6\,\tau)\,d\tau}{(-1+\sigma\,\cosh(\upsilon\,\tau))}.$$

From the reference [145] in page **511**, the integrals of the right-hand side mentioned above can be evaluated through the formula

$$\int_0^{+\infty} \frac{\cos(ax)dx}{(c+b\cosh(\beta x))} = \frac{\pi \sinh\left(\frac{a}{\beta} arc\cos\left(\frac{c}{b}\right)\right)}{\beta\sqrt{b^2-c^2}\sinh\left(\frac{a\pi}{\beta}\right)}, [b > |c| > 0].$$

The necessary conditions being fulfilled, because $\sigma > 1 > 0$, one obtains finally

$$I_2 = \frac{2\pi\upsilon}{g_0\sqrt{\sigma^2-1}}\Big[\frac{b_0\sin(2\tau_0)\sinh\left(\frac{2}{\upsilon}arc\cos\left(-\frac{1}{\sigma}\right)\right)}{\sinh\left(\frac{2\pi}{\upsilon}\right)} + \frac{2b_1\sin(4\tau_0)\sinh\left(\frac{4}{\upsilon}arc\cos\left(-\frac{1}{\sigma}\right)\right)}{\sinh\left(\frac{4\pi}{\upsilon}\right)} + \frac{3b_2\sin(6\tau_0)\sinh\left(\frac{6}{\upsilon}arc\cos\left(-\frac{1}{\sigma}\right)\right)}{\sinh\left(\frac{6\pi}{\upsilon}\right)}\Big]. \quad (65)$$

Let's evaluate I_3.

$$I_3 = \frac{\upsilon^4\sigma^2}{4g_0}\int_{-\infty}^{+\infty} \frac{\sinh^2(\upsilon\tau)d\tau}{(-1+\sigma\cosh(\upsilon\tau))^3} = \frac{\upsilon^4\sigma^2}{2g_0}\int_0^{+\infty} \frac{\sinh^2(\upsilon\tau)d\tau}{(-1+\sigma\cosh(\upsilon\tau))^3}$$

With the integration by part method, one obtains

$$I_3 = \frac{\upsilon^4\sigma^2}{2g_0}\left(\left[-\frac{\sinh(\upsilon\,\tau)}{2\sigma\,\upsilon\,\left(-1+\sigma\,\cosh(\upsilon\,\tau)\right)^2}\right]_0^{+\infty} + \frac{1}{2\sigma}\int_0^{+\infty}\frac{\cosh(\upsilon\,\tau)\,d\tau}{\left(-1+\sigma\,\cosh(\upsilon\,\tau)\right)^2}\right)$$

$$= \frac{\upsilon^4\sigma^2}{2g_0}\left(0+\frac{1}{2\sigma}\int_0^{+\infty}\frac{\cosh(\upsilon\,\tau)\,d\tau}{\left(-1+\sigma\,\cosh(\upsilon\,\tau)\right)^2}\right) = \frac{\upsilon^4\sigma}{4g_0}\int_0^{+\infty}\frac{\cosh(\upsilon\,\tau)\,d\tau}{\left(-1+\sigma\,\cosh(\upsilon\,\tau)\right)^2}$$

The last integral necessary for the calculation of I_3 can be obtained directly from Maple software. Thus, after some algebraic manipulations of the result given by Maple software, one obtains:

$$I_3 = \frac{\upsilon^4\sigma}{4g_0}\left(\left[\frac{2\sigma}{\upsilon\left(\sigma^2-1\right)^{\frac{3}{2}}}\arctan\left(\sqrt{\frac{\sigma+1}{\sigma-1}}\tanh\left(\frac{\upsilon\tau}{2}\right)\right)\right]_0^{+\infty} + \left[\frac{\sinh(\upsilon\tau)}{\upsilon\left(\sigma^2-1\right)\left(-1+\sigma\cosh(\upsilon\tau)\right)}\right]_0^{+\infty}\right)$$

$$= \frac{\upsilon^4\sigma}{4g_0}\left(\frac{2\sigma}{\upsilon\left(\sigma^2-1\right)^{\frac{3}{2}}}\arctan\left(\sqrt{\frac{\sigma+1}{\sigma-1}}\right) + \frac{1}{\upsilon\sigma\left(\sigma^2-1\right)}\right),$$

and finally

$$I_3 = \frac{\upsilon^3}{4g_0\left(\sigma^2-1\right)}\left(1+\frac{2\sigma^2}{\sqrt{\sigma^2-1}}\arctan\left(\sqrt{\frac{\sigma+1}{\sigma-1}}\right)\right) \tag{66}$$

Inserting eq.(65) and eq.(66) into eq.(60) leads to the following Melnikov's function

$$M^{\pm}(\tau_0) = -\frac{\gamma\upsilon^4}{4g_0\left(\sigma^2-1\right)}\left(1+\frac{2\sigma^2}{\sqrt{\sigma^2-1}}\arctan\left(\sqrt{\frac{\sigma+1}{\sigma-1}}\right)\right) - \frac{\pi\upsilon V_0}{g_0\sqrt{\sigma^2-1}}\times \tag{67}$$

$$\left[\frac{b_0\sinh\left(\frac{2}{\upsilon}arc\cos\left(\frac{-1}{\sigma}\right)\right)\sin(2\tau_0)}{\sinh\left(\frac{2\pi}{\upsilon}\right)} + \frac{2b_1\sinh\left(\frac{4}{\upsilon}arc\cos\left(\frac{-1}{\sigma}\right)\right)\sin(4\tau_0)}{\sinh\left(\frac{4\pi}{\upsilon}\right)} + \frac{3b_2\sinh\left(\frac{6}{\upsilon}arc\cos\left(\frac{-1}{\sigma}\right)\right)\sin(6\tau_0)}{\sinh\left(\frac{6\pi}{\upsilon}\right)}\right].$$

The Smale-Birkhoff theorem for the determination of the onset of homoclinic chaos states that the required condition for the occurrence of chaos is that the Melnikov function should have simple zero. To find analytically the condition for Melnikov's function to have simples zero is generally very cumbersome, so that some approximations are usually necessary to accomplish the task. At these approximations which create a gap between the exact solution and the approximative one, we should not also forget that the **MM** itself is an approximative method. Therefore, one should not expect a perfect concordance between the results deriving from the **MM** and those provided by numerical simulations.

The comparison of Fourier coefficients $b_j(m)$, j=0,1,2 shows through Fig.(6) that, one can neglect b_1 and $b_2(m)$ in front of b_0(m). Hence, the approximate Melnikov function admits simple zero if $M(\tau_0)$=0 and $\frac{dM(\tau_0)}{d\tau_0} \neq 0$ at $\tau = \tau_0$. That is to say

$$\sin(2\tau_0) = -\frac{\gamma\upsilon^3\sinh\left(\frac{2\pi}{\upsilon}\right)}{4\pi V_0\sqrt{\sigma^2-1}b_0(m)\sinh\left(\frac{2}{\upsilon}arc\cos\left(-\frac{1}{\sigma}\right)\right)}\left(1+\frac{2\sigma^2}{\sqrt{\sigma^2-1}}\arctan\left(\sqrt{\frac{\sigma+1}{\sigma-1}}\right)\right)$$

Thus, the occurrence condition of the homoclinic chaos is obtained by solving $|\sin(2\tau_0)| \leq 1$. That leads to

$$\ell(V_0, m, \upsilon, g_1, \gamma) = \frac{V_0}{\gamma} - \frac{\upsilon^3 \sinh\left(\frac{2\pi}{\upsilon}\right)\left(1 + \frac{2\sigma^2}{\sqrt{\sigma^2-1}}\arctan\left(\sqrt{\frac{\sigma+1}{\sigma-1}}\right)\right)}{4\pi\sqrt{\sigma^2-1}b_0(m)\sinh\left(\frac{2}{\upsilon}arc\cos\left(-\frac{1}{\sigma}\right)\right)} \geq 0. \tag{68}$$

This inequality shows how the parameters must be linked to produce a chaotic behaviour of the condensate, and will be very helpful in the next to verify the reliability of the theoretical investigations, compared to numerical simulations.

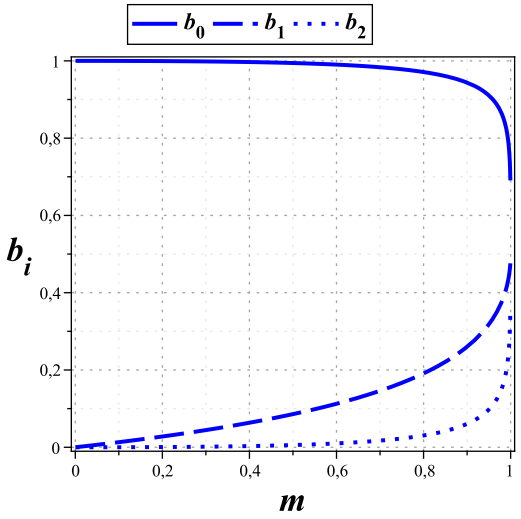

Figure 6: Plot of Fourier coefficients b_i, (i=0,1,2) versus the shape parameter m

II.4.2 Case of an undamped condensate subjected to inelastic collisions

In this subsection, we take into account the irreversible effects in the dynamical behaviour of the condensate, always in the case of repulsive two-body and attractive three-body elastic atom-atom collisions. We neglect the damping parameter $\gamma(\gamma = 0)$ not only for a possible analytical treatment, but especially because the two-and three-body inelastic atom-atom collisions are viewed as dissipation phenomena. Thus, according to eq.(37) of the previous section, the dynamics of such a condensate is governed by the following system

$$\begin{cases} \dfrac{d^2R}{d\tau^2} - \left[\alpha^2 + \beta + \dfrac{V_0}{2}\left(b_0(m) + b_1(m) + b_2(m) - b_0(m)\cos(2\tau) - b_1(m)\cos(4\tau) - b_2(m)\cos(6\tau)\right)\right]R \\ -R\left(\dfrac{d\theta}{d\tau}\right)^2 - (\upsilon + 2\alpha)R\dfrac{d\theta}{d\tau} - g_0R^3 - g_1R^5 = 0 \\ R\dfrac{d^2\theta}{d\tau^2} + 2\dfrac{dR}{d\tau}\dfrac{d\theta}{d\tau} + (\upsilon + 2\alpha)\dfrac{dR}{d\tau} - \gamma_0R + \gamma_1R^3 + \gamma_2R^5 = 0. \end{cases} \tag{69}$$

II.4.2.1. Amplitude equation governing the dynamics of the condensate

Before applying the Melnikov method, it is necessary to separate the two variables of eq.(69). Hence, we multiply the second equation of this system by $R(\tau)$. As result, one obtains

$$\frac{d}{d\tau}\left[R^2\left(\frac{d\theta}{d\tau}+\left(\frac{\upsilon+2\alpha}{2}\right)\right)\right]=\gamma_0R^2-\gamma_1R^4-\gamma_2R^6.$$

The integration of this equation between $-\infty$ and τ with the assumption that the real amplitude of the condensate must be null when the spatiotemporal variable τ approaches infinity, permits to separate the two variables of eq.(69) as follows

$$\frac{d\theta}{d\tau}=\frac{1}{R^2}\int_{-\infty}^{\tau}\left(\gamma_0R^2(\tau)-\gamma_1R^4(\tau)-\gamma_2R^6(\tau)\right)d\tau-\left(\frac{\upsilon+2\alpha}{2}\right). \tag{70}$$

The boundary conditions on the wave function due to the fact that the wave amplitude must be null at $\tau=\pm\infty$ leads to

$$\int_{-\infty}^{+\infty}\left(\gamma_0R^2(\tau)-\gamma_1R^4(\tau)-\gamma_2R^6(\tau)\right)d\tau=0. \tag{71}$$

eq.(71) represents one constraint relation between parameters modeling inelastic processes. Inserting eq.(70) in the first equation of system eq.(69), we obtain the following nonlinear integro-differential equation governing the real amplitude of the traveling wave.

$$\begin{aligned}&\frac{d^2R}{d\tau^2}-\left[\frac{a^2}{4}+\frac{V_0}{2}\left(b_0(m)+b_1(m)+b_2(m)-b_0(m)\cos(2\tau)-b_1(m)\cos(4\tau)-b_2(m)\cos(6\tau)\right)\right]R\\&-g_0R^3-g_1R^5=\frac{1}{R^3(\tau)}\left[\int_{-\infty}^{\tau}\left(\gamma_0R^2(\tau)-\gamma_1R^4(\tau)-\gamma_2R^6(\tau)\right)d\tau\right]^2,\end{aligned} \tag{72}$$

with the expression of the constant a given by $a^2=4\beta-\upsilon^2-4\alpha\upsilon$.
As in the previous subsection, we assume the depth of optical lattice V_0, and parameters related to atomic feeding and inelastic atom-atom collisions γ_i, i=0,1,2 of small amplitudes. Furthermore, we admit γ_i more smaller than V_0. To bring closer the two terms of perturbation (V_0 and γ_i), we assume the following scale transformation. $V_0\rightarrow\epsilon V_0$, $\gamma_0\rightarrow\sqrt{\epsilon}\gamma_0$, $\gamma_1\rightarrow\sqrt{\epsilon}\gamma_1$ and $\gamma_2\rightarrow\sqrt{\epsilon}\gamma_2$. It is obvious that when $\epsilon\ll1$, $\sqrt{\epsilon}$ is bigger than ϵ. Thus, to multiply the small values of parameters modeling the atomic feeding and inelastic collisions with $\sqrt{\epsilon}$ will bring closer the two terms of perturbation, avoiding the inelastic processes to be negligible. This integro-differential equation eq.(72) can be rewritten in the form of a first order system as

$$\begin{cases}\dot{R}=X\\[2ex]\dot{X}=\dfrac{a^2}{4}R+g_0R^3+g_1R^5+\epsilon\Big[\dfrac{V_0}{2}\left(b_0+b_1+b_2-b_0\cos(2\tau)-b_1\cos(4\tau)-b_2\cos(6\tau)\right)R\\[2ex]+\dfrac{1}{R^3(\tau)}\left(\displaystyle\int_{-\infty}^{\tau}\left(\gamma_0R^2(\tau)-\gamma_1R^4(\tau)-\gamma_2R^6(\tau)\right)d\tau\right)^2\Big].\end{cases} \tag{73}$$

II.4.2.2. Determination of state vectors generating the two homoclinic separatrices.

The unperturbed system deriving from eq.(73) has the same form as the one of the previous subsection, with the difference that the velocity of the optical lattice v is replaced by the parameter a aforementioned. We conclude that this unperturbed system has three fixed points. One unstable fixed point at $(0,0)$ which is a saddle point, and two stables fixed points at $(-R_1',0)$ and $(+R_1',0)$ which are centers, with

$$R_1' = \sqrt{-\frac{g_0}{2g_1}\left(1+\sqrt{1-\frac{g_1 a^2}{g_0^2}}\right)}.$$

The components of the state vector generating the homoclinic separatrices deduced from the previous section can be written as

$$\begin{cases} R_0^{\pm}(\tau) = \pm\dfrac{a}{\sqrt{g_0\Big(-1+\sigma'\cosh(a\tau)\Big)}} \\ \\ X_0^{\pm}(\tau) = \pm\dfrac{a^2\sigma'\sinh(a\tau)}{2\sqrt{g_0}\Big(-1+\sigma'\cosh(a\tau)\Big)^{3/2}} \end{cases} \tag{74}$$

with $\sigma' = \sqrt{1-\dfrac{4g_1a^2}{3g_0^2}}$.

II.4.2.2. The Melnikov approach

According to eq.(16), the Melnikov function deduced from the perturbed system eq.(73) is given by

$$\overrightarrow{M}(\tau_0) = \int_{-\infty}^{+\infty} f\left[S_0(\tau)\right] \wedge g\left[S_0(\tau), \tau+\tau_0\right] d\tau, \tag{75}$$

with $S_0 = \begin{bmatrix} R_0 \\ X_0 \end{bmatrix}$, $f = \begin{bmatrix} X \\ \dfrac{a^2}{4}R + g_0R^3 + g_1R^5 \end{bmatrix}$, $g\left(S(\tau), \tau+\tau_0\right) = \begin{bmatrix} 0 \\ g(\tau) \end{bmatrix}$, and

$g(\tau) = \dfrac{V_0}{2}\Big(b_0 + b_1 + b_2 - b_0\cos(2\tau+2\tau_0) - b_1\cos(4\tau+4\tau_0) - b_2\cos(6\tau+6\tau_0)\Big)R$

$+ \dfrac{1}{R^3(\tau)}\left(\displaystyle\int_{-\infty}^{\tau}\left(\gamma_0R^2(\tau) - \gamma_1R^4(\tau) - \gamma_2R^6(\tau)\right)d\tau\right)^2$.

Finally, the algebraic expression of the Melnikov function is given by

$$M(\tau_0) = \int_{-\infty}^{+\infty} X_0(\tau)\, g_0(\tau)\, d\tau, \tag{76}$$

with $g_0(\tau) = \dfrac{V_0}{2}\Big(b_0 + b_1 + b_2 - b_0\cos(2\tau+2\tau_0) - b_1\cos(4\tau+4\tau_0) - b_2\cos(6\tau+6\tau_0)\Big)R_0 +$

$\dfrac{1}{R_0^3(\tau)}\left(\displaystyle\int_{-\infty}^{\tau}\left(\gamma_0R_0^2(\tau) - \gamma_1R_0^4(\tau) - \gamma_2R_0^6(\tau)\right)d\tau\right)^2$

As in the previous subsection, this Melnikov's function can be rewritten in the form

$$M(\tau_0) = \frac{V_0}{2}\left[b_0(m) + b_1(m) + b_2(m)\right] I_1' - \frac{V_0}{2} I_2' + T, \tag{77}$$

with I_1', I_2' and T given by the following integrals

$$I_1' = \int_{-\infty}^{+\infty} R_0(\tau) X_0(\tau) d\tau, \tag{78}$$

$$I_2' = \int_{-\infty}^{+\infty} \left[b_0(m)\cos(2\tau + 2\tau_0) + b_1(m)\cos(4\tau + 4\tau_0) + b_2(m)\cos(6\tau + 6\tau_0)\right] R_0(\tau) X_0(\tau) d\tau, \tag{79}$$

$$T = \int_{-\infty}^{+\infty} \frac{X_0(\tau)}{R_0^3(\tau)} \left(\int_{-\infty}^{\tau} \left(\gamma_0 R_0^2(\tau) - \gamma_1 R_0^4(\tau) - \gamma_2 R_0^6(\tau)\right) d\tau \right)^2 d\tau. \tag{80}$$

According to the previous subsection, $I_1' = 0$ and I_2' is obtained by replacing in the expression of I_2 the speed of the optical lattice υ by a, and σ by σ'.

The plots of $R_0(\tau)$ and $X_0(\tau)$ versus the spatiotemporal variable τ reveal that these functions are null for τ belonging to the interval $]-\infty; -\tau_c[\cup]\tau_c; +\infty[$, where τ_c represents the value of τ corresponding to $R_0(\tau)$ and $X_0(\tau)$ very close to zero. It is to point out that this value of τ_c depends on other parameters. As an example, in Fig.(5), $R_0^2(\tau) = 0.0001$ leads to $\tau = 5.22$. Henceforth, we consider τ in the interval $[-\tau_c; +\tau_c]$. Hence T can be rewritten as

$$T = \int_{-\tau_c}^{+\tau_c} \frac{X_0(\tau)}{R_0^3(\tau)} \left(\int_{-\tau_c}^{\tau} \left(\gamma_0 R_0^2(\tau) - \gamma_1 R_0^4(\tau) - \gamma_2 R_0^6(\tau)\right) d\tau \right)^2 d\tau. \tag{81}$$

The Melnikov function necessary to predict the onset of chaos in the dynamics of the condensate is then given by

$$\begin{aligned} M^{\pm}(\tau_0) \;=\; & -\frac{\pi a V_0}{g_0\sqrt{\sigma'^2 - 1}} \Big[\frac{b_0 \sin(2\tau_0) \sinh\left(\frac{2}{a} arc\cos\left(-\frac{1}{\sigma'}\right)\right)}{\sinh\left(\frac{2\pi}{a}\right)} + \frac{2b_1 \sin(4\tau_0) \sinh\left(\frac{4}{a} arc\cos\left(-\frac{1}{\sigma'}\right)\right)}{\sinh\left(\frac{4\pi}{a}\right)} \\ & + \frac{3b_2 \sin(6\tau_0) \sinh\left(\frac{6}{a} arc\cos\left(-\frac{1}{\sigma'}\right)\right)}{\sinh\left(\frac{6\pi}{a}\right)} \Big] + T. \end{aligned} \tag{82}$$

The expression of T is very cumbersome to obtain. From multiple integrations via Maple software and integrals table and series [145], T is derived in section Appendix A.

As in the previous subsection, neglecting $b_1(m)$ and $b_2(m)$ in front of $b_0(m)$, the approximate condition for the occurrence of the homoclinic chaos deduced from eq.(82) is given by

$$\delta \geq \left| \frac{g_0\sqrt{\sigma'^2 - 1} T \sinh\left(\frac{2\pi}{a}\right)}{a\pi \sinh\left(\frac{2}{a} arc\cos\left(-\frac{1}{\sigma'}\right)\right)} \right|, \tag{83}$$

where $\delta = V_0 b_0(m)$ in fact represents the amplitude of our trapping potential, and $||$ denoting the absolute value. The advantage to gather together V_0 and $b_0(m)$ in δ is the possibility to change gradually the geometry of the trapping potential, by acting on the shape parameter m. That will be very helpful in experiments.

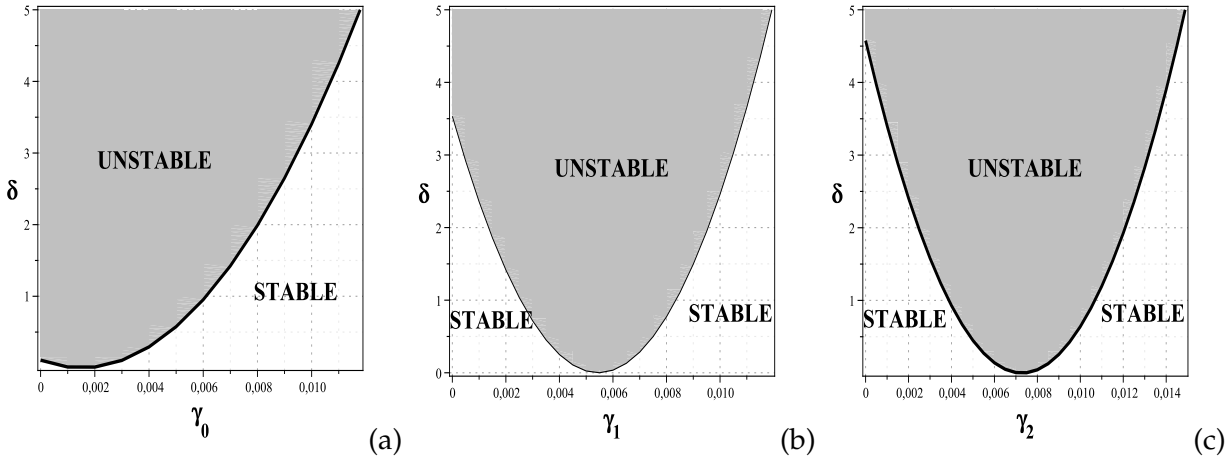

Figure 7: Unstable and stable zones in parameter space (γ_i, δ), (i=0,1,2), deduced from eq.(83). Modulated lattice potential depth δ versus (a) the feeding parameter γ_0 (b) the dipolar relaxation parameter γ_1 (c) the three-body recombination factor γ_2. The other parameters used are: $a = 2$, $g_0 = 0.75$, $g_1 = -0.9$, $\gamma_0 = 10^{-2}$, $\gamma_1 = 10^{-4}$, $\gamma_2 = 10^{-3}$, $\tau_c = 5$.

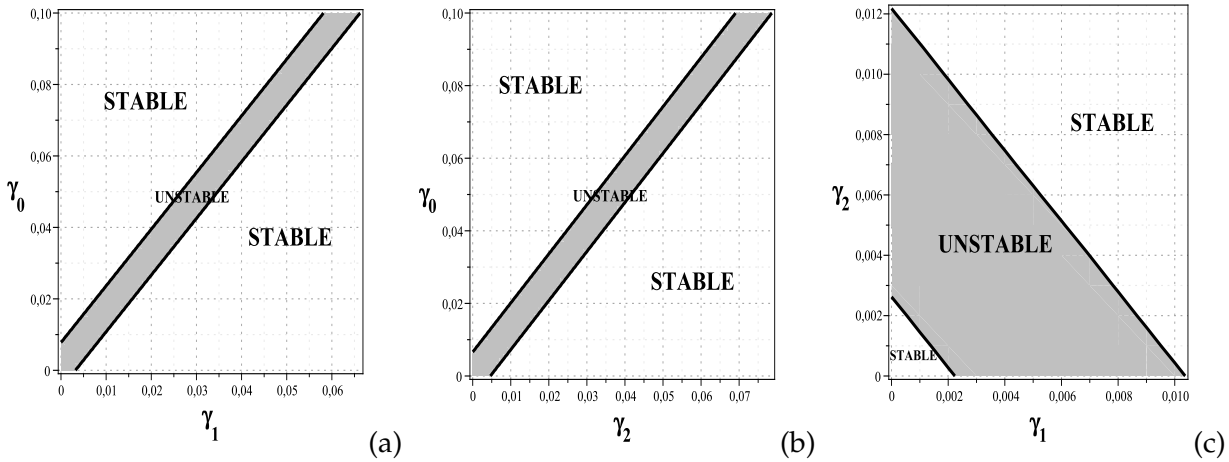

Figure 8: Unstable and stable zones in parameter space (γ_i, γ_j), (i,j=0,1,2), deduced from eq.(83). (a) The feeding parameter γ_0 versus the dipolar relaxation parameter γ_1 (b) The feeding parameter γ_0 versus the three-body recombination factor γ_2 (c) The three-body recombination factor γ_2 versus the dipolar relaxation parameter γ_1. The other parameters used are: $a = 2$, $g_0 = 0.75$, $g_1 = -0.9$, $\gamma_0 = 10^{-2}$, $\gamma_1 = 10^{-4}$, $\gamma_2 = 10^{-3}$, $V_0 = 2$, $m = 0.8$, $\tau_c = 5$.

II.5 Analytical study of a BEC with attractive two-body and repulsive three-body interactions loaded into a moving optical Fourier-synthesized lattice

In this section we consider a condensate with attractive two-body and repulsive three-body atom-atom elastic collisions. Thus, the parameter g_0 is a negative number while the parameter g_1 is a positive number. It is well known today through the Feshbach resonance techniques that, the s-wave scattering length can vary from positive to negative values, as shown in the Bose-Einstein condensation of ^{85}Rb [154, 155]. From the previous case, one can obtain the current case through this technique, or directly by considering a condensate with an attractive species.

II.5.1 Case of a damped condensate not subjected to inelastic collisions

In this subsection, the condensate initially on the ground state of the optical lattice, evolves according to the nonlinear system eq.(37). Under the condition eq.(40), the two equations of system eq.(37) can be summarized by the nonlinear differential equation eq.(41). As in the previous section, we assume the depth V_0 of the optical lattice and the parameters γ_i related to inelastic processes as of small amplitudes. Accordingly, the differential equation eq.(41) can be rewritten as a first order system as shown in eq.(42). Now, let us consider the unperturbed system given by eq.(43).

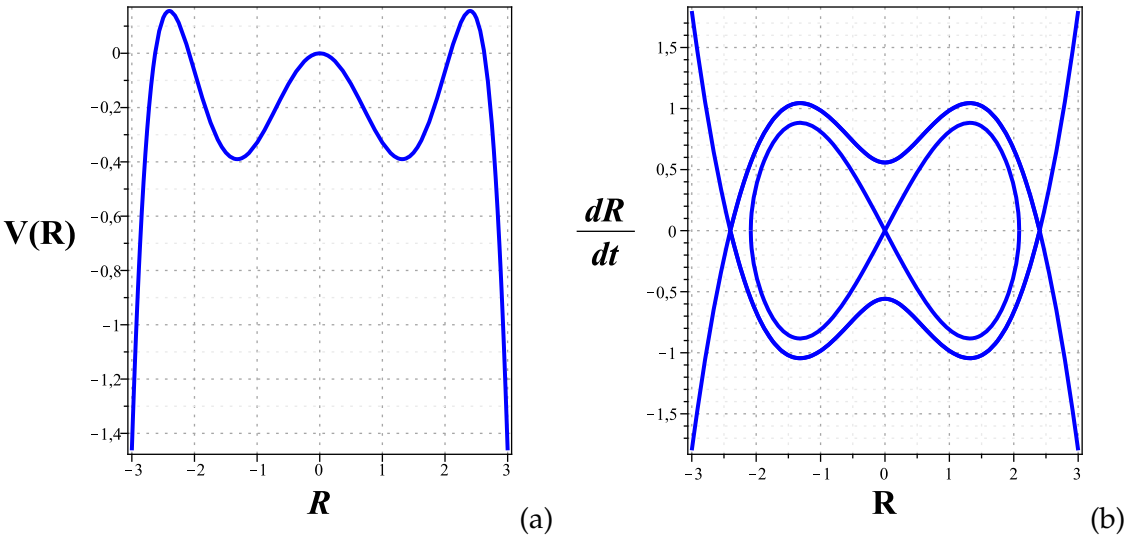

Figure 9: (a)A configuration of the unbounded ϕ^6 potential with two wells (b) local bifurcation near the fixed points of the corresponding potential. The other parameters used are: $\upsilon = 2$, $g_0 = -0.75$, $g_1 = 0.1$

II.5.1.1. Fixed points of the unperturbed system and their stabilities

Working on the hypotheses $g_0 < 0$ and $g_1 > 0$, the potential energy U(R) defined in eq.(44) is an unbounded ϕ^6 potential, and can be a (i) zero-well, (ii) single-well or (iii) double-well potential.

In the interesting case where the potential energy has two wells, explicitly under the condition

$$g_0^2 - g_1 \upsilon^2 > 0, \tag{84}$$

the integrable system eq.(43) has five equilibrium points.
In the previous section, we have studied the case of homoclinic orbits only. Now, we focalize our attention on the case of the coexistence of homoclinic and heteroclinic orbits, to determine how heteroclinic orbits act on the dynamical behaviour of the condensate. The unperturbed system aforementioned under the condition eq.(84) will exhibit simultaneously homoclinic and heteroclinic separatrices if the potential energy U(R) intersects the R-axis three or five times. This condition is fulfilled if the parameters related to two-and three-body elastic collisions are linked as

$$3g_0^2 - 4g_1 \upsilon^2 \geq 0. \tag{85}$$

It is obvious that if eq.(85) is satisfied, then eq.(84) will also be satisfied. Hence, these two conditions can be reduced to eq.(85).
Under the condition eq.(85), the unperturbed system possesses three unstable hyperbolic fixed points at $(0,0)$, $(-R_2,0)$ and $(+R_2,0)$ and two stable nonhyperbolic fixed points at $(-R_1,0)$ and $(+R_1,0)$. Proceeding as in the previous section, the three hyperbolic fixed points are saddle points whereas the two nonhyperbolic fixed points are centers. The five fixed points can also be seen on the potential energy displayed in Fig.9(a), as maxima and minima of this curve. R_1 and R_2 mentioned above, solution of $\frac{dU(R)}{dR} = 0$ are given by the following expressions

$$\begin{cases} R_1 = \sqrt{-\frac{g_0}{2g_1}\left(1 - \sqrt{1 - \frac{g_1\upsilon^2}{g_0^2}}\right)} \\ R_2 = \sqrt{-\frac{g_0}{2g_1}\left(1 + \sqrt{1 - \frac{g_1\upsilon^2}{g_0^2}}\right)}. \end{cases} \tag{86}$$

II.5.1.2. Determination of state vectors generating the two homoclinic separatrices

The unperturbed system as function of the Hamiltonian is given by eq.(48). The Hamiltonian of this system is expressed in eq.(49), and finally the equation of integral curves is presented in eq.(50). As clearly visible in the Fig.9(b), the unstable fixed point $S_1(0,0)$ belongs to homoclinic separatrices. Thus, as in the previous section, the integral curve generating the homoclinic separatrices is expressed in eq.(51). From this equation, one has

$$\frac{dR_0}{R_0\sqrt{R_0^4 + \frac{3g_0}{2g_1}R_0^2 + \frac{3\upsilon^2}{4g_1}}} = \pm\sqrt{\frac{g_1}{3}}d\tau.$$

With the change of variable $R_0^2 = u$, one obtains

$$\int \frac{du}{u\sqrt{u^2 + \dfrac{3g_0}{2g_1}u + \dfrac{3\upsilon^2}{4g_1}}} = \pm 2\sqrt{\frac{g_1}{3}}\tau. \tag{87}$$

As in the previous section, the integration of the left-hand side of eq.(87) gives

$$\frac{1}{\sqrt{\dfrac{3\upsilon^2}{4g_1}}} arc\cosh\left(\frac{\dfrac{3\upsilon^2}{2g_1} + \dfrac{3g_0 u}{2g_1}}{u\sqrt{\dfrac{9g_0^2 - 12g_1\upsilon^2}{4g_1^2}}}\right) = \pm 2\sqrt{\frac{g_1}{3}}\tau.$$

This equation can be rewritten as $arc\cosh\left(\dfrac{3g_0 + \dfrac{3\upsilon^2}{u}}{\sqrt{9g_0^2 - 12g_1\upsilon^2}}\right) = \pm\upsilon\tau.$

The unknown variable being $u(\tau)$, can then be determined from the above equation. One obtains

$$u(\tau) = \frac{3\upsilon^2}{-3g_0 + \sqrt{9g_0^2 - 12g_1\upsilon^2}\cosh(\upsilon\tau)}.$$

From $R_0^2 = u$, one obtains finally

$$R_0 = \pm\frac{\upsilon}{\sqrt{-g_0(1 + \sigma\cosh(\upsilon\tau))}}, \tag{88}$$

with $\sigma = \sqrt{1 - \dfrac{4g_1\upsilon^2}{3g_0^2}}$.

According to our work hypothesis defined in eq.(85), it is obvious to observe that $0 < \sigma < 1$. Thus, the components of the state vector generating the homoclinic separatrices are given as follows

$$\begin{cases} R_{hom}^{\pm}(\tau) = \pm\dfrac{\upsilon}{\sqrt{-g_0\Big(1 + \sigma\cosh(\upsilon\tau)\Big)}} \\ X_{hom}^{\pm}(\tau) = \pm\dfrac{\upsilon^2\sigma\sinh(\upsilon\tau)}{2\sqrt{-g_0}\Big(1 + \sigma\cosh(\upsilon\tau)\Big)^{3/2}}. \end{cases} \tag{89}$$

X_{hom}^{+} corresponds to R_{hom}^{-} and X_{hom}^{-} corresponds to R_{hom}^{+}, hom denoting an abbreviation of homoclinic. The separatrices obtained through theoretical investigations and displayed in Fig.10(c) is exactly the one obtained directly via a numerical integration and shown in Fig.9(c).

It comes from Fig.10 that this undamped condensate without trapping potential exhibits solitonic solutions as bright soliton for $R_{hom}^2(\tau)$ and black soliton for $X_{hom}^2(\tau)$. Once again, these solitary waves can be interpreted as a balance between the both parts of the nonlinearity. Now, let's find out how the two-and three-body elastic atom-atom collisions impact on the width at mid-height $\Delta\tau$ of the condensate, for the unperturbed system. The maximum value of $R_{hom}^2(\tau)$

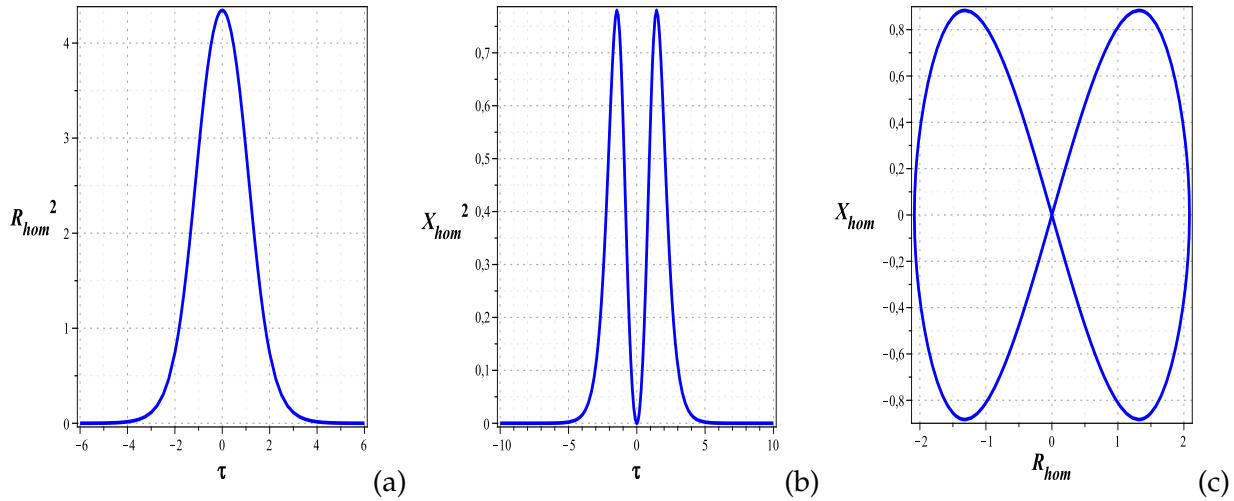

Figure 10: (a) Spatiotemporal evolution of the particle number density of condensate (bright soliton). (b) Spatiotemporal evolution of the first excited state of condensate (black soliton or kink). (c) The homoclinic separatrices deduced from eq.(89). The other parameters used are: $\upsilon = 2$, $g_0 = -0.75$, $g_1 = 0.1$

is obtained for $\tau = 0$. That leads to $R_{max}^2 = \dfrac{\upsilon^2}{-g_0(1+\sigma)}$. Solving $R_{hom}^2(\tau) = \dfrac{R_{max}^2}{2}$, one obtains $\tau = \pm\dfrac{1}{\upsilon} arc\cosh\left(2+\dfrac{1}{\sigma}\right)$. Thus, the spatiotemporal extension of the condensate is the gap between these two values of τ, as specified below

$$\Delta\tau = \frac{2}{\upsilon} arc\cosh(2+\frac{1}{\sigma}). \tag{90}$$

This equation reveals that when the scattering length is increasingly varied while the parameter of the three-body elastic atom-atom collisions is kept constant, the density and the spatiotemporal extension of the condensate increase.
The same behaviour is observed when the parameter related to three-body elastic atom-atom collisions is increasingly varied while the scattering length is kept constant.

II.5.1.3. Determination of the state vector generating the heteroclinic separatrix

The starting point is the equation of integral curves given by eq.(50). These heteroclinic separatrix in phase space (R, X) intersect the R-axis at $\pm R_2$. To determine the value of the constant C_0 appearing in the integral curves, it is obvious to observe that $(-R_2, 0)$ and $(+R_2, 0)$ belong to the heteroclinic separatrix. That leads to

$$C_0 = -\frac{\upsilon^2}{4}R_2^2 - \frac{g_0}{2}R_2^4 - \frac{g_1}{3}R_2^6.$$

Inserting this expression of the constant C_0 in eq.(50) leads to the integral curve characterizing the heteroclinic separatrix, given by

$$X_0^2 = \frac{\upsilon^2}{4}\left(R_0^2 - R_2^2\right) + \frac{g_0}{2}\left(R_0^4 - R_2^4\right) + \frac{g_1}{3}\left(R_0^6 - R_2^6\right). \tag{91}$$

Let's integrate it.

$$\begin{aligned} X_0^2 &= \frac{\upsilon^2}{4}\left(R_0^2 - R_2^2\right) + \frac{g_0}{2}\left(R_0^2 - R_2^2\right)\left(R_0^2 - R_2^2 + 2R_2^2\right) + \frac{g_1}{3}\left[\left(R_0^2 - R_2^2\right)^3 + 3R_0^2R_2^2\left(R_0^2 - R_2^2\right)\right] \\ &= \left(R_0^2 - R_2^2\right)\left[\frac{\upsilon^2}{4} + \frac{g_0}{2}\left(R_0^2 - R_2^2 + 2R_2^2\right) + \frac{g_1}{3}\left(\left(R_0^2 - R_2^2\right)^2 + 3(R_0^2 - R_2^2 + R_2^2)R_2^2\right)\right] \quad (92) \\ &= \left(R_0^2 - R_2^2\right)\left[\frac{\upsilon^2}{4} + g_0R_2^2 + g_1R_2^4 + \frac{g_0}{2}\left(R_0^2 - R_2^2\right) + \frac{g_1}{3}\left(\left(R_0^2 - R_2^2\right)^2 + 3\left(R_0^2 - R_2^2\right)R_2^2\right)\right] \end{aligned}$$

$(+R_2, 0)$ being a fixed point of the unperturbed system, $\frac{\upsilon^2}{4} + g_0R_2^2 + g_1R_2^4 = 0$. Hence, the differential equation modeling the heteroclinic separatrix becomes

$$X_0 = \pm\left(R_0^2 - R_2^2\right)\sqrt{\frac{g_0}{2} + g_1R_2^2 + \frac{g_1}{3}\left(R_0^2 - R_2^2\right)}. \tag{93}$$

The heteroclinic separatrix belonging to the interval $[-R_2, +R_2]$, we change the variable as follows: $u = R_2^2 - R_0^2$. It is clear that u is a positive number, and $du = -2R_0dR_0$. Replacing X_0 by $\frac{dR_0}{d\tau}$ in eq.(93), we obtain

$$\frac{dR_0}{d\tau} = \pm u\sqrt{\frac{g_0}{2} + g_1R_2^2 - \frac{g_1}{3}u}.$$

Next, we insert the new expression of $R_0(\tau)$ in the equation above and obtain

$$\frac{\frac{du}{d\tau}}{2\sqrt{R_2^2 - u}} = \pm u\sqrt{\frac{g_0}{2} + g_1R_2^2 - \frac{g_1}{3}u}.$$

Subsequently, we expand the contents of the two square root, and the outcome of that is given by

$$\frac{du}{u\sqrt{u^2 - \left(4R_2^2 + \frac{3g_0}{2g_1}\right)u + \left(\frac{3g_0}{2g_1} + 3R_2^2\right)R_2^2}} = \pm 2\sqrt{\frac{g_1}{3}}d\tau.$$

Let's integrate the both sides of the above equation. We obtain

$$\int \frac{du}{u\sqrt{u^2 - \left(4R_2^2 + \frac{3g_0}{2g_1}\right)u + \left(\frac{3g_0}{2g_1} + 3R_2^2\right)R_2^2}} = \pm 2\sqrt{\frac{g_1}{3}}\tau. \tag{94}$$

This indefinite integral was already encountered in the previous section, and the required conditions for the use of the aforementioned formula are satisfied.

$$\Delta = 4\left(\frac{3g_0R_2^2}{2g_1} + 3R_2^4\right) - \left(4R_2^2 + \frac{3g_0}{2g_1}\right)^2 = -\left(2R_2^2 + \frac{3g_0}{2g_1}\right)^2 < 0,$$

and it is easy to prove that $\left(\frac{3g_0}{2g_1}+3R_2^2\right)R_2^2>0$. Hence, eq.(94) can be rewritten as

$$\frac{1}{\sqrt{R_2^2\left(3R_2^2+\frac{3g_0}{2g_1}\right)}}arc\cosh\left(\frac{2R_2^2\left(3R_2^2+\frac{3g_0}{2g_1}\right)-\left(4R_2^2+\frac{3g_0}{2g_1}\right)u}{\left(2R_2^2+\frac{3g_0}{2g_1}\right)u}\right)=\pm2\sqrt{\frac{g_1}{3}}\tau,$$

which can be more simplified as follow

$$arc\cosh\left(\frac{2R_2^2\left(3R_2^2+\frac{3g_0}{2g_1}\right)-\left(4R_2^2+\frac{3g_0}{2g_1}\right)u}{\left(2R_2^2+\frac{3g_0}{2g_1}\right)u}\right)=\pm2R_2\sqrt{\left(3R_2^2+\frac{3g_0}{2g_1}\right)}\sqrt{\frac{g_1}{3}}\tau.$$

Remembering that the unknown variable is $u(\tau)$, we obtain

$$\frac{2R_2^2\left(3R_2^2+\frac{3g_0}{2g_1}\right)}{\left(2R_2^2+\frac{3g_0}{2g_1}\right)u}-\frac{\left(4R_2^2+\frac{3g_0}{2g_1}\right)}{\left(2R_2^2+\frac{3g_0}{2g_1}\right)}=\cosh\left(2\sqrt{\left(3R_2^2+\frac{3g_0}{2g_1}\right)}\sqrt{\frac{g_1R_2^2}{3}}\tau\right).$$

By continuing to simplify this equation, it can be rewritten as follows

$$\frac{2R_2^2\left(3R_2^2+\frac{3g_0}{2g_1}\right)}{u}=\left(4R_2^2+\frac{3g_0}{2g_1}\right)+\left(2R_2^2+\frac{3g_0}{2g_1}\right)\cosh\left(2\sqrt{\left(3R_2^2+\frac{3g_0}{2g_1}\right)\frac{g_1R_2^2}{3}}\tau\right).$$

Finally the value of the unknown variable is given by

$$u(\tau)=\frac{2R_2^2\left(3R_2^2+\frac{3g_0}{2g_1}\right)}{\left(4R_2^2+\frac{3g_0}{2g_1}\right)+\left(2R_2^2+\frac{3g_0}{2g_1}\right)\cosh\left(2\sqrt{\left(3R_2^2+\frac{3g_0}{2g_1}\right)\frac{g_1R_2^2}{3}}\tau\right)}.$$

Thereafter, we replace $u(\tau)$ by its expression function of $R_0(\tau)$, and we obtain

$$R_2^2-R_0^2=\frac{2R_2^2\left(3R_2^2+\frac{3g_0}{2g_1}\right)}{\left(4R_2^2+\frac{3g_0}{2g_1}\right)+\left(2R_2^2+\frac{3g_0}{2g_1}\right)\cosh\left(2\sqrt{\left(3R_2^2+\frac{3g_0}{2g_1}\right)\frac{g_1R_2^2}{3}}\tau\right)},$$

$$R_0(\tau)=\pm R_2\sqrt{1-\frac{2\left(3R_2^2+\frac{3g_0}{2g_1}\right)}{\left(4R_2^2+\frac{3g_0}{2g_1}\right)+\left(2R_2^2+\frac{3g_0}{2g_1}\right)\cosh\left(2\sqrt{\left(3R_2^2+\frac{3g_0}{2g_1}\right)\frac{g_1R_2^2}{3}}\tau\right)}}.$$

This expression can be more simplified as follows

$$R_0(\tau) = \pm R_2 \sqrt{\frac{1-\cosh\left(2\sqrt{\left(3R_2^2+\frac{3g_0}{2g_1}\right)\frac{g_1R_2^2}{3}}\tau\right)}{-\frac{4R_2^2+\frac{3g_0}{2g_1}}{2R_2^2+\frac{3g_0}{2g_1}}-\cosh\left(2\sqrt{\left(3R_2^2+\frac{3g_0}{2g_1}\right)\frac{g_1R_2^2}{3}}\tau\right)}}.$$

Let's evaluate the quantities inside the square root, by replacing R_2 by its value given in eq.(86). One obtains:

$$3R_2^2+\frac{3g_0}{2g_1} = \frac{3\sqrt{g_0^2-g_1\upsilon^2}}{2g_1} = -\frac{3g_0}{2g_1}\sqrt{1-\frac{g_1\upsilon^2}{g_0^2}}$$

$$\frac{g_1R_2^2}{3} = \frac{-g_0+\sqrt{g_0^2-g_1\upsilon^2}}{6} = -\frac{g_0}{6}\left(1+\sqrt{1-\frac{g_1\upsilon^2}{g_0^2}}\right)$$

$$4R_2^2+\frac{3g_0}{2g_1} = \frac{-g_0+4\sqrt{g_0^2-g_1\upsilon^2}}{2g_1} = -\frac{g_0}{2g_1}\left(1+4\sqrt{1-\frac{g_1\upsilon^2}{g_0^2}}\right)$$

$$2R_2^2+\frac{3g_0}{2g_1} = \frac{g_0+2\sqrt{g_0^2-g_1\upsilon^2}}{2g_1} = -\frac{g_0}{2g_1}\left(-1+2\sqrt{1-\frac{g_1\upsilon^2}{g_0^2}}\right)$$

Only for sake of simplicity, let's pose $\mu = \sqrt{1-\frac{g_1\upsilon^2}{g_0^2}}$, $\Gamma = -\frac{4R^2+\frac{3g_0}{2g_1}}{2R^2+\frac{3g_0}{2g_1}}$ and $\omega = \left(2\sqrt{\left(3R_2^2+\frac{3g_0}{2g_1}\right)\frac{g_1R_2^2}{3}}\right)$.

Thus, Γ and ω can be rewritten as follows $\Gamma = \frac{1+4\mu}{1-2\mu}$ and $\omega = -g_0\sqrt{\frac{\mu(1+\mu)}{g_1}}$.

Finally, the abscissa of the state vector is given by

$$R_0(\tau) = \pm R_2\sqrt{\frac{1-\cosh(\omega\tau)}{\Gamma-\cosh(\omega\tau)}}. \tag{95}$$

According to our work hypothesis given in eq.(85), μ and Γ must fulfill the following inequalities: $\frac{1}{2} < \mu < 1$ and $\Gamma < -5$.

In summary, the components of the state vector generating the heteroclinic separatrix are given by

$$\begin{cases} R_{het}^{\pm}(\tau) = \pm R_2\sqrt{\frac{1-\cosh(\omega\tau)}{\Gamma-\cosh(\omega\tau)}} \\ X_{het}^{\pm}(\tau) = \pm\frac{\frac{R_2\omega(1-\Gamma)\sinh(\omega\tau)}{(\Gamma-\cosh(\omega\tau))^2}}{2\sqrt{\frac{1-\cosh(\omega\tau)}{\Gamma-\cosh(\omega\tau)}}}. \end{cases} \tag{96}$$

The signs $\pm$ must be understood as follows: X_{het}^{+} corresponds to R_{het}^{+} and X_{het}^{-} corresponds to R_{het}^{-}, het denoting the abbreviation of heteroclinic. Once more, it is to note that the heteroclinic

separatrix presented in Fig.11(c) obtained through this analytical treatment is exactly the one obtained directly in Fig.9(b) through the numerical integration. It comes from Fig.11 that an un-

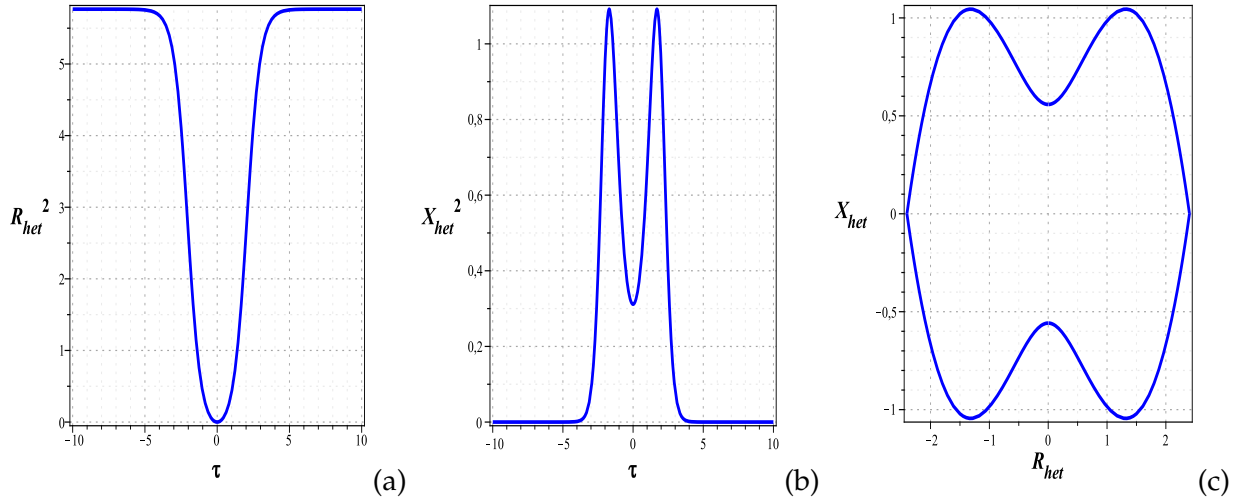

Figure 11: (a) Spatiotemporal evolution of the particle number density of condensate (black solitons). (b) Spatiotemporal evolution of the first excited state of condensate (gray solitons). (c) The heteroclinic separatrix deduced from eq.(96). The other parameters used are: $\upsilon = 2$, $g_0 = -0.75$, $g_1 = 0.1$

damped condensate without trapping potential exhibits solitonic solutions as black solitons for heteroclinic depression $R^2_{het}(\tau)$ and gray solitons for the first excited state $X^2_{het}(\tau)$. Once again, these solitary waves can be interpreted as a balance between the both parts of the nonlinearity.

II.5.1.4. The Melnikov analysis

a) Global bifurcations of homoclinic orbits

As in the previous section, the Melnikov function for homoclinic bifurcations can be expressed as

$$M(\tau_0) = \frac{V_0}{2}\left[b_0(m) + b_1(m) + b_2(m)\right] J_1 - \frac{V_0}{2} J_2 - \gamma \upsilon J_3. \tag{97}$$

The quantities J_1, J_2 and J_3 are given by

$$J_1 = \int_{-\infty}^{+\infty} R_{hom}(\tau) X_{hom}(\tau) d\tau, \tag{98}$$

$$J_2 = \int_{-\infty}^{+\infty} \left[b_0 \cos(2\tau + 2\tau_0) + b_1 \cos(4\tau + 4\tau_0) + b_2 \cos(6\tau + 6\tau_0)\right] R_{hom}(\tau) X_{hom}(\tau) d\tau, \tag{99}$$

$$J_3 = \int_{-\infty}^{+\infty} X^2_{hom}(\tau) d\tau. \tag{100}$$

Let's begin the evaluation of these integrals by calculating the product $R_{hom}(\tau)X_{hom}(\tau)$, given by $R_{hom}(\tau)X_{hom}(\tau) = \dfrac{\upsilon^3 \sigma \sinh(\upsilon\tau)}{2g_0(1+\sigma\cosh(\upsilon\tau))^2}$.
It is clear that this product is an odd function, and consequently, $J_1 = 0$.

J_2 can be rewritten as

$$J_2 = -\frac{b_0 \upsilon^3 \sigma \sin(2\tau_0)}{g_0} \int_0^{+\infty} \frac{\sinh(\upsilon\tau)\sin(2\tau)d\tau}{(1+\sigma\cosh(\upsilon\tau))^2} - \frac{b_1 \upsilon^3 \sigma \sin(4\tau_0)}{g_0} \int_0^{+\infty} \frac{\sinh(\upsilon\tau)\sin(4\tau)d\tau}{(1+\sigma\cosh(\upsilon\tau))^2} - \frac{b_2 \upsilon^3 \sigma \sin(6\tau_0)}{g_0} \int_0^{+\infty} \frac{\sinh(\upsilon\tau)\sin(6\tau)d\tau}{(1+\sigma\cosh(\upsilon\tau))^2} \tag{101}$$

Each integral of eq.(101) can be calculated by the integration by parts method, as shown below.

$$\int_0^{+\infty} \frac{\sinh(\upsilon\tau)\sin(2\tau)d\tau}{(1+\sigma\cosh(\upsilon\tau))^2} = \left[-\frac{\sin(2\,\tau)}{\sigma\,\upsilon\,(1+\sigma\,\cosh(\upsilon\,\tau))}\right]_0^{+\infty} + 2\int_0^{+\infty} \frac{\cos(2\,\tau)\,d\tau}{\sigma\,\upsilon\,(1+\sigma\,\cosh(\upsilon\,\tau))}$$
$$= \left(0 + 2\int_0^{+\infty} \frac{\cos(2\,\tau)\,d\tau}{\sigma\,\upsilon\,(1+\sigma\,\cosh(\upsilon\,\tau))}\right) = \frac{2}{\upsilon\sigma}\int_0^{+\infty} \frac{\cos(2\,\tau)\,d\tau}{(1+\sigma\,\cosh(\upsilon\,\tau))}$$

From this result, one can deduce the two remaining integrals.

$$\int_0^{+\infty} \frac{\sinh(\upsilon\tau)\sin(4\tau)d\tau}{(1+\sigma\cosh(\upsilon\tau))^2} = \frac{4}{\upsilon\sigma}\int_0^{+\infty} \frac{\cos(4\,\tau)\,d\tau}{(1+\sigma\,\cosh(\upsilon\,\tau))},$$

and

$$\int_0^{+\infty} \frac{\sinh(\upsilon\tau)\sin(6\tau)d\tau}{(1+\sigma\cosh(\upsilon\tau))^2} = \frac{6}{\upsilon\sigma}\int_0^{+\infty} \frac{\cos(6\,\tau)\,d\tau}{(1+\sigma\,\cosh(\upsilon\,\tau))}.$$

The integrals of the right-hand side expressed above can be evaluated through the following formula given in page **511** of the reference [145].

$$\int_0^{+\infty} \frac{\cos(ax)dx}{(c+b\cosh(\beta x))} = \frac{\pi}{\beta\sqrt{c^2-b^2}} \frac{\sin\left(\frac{a}{\beta} arc\cosh\left(\frac{c}{b}\right)\right)}{\sinh\left(\frac{a\pi}{\beta}\right)}, [c > b > 0]$$

The required conditions being fulfilled, because $1 > \sigma > 0$, one finally obtains

$$J_2 = -\frac{2\pi\upsilon}{g_0\sqrt{1-\sigma^2}}\Big[\frac{b_0\sin(2\tau_0)\sin\left(\frac{2}{\upsilon} arc\cosh\left(\frac{1}{\sigma}\right)\right)}{\sinh\left(\frac{2\pi}{\upsilon}\right)} + \frac{2b_1\sin(4\tau_0)\sin\left(\frac{4}{\upsilon} arc\cosh\left(\frac{1}{\sigma}\right)\right)}{\sinh\left(\frac{4\pi}{\upsilon}\right)} + \frac{3b_2\sin(6\tau_0)\sin\left(\frac{6}{\upsilon} arc\cosh\left(\frac{1}{\sigma}\right)\right)}{\sinh\left(\frac{6\pi}{\upsilon}\right)}\Big]. \tag{102}$$

Now, let's evaluate the integral J_3.

$$J_3 = -\frac{\upsilon^4\sigma^2}{4g_0}\int_{-\infty}^{+\infty} \frac{\sinh^2(\upsilon\tau)d\tau}{(1+\sigma\cosh(\upsilon\tau))^3} = -\frac{\upsilon^4\sigma^2}{2g_0}\int_0^{+\infty} \frac{\sinh^2(\upsilon\tau)d\tau}{(1+\sigma\cosh(\upsilon\tau))^3}.$$

With the integration by parts method, one obtains

$$J_3 = -\frac{\upsilon^4\sigma^2}{2g_0}\left(\left[-\frac{\sinh(\upsilon\,\tau)}{2\sigma\,\upsilon\,(1+\sigma\,\cosh(\upsilon\,\tau))^2}\right]_0^{+\infty} + \frac{1}{2\sigma}\int_0^{+\infty}\frac{\cosh(\upsilon\,\tau)\,d\tau}{(1+\sigma\,\cosh(\upsilon\,\tau))^2}\right)$$

$$= -\frac{\upsilon^4\sigma^2}{2g_0}\left(0 + \frac{1}{2\sigma}\int_0^{+\infty}\frac{\cosh(\upsilon\,\tau)\,d\tau}{(1+\sigma\,\cosh(\upsilon\,\tau))^2}\right) = -\frac{\upsilon^4\sigma}{4g_0}\int_0^{+\infty}\frac{\cosh(\upsilon\,\tau)\,d\tau}{(1+\sigma\,\cosh(\upsilon\,\tau))^2}$$

This last integral can be carried out directly from Maple software. Thus, after some algebraic manipulations of the result given by Maple, and verified with the reference [145] in page **126**, one obtains

$$J_3 = -\frac{\upsilon^4\sigma}{4g_0}\left[\frac{-2\sigma}{\upsilon\,(1-\sigma^2)^{3/2}}arc\tanh\left(\sqrt{\frac{1-\sigma}{1+\sigma}}\tanh\left(\frac{\upsilon\tau}{2}\right)\right)\right]_0^{+\infty} - \frac{\upsilon^4\sigma}{4g_0}\left[\frac{\sinh(\upsilon\tau)}{\upsilon\,(1-\sigma^2)\,(1+\sigma\cosh(\upsilon\tau))}\right]_0^{+\infty}$$

$$= -\frac{\upsilon^4\sigma}{4g_0}\left(\frac{-2\sigma}{\upsilon\,(1-\sigma^2)^{3/2}}arc\tanh\left(\sqrt{\frac{1-\sigma}{1+\sigma}}\right) + \frac{1}{\upsilon\sigma\,(1-\sigma^2)}\right),$$

and finally

$$J_3 = -\frac{\upsilon^3}{4g_0\,(1-\sigma^2)}\left(1 - \frac{2\sigma^2}{\sqrt{1-\sigma^2}}arc\tanh\left(\sqrt{\frac{1-\sigma}{1+\sigma}}\right)\right). \tag{103}$$

The Melnikov function for homoclinic bifurcations is then given by

$$M^{\pm}(\tau_0) = \frac{\gamma\upsilon^4}{4g_0\,(1-\sigma^2)}\left(1 - \frac{2\sigma^2}{\sqrt{1-\sigma^2}}arc\tanh\left(\sqrt{\frac{1-\sigma}{1+\sigma}}\right)\right) + \frac{\pi\upsilon V_0}{g_0\sqrt{1-\sigma^2}}\times \tag{104}$$

$$\left[\frac{b_0\sin(2\tau_0)\sin\left(\frac{2}{\upsilon}arc\cosh\left(\frac{1}{\sigma}\right)\right)}{\sinh\left(\frac{2\pi}{\upsilon}\right)} + \frac{2b_1\sin(4\tau_0)\sin\left(\frac{4}{\upsilon}arc\cosh\left(\frac{1}{\sigma}\right)\right)}{\sinh\left(\frac{4\pi}{\upsilon}\right)} + \frac{3b_2\sin(6\tau_0)\sin\left(\frac{6}{\upsilon}arc\cosh\left(\frac{1}{\sigma}\right)\right)}{\sinh\left(\frac{6\pi}{\upsilon}\right)}\right].$$

To seek the simple zeros of $M(\tau_0)$ corresponding to homoclinic bifurcations is analytically very difficult. But, as in the previous section, the study of the Fourier coefficients $b_0(m)$, $b_1(m)$ and $b_2(m)$ versus the lattice shape parameter m reveals that we can neglect $b_1(m)$ and $b_2(m)$ in front of $b_0(m)$. Thus, according to the Smale-Birkhoff theorem, the approximate condition for the occurrence of the homoclinic chaos is given by

$$\rho(V_0, m, \upsilon, \gamma, g_1) = \frac{V_0}{\gamma} - \frac{\upsilon^3\left[1 - \frac{2\sigma^2}{\sqrt{1-\sigma^2}}arc\tanh\left(\sqrt{\frac{1-\sigma}{1+\sigma}}\right)\right]\sinh\left(\frac{2\pi}{\upsilon}\right)}{4\pi\sqrt{1-\sigma^2}b_0(m)\left|\sin\left(\frac{2}{\upsilon}arc\cosh(\sigma^{-1})\right)\right|} \geq 0 \tag{105}$$

where the symbol || denotes the absolute value.

b) Global bifurcations of heteroclinic orbits

The Melnikov function characterizing the heteroclinic bifurcations is given by the following expression

$$M(\tau_0) = \frac{V_0}{2}\left[b_0(m) + b_1(m) + b_2(m)\right] Y_1 - \frac{V_0}{2} Y_2 - \gamma \upsilon Y_3, \tag{106}$$

where the quantities Y_1, Y_2 and Y_3 denote the following integrals

$$Y_1 = \int_{-\infty}^{+\infty} R_{het}(\tau) X_{het}(\tau) d\tau, \tag{107}$$

$$Y_2 = \int_{-\infty}^{+\infty} \left[b_0 \cos(2\tau + 2\tau_0) + b_1 \cos(4\tau + 4\tau_0) + b_2 \cos(6\tau + 6\tau_0)\right] R_{het}(\tau) X_{het}(\tau) d\tau, \tag{108}$$

and

$$Y_3 = \int_{-\infty}^{+\infty} X_{het}^2(\tau) d\tau. \tag{109}$$

Let's start the evaluation of these integrals by calculating the product of function $R_{het}X_{het}$.

$$R_{het}(\tau)X_{het}(\tau) = \frac{R_2^2\omega\ (1-\Gamma)\sinh(\omega\tau)}{2\left(\Gamma - \cosh(\omega\tau)\right)^2}.$$

This product being an odd function, $Y_1 = 0$.
To evaluate Y_2, we expand the term preceding the product $R_{het}(\tau)X_{het}(\tau)$ and we retain only the odd part of the expansion. Thus, this integral can be rewritten as

$$\begin{aligned} Y_2 \;=\; & -R_2^2\omega\ (1-\Gamma)\left[b_0(m)\sin(2\tau_0)\int_0^{+\infty}\frac{\sinh(\omega\tau)\sin(2\tau)d\tau}{\left(\Gamma-\cosh(\omega\tau)\right)^2} + b_1(m)\sin(4\tau_0)\int_0^{+\infty}\frac{\sinh(\omega\tau)\sin(4\tau)d\tau}{\left(\Gamma-\cosh(\omega\tau)\right)^2}\right] \\ & -R_2^2\omega\ (1-\Gamma)\, b_2(m)\sin(6\tau_0)\int_0^{+\infty}\frac{\sinh(\omega\tau)\sin(6\tau)d\tau}{\left(\Gamma-\cosh(\omega\tau)\right)^2} \end{aligned} \tag{110}$$

Let's evaluate each integral of eq.(110).

$$\int_0^{+\infty}\frac{\sinh(\omega\tau)\sin(2\tau)d\tau}{\left(\Gamma-\cosh(\omega\tau)\right)^2} = \left[\frac{\sin(2\tau)}{\omega\ \left(\Gamma-\cosh(\omega\tau)\right)}\right]_0^{+\infty} - \frac{2}{\omega}\int_0^{+\infty}\frac{\cos(2\tau)\,d\tau}{\Gamma-\cosh(\omega\tau)}$$

$$= 0 - \frac{2}{\omega}\int_0^{+\infty}\frac{\cos(2\tau)\,d\tau}{\Gamma-\cosh(\omega\tau)} = -\frac{2}{\omega}\int_0^{+\infty}\frac{\cos(2\tau)\,d\tau}{\Gamma-\cosh(\omega\tau)}$$

It is already known in page **511** of the reference [145] that there is a formula for the evaluation of this integral. The use of this formula leads to

$$\int_0^{+\infty}\frac{\sinh(\omega\tau)\sin(2\tau)d\tau}{\left(\Gamma-\cosh(\omega\tau)\right)^2} = \frac{2}{\omega}\int_0^{+\infty}\frac{\cos(2\tau)\,d\tau}{-\Gamma+\cosh(\omega\tau)} = \frac{2\pi\sin\left(\frac{2}{\omega}arc\cosh(-\Gamma)\right)}{\omega^2\sqrt{\Gamma^2-1}\sinh\left(\frac{2\pi}{\omega}\right)},$$

$$\int_0^{+\infty} \frac{\sinh(\omega\tau)\sin(4\tau)d\tau}{(\Gamma-\cosh(\omega\tau))^2} = \frac{4}{\omega}\int_0^{+\infty} \frac{\cos(4\tau)\,d\tau}{-\Gamma+\cosh(\omega\tau)} = \frac{4\pi\sin\left(\frac{4}{\omega}arc\cosh(-\Gamma)\right)}{\omega^2\sqrt{\Gamma^2-1}\sinh\left(\frac{4\pi}{\omega}\right)},$$

$$\int_0^{+\infty} \frac{\sinh(\omega\tau)\sin(6\tau)d\tau}{(\Gamma-\cosh(\omega\tau))^2} = \frac{6}{\omega}\int_0^{+\infty} \frac{\cos(6\tau)\,d\tau}{-\Gamma+\cosh(\omega\tau)} = \frac{6\pi\sin\left(\frac{6}{\omega}arc\cosh(-\Gamma)\right)}{\omega^2\sqrt{\Gamma^2-1}\sinh\left(\frac{6\pi}{\omega}\right)}.$$

The integral Y_2 is then given by

$$\begin{aligned} Y_2 &= -\frac{2\pi R_2^2\,(1-\Gamma)}{\omega\sqrt{\Gamma^2-1}}\Big[\frac{b_0(m)\sin(2\tau_0)\sin\left(\frac{2}{\omega}arc\cosh(-\Gamma)\right)}{\sinh\left(\frac{2\pi}{\omega}\right)} + \frac{2b_1(m)\sin(4\tau_0)\sin\left(\frac{4}{\omega}arc\cosh(-\Gamma)\right)}{\sinh\left(\frac{4\pi}{\omega}\right)} \\ &+\frac{3b_2(m)\sin(6\tau_0)\sin\left(\frac{6}{\omega}arc\cosh(-\Gamma)\right)}{\sinh\left(\frac{6\pi}{\omega}\right)}\Big]. \end{aligned} \tag{111}$$

Now, let's evaluate Y_3.

$$X_{het}^2 = \frac{R_2^2(1-\Gamma)^2\omega^2(1+cosh(\omega\tau))}{4(-\Gamma+cosh(\omega\tau))^3}.$$

With the change of variable $\omega\tau = x$, one has

$$Y_3 = 2\int_0^{+\infty} X_{het}^2(\tau)d\tau = \frac{R_2^2(1-\Gamma)^2\omega}{2}\int_0^{+\infty}\frac{(1+cosh(x))dx}{(-\Gamma+cosh(x))^3}.$$

Via the Maple software, Y_3 is finally given by

$$Y_3 = \frac{R_2^2\omega}{4(1+\Gamma)}\left[2+\Gamma-\frac{2(1+2\Gamma)}{\sqrt{\Gamma^2-1}}arc\tanh\left(\sqrt{\frac{\Gamma+1}{\Gamma-1}}\right)\right]. \tag{112}$$

Inserting Y_1, Y_2 and Y_3 into the Melnikov function defined in eq.(106) one obtains

$$\begin{aligned} M^{\pm}(\tau_0) &= -\frac{R_2^2\gamma\omega v}{4(1+\Gamma)}\left[2+\Gamma-\frac{2(1+2\Gamma)}{\sqrt{\Gamma^2-1}}arc\tanh\left(\sqrt{\frac{\Gamma+1}{\Gamma-1}}\right)\right] + \frac{\pi V_0 R_2^2(1-\Gamma)}{\omega\sqrt{\Gamma^2-1}}\times \\ &\left[\frac{b_0\sin(2\tau_0)\sin\left(\frac{2}{\omega}arc\cosh(-\Gamma)\right)}{\sinh\left(\frac{2\pi}{\omega}\right)} + \frac{2b_1\sin(4\tau_0)\sin\left(\frac{4}{\omega}arc\cosh(-\Gamma)\right)}{\sinh\left(\frac{4\pi}{\omega}\right)} + \frac{3b_2\sin(6\tau_0)\sin\left(\frac{6}{\omega}arc\cosh(-\Gamma)\right)}{\sinh\left(\frac{6\pi}{\omega}\right)}\right]. \end{aligned} \tag{113}$$

Applying the Smale-Birkhoff theorem under the fulfilled conditions $b_1(m) << b_0(m)$ and $b_2(m) << b_0(m)$, the approximate condition of apparition of the heteroclinic chaos is given by

$$\varpi(V_0,m,g_1,\gamma,\upsilon)=\frac{V_0}{\gamma}+\frac{\upsilon\omega^2 sinh\left(\frac{2\pi}{\omega}\right)\left(2+\Gamma-\frac{2(1+2\Gamma)}{\sqrt{\Gamma^2-1}}arc\tanh\left(\sqrt{\frac{\Gamma+1}{\Gamma-1}}\right)\right)}{4\pi\sqrt{\Gamma^2-1}b_0(m)\left|sin\left(\frac{2}{\omega}arc\cosh(-\Gamma)\right)\right|}\geq 0, \quad (114)$$

with the symbol || denoting the absolute value.

II.5.2 Case of an undamped condensate subjected to inelastic collisions

As in the previous section, in this subsection we take into account the inelastic processes in the dynamics of the condensate,always in the framework of attractive two-body and repulsive three-body elastic atom-atom collisions. We neglect the damping parameter γ, not only for a possible analytical treatment, but especially because the two-body and three-body inelastic atom-atom collisions are viewed as dissipation phenomena. The dynamics of such a condensate is governed by the nonlinear system eq.(69), and the amplitude equation deriving from this system is given by eq.(72). This amplitude equation is written as a first order system in eq.(73). The unperturbed system deriving from eq.(73) possesses three unstable hyperbolic fixed points at $(0,0)$, $(-R_2^{'},0)$ and $(+R_2^{'},0)$ and two stable nonhyperbolic fixed points at $(-R_1^{'},0)$ and $(+R_1^{'},0)$. The expressions of $R_1^{'}$ and $R_2^{'}$ aforementioned are given by

$$\begin{cases} R_1'=\sqrt{-\frac{g_0}{2g_1}\left(1-\sqrt{1-\frac{g_1a^2}{g_0^2}}\right)} \\ R_2'=\sqrt{-\frac{g_0}{2g_1}\left(1+\sqrt{1-\frac{g_1a^2}{g_0^2}}\right)}. \end{cases} \quad (115)$$

II.5.2.1. The Melnikov analysis for homoclinic orbits

The state vector generating the homoclinic separatrices in this case is obtained by replacing in eq.(89) the velocity of the optical lattice υ by $a=\sqrt{4\beta-\upsilon^2-4\alpha\upsilon}$. That implies also to replace σ by its new expression $\sigma'=\sqrt{1-\frac{4g_1a^2}{3g_0^2}}$, with $0<\sigma'<1$. Thus, one obtains the following components

$$\begin{cases} R_{hom}^{\pm}(\tau)=\pm\dfrac{a}{\sqrt{-g_0\Big[1+\sigma'\cosh(a\tau)\Big]}} \\ X_{hom}^{\pm}(\tau)=\pm\dfrac{a^2\sigma'\sinh(a\tau)}{2\sqrt{-g_0\Big[1+\sigma'\cosh(a\tau)\Big]}^3}, \end{cases} \quad (116)$$

with $\sigma'=\sqrt{1-\frac{4g_1a^2}{3g_0^2}}$. The corresponding Melnikov function can be expressed as

$$M(\tau_0)=\frac{V_0}{2}\left[b_0(m)+b_1(m)+b_2(m)\right]J_1'-\frac{V_0}{2}J_2'+\Sigma, \quad (117)$$

where the quantities J_1', J_2' and Σ are given by

$$J_1' = \int_{-\infty}^{+\infty} R_{hom}(\tau) X_{hom}(\tau) d\tau, \tag{118}$$

$$J_2' = \int_{-\infty}^{+\infty} \left[b_0 \cos(2\tau + 2\tau_0) + b_1 \cos(4\tau + 4\tau_0) + b_2 \cos(6\tau + 6\tau_0) \right] R_{hom}(\tau) X_{hom}(\tau) d\tau, \tag{119}$$

and

$$\Sigma = \int_{-\infty}^{+\infty} \frac{X_{hom}(\tau)}{R_{hom}^3(\tau)} \left(\int_{-\infty}^{\tau} \left(\gamma_0 R_{hom}^2(\tau) - \gamma_1 R_{hom}^4(\tau) - \gamma_2 R_{hom}^6(\tau) \right) d\tau \right)^2 d\tau. \tag{120}$$

According to the previous subsection, $J_1' = 0$, and J_2' is obtained by replacing in the expression of J_2 defined in eq.(102) the velocity of optical lattice υ by a and σ by σ'. Thus, one obtains

$$\begin{aligned} J_2' &= -\frac{2\pi a}{g_0\sqrt{1-\sigma'^2}} \Big[\frac{b_0 \sin(2\tau_0) \sin\left(\frac{2}{a} arc\cosh\left(\frac{1}{\sigma'} \right) \right)}{\sinh\left(\frac{2\pi}{a} \right)} + \frac{2b_1 \sin(4\tau_0) \sin\left(\frac{4}{a} arc\cosh\left(\frac{1}{\sigma'} \right) \right)}{\sinh\left(\frac{4\pi}{a} \right)} \\ &+ \frac{3b_2 \sin(6\tau_0) \sin\left(\frac{6}{a} arc\cosh\left(\frac{1}{\sigma'} \right) \right)}{\sinh\left(\frac{6\pi}{a} \right)} \Big]. \end{aligned} \tag{121}$$

The expression of Σ is obtained with the help of the Maple software, with the remark that $R_{hom}(\tau)$ and $X_{hom}(\tau)$ are practically null for $]-\infty, \tau_c[\cup]\tau_c, +\infty[$ (see Fig.(10)), where the symbol $\cup$ stands for the union operator. Therefore, Σ is evaluated with the spatiotemporal variable τ taken between $-\tau_c$ and τ_c. In fact, τ_c represents the value of τ for which $R_{hom}^2(\tau)$, $R_{hom}^4(\tau)$ and $R_{hom}^6(\tau)$ can be assumed close to zero, and it value depends on the set of parameters used. For example, taking the set of parameters as those used to plot the particle number density of the condensate for the unperturbed system deriving from eq.(73), when we solve $R_{hom}^2(\tau) = 0.0001$ we have as solution $\tau = 6.52$. $R_{hom}^4(\tau) = 0.0001$ leads to $\tau = 4.22$ and $R_{hom}^6(\tau) = 0.0001$ gives as solution $\tau = 3.45$. Henceforth, we give to τ_c the value 4 to numerical simulations. Consequently, Σ can be expressed as

$$\Sigma = \int_{-\tau_c}^{+\tau_c} \frac{X_{hom}(\tau)}{R_{hom}^3(\tau)} \left(\int_{-\tau_c}^{\tau} \left(\gamma_0 R_{hom}^2(\tau) - \gamma_1 R_{hom}^4(\tau) - \gamma_2 R_{hom}^6(\tau) \right) d\tau \right)^2 d\tau. \tag{122}$$

Thus, the Melnikov function for homoclinic orbits is then given by

$$\begin{aligned} M^{\pm}(\tau_0) &= \frac{\pi a V_0}{g_0\sqrt{1-\sigma'^2}} \Big[\frac{b_0 \sin(2\tau_0) \sin\left(\frac{2}{a} arc\cosh\left(\frac{1}{\sigma'} \right) \right)}{\sinh\left(\frac{2\pi}{a} \right)} + \frac{2b_1 \sin(4\tau_0) \sin\left(\frac{4}{a} arc\cosh\left(\frac{1}{\sigma'} \right) \right)}{\sinh\left(\frac{4\pi}{a} \right)} \\ &+ \frac{3b_2 \sin(6\tau_0) \sin\left(\frac{6}{a} arc\cosh\left(\frac{1}{\sigma'} \right) \right)}{\sinh\left(\frac{6\pi}{a} \right)} \Big] + \Sigma. \end{aligned} \tag{123}$$

The expression of Σ, resulting from cumbersome integrals is given in section Appendix B.
By applying the Melnikov criterion on the Melnikov function corresponding to homoclinic bifurcations, the occurrence condition of the homoclinic chaos is then given by the following inequality

$$\delta \geq \left| \frac{g_0\sqrt{1-\sigma'^2}\Sigma \sinh\left(\frac{2\pi}{a}\right)}{a\pi \sin\left(\frac{2}{a} arc\cosh\left(\frac{1}{\sigma'}\right)\right)} \right|. \tag{124}$$

$\delta = V_0 b_0(m)$ represents the amplitude of the optical lattice potential in the case of approximations $b_1(m) << b_0(m)$ and $b_2(m) << b_0(m)$.

II.5.2.2. The Melnikov analysis for heteroclinic orbits

The state vector generating the heteroclinic separatrix in this case is obtained by replacing in eq.(96) R_2 by R_2' defined in eq.(115), μ by $\mu' = \sqrt{1-\frac{g_1 a^2}{g_0^2}}$, Γ by $\Gamma' = -\frac{4R_2'^2 + \frac{3g_0}{2g_1}}{2R_2'^2 + \frac{3g_0}{2g_1}} = \frac{1+4\mu'}{1-2\mu'}$ and ω by $\omega' = -g_0\sqrt{\frac{\mu'(1+\mu')}{g_1}}$.
These changes are due to the fact that, to take into account the inelastic processes implies the replacement of the velocity of the optical lattice v by $a = \sqrt{4\beta - v^2 - 4\alpha v}$, as it is well visible in eq.(72). One will not forget that these constants must fulfill the following inequalities: $\frac{1}{2} < \mu' < 1$ and $\Gamma' < -5$.
Hence, the components of the state vector generating the heteroclinic separatrix is given by

$$\begin{cases} R_{het}^{\pm}(\tau) = \pm R_2' \sqrt{\dfrac{1-\cosh(\omega'\tau)}{\Gamma' - \cosh(\omega'\tau)}} \\ X_{het}^{\pm}(\tau) = \dfrac{R_2'\omega'(1-\Gamma')\sinh(\omega'\tau)}{(\Gamma' - \cosh(\omega'\tau))^2} \Big/ 2\sqrt{\dfrac{1-\cosh(\omega'\tau)}{\Gamma' - \cosh(\omega'\tau)}} \end{cases}. \tag{125}$$

The Melnikov function corresponding to heteroclinic bifurcations can be written as

$$M(\tau_0) = \frac{V_0}{2}\left[b_0(m) + b_1(m) + b_2(m)\right] Y_1' - \frac{V_0}{2} Y_2' + F, \tag{126}$$

with the quantities Y_1', Y_2' and F given by

$$Y_1' = \int_{-\infty}^{+\infty} R_{het}(\tau) X_{het}(\tau) d\tau, \tag{127}$$

$$Y_2' = \int_{-\infty}^{+\infty} \left[b_0\cos(2\tau + 2\tau_0) + b_1\cos(4\tau + 4\tau_0) + b_2\cos(6\tau + 6\tau_0)\right] R_{het}(\tau) X_{het}(\tau) d\tau, \tag{128}$$

and

$$F=\int_{-\infty}^{+\infty}\frac{X_{het}(\tau)}{R_{het}^{3}(\tau)}\left[\int_{-\infty}^{\tau}\left(\gamma_0 R_{het}^{2}(\tau)-\gamma_1 R_{het}^{4}(\tau)-\gamma_2 R_{het}^{6}(\tau)\right)d\tau\right]^{2}d\tau. \tag{129}$$

As in the previous subsection, the product $R_{het}\left(\tau\right)X_{het}\left(\tau\right)$ is an odd function. Therefore, $Y_1'=0$. Y_2' is obtained by replacing into the expression of Y_2, R_2 by R_2', Γ by Γ' and ω by ω'. Hence we obtain

$$\begin{aligned}Y_2' &= -\frac{2\pi R_2'^2\ (1-\Gamma')}{\omega'\sqrt{\Gamma'^2-1}}\Big[\frac{b_0(m)\sin(2\tau_0)\sin\left(\frac{2}{\omega'}arc\cosh(-\Gamma')\right)}{\sinh\left(\frac{2\pi}{\omega'}\right)}+\frac{2b_1(m)\sin(4\tau_0)\sin\left(\frac{4}{\omega'}arc\cosh(-\Gamma')\right)}{\sinh\left(\frac{4\pi}{\omega'}\right)}\\ &+\frac{3b_2(m)\sin(6\tau_0)\sin\left(\frac{6}{\omega'}arc\cosh(-\Gamma')\right)}{\sinh\left(\frac{6\pi}{\omega'}\right)}\Big]\end{aligned} \tag{130}$$

Now, let's focalize our mind on the calculation of F. It comes from Fig.(11) that $X_{het}(\tau)$ is practically null for $]-\infty;\tau_c[\cup]\tau_c;+\infty[$, where the value of τ_c depends of the set of parameters used. Another remark is that F cannot be evaluated for $\tau=0$. But in terms of area, we approximate the value of F by avoiding the vicinity of $\tau=0$. With this remark, F can be rewritten as

$$F=\int_{-\tau_c}^{+\tau_c}\frac{X_{het}(\tau)}{R_{het}^{3}(\tau)}\left(\int_{-\tau_c}^{\tau}\left(\gamma_0 R_{het}^{2}(\tau)-\gamma_1 R_{het}^{4}(\tau)-\gamma_2 R_{het}^{6}(\tau)\right)d\tau\right)^{2}d\tau. \tag{131}$$

Finally, the Melnikov function of heteroclinic orbits deriving from the perturbed system eq.(73) is given by

$$\begin{aligned}M^{\pm}(\tau_0) &= \frac{\pi R_2'^2 V_0\ (1-\Gamma')}{\omega'\sqrt{\Gamma'^2-1}}\Big[\frac{b_0(m)\sin(2\tau_0)\sin\left(\frac{2}{\omega'}arc\cosh(-\Gamma')\right)}{\sinh\left(\frac{2\pi}{\omega'}\right)}\\ &+\frac{2b_1(m)\sin(4\tau_0)\sin\left(\frac{4}{\omega'}arc\cosh(-\Gamma')\right)}{\sinh\left(\frac{4\pi}{\omega'}\right)}+\frac{3b_2(m)\sin(6\tau_0)\sin\left(\frac{6}{\omega'}arc\cosh(-\Gamma')\right)}{\sinh\left(\frac{6\pi}{\omega'}\right)}\Big]+F.\end{aligned} \tag{132}$$

The derivation of F is given in Appendix C.

Recalling that one can neglect $b_1(m)$ and $b_2(m)$ in front of $b_0(m)$ the approximate condition for the occurrence of the heteroclinic chaos deduced from eq.(132) is given by the following expression.

$$\delta\geq\left|\frac{\omega'\sqrt{\frac{\Gamma'+1}{\Gamma'-1}}F\sinh\left(\frac{2\pi}{\omega'}\right)}{\pi R_2'^2\sin\left(\frac{2}{\omega'}arc\cosh(-\Gamma')\right)}\right|. \tag{133}$$

with $\delta=V_0b_0(m)$ the amplitude of the optical lattice potential in the case of approximations $b_1(m)<<b_0(m)$ and $b_2(m)<<b_0(m)$.

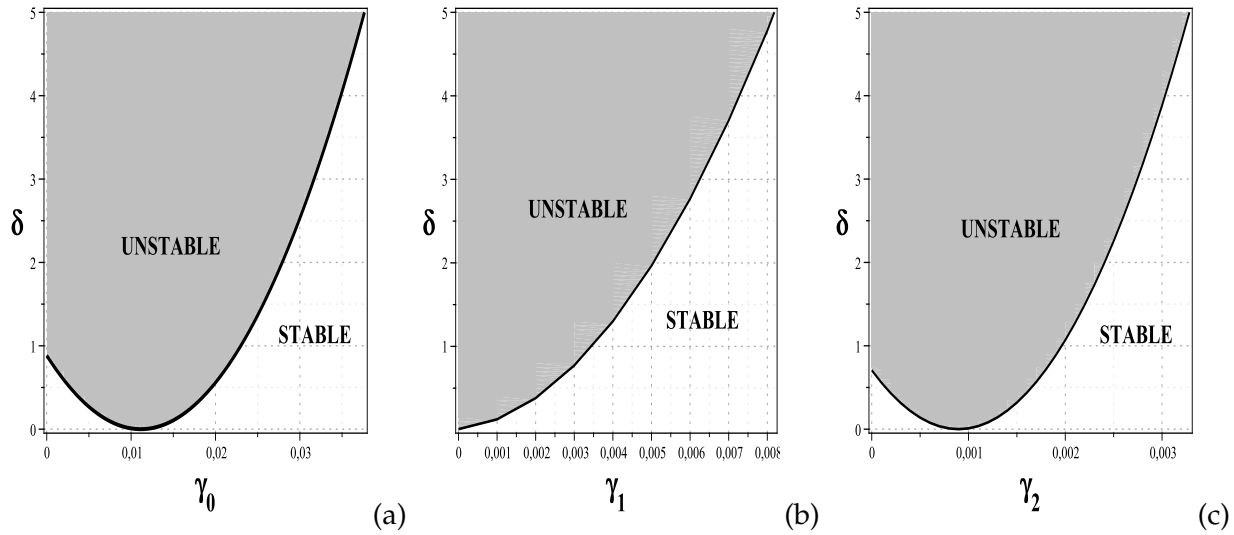

Figure 12: Stable and unstable zones in parameter space (γ_i, δ), (i=0,1,2) for homoclinic bifurcations. Modulated lattice potential depth δ versus (a) The feeding parameter γ_0 (b) The dipolar relaxation parameter γ_1 (c) The three-body recombination factor γ_2. The other parameters used are: a=2, $g_0 = -0.75$, $g_1 = 0.1$, $\gamma_0 = 10^{-2}$, $\gamma_1 = 10^{-5}$, $\gamma_2 = 10^{-3}$, $\tau_c = 4$.

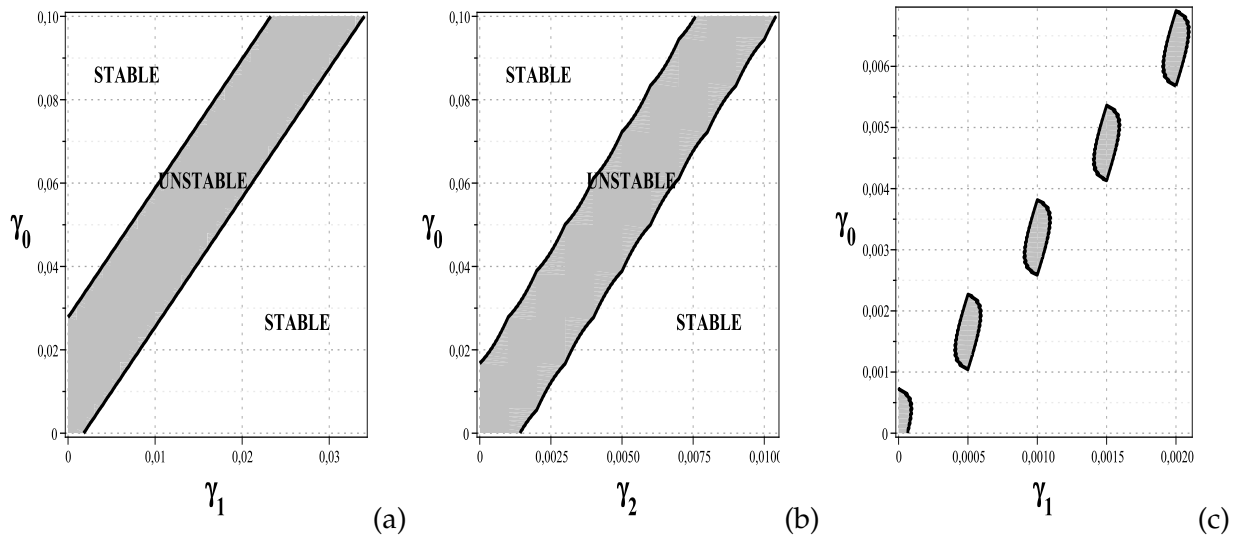

Figure 13: Stable and unstable zones in parameter space (γ_i, γ_j), (i=0,1,2) for homoclinic bifurcations (a) Feeding parameter versus the dipolar relaxation parameter for $\gamma_2 = 10^{-3}$ (b) Feeding parameter versus the three-body inelastic recombination factor for $\gamma_1 = 10^{-5}$ (c) Discrete unstable regions in parameter space (γ_1, γ_0) for $\gamma_2 = 10^{-5}$, $V_0 = 0.02$, $\tau_c = 5$. The other parameters used are: a=2, $g_0 = -0.75$, $g_1 = 0.1$, $m = 0.5$, $V_0 = 2$, $\tau_c = 4$

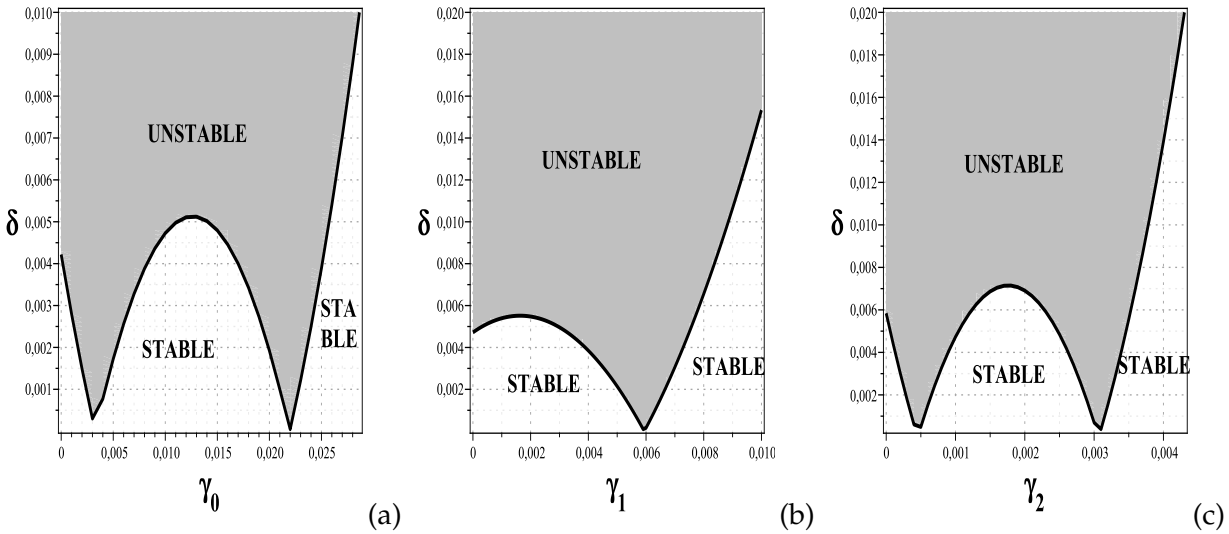

Figure 14: Unstable and stable zones in parameter space (γ_i, δ), (i=0,1,2) for heteroclinic bifurcations. Modulated lattice potential depth δ versus (a) Feeding parameter γ_0 (b) The dipolar relation parameter γ_1 (c) The three-body inelastic recombination factor γ_2. The other parameters used are: $a = 2$, $g_0 = -0.75$, $g_1 = 0.1$, $\gamma_0 = 10^{-2}$, $\gamma_1 = 10^{-5}$, $\gamma_2 = 10^{-3}$, $\tau_c = 4$, $\tau_i = 0.005$, $V_0 = 2$.

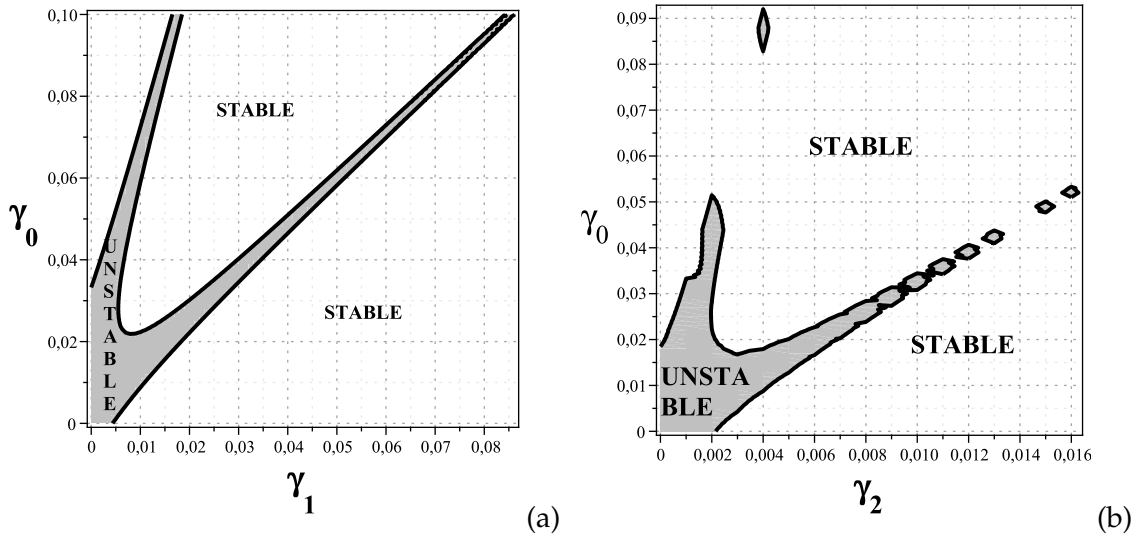

Figure 15: Unstable and stable zones in parameter space (γ_i, γ_j), i=0,1,2 for heteroclinic bifurcations (a) Feeding parameter versus the dipolar relation parameter for $\gamma_2 = 10^{-3}$ (b) Feeding parameter versus the three-body inelastic recombination factor for $\gamma_1 = 10^{-5}$. The other parameters used are: $a = 2$, $g_0 = -0.75$, $g_1 = 0.1$, $m = 0.5$, $\tau_c = 4$, $\tau_i = 0.005$, $V_0 = 2$.

II.6 Conclusion

In this chapter, the different methods used in this thesis are presented. Subsequently, the model considered (a damped condensate governed by the Gross-Pitaevskii-Ginzburg equation) is described, and an analytical treatment through the Melnikov method is made to predict the onsets of chaos in the dynamical behaviour of the condensate. Some zones of instability are plotted in different parameter spaces, and the study reveals that for a fixed number of atoms in the condensate, repulsive two-body and attractive three-body elastic collisions tend to increase the density and decrease the spatiotemporal extension of the condensate, while attractive two-body and repulsive three-body elastic collisions tend to increase the density and the spatiotemporal extension of the condensate.

CHAPTER III

RESULTS AND DISCUSSION

III.1 Introduction

The previous chapter has introduced five problems, and the aim of this chapter is to answer at these questions. The next sections are devoted to a comparative study between analytical and numerical investigations. Although we do not expect a perfect concordance between these two types of study, a comparison is nevertheless made, and the role of different parameters in the enhancement or annihilation of the chaotic behaviour of the condensate is established. In the first part of each section, we begin by the study of the condensate without inelastic collisions between atoms, inelastic collisions which will be subsequently considered in the second part.
In the first part of each section, excepted the control parameter, we give to parameters the values usually considered in experiments[156, 157]. The conditions of chaos occurrence obtained in the previous chapter are then used to determine if the control parameter enhances or annihilates the chaotic behaviour of the condensate. Subsequently, the critical value of the control parameter which in Melnikov's sense represents the beginning or the end of the instability in the dynamical behaviour of the condensate is determined. With the same set of parameters used in the analytical treatment, the numerical simulations start with the plot of the bifurcation diagram, with initial conditions taken at stable fixed points. Each bifurcation diagram combined with the corresponding curve of the largest Lyapunov exponent provide the critical value of the control parameter on the onset or at the end of the instability. A comparison of these two critical values of control parameter is made to verify the reliability of the analytical study, although we do not expect a perfect equality between them. In fact, the **MM** is a perturbative method, generally related to transient chaos, while bifurcation diagram provide information solely concerning steady chaos. In addition, some Poincaré sections, phase portraits, and basins of attraction are plotted to determine the transition route to chaos taken by each control parameter.
In the second part of these sections, the inelastic collisions between atoms are taken into account in the dynamical behaviour of the condensate. Once more, coupling analytical and numerical studies, the impacts of parameters related to inelastic collisions between atoms on the chaotic behaviour of the condensate are determined, and the results are compared with the findings of other authors, but with bosonic atoms trapped by a magnetic field and studied analytically by a variational approach.

III.2 Transitions to chaos in the dynamical behaviour of a BEC with repulsive two-body and attractive three-body interactions loaded into a moving optical Fourier-synthesized lattice

According to previous chapter, we will not forget that the system eq.(37) modeling the dynamics of the condensate exhibits only homoclinic orbits. To verify the reliability of the analytical study, we have performed computer simulations on the perturbed system eq.(37), using the fourth-order Runge-Kutta and Euler-Cromer methods defined in the previous chapter.

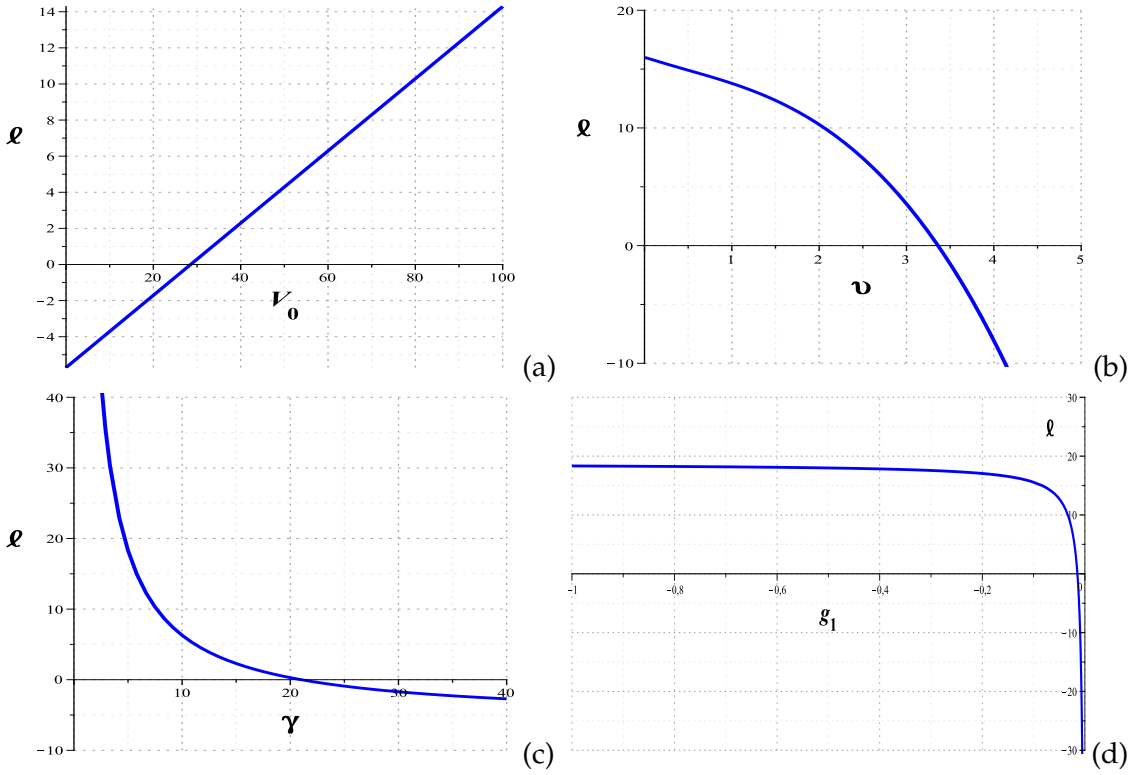

Figure 16: Plot of the threshold function of homoclinic chaos versus (a) The optical intensity V_0 (b) The velocity of the optical lattice υ, with $V_0 = 80$ (c) The damping parameter γ, with $V_0 = 120$ (d) The elastic three-body recombination factor g_1, with $V_0 = 120$. The other parameters used are: $\upsilon = 2$, $g_0 = 0.75$, $g_1 = -0.9$, $m = 0.8$, $\gamma = 5$.

III.2.1 Case of a BEC of atoms not subjected to inelastic collisions

a) Bifurcation responses with the optical lattice depth V_0 as control parameter

We give to parameters the values usually considered in experiments. Thus, we consider the following set of data: $g_0 = 0.75$, $g_1 = -0.9$, $\upsilon = 2$, $\gamma = 5$, $m = 0.8$, $\epsilon = 0.05$. It is clear on the Fig.16(a) deriving from the analytical prediction of the homoclinic chaos defined in eq.(68) that the critical value of the optical depth is $V_{0c} = 28.54$. According to this curve, the dynamics of the condensate will be regular for V_0 taken between 0 and 28.54, and chaotic for V_0 beyond 28.54.

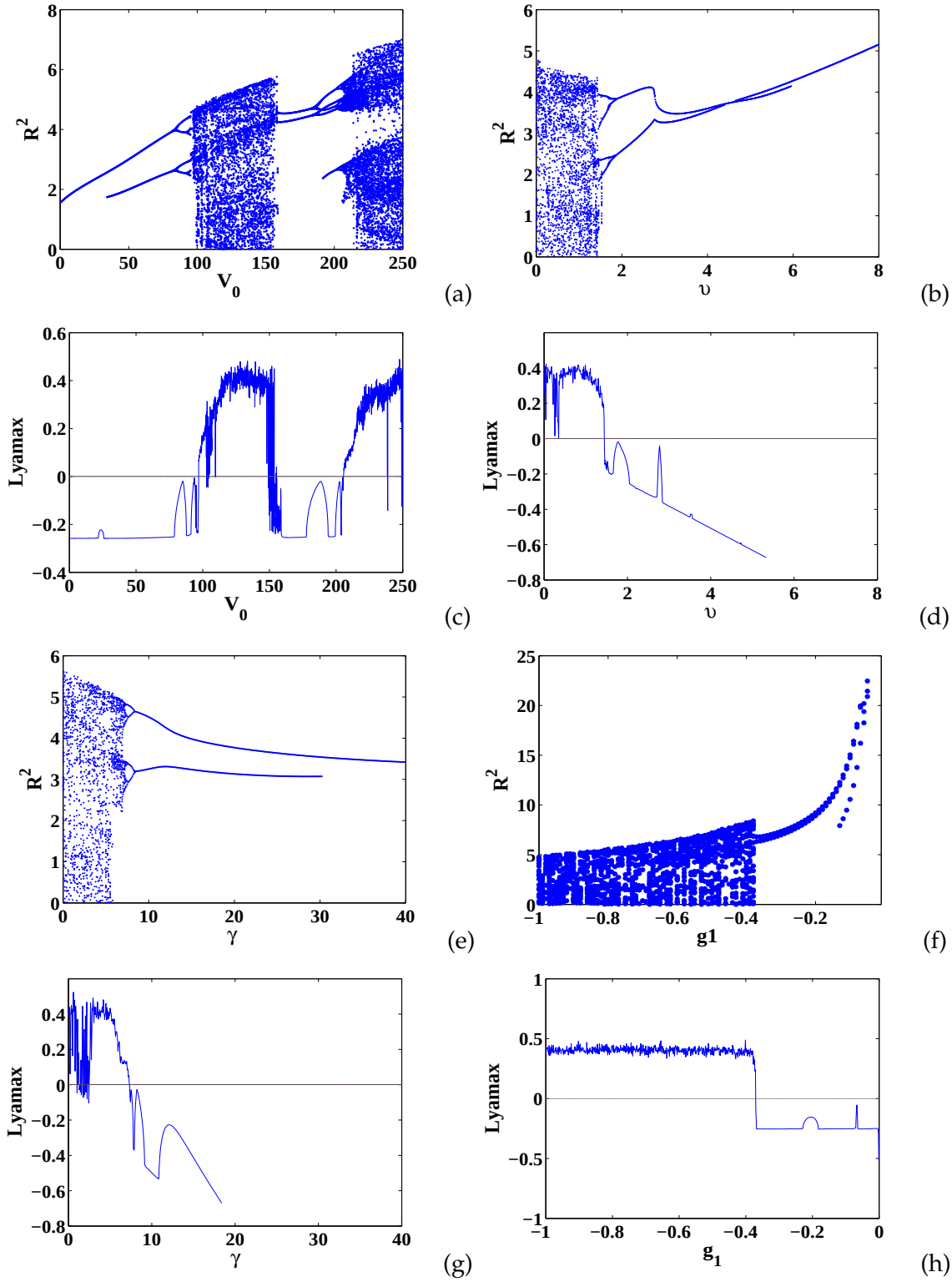

Figure 17: Bifurcation diagrams and corresponding Lyapunov exponents deduced from eq.(42) (a)-(c) The optical intensity V_0 as control parameter (b)-(d) The optical velocity υ as control parameter (e)-(g) The damping parameter γ as control parameter (f)-(h) The elastic three-body recombination factor as control parameter. The other parameters used are: $\upsilon = 2$, $g_0 = 0.75$, $g_1 = -0.9$, $\epsilon = 0.05$, $m = 0.8$, $\gamma = 5$, the initial conditions taken at the stable fixed point ($R = R_1 = 1.24503913$, $dR/d\tau = 0$).

Let's note that in Melnikov's sense, this critical value indicates the beginning of the instability and not the chaos. Visibly, this control parameter enhances the homoclinic chaos in the dynamical behaviour of the condensate. Subsequently, to verify the reliability of the analytical study, we plot with the same set of data the bifurcation diagram shown in Fig.17(a). It comes from this curve that the optical depth enhances really the chaos in the dynamics of the condensate as predicted by the **MM**.

Now, let's determine the transition route to chaos when the control parameter evolves. As the depth of the optical lattice is gradually increased, the fixed point $(R_1, 0)$ loses stability, giving birth to periodic oscillations of the condensate, as one can observe on the Poincaré section displayed in Fig.18(a) for $V_0 = 20$, which exhibits a point attractor. This result is confirmed with the corresponding phase portrait depicted in Fig.19(a) which exhibits a period-1 limit cycle. As the control parameter V_0 continues to evolve, around 34.2, a second bifurcation occurs, culminating in period-2 oscillations of the condensate, clearly visible on the bifurcation diagram, with the birth of another branch. It is the beginning of the instability in the dynamics of the condensate. The Poincaré section depicted in Fig.18(b) and the phase portrait shown in Fig.19(b) for $V_0 = 50$ exhibit two points attractors and a period-2 attractor respectively, confirming the result of the bifurcation diagram. By continuing to vary increasingly the control parameter, in the vicinity of $V_0 = 84.0$, each branch of the bifurcation diagram is separated into two branches, and the dynamics of the condensate undergoes another period doubling bifurcation, leading to period-4 oscillations, as clearly exhibited on the Poincaré section depicted in Fig.18(c) for $V_0 = 90$, which shows four point attractors, and on the phase portrait depicted in Fig.19(c) for $V_0 = 90$, which shows a period-4 attractor. From $V_0 = 84.0$, as the control parameter evolves, one observes on the bifurcation diagram that around $V_0 = 94.6$, the dynamics of the condensate undergoes another period doubling bifurcation leading to period-6 oscillations, as shown on the Poincaré section in Fig.18(d) which exhibits six point attractors, and on the phase portrait in Fig.19(d) which shows a period-6 attractor for $V_0 = 95$. From this bifurcation point($V_0 = 94.6$), as the control parameter evolves, in the vicinity of $V_0 = 96.9$, the bifurcation diagram becomes very messy, and the largest Lyapunov exponent plotted in Fig.17(c) crosses the V_0 axis and becomes a positive number. The dynamics of the condensate enters into an aperiodic regime, characterized by a symmetric strange attractor as Poincaré sections, as depicted in Fig.18(e) for $V_0 = 120$. In the corresponding phase portrait depicted in Fig.19(e), the phase orbits evolve in a finite region and exhibit confusion, which is the chaotic feature. In this range of control parameter, the dynamical behaviour of the condensate becomes unpredictable and the butterfly effect is present. This bifurcation diagram and the corresponding Lyapunov exponent present in the chaotic zone an open window of regular oscillations for V_0 between 155.40 and 205.60. From this study, we deduce that the transition route to homoclinic chaos is the period-doubling scenario. Now, let's examine the bifurcation points. The Feigenbaum numbers corresponding to these bifurcation points are $\delta_1 = \dfrac{84.0 - 34.2}{94.6 - 84.0} = 4.698113208$ and $\delta_2 = \dfrac{94.6 - 84.0}{96.9 - 94.6} = 4.608695652$. It is clear that the universality of chaos is recognized in this physical system.

According to numerical simulations, the instability of the condensate begins at $V_0 = 34.2$, the critical value of the control parameter. The gap of 16.54% as relative uncertainty between these

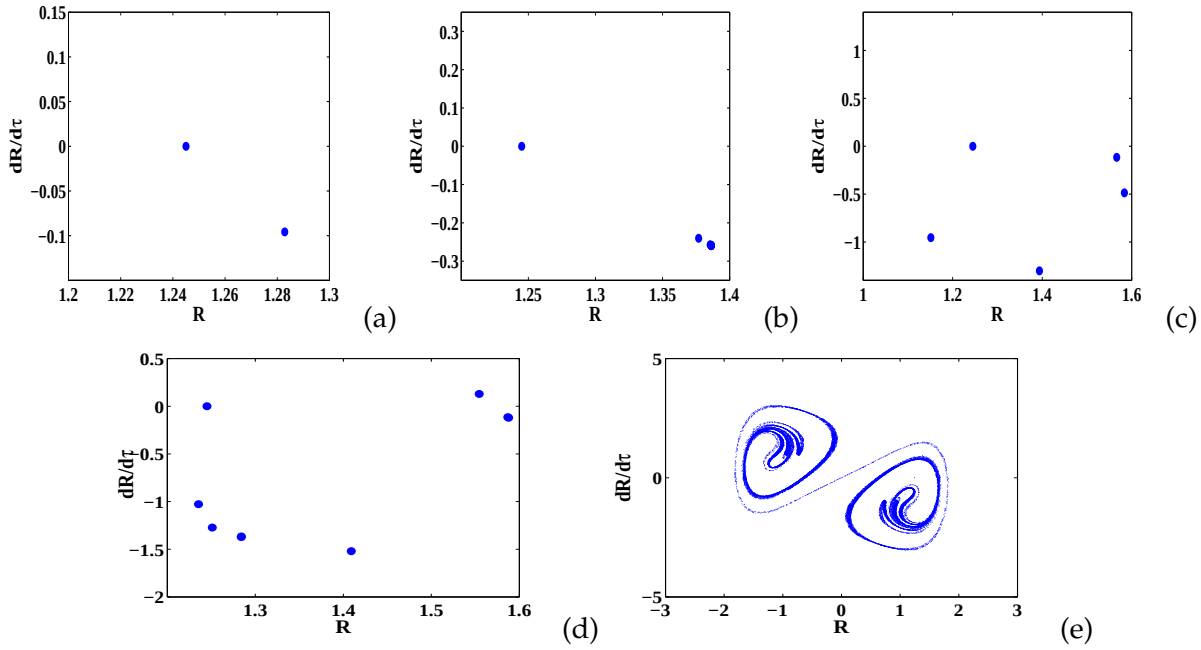

Figure 18: Poincaré sections deduced from eq.(42) with the optical depth V_0 as control parameter. (a) $V_0 = 20$ (b) $V_0 = 50$ (c) $V_0 = 90$ (d) $V_0 = 95$ (e) $V_0 = 120$. The other parameters used are: $\upsilon = 2$, $g_0 = 0.75$, $g_1 = -0.9$, $\epsilon = 0.05$, $m = 0.8$, $\gamma = 5$, the initial conditions taken at the stable fixed point ($R = R_1 = 1.24503913$, $dR/d\tau = 0$).

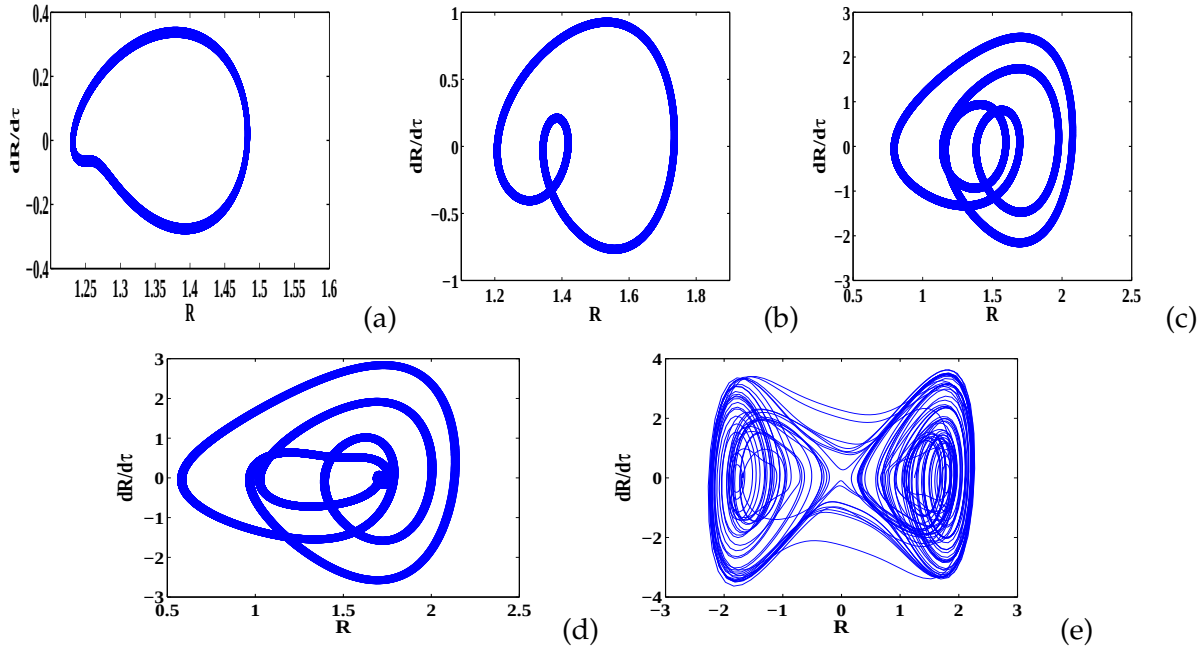

Figure 19: Phase portraits deduced from eq.(42) with the optical depth V_0 as control parameter. (a) $V_0 = 20$ (b) $V_0 = 50$ (c) $V_0 = 90$ (d) $V_0 = 95$ (e) $V_0 = 120$. The other parameters used are: $\upsilon = 2$, $g_0 = 0.75$, $g_1 = -0.9$, $\epsilon = 0.05$, $m = 0.8$, $\gamma = 5$, the initial conditions taken at the stable fixed point ($R = R_1 = 1.24503913$, $dR/d\tau = 0$).

values proves the reliability of our analytical analysis. Remembering that the **MM** is an approximate method, and moreover that some terms were neglected in the Melnikov function to solve analytically the problem, one can understand the gap between these two critical values.

To make sure that when the optical depth evolves the stability of the condensate is progressively

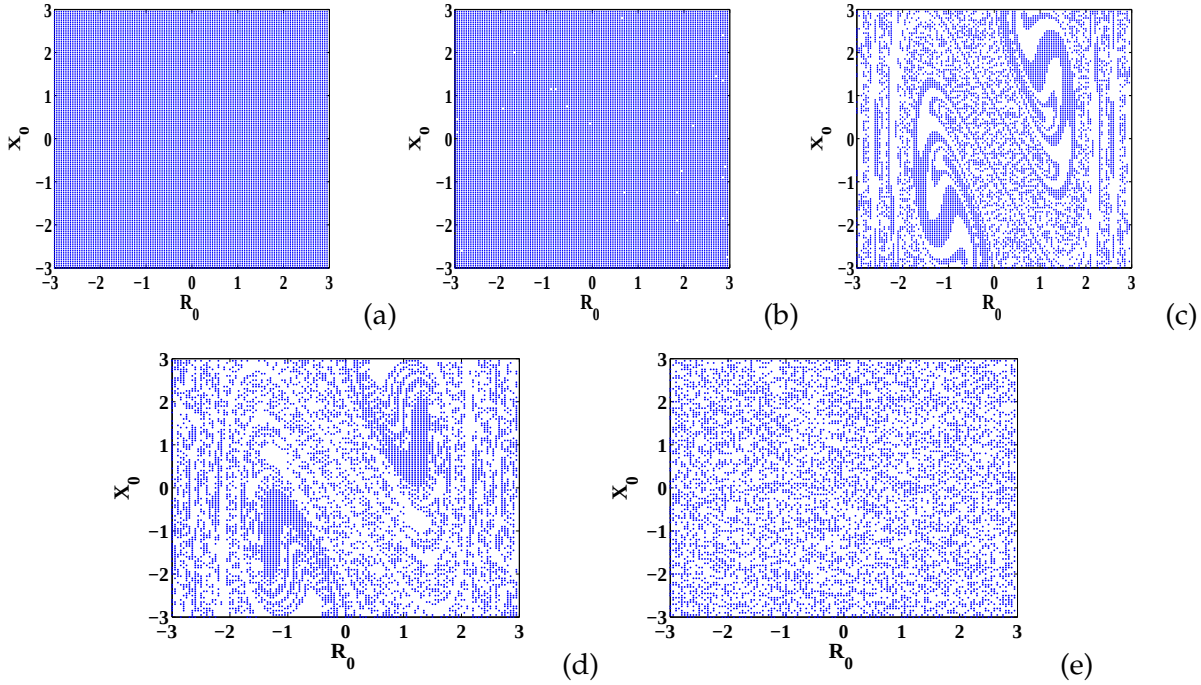

Figure 20: Basin of attraction deduced from eq.(42) with the optical depth V_0 as control parameter. (a) $V_0 = 20$ (b) $V_0 = 50$ (c) $V_0 = 90$ (d) $V_0 = 95$ (e) $V_0 = 120$. The other parameters used are: $\upsilon = 2$, $g_0 = 0.75$, $g_1 = -0.9$, $\epsilon = 0.05$, $m = 0.8$, $\gamma = 5$, the initial conditions taken at the stable fixed point ($R = R_1 = 1.24503913$, $dR/d\tau = 0$).

destroyed and leads to chaos, we study the effect of the optical depth on the basin of attraction. In fact, the basin of attraction is defined as a set of points taken as initial conditions, which are attracted to a fixed point or attracted to an invariant set. By using the same set of data considered to plot the bifurcation diagram, we perform a scan of the initial conditions in the phase space $(R, X = dR/d\tau)$ for various values of the optical depth V_0. One observes that when V_0 is less than the critical value obtained numerically, the basin of attraction is regular as shown in Fig.20(a) for $V_0 = 20$. When the optical depth V_0 is greater than the critical value, the regular shape of the basin of attraction is progressively destroyed and the fractal behaviour becomes more and more visible, as one can see on figures Fig.20(b) for $V_0 = 50$, Fig.20(c) for $V_0 = 90$ and on the Fig.20(d) for $V_0 = 95$. In Fig.20(e) corresponding to $V_0 = 120$, the chaotic state of the condensate is very visible, with the total destruction of the basin of attraction. It is worth noting that Fig.20 represents the basins of attraction of motion around the two fixed points $(-R_1, 0)$ and $(+R_1, 0)$ of potential well.

The spatiotemporal evolution of the condensate presented in Fig.(21) confirms the period-doubling scenario as transition route to homoclinic chaos when the optical depth V_0 evolves.

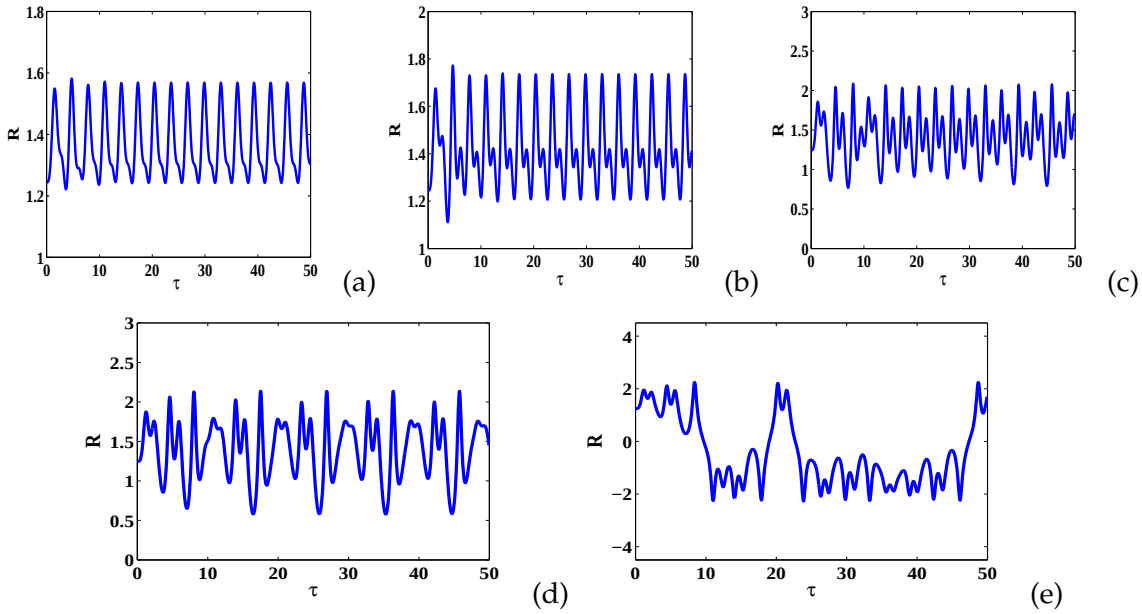

Figure 21: Spatiotemporal evolution of the condensate deduced from eq.(42) with the optical depth V_0 as control parameter. (a) periodic oscillations for $V_0 = 20$ (b) period-2 oscillations for $V_0 = 50$ (c) period-4 oscillations for $V_0 = 90$ (d) period-6 oscillations for $V_0 = 95$ (e) chaotic oscillations for $V_0 = 120$. The other parameters used are: $\upsilon = 2$, $g_0 = 0.75$, $g_1 = -0.9$, $\epsilon = 0.05$, $m = 0.8$, $\gamma = 5$, the initial conditions taken at the stable fixed point ($R = R_1 = 1.24503913$, $dR/d\tau = 0$).

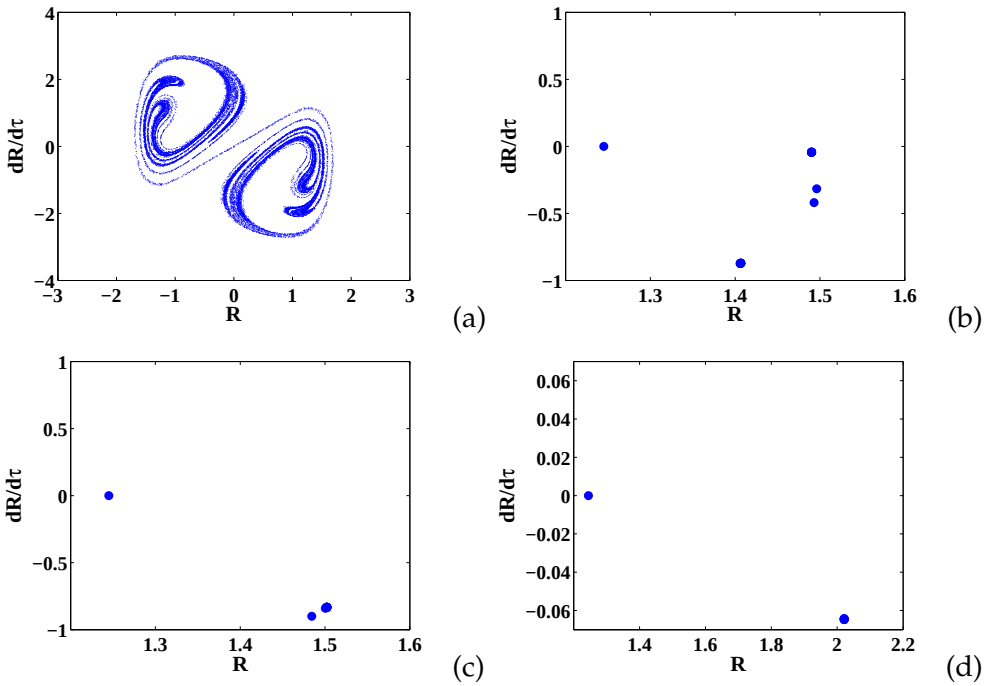

Figure 22: Poincaré sections deduced from eq.(42) with the velocity of the optical lattice υ as control parameter. (a) $\upsilon = 1$ (b) $\upsilon = 1.70$ (c) $\upsilon = 2$ (d) $\upsilon = 7$. The other parameters used are: $V_0 = 80$, $g_0 = 0.75$, $g_1 = -0.9$, $\epsilon = 0.05$, $m = 0.8$, $\gamma = 5$, the initial conditions taken at the stable fixed point ($R = R_1 = 1.24503913$, $dR/d\tau = 0$).

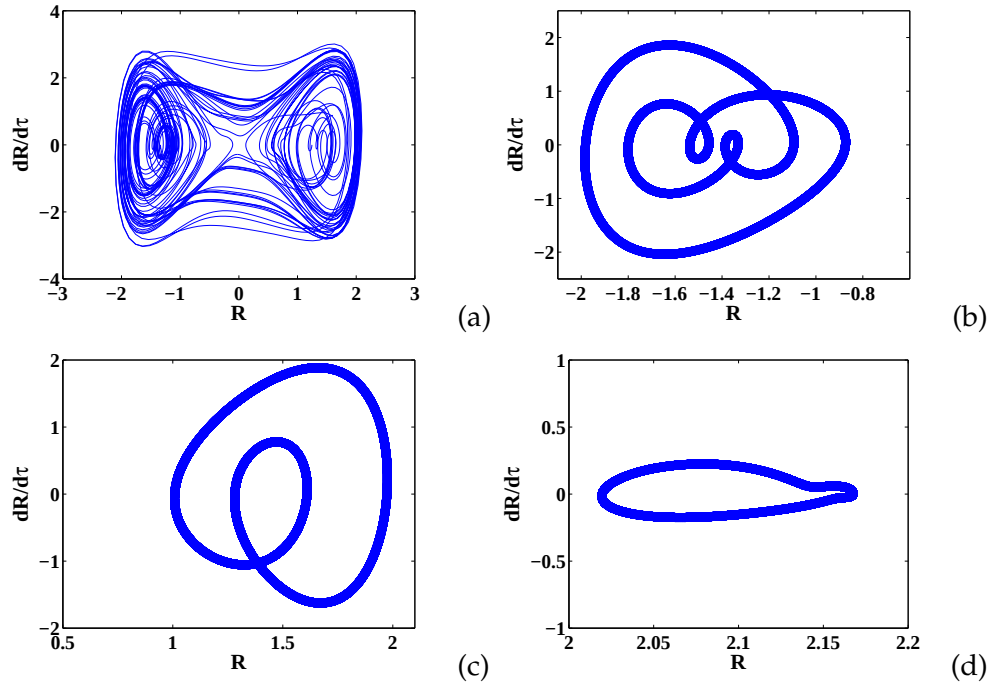

Figure 23: Phase portraits deduced from eq.(42) with the velocity of the optical lattice υ as control parameter. (a) $\upsilon = 1$ (b) $\upsilon = 1.70$ (c) $\upsilon = 2$ (d) $\upsilon = 7$. The other parameters used are: $V_0 = 80$, $g_0 = 0.75$, $g_1 = -0.9$, $\epsilon = 0.05$, $m = 0.8$, $\gamma = 5$, the initial conditions taken at the stable fixed point ($R = R_1 = 1.24503913$, $dR/d\tau = 0$.

b) Bifurcation responses with the velocity of the optical lattice υ as control parameter

In this paragraph, the velocity of the optical lattice υ is considered as control parameter. For the remaining parameters, we give the values: $m = 0.8$, $g_0 = 0.75$, $g_1 = -0.9$, $\gamma = 5$, $\epsilon = 0.05$, and $V_0 = 80$. The analytical prediction of homoclinic chaos defined in eq.(68) and plotted in Fig.16(b) indicates that the dynamics of the condensate will be chaotic for υ between 0 and 3.33, corresponding to positive values of the threshold function ℓ. This analytical study reveals that the velocity of the optical lattice annihilates the chaotic behaviour of the condensate when its values increase, and the critical value of the velocity is $\upsilon_c = 3.33$. Numerically, the bifurcation diagram and the largest Lyapunov exponent depicted in figures 17(b) and 17(d) respectively, reveal that the velocity of the optical lattice reduces the chaotic behaviour of the condensate when its values evolve.

Through the Poincaré sections and phase portraits, let's determine the transition route leading to regular oscillations. As the control parameter υ evolves, in the vicinity of 1.53 the chaotic dynamics (see Poincaré section and phase portrait plotted respectively in figures 22(a) and 23(a) for $\upsilon = 1$ which exhibit a symmetric strange attractor and erratic phase orbits respectively) of the condensate disappears, as indicates the largest Lyapunov exponent depicted in Fig.17(d) which becomes a negative number. The outcome of that is the birth of period-4 oscillations, as one can see through the Poincaré section and phase portrait plotted in figures 22(b) and 23(b) respectively, for $\upsilon = 1.70$. By continuing to increase the control parameter, close to 1.85, the

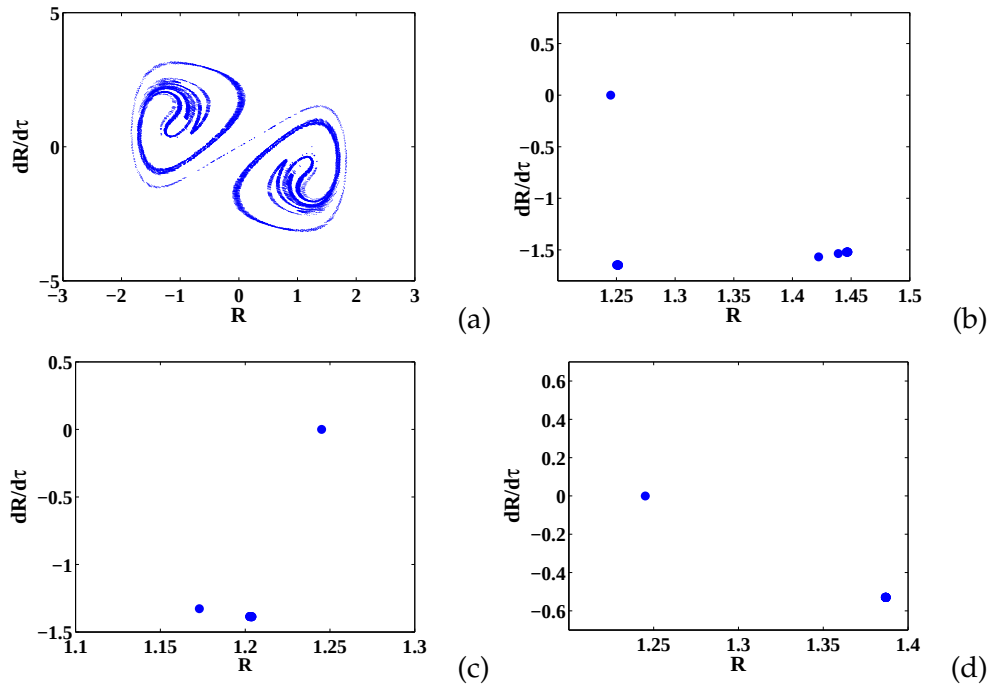

Figure 24: Poincaré sections deduced from eq.(42) with the dissipation parameter γ as control parameter. (a) $\gamma = 4$ (b) $\gamma = 8$ (c) $\gamma = 10$ (d) $\gamma = 35$. The other parameters used are: $V_0 = 120$, $g_0 = 0.75$, $g_1 = -0.9$, $\epsilon = 0.05$, $m = 0.8$, the initial conditions taken at the stable fixed point ($R = R_1 = 1.24503913$, $dR/d\tau = 0$).

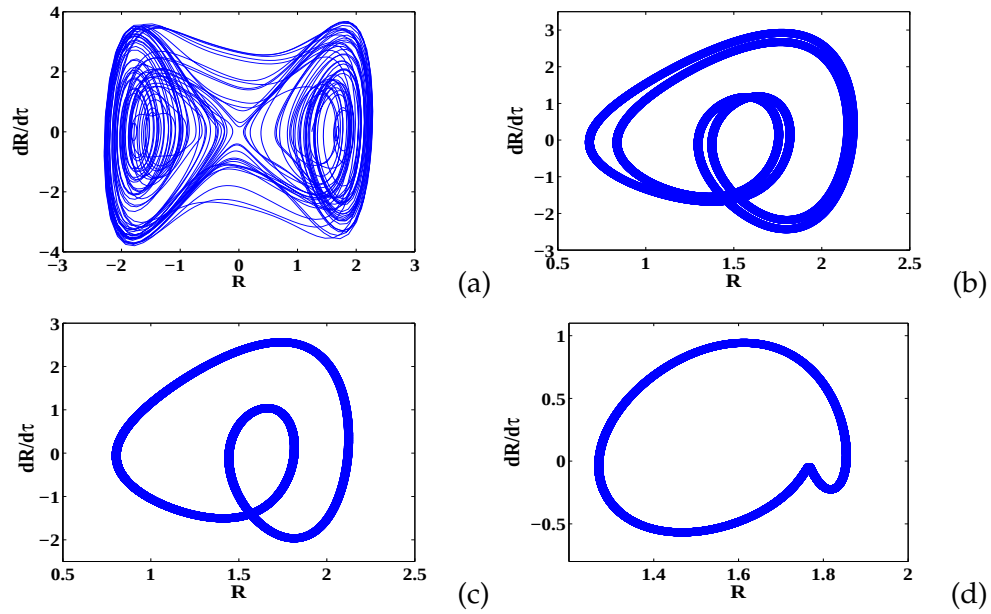

Figure 25: Phase portaits deduced from eq.(42) with the dissipation parameter γ as control parameter. (a) $\gamma = 4$ (b) $\gamma = 8$ (c) $\gamma = 10$ (d) $\gamma = 35$. The other parameters used are: $V_0 = 120$, $g_0 = 0.75$, $g_1 = -0.9$, $\epsilon = 0.05$, m=0.8, the initial conditions taken at the stable fixed point ($R = R_1 = 1.24503913$, $dR/d\tau = 0$).

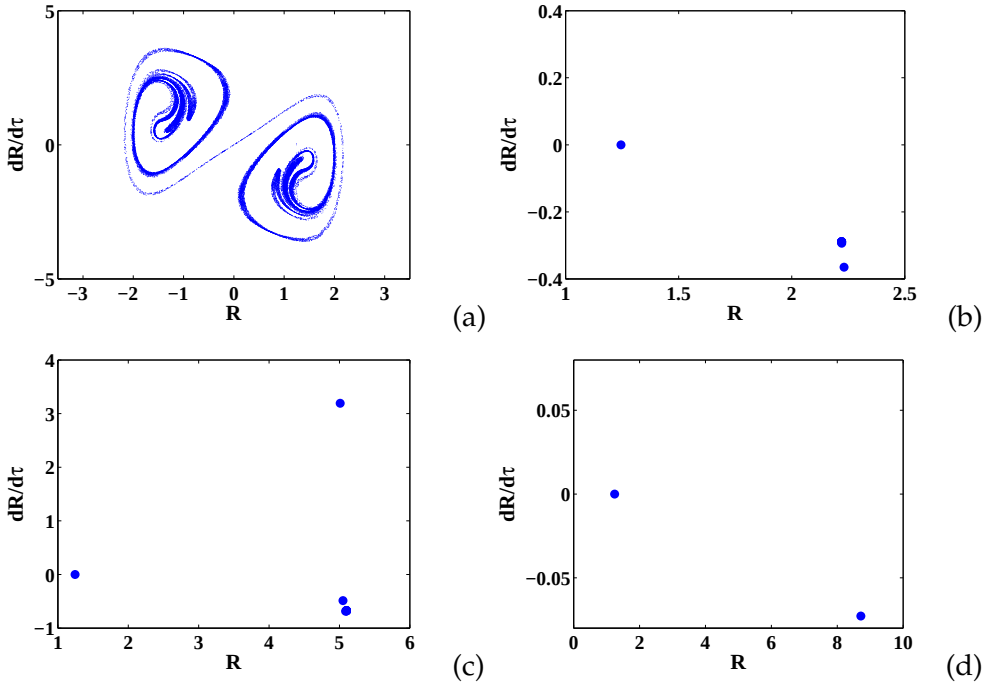

Figure 26: Poincaré sections deduced from eq.(42) with the strength of three-body elastic atom-atom interaction g_1 as control parameter. (a) $g_1 = -0.5$ (b) $g_1 = -0.2$ (c) $g_1 = -0.03$ (d) $g_1 = -0.01$. The other parameters used are: $V_0 = 120$, $g_0 = 0.75$, $\epsilon = 0.05$, $m = 0.8$, $\gamma = 5$, the initial conditions taken at the stable fixed point ($R = R_1 = 1.24503913$, $dR/d\tau = 0$).

dynamics of the condensate undergoes another period-doubling bifurcation, leading to period-2 oscillations, as one can see on the Poincré section and phase portrait depicted in figures 22(c) and 23(c) respectively, for $\upsilon = 2$. These period-2 oscillations of the condensate persist until the control parameter reaches the value 6.0, where another bifurcation leads the condensed atoms in a periodic regime as well visible on the Poincaré section and phase portrait shown in figures 22(d) and 23(d) respectively, for $\upsilon = 7$). This numerical study reveals that the critical value of the velocity of the optical lattice is 6.0. The gap of 44.5% between these two critical values can be explained as above. The study reveals that this gap decreases when the value of the optical depth increases. Once more, from chaotic oscillations, the transition route leading to regular oscillations is the period-doubling scenario.

c) Bifurcation responses with the dissipation parameter γ as control parameter

Here, we use as control parameter the dissipation coefficient γ, and for remaining parameters we give the values: $m = 0.8$, $g_0 = 0.75$, $g_1 = -0.9$, $\upsilon = 2$, $\epsilon = 0.05$, and $V_0 = 120$. The analytical prediction of homoclinic chaos defined in eq.(68) and plotted in Fig.16(c) reveals that the dynamics of condensed atoms will be chaotic for γ taken between 0 and 21.0, corresponding to positive values of the threshold function ℓ. The control parameter here annihilates or reduces the chaotic behaviour of the condensate, and the periodic oscillations are predicted around the critical value $\gamma_c = 21.0$. Subsequently, with the same set of data, we plot the bifurcation diagram

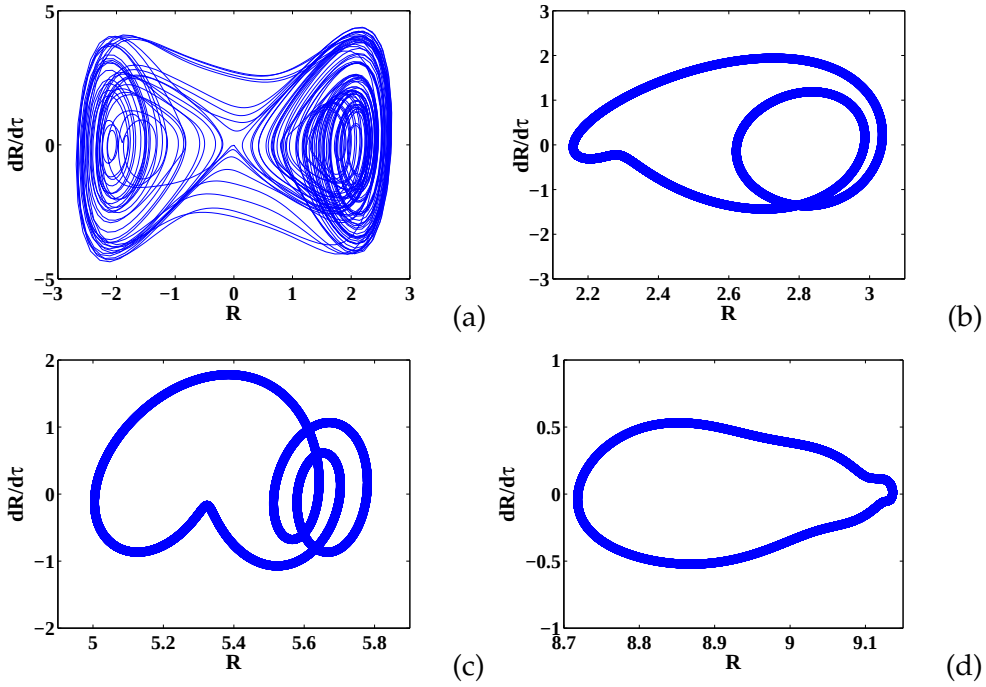

Figure 27: Phase portraits deduced from eq.(42) with the strength of three-body elastic atom-atom interaction g_1 as control parameter. (a) $g_1 = -0.5$ (b) $g_1 = -0.2$ (c) $g_1 = -0.03$ (d) $g_1 = -0.01$. The other parameters used are: $V_0 = 120$, $g_0 = 0.75$, $\epsilon = 0.05$, $m = 0.8$, $\gamma = 5$, the initial conditions taken at the stable fixed point ($R = R_1 = 1.24503913$, $dR/d\tau = 0$).

and the largest Lyapunov exponent, shown in figures 17(e) and 17(g) respectively. These curves confirm really that this control parameter reduces the chaotic behaviour of the condensate. For this set of data, as the control parameter γ evolves, the chaotic oscillations initially present(see the Poincaré section and the phase portrait plotted respectively in figures 24(a) and 25(a) for $\gamma = 4$) disappear around $\gamma = 7.50$, giving rise to period-4 oscillations as one can see on the Poincaré section in Fig.24(b) which exhibits four point attractors and on the phase portrait in Fig.25(b) which exhibits a period-4 attractor, for $\gamma = 8$. Beyond the first bifurcation point, in the vicinity of 8.30, the dynamics of condensed atoms undergoes another period-doubling bifurcation, culminating in period-2 oscillations. That can be observed on the Poincaré section and phase portrait plotted in figures 24(c) and 25(c) respectively, for $\gamma = 10$. The period-2 oscillations persist until the control parameter reaches the value 30.0, where the dynamics of the condensate bifurcates into a periodic regime, as clearly visible on the Poincaré section(a point attractor) and on the phase portrait(limit-1 cycle) depicted in figures 24(d) and 25(d) for $\gamma = 35$. Once again, the period-doubling scenario is the route leading to regular oscillations when the dissipation parameter evolves. The relative uncertainty between these critical values is 30%, and can be explained as above.

d) Bifurcation responses with the strength of three-body elastic atom-atom interaction as control parameter

We consider as control parameter the strength of three-body elastic atom-atom collisions assumed to be a negative number. In addition, we use the following set of data for remaining parameters: $m = 0.8$, $g_0 = 0.75$, $\gamma = 5$, $\upsilon = 2$, $\epsilon = 0.05$, and $V_0 = 120$. It comes from Fig.16(d) deriving from the analytical prediction of Melnikov's chaos given by eq.(68) that the dynamics of the condensate will be chaotic for g_1 under -0.0145. Therefore this control parameter reduces the chaotic behaviour of the condensate, and its critical value at the onset of regular oscillation is $g_{1c} = -0.0145$. The bifurcation diagram and the largest Lyapunov exponent depicted in figures 17(f) and 17(h) respectively, prove that the control parameter reduces really the chaotic behaviour of condensed atoms. These curves reveal that by increasing gradually the control parameter, the erratic oscillations are progressively annihilated, and the outcome of that are regular oscillations in the vicinity of -0.02.

Let's determine the regularization route leading to periodic oscillations. For g_1 between 0 and

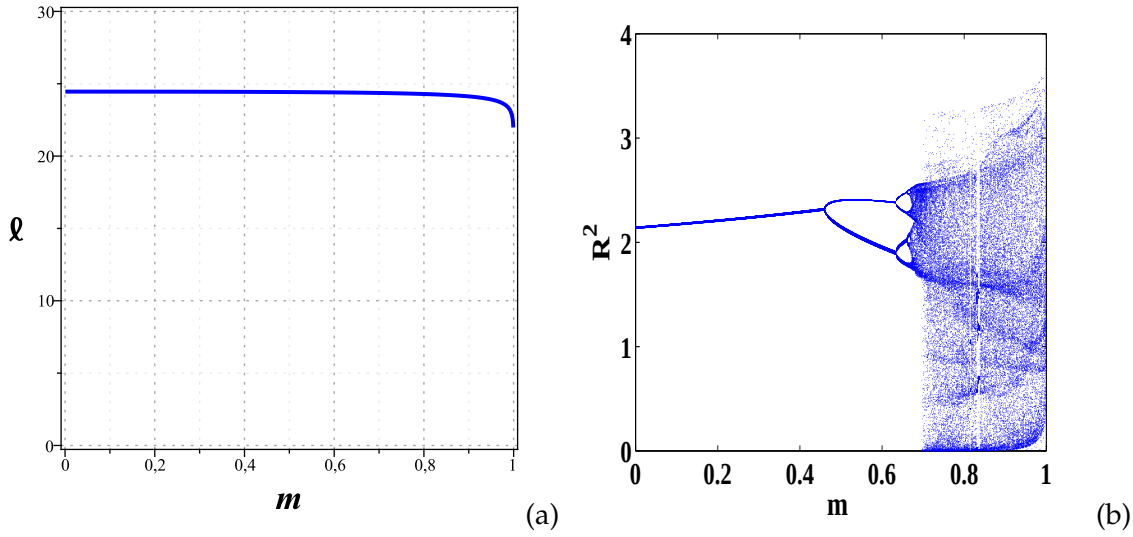

Figure 28: (a) Plot of the homoclinic threshold function of chaos occurrence versus the optical shape parameter m (b) Bifurcation diagram deduced from eq.(42) with the optical shape parameter m as control parameter. The other parameters used are: $\upsilon = 2$, $g_0 = 0.75$, $g_1 = -0.9$, $\epsilon = 0.03$, $V_0 = 150$, $\gamma = 5$, the initial conditions taken at the stable fixed point($R = R_1 = 1.24503913$, $dR/d\tau = 0$).

-0.38, the dynamics of the condensate is chaotic, as illustrated by the figures 26(a) and 27(a) for $g_1 = -0.5$, where the Poincaré section exhibits a strange attractor hallmark of chaotic oscillations, and the phase portrait exhibits erratic phase orbits located in a finite region. As the control parameter evolves, in the vicinity of $g_1 = -0.38$, the dynamics of the condensate undergoes a period-doubling bifurcation and culminates in a period-2 oscillations regime as one can observe in figures 26(b) and 27(b) for $g_1 = -0.2$, with two points attractor as Poincaré section. By continuing to increase the control parameter, this period-2 attractor undergoes another bifurcation when its value reaches -0.13, leading to a period-3 attractor as illustrated in figures 26(c)(three

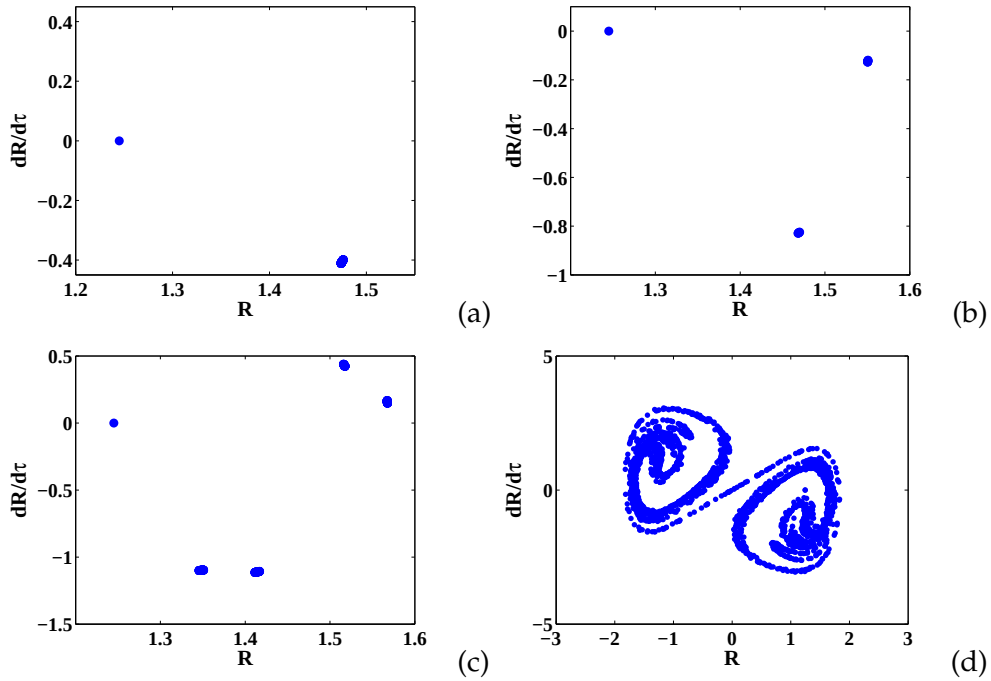

Figure 29: Poincaré sections deduced from eq.(42) with the shape parameter m as control parameter. (a) $m = 0.1$ (b) $m = 0.5$ (c) $m = 0.65$ (d) $m = 0.9$. The other parameters used are: $V_0 = 150$, $g_0 = 0.75$, $\epsilon = 0.03$, $g_1 = -0.9$, $\gamma = 5$, the initial conditions taken at the stable fixed point ($R = R_1 = 1.24503913$, $dR/d\tau = 0$).

points attractor) and 27(c) for $g_1 = -0.03$. By continuing to vary gradually the control parameter, the regular or periodic regime appear around -0.02, as one can observe on the following Poincaré section and phase portrait shown in figures 26(d) and 27(d) respectively, for $g_1 = -0.01$. Once more, the period-doubling scenario is the route governing the transition to homoclinic chaos. The relative uncertainty between the two critical values is 27.50%.

e) Bifurcation responses with the optical lattice shape m as control parameter

Here, as above, the data used are: $g_0 = 0.75$, $g_1 = -0.9$, $\upsilon = 2$, $\gamma = 5$. To ϵ and V_0 we give the values 0.03 and 150 respectively. The figure 28(a) deriving from the analytical prediction of homoclinic chaos defined in eq.(68) shows that for this set of parameters, the threshold function ℓ is always positive for all values of the shape parameter m. According to the **MM** which predicts the beginning or the end of the instability, the dynamics of the condensate is always chaotic. In Melnikov's sense, it means that there is no periodic oscillations in the dynamical behaviour of the condensate. On the bifurcation diagram plot in Fig.28(b), this information is not well visible, because the two branches of this diagram are very close for small values of the shape parameter m. On contrary, on the Poincaré section and phase portrait depicted in figures 29(a) and 30(a) for m=0.1, it is clear that the dynamics of condensed atoms exhibits period-2 oscillations. The depth analysis of Poincaré sections and phase portraits reveals that for very weak values of the shape parameter m, the dynamics of the condensate always exhibits period-2 oscillations with

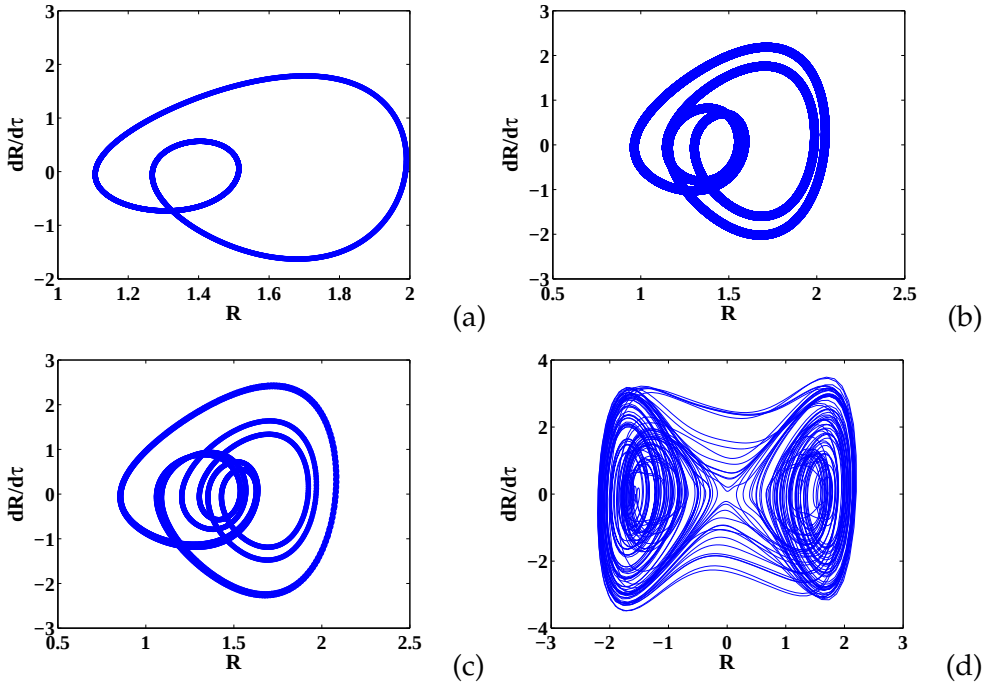

Figure 30: Phase portraits deduced from eq.(42) with the shape parameter m as control parameter. (a) $m = 0.1$ (b) $m = 0.5$ (c) $m = 0.65$ (d) $m = 0.9$. The other parameters used are: $V_0 = 150$, $g_0 = 0.75$, $\epsilon = 0.03$, $g_1 = -0.9$, $\gamma = 5$, the initial conditions taken at the stable fixed point ($R = R_1 = 1.24503913$, $dR/d\tau = 0$).

two points attractor very close. This result is in perfect accord with the analytical prediction which reveals no periodic oscillations. Let's determine the transition route to homoclinic chaos. As the control parameter evolves, the period-2 oscillations persist until the control parameter m reaches the value 0.465 where the dynamics of the condensate bifurcates in period-4 oscillations, as one can see on the Poincaré section and phase portrait depicted in figures 29(b) and 30(b) respectively, for m=0.5. Once again, the four points attractor are two by two paired. As the control parameter m continues to evolve, in the vicinity of 0.638 the dynamics of the condensate culminates in period-8 oscillations, as quite visible on the Poincaré section and phase portrait depicted in figures 29(c)and 30(c) respectively, for m=0.65. This Poincaré section seems to exhibit four points attractor instead of eight points attractor. In fact, after the transient regime has disappeared, the phase orbits are two by two very close. That justifies why these points attractor are two by two paired. By continuing to vary increasingly the control parameter, close to 0.675 the dynamical behaviour of the condensate enters in an aperiodic regime, as quite visible on the Poincaré section which exhibits a symmetric strange attractor, hallmark of chaotic oscillations. The dynamics of the condensate is then very sensitive to initial conditions. The analysis of bifurcation points obtained numerically reveals once again the universality of chaos through the Feigenbaum number given here by $\delta_1 = \dfrac{0.638 - 0.465}{0.675 - 0.638} = 4.675675676.$

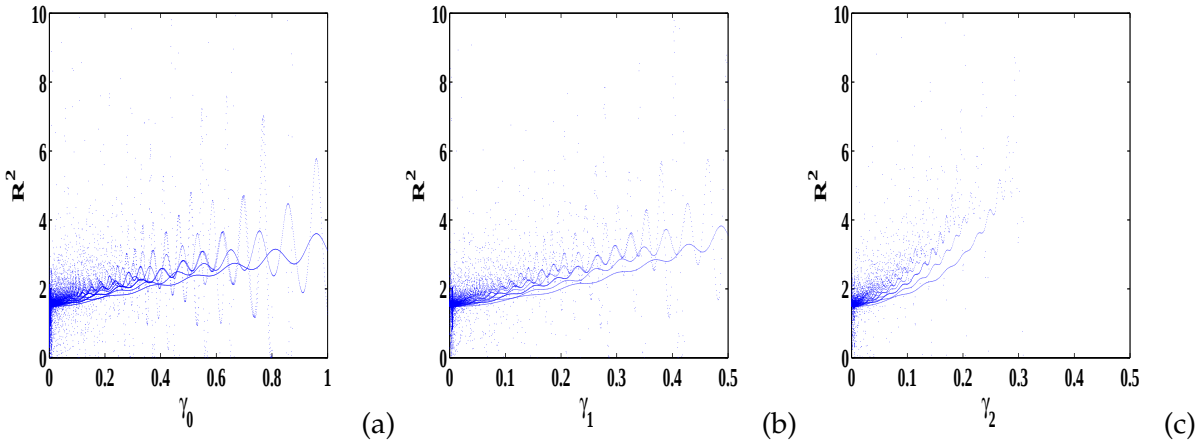

Figure 31: Bifurcation diagrams deduced from eq(69). (a) The feeding rate γ_0 as control parameter with $\gamma_1 = 10^{-4}$, $\gamma_2 = 10^{-3}$ (b) The parameter of dipolar relaxation γ_1 as control parameter with $\gamma_0 = 10^{-2}$, $\gamma_2 = 10^{-3}$ (c) The three-body inelastic recombination factor γ_2 as control parameter with $\gamma_0 = 10^{-2}$, $\gamma_1 = 10^{-4}$. The other parameters used are: $V_0 = 2$, $\upsilon = 0.0001$, $\alpha = 0$, $\beta = 1$, $g_0 = -0.75$, $g_1 = 0.1$, m=0.8, $\epsilon = 0.05$, the initial conditions taken at the stable fixed point ($R = R_1^{'} = 1.24503913$, $dR/d\tau = 0$).

III.2.2 Case of a BEC of atoms subjected to inelastic collisions

This subsection is planned as follows. Firstly, we analyze thoroughly the analytical condition for apparition of chaotic oscillations in the dynamics of condensed atoms obtained in eq.(83).
Secondly, our analytical results are compared to numerical simulations(Bifurcation diagrams and Poincaré sections).
Thirdly, to verify the reliability of our investigations, we compare our results with those of references [22, 24, 25, 26] in which the condensate was studied by a variational approach.
From eq.(83), via Maple software, some regions of instability are plotted in parameter space, as shown in figures (7) and (8). For each parameter space, we take a point inside of the unstable and stable zones, and we plot the corresponding Poincaré sections to verify the analytical predictions. The aim of our study being the impact of inelastic processes (atomic pumping and inelastic collisions) on the dynamical behaviour of condensed atoms, we focus our attention on the cases in which the instability regions in parameter space (γ_i, γ_j) have approximately linear boundaries, and we attempt to find a connection between parameters related to inelastic collisions between bosonic atoms and atomic feeding for the occurrence of chaotic oscillations.
Let's consider the Fig.7(a) in parameter space (γ_0, δ). The point with components $(\gamma_0 = 0.002, \delta = 1)$ is inside of the unstable zone coloured in gray. With these parameters, the Poincaré section depicted in Fig.32(a) exhibits a strange attractor, hallmark of chaotic oscillations of the condensate. On the contrary, the point $(\gamma_0 = 0.01, \delta = 0.1)$ is outside of the unstable region. The corresponding Poincaré section depicted in Fig.32(b) shows a set of five points attractor, characterizing the period-5 limit cycle in phase space. The deep analysis of Poincaré sections reveals that, when one increases the parameter related to atomic feeding γ_0 while δ is kept constant, the number of points characterizing the Poincaré sections decreases progressively. The periodic oscillations

are finally obtained for very large values of γ_0. This result is also quite visible on the bifurcation diagram shown in Fig.31(a). For fixed values of optical depth, as the feeding parameter evolves, from chaotic oscillations the dynamics of the condensate undergoes a period-doubling cascade culminating in periodic oscillations.

By continuing with the parameter space (γ_i, γ_j), and particularly in the parameter space (γ_2, γ_0),

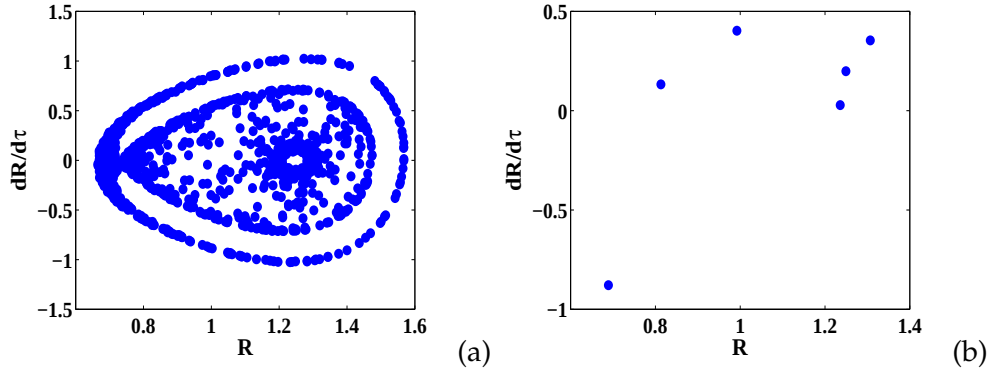

Figure 32: Poincaré sections deriving from eq.(69). (a) The point $(\gamma_0 = 0.002, \delta = 1)$ taken inside the unstable zone (b) The point $(\gamma_0 = 0.01, \delta = 0.1)$ taken inside the stable zone . The other parameters used are: $g_0 = 0.75$, $g_1 = -0.9$, $\upsilon = 0.0001$, $m = 0.8$, $\alpha = 0$, $\beta = 1$, $\gamma_1 = 10^{-4}$, $\gamma_2 = 10^{-3}$, $\epsilon = 0.05$. Initial conditions $(R = R_1^{'} = 1.24503913, dR/d\tau = 0)$.

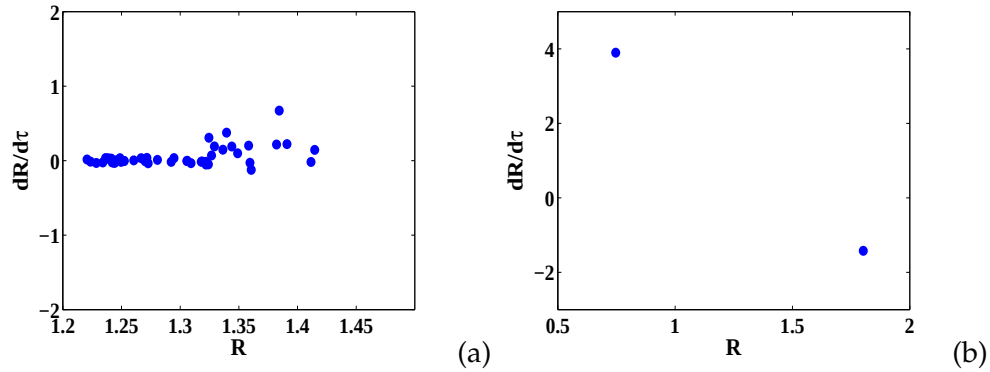

Figure 33: Poincaré sections deriving from eq.(69). (a) The point $(\gamma_2 = 0.03, \gamma_0 = 0.04)$ taken inside the unstable zone (b) The point $(\gamma_2 = 0.07, \gamma_0 = 0.04)$ taken inside the stable zone . The other parameters used are: $g_0 = 0.75$, $g_1 = -0.9$, $V_0 = 2$, $m = 0.8$, $\upsilon = 0.0001$, $\alpha = 0$, $\beta = 1$, $\gamma_1 = 10^{-4}$, $\gamma_2 = 10^{-3}$, $\epsilon = 0.05$. Initial conditions $(R = R_1^{'} = 1.24503913, dR/d\tau = 0)$.

reasoning as above, the point with coordinates $(\gamma_2 = 0.03, \gamma_0 = 0.04)$ is inside of the unstable region coloured in gray. The Poncaré section depicted in Fig.33(a) exhibits a set of points randomly confined in a finite region, characterizing a chaotic regime. by using the same set of data, and taking the point with coordinates $(\gamma_2 = 0.07, \gamma_0 = 0.04)$ which is outside of the zone of instability, after the transient regime had died out, the Poincaré section plotted in Fig.33(b) exhibits a set of two point attractors, signature in phase space of a period-2 limit cycle. It comes from Fig.31 that, for fixed values of optical depth and feeding parameter, as parameters related to inelastic

collisions between bosonic atoms evolve, the regularization route is ensured.
Furthermore, with the remark that the curves delimiting the unstable region given by $-0.0060 \leq \gamma_0 - 1.35\gamma_2 \leq 0.0070$ in parameter space (γ_2, γ_0) and $-0.0050 \leq \gamma_0 - 1.58\gamma_1 \leq 0.0085$ in parameter space (γ_1, γ_0) are approximately linear, we can deduce the following quotients between these parameters for the occurrence of chaotic oscillations. $\frac{\gamma_0}{\gamma_2} = 1.35$ and $\frac{\gamma_0}{\gamma_1} = 1.58$. These ratios indicate that the parameters related to atomic feeding, dipolar relaxation and three-body inelastic collisions must be approximately in the same order for the occurrence of homoclinic chaos in the dynamical behaviour of the condensate.

III.3 Transitions to chaos in the dynamics of a BEC with attractive two-body and repulsive three-body interactions loaded into a moving optical Fourier-synthesized lattice

III.3.1 Case of a BEC of atoms not subjected to inelastic collisions

In this subsection, through the fourth-order Runge-Kutta and Euler-Cromer methods, we perform computer simulations on the perturbed system eq.(42) firstly, to verify the reliability of the analytical study, and secondly to determine the transition route to chaos.

III.3.1.1. Bifurcation responses of homoclinic trajectories

The initial conditions used in this subsection are taken at the stable fixed point (R_1,0). We eliminate the transient regime so that the fixed point considered as initial conditions don't appear in Poincaré sections. Such was not the case in the previous section. Furthermore, to ϵ we give the value 0.01.

a) Bifurcation responses with the depth V_0 of the optical lattice as control parameter

We use the following experimental set of data: $g_0 = -0.75$, $g_1 = 0.1$, $\upsilon = 1.5$, $\gamma = 0.05$ and $m = 0.5$. It comes from the condition for apparition of homoclinic chaos expressed in eq.(105) and depicted in Fig.34(a) that, the threshold function $\rho(V_0, m, \upsilon, \gamma, g_1)$ versus the depth of the optical lattice is positive for V_0 beyond 0.2618. It is clear that this control parameter enhances the dynamical behaviour of the condensate. In Melnikov's sense, the critical value $V_{0c} = 0.2618$ of the control parameter indicates the beginning of the instability in the dynamics of condensed atoms.
Let's verify this analytical prediction by numerical simulations. The bifurcation diagram and the largest Lyapunov exponent depicted in figures 35(a) and 35(c) indicate really that the chaos is enhanced in the dynamics of the condensate as predicted by the analytical study. Let's determine the transition route leading to chaotic oscillations. As the control parameter evolves, the point attractor (R_1,0) loses stability via a supercritical Hopf bifurcation, resulting in a periodic attractor. The outcome of that is the birth of periodic oscillations around the fixed point(R_1,0), as illustrated in Fig.36(a) with a point attractor as Poincaré section and in Fig.37(a) with a closed

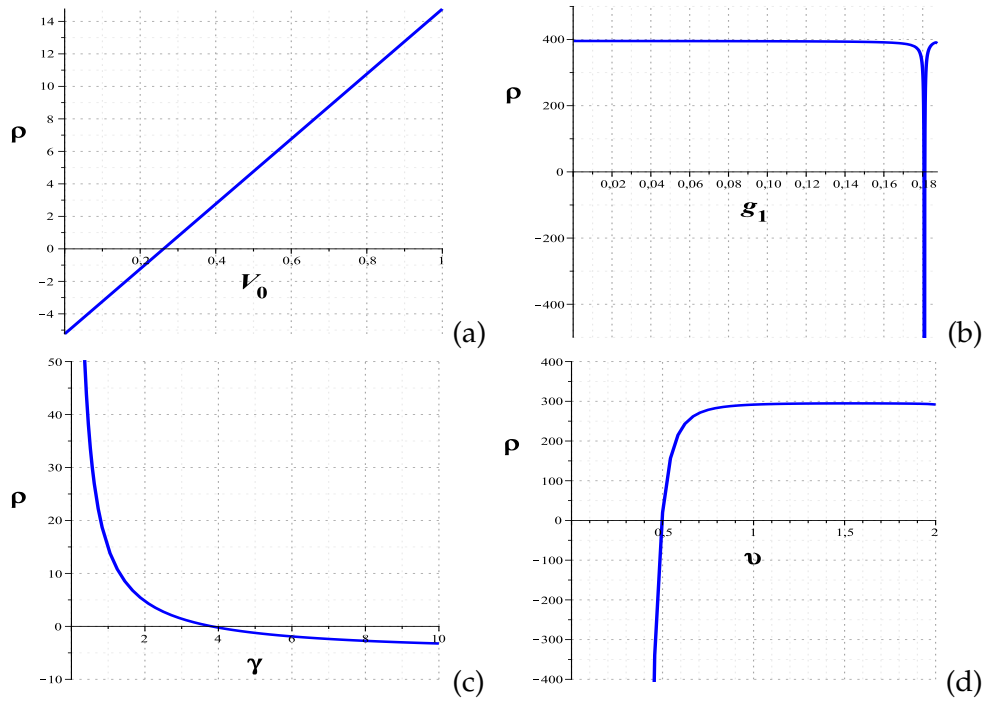

Figure 34: Plot of the homoclinic threshold function $\rho(V_0, m, \upsilon, \gamma, g_1)$ of chaos occurrence versus (a) The optical intensity V_0 (b) The elastic three-body recombination factor g_1, with $V_0 = 20$ (c) The damping parameter γ, with $V_0 = 20$ (d) The velocity of the optical lattice υ, with $V_0 = 15$. The other parameters used are: $\upsilon = 1.5$, $g_0 = -0.75$, $g_1 = 0.1$, $m = 0.5$, $\gamma = 0.05$.

curve as phase portrait. By continuing to vary increasingly the control parameter, in the vicinity of $V_0 = 0.50$, this periodic attractor undergoes a secondary supercritical Hopf bifurcation or a Neimark bifurcation, characterized by the birth of a second frequency incommensurate with the former one. The outcome of that is the birth of two-period quasi-periodic oscillations, as one can see on the Poincaré section depicted in Fig.36(b) which exhibits a closed curve and on the phase portrait depicted in Fig.37(b) which exhibits a quasi-periodic attractor. As the control parameter is gradually increased, around $V_0 = 1.35$ via another Hopf bifurcation, the dynamics of the condensate bifurcates into period-2 oscillations, as one sees on the Poincaré section plotted in Fig.36(c), which exhibits two points attractor, and on the phase portrait depicted in Fig.37(c) which exhibits a period-2 attractor. These period-2 oscillations persist as the control parameter evolves until the vicinity of $V_0 = 1.55$, where another Hopf bifurcation leads the condensate into another quasi-periodic regime, but with two loops as Poincaré section, as shown in Fig.36(d-e) and in phase portraits displayed in Fig.37(d-e) which exhibit quasi-periodic attractors. By continuing to increase gradually the control parameter, the quasi-periodic oscillations persist until its value approaches $V_0 = 13.95$, where the largest Lyapunov exponent depicted in Fig.35(c) crosses the V_0 axis, and becomes a positive number. At this bifurcation point, another Hopf bifurcation leads the condensate to chaos, as quite visible on the Poincaré section depicted in Fig.36(e) which exhibits a symmetric strange attractor, hallmark of a chaotic dynamics. The phase portrait shown in Fig.37(e) presents erratic phase orbits confined randomly in a finite region. The behaviour of

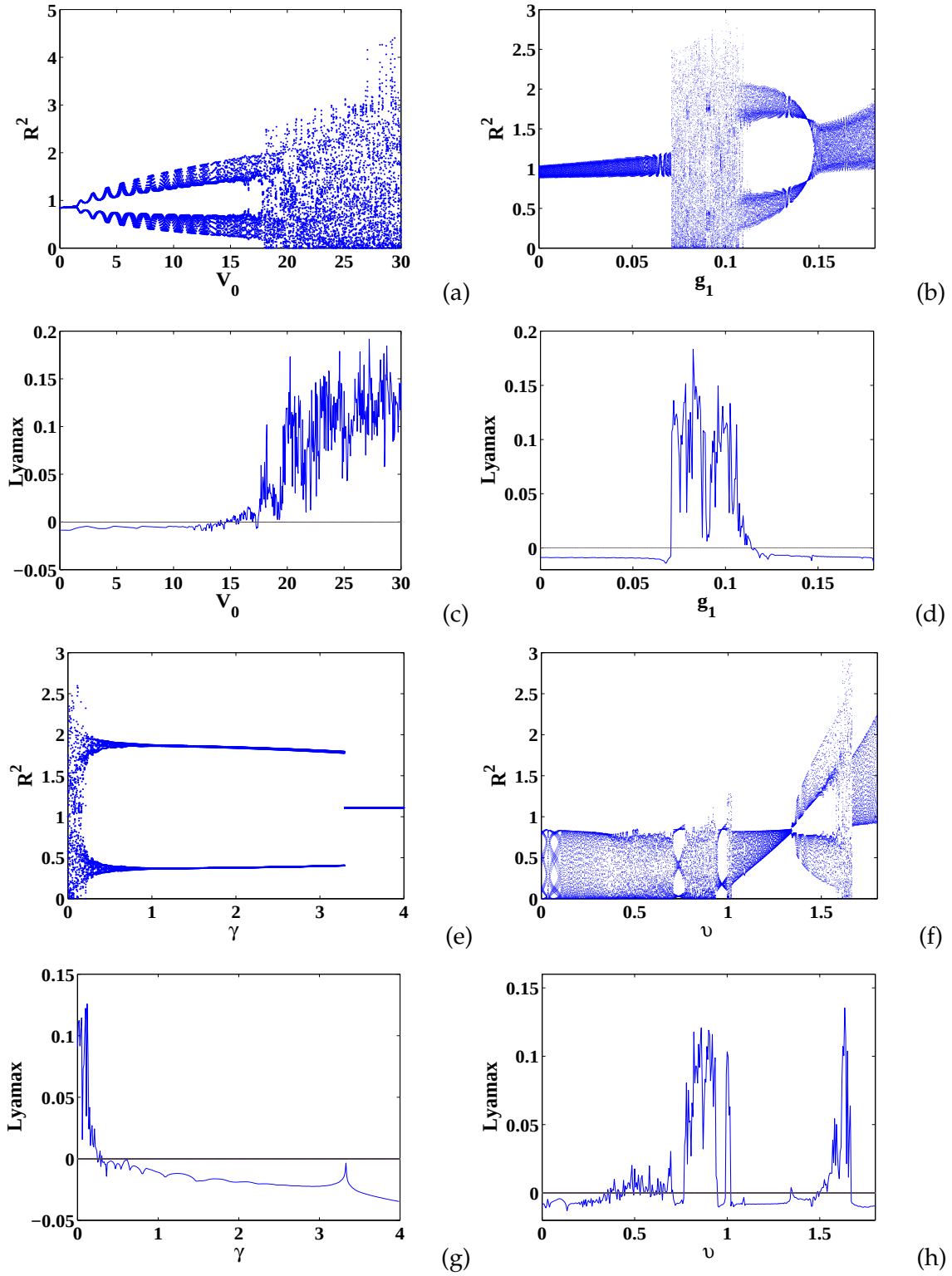

Figure 35: Bifurcation diagrams and corresponding Lyapunov exponents of homoclinic bifurcations, deduced from eq.(42) (a)-(c) The optical intensity V_0 as control parameter (b)-(d) The elastic three-body recombination factor as control parameter (e)-(g) The damping parameter γ as control parameter (f)-(h) The optical velocity υ as control parameter . The other parameters used are: $\upsilon = 1.5$, $g_0 = -0.75$, $g_1 = 0.1$, $\epsilon = 0.01$, $m = 0.5$, $\gamma = 0.05$, the initial conditions taken at the stable fixed point ($R = R_1 = 0.9193815805$, $dR/d\tau = 0$).

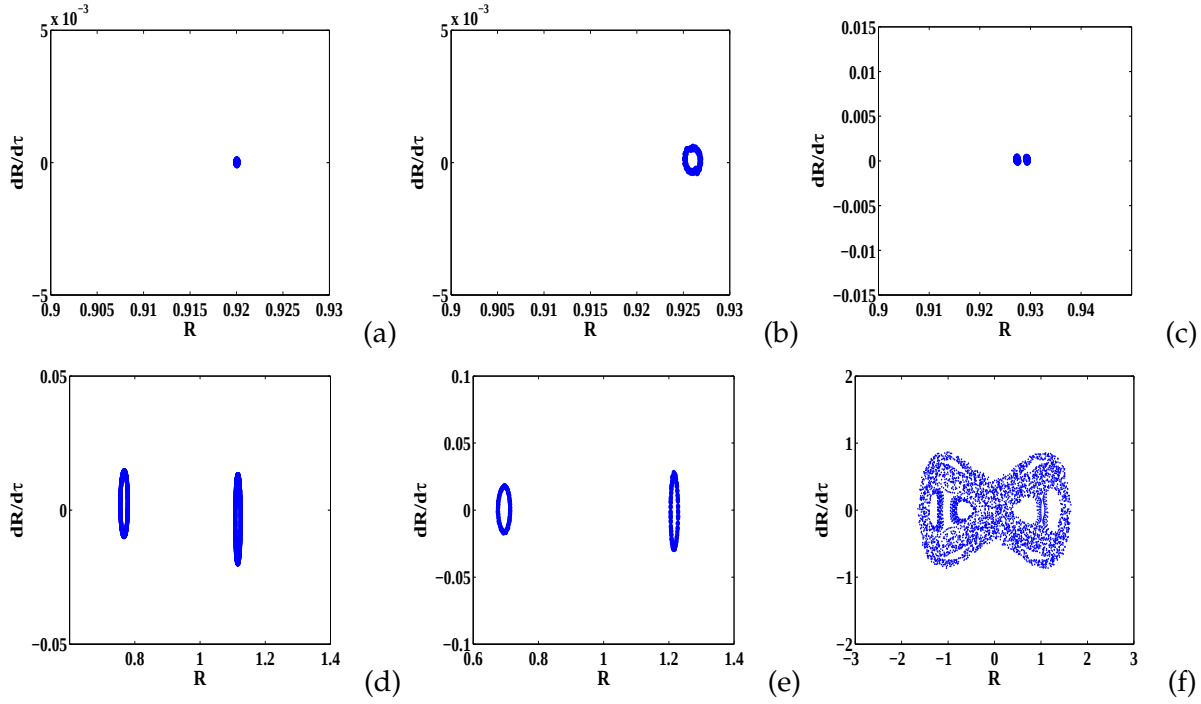

Figure 36: Poincaré sections of homoclinic bifurcations, deduced from eq.(42) with the optical intensity V_0 as control parameter. (a) $V_0 = 0.1$ (b) $V_0 = 1$ (c) $V_0 = 1.35$ (d) $V_0 = 5$ (e) $V_0 = 10$ (f) $V_0 = 20$. The other parameters used are: $\upsilon = 1.5$, $g_0 = -0.75$, $g_1 = 0.1$, $\epsilon = 0.01$, $m = 0.5$, $\gamma = 0.05$, the initial conditions taken at the stable fixed point ($R = R_1 = 0.9193815805$, $dR/d\tau = 0$).

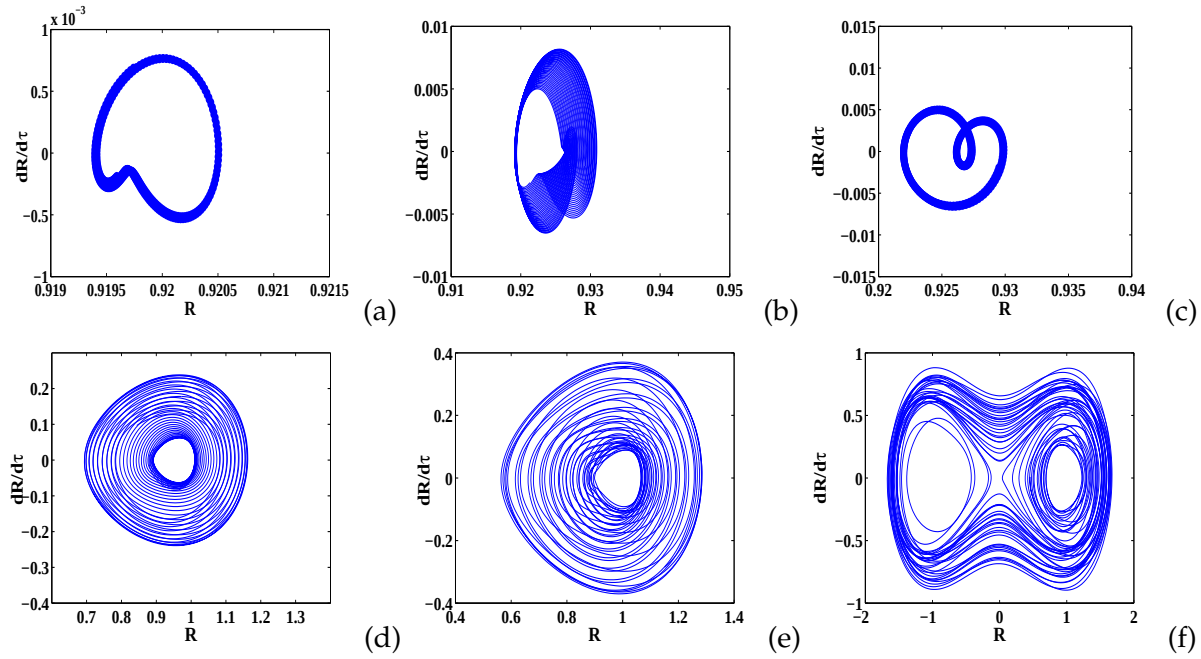

Figure 37: Phase portraits of homoclinic bifurcations, deduced from eq.(42) with the optical intensity V_0 as control parameter. (a) $V_0 = 0.1$ (b) $V_0 = 1$ (c) $V_0 = 1.35$ (d) $V_0 = 5$ (e) $V_0 = 10$ (f) $V_0 = 20$. The other parameters used are: $\upsilon = 1.5$, $g_0 = -0.75$, $g_1 = 0.1$, $\epsilon = 0.01$, $m = 0.5$, $\gamma = 0.05$, the initial conditions taken at the stable fixed point ($R = R_1 = 0.9193815805$, $dR/d\tau = 0$).

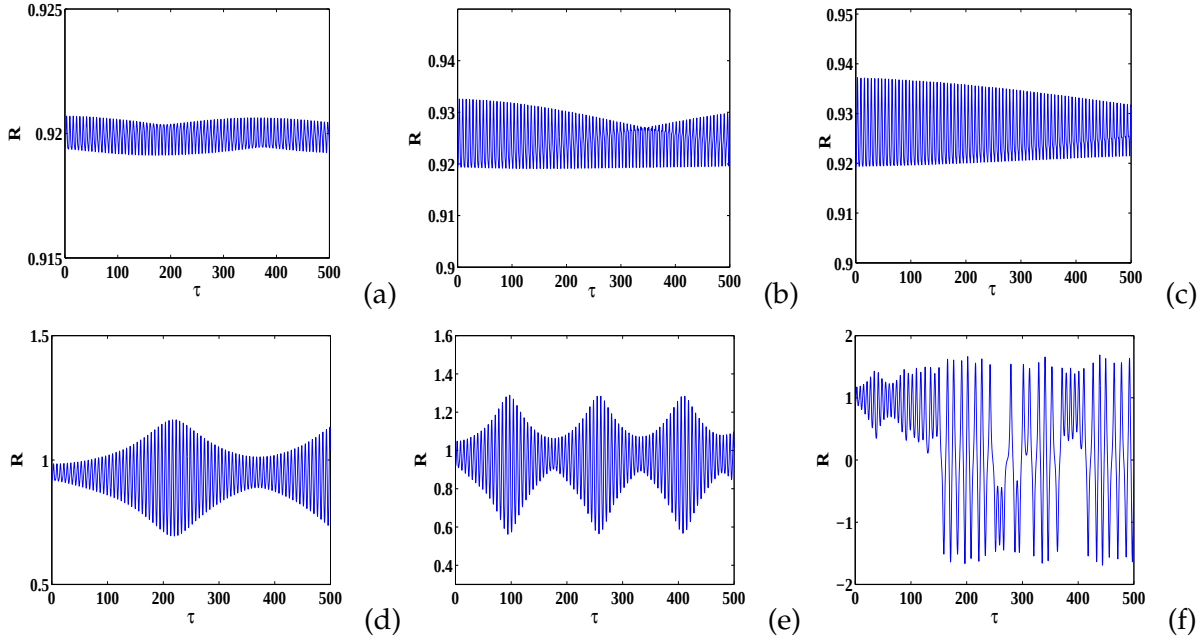

Figure 38: Spatiotemporal evolution of condensate in the case of homoclinic bifurcations, deduced from eq.(42) with the optical intensity V_0 as control parameter. (a) $V_0 = 0.1$ (b) $V_0 = 1$ (c) $V_0 = 1.35$ (d) $V_0 = 5$ (e) $V_0 = 10$ (f) $V_0 = 20$. The other parameters used are: $\upsilon = 1.5$, $g_0 = -0.75$, $g_1 = 0.1$, $\epsilon = 0.01$, $m = 0.5$, $\gamma = 0.05$, the initial conditions taken at the stable fixed point ($R = R_1 = 0.9193815805$, $dR/d\tau = 0$).

the condensate in this condition is very sensitive to initial conditions, and unpredictable. For this control parameter, it is clear that to each limit cycle corresponds a torus attractor and to the period-doubling of limit cycle corresponds torus-doubling of torus attractors. One recognizes here the torus-doubling bifurcation route to chaos. Furthermore, from two-period quasi-periodic oscillations of the condensate, its dynamical behaviour becomes directly chaotic. One recognizes the Ruelle-Takens and Newhouse results [158, 159] in the so-called Ruelle-Takens scenario route to chaos. That is to say that the chaotic oscillations can be obtained for finite incommensurate frequencies, particularly the birth of the third incommensurate frequencies can lead directly to chaos under very weak perturbations, contrary to the Landau theory which predicts more incommensurate frequencies for the occurrence of chaos. The gap of 47.64% as relative uncertainty between the two critical values seems so large that one can condemn the theoretical study. In fact, one cannot expect a good quantitative agreement between the two kinds of findings, because the **MM** is a perturbative method generally related to transient chaos, while bifurcation diagrams provide information solely concerning steady chaos.

In addition, one observes on the spatiotemporal evolutions of the condensate that, in the case of periodic oscillations corresponding to very weak values of optical depth V_0, the real amplitude of the wave function of the condensate is virtually constant, as well visible on the Fig.21(a-b-c) for V_0 taking respectively the values 0.1, 1.0 and 1.35. One can deduce a solitonic solution for eq.(42) as bright solitons. Subsequently, when the control parameter V_0 continues to increase, progressively, the spatiotemporal evolutions of the real amplitude of the condensate appear like

waves envelope, as shown in Fig.21(d-e) for V_0 respectively 5.0 and 10.0. One recognizes the envelope solitons as solitonic solutions of eq.(42). The Fig.21(f) exhibits the erratic oscillations for $V_0 = 20$, as predicted by the bifurcation diagram and the largest Lyapunov exponent. Roughly speaking, the stable dynamics of the condensate is governed by the solitary waves, of type bright solitons and envelope solitons. These solitonic solutions of eq.(42) can be interpreted as a perfect balance between dissipation and nonlinearities.

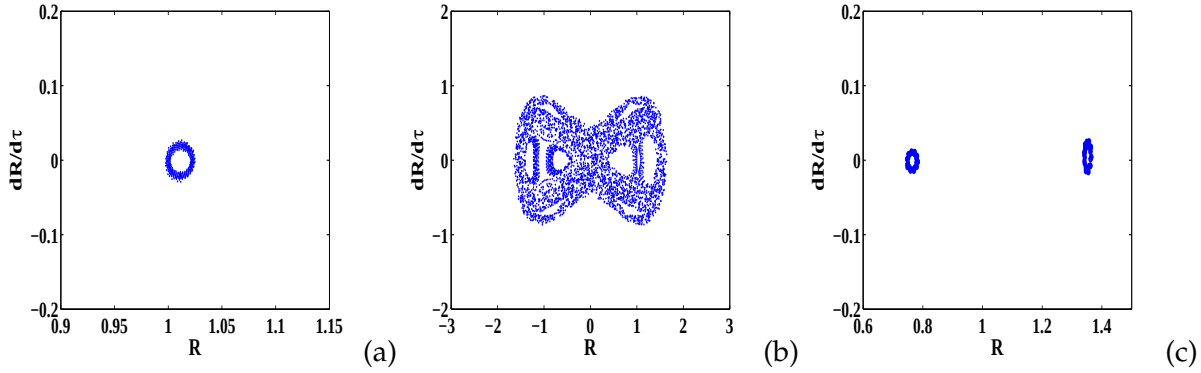

Figure 39: Poincaré sections of homoclinic bifurcations, deduced from eq.(42) with the strength of three-body elastic atom-atom interaction g_1 as control parameter. (a) $g_1 = 0.05$ (b) $g_1 = 0.1$ (c) $g_1 = 0.13$. The other parameters used are: $V_0 = 20$, $g_0 = -0.75$, $\epsilon = 0.01$, $m = 0.5$, $\gamma = 0.05$, the initial conditions taken at the stable fixed point ($R = R_1 = 0.9193815805$, $dR/d\tau = 0$).

b) Bifurcation responses with the strength of the three-body recombination g_1 as control parameter

We use the same set of data as above, and to V_0 we give the value 20. Remembering our work hypothesis defined in eq.(84) and eq.(85), g_1 must be taken between 0 and 0.1875. The condition for the occurrence of the Melnikov chaos deduced from eq.(105) and plotted in Fig.34(b) shows that the threshold function $\rho(V_0, m, \upsilon, g_1, \gamma)$ is always positive, excepted the vicinity of 0.1810 where the threshold function is not defined. Therefore, the dynamics of the condensate will remain chaotic when the control parameter varies between 0 and 0.1875. But, in Melnikov's sense, it means that for this set of data, there are no periodic oscillations. The bifurcation diagram plotted in Fig.35(b) confirms that, because it begins by a large branch instead of a tiny branch as in the case of periodic oscillations. The beginning of this bifurcation diagram corresponding to the negative part of the largest Lyapunov exponent shown in Fig.35(d) corresponds in fact to quasi-periodic oscillations, as clearly seen on the Poincaré section (closed curve), and on the phase portrait(quasi-periodic attractor), displayed in figures 39(a) and 40(a) respectively, for $g_1 = 0.05$. By continuing to vary increasingly the control parameter, in the vicinity of 0.0701, via a Hopf bifurcation, the dynamics of the condensate experiences suddenly a chaotic regime, as clearly visible on the largest Lyapunov exponent displayed in Fig.35(d) which crosses the g_1 axis, becoming a positive number. The Poincaré section and the phase portrait depicted in Fig.39(b) and Fig.40(b) respectively, for $g_1 = 0.1$ present a strange attractor and erratic phase orbits. In

fact, for g_1 taken between 0.0701 and 0.1135, the eigenvalues corresponding to the stable fixed points are very close to the imaginary complex number j ($j^2 = -1$). One understands the Hopf bifurcation leading to the chaotic oscillations of the condensate in the vicinity of $g_1 = 0.0701$, and the torus-doubling bifurcation observed around $g_1 = 0.1135$ which culminates in another quasi-periodic regime, with a Poincaré section exhibiting two closed curves as displayed in Fig.39(c) for $g_1 = 0.13$.

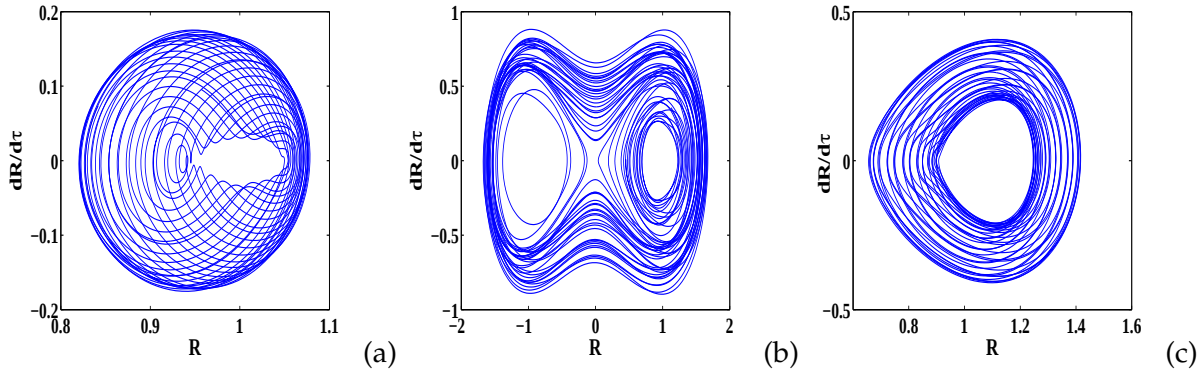

Figure 40: Phase portraits of homoclinic bifurcations, deduced from eq.(42) with the strength of three-body elastic atom-atom interaction g_1 as control parameter. (a) $g_1 = 0.05$ (b) $g_1 = 0.1$ (c) $g_1 = 0.13$. The other parameters used are: $V_0 = 20$, $g_0 = -0.75$, $\epsilon = 0.01$, $m = 0.5$, $\gamma = 0.05$, the initial conditions taken at the stable fixed point ($R = R_1 = 0.9193815805$, $dR/d\tau = 0$).

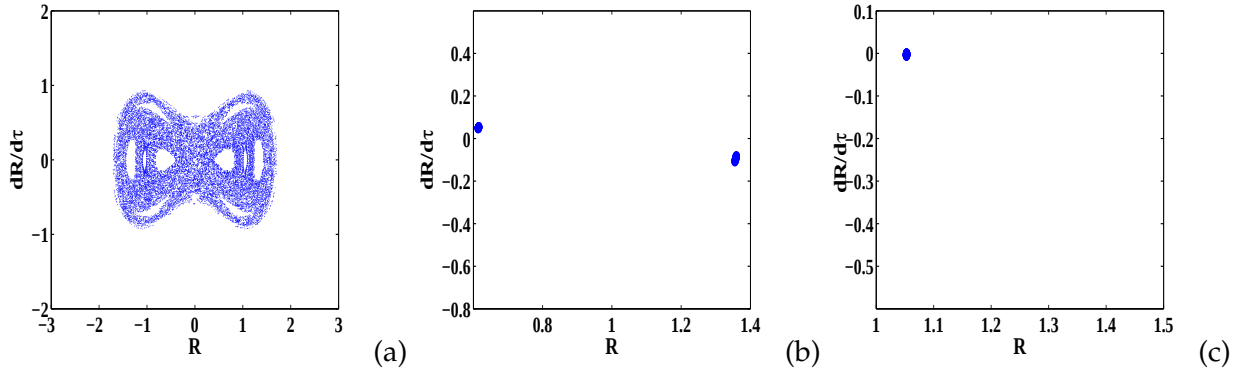

Figure 41: Poincaré sections of homoclinic bifurcations, deduced from eq.(42) with the dissipation parameter γ as control parameter. (a) $\gamma = 0.01$ (b) $\gamma = 2$ (c) $\gamma = 3.5$. The other parameters used are: $V_0 = 20$, $g_0 = -0.75$, $g_1 = 0.1$, $\epsilon = 0.01$, $m = 0.5$, the initial conditions taken at the stable fixed point ($R = R_1 = 0.9193815805$, $dR/d\tau = 0$).

c) Bifurcation responses with the damping coefficient γ as control parameter

We continue with the same set of data as above, but to g_1 and V_0 we give the value 0.1 and 20 respectively. The threshold function $\rho(V_0, m, \upsilon, g_1, \gamma)$ expressed in eq.(105) is plotted versus the control parameter γ in Fig.34(c). It comes from this curve that, when the dissipation parameter

evolves, the dynamics of the condensate remains chaotic until the control parameter reaches the value 3.81, where the condensate undergoes a bifurcation culminating in a periodic regime. According to this analytical treatment, it is clear that the dissipation coefficient reduces the chaotic behaviour of the condensate. Numerically, the bifurcation diagram and the largest Lyapunov exponent plotted in figures 35(e) and 35(g) respectively, show that when the dissipation coefficient varies increasingly, the chaotic behaviour of the condensate is progressively reduced until the vicinity of 3.305 where a period-doubling bifurcation leads the condensate to a periodic regime. The gap between the two critical values is 13.25% as relative uncertainty. The Poincaré sections and phase portraits shown in figures 41(a-b-c) and 42(a-b-c) allow us to conclude that the regularization route is via the period-doubling scenario.

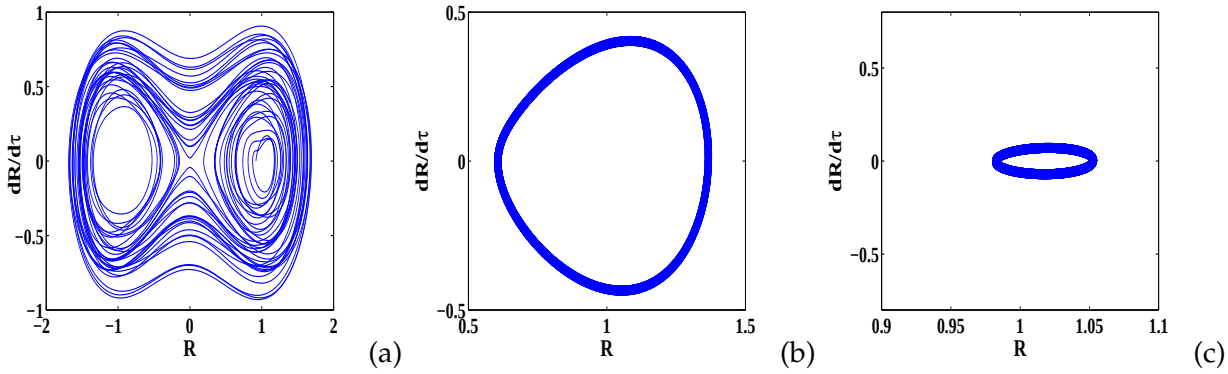

Figure 42: Phase portraits of homoclinic bifurcations, deduced from eq.(42) with the dissipation parameter γ as control parameter. (a) $\gamma = 0.01$ (b) $\gamma = 2$ (c) $\gamma = 3.5$. The other parameters used are: $V_0 = 20$, $g_0 = -0.75$, $g_1 = 0.1$, $\epsilon = 0.01$, $m = 0.5$, the initial conditions taken at the stable fixed point ($R = R_1 = 0.9193815805$, $dR/d\tau = 0$).

d) Bifurcation responses with the velocity of the optical lattice υ as control parameter

We consider as above, the following set of data: $g_0 = -0.75$, $g_1 = 0.1$, $V_0 = 15$, $\gamma = 0.05$, $m = 0.5$. Our work hypothesis expressed in eq.(84) and eq.(85) constraints the control parameter υ to vary between 0 and 2.053. The threshold function $\rho(V_0, m, \upsilon, g_1, \gamma)$ deriving from eq.(105) and plotted in Fig.34(d) reveals that when the control parameter evolves, the stability of the condensate is progressively destroyed, and its chaotic behaviour is obtained in the vicinity of $\upsilon = 0.50$.
Numerically, through the largest Lyapunov exponent displayed in Fig.35(h), the numerical simulations reveal that the dynamics of the condensate becomes chaotic for the velocity of optical lattice more greater than 0.355. Therefore, this control parameter enhances the chaotic dynamics of the condensate. Through the Poincaré sections and phase portraits depicted in figures 43(a-b-c-d) and 44(a-b-c-d) respectively, it is clear that the quasi-periodicity is the route leading to chaotic oscillations. In the chaotic zone, there are open windows of quasi-periodic oscillations, as clearly visible on the largest Lyapunov exponent for υ between 1.02 and 1.49. That is well visible on the Poincaré section (closed curves) and phase portrait shown in figures 43(e) and 44(e) respectively, for $\upsilon = 1.3$. The relative uncertainty between the two critical values is 29.0%.

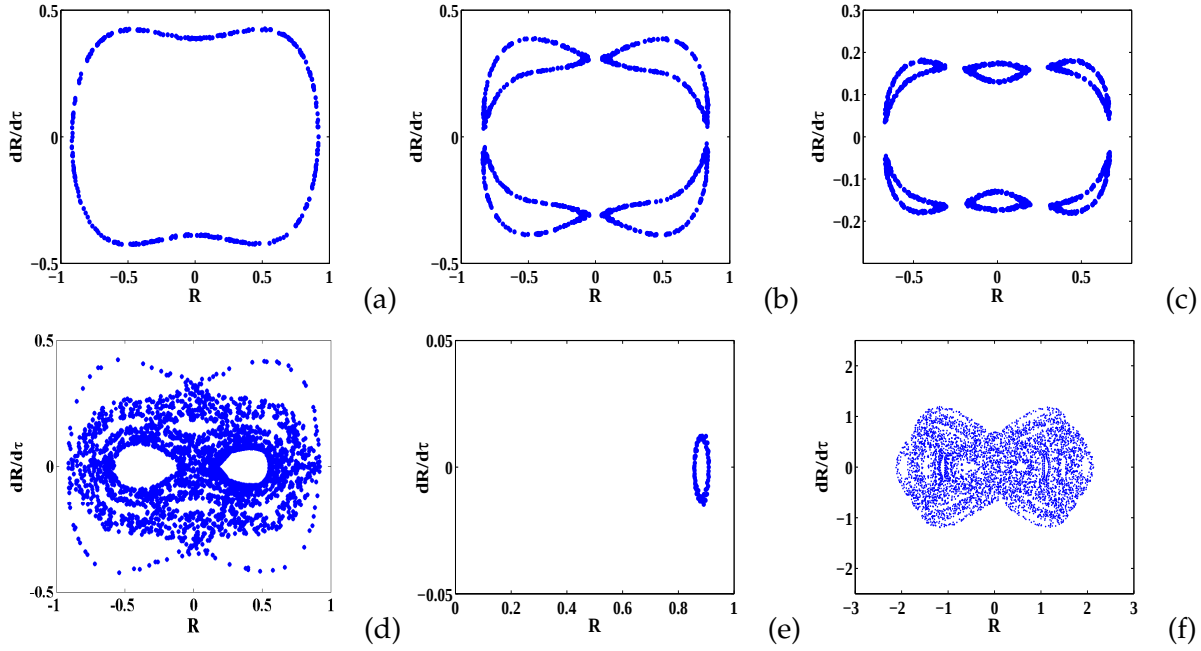

Figure 43: Poincaré sections of homoclinic bifurcations, deduced from eq.(42) with the velocity of optical lattice υ as control parameter. (a) $\upsilon = 0.01$ (b) $\upsilon = 0.1$ (c) $\upsilon = 0.3$ (d) $\upsilon = 0.4$ (e) $\upsilon = 1.3$ (f) $\upsilon = 1.5$. The other parameters used are: $V_0 = 15$, $g_0 = -0.75$, $g_1 = 0.1$, $\epsilon = 0.01$, $m = 0.5$, $\gamma = 0.05$, the initial conditions taken at the stable fixed point ($R = R_1 = 0.9193815805$, $dR/d\tau = 0$).

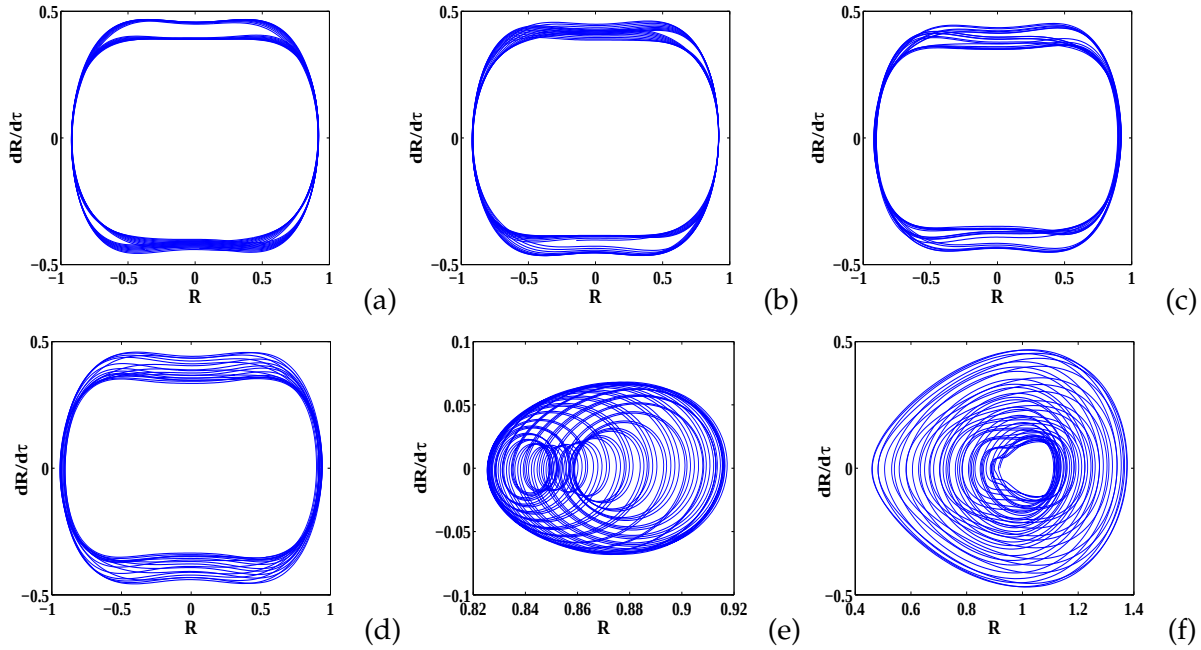

Figure 44: Phase portraits of homoclinic bifurcations, deduced from eq.(42) with the velocity of optical lattice υ as control parameter. (a) $\upsilon = 0.01$ (b) $\upsilon = 0.1$ (c) $\upsilon = 0.3$ (d) $\upsilon = 0.4$ (e) $\upsilon = 1.3$ (f) $\upsilon = 1.5$. The other parameters used are: $V_0 = 15$, $g_0 = -0.75$, $g_1 = 0.1$, $\epsilon = 0.01$, $m = 0.5$, $\gamma = 0.05$, the initial conditions taken at the stable fixed point ($R = R_1 = 0.9193815805$, $dR/d\tau = 0$).

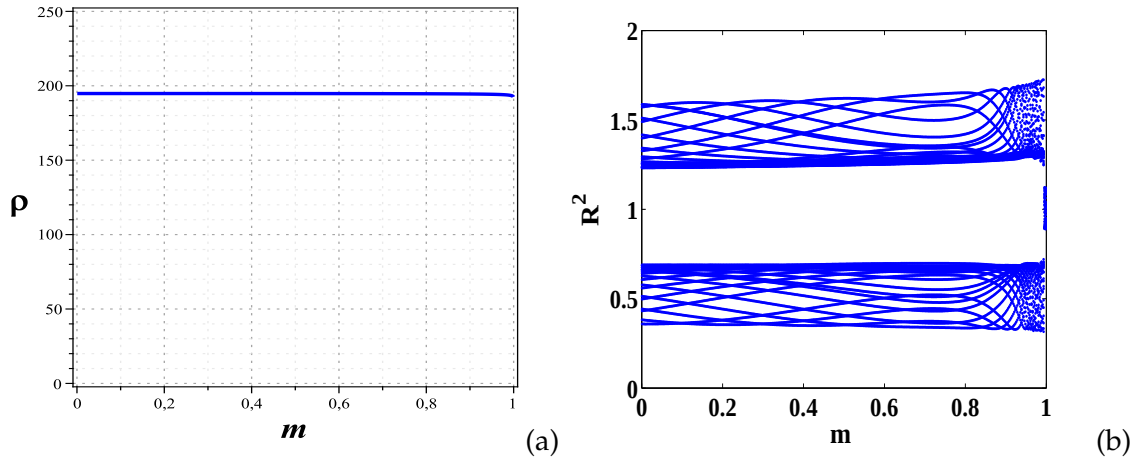

Figure 45: (a) Plot of the homoclinic threshold function $\rho(V_0, m, \upsilon, \gamma, g_1)$ of chaos occurrence versus the optical shape parameter m. (b) Bifurcation diagram of homoclinic bifurcations, deduced from eq.(42) with the shape parameter m as control parameter. The other parameters used are: $V_0 = 10$, $g_0 = -0.75$, $g_1 = 0.1$, $\epsilon = 0.01$, $\upsilon = 1.5$, $\gamma = 0.05$, the initial conditions taken at the stable fixed point ($R = R_1 = 0.9193815805$, $dR/d\tau = 0$).

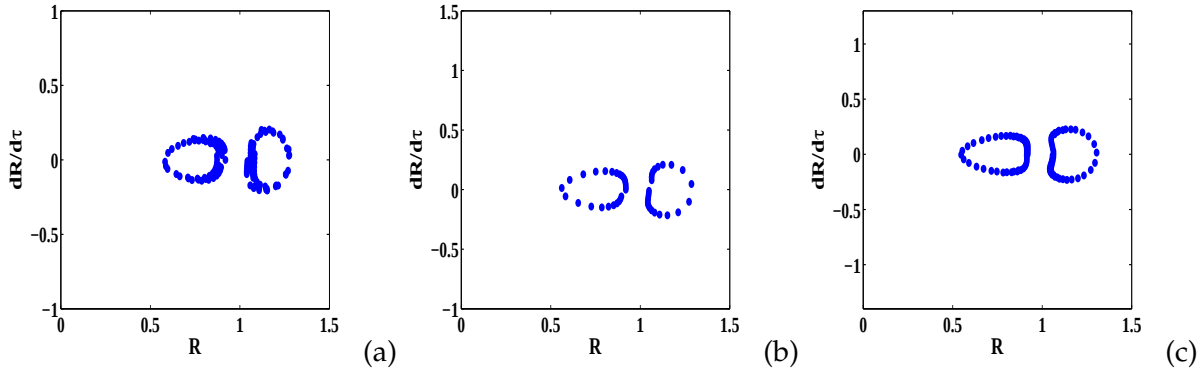

Figure 46: Poincaré sections of homoclinic bifurcations, deduced from eq.(42) with the shape parameter m as control parameter. (a) $m = 0.1$ (b) $m = 0.5$ (c) $m = 0.8$. The other parameters used are: $V_0 = 10$, $g_0 = -0.75$, $g_1 = 0.1$ $\epsilon = 0.01$, $\gamma = 0.05$, $\upsilon = 1.5$, the initial conditions taken at the stable fixed point ($R = R_1 = 0.9193815805$, $dR/d\tau = 0$).

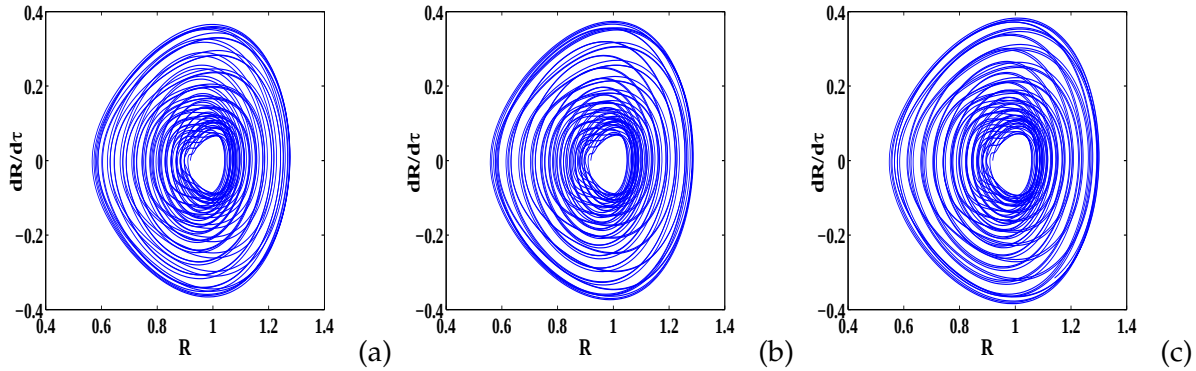

Figure 47: Phase portraits of homoclinic bifurcations, deduced from eq.(42) with the shape parameter m as control parameter. (a) $m = 0.1$ (b) $m = 0.5$ (c) $m = 0.8$. The other parameters used are: $V_0 = 10$, $g_0 = -0.75$, $g_1 = 0.1$, $\epsilon = 0.01$, $\gamma = 0.05$, $\upsilon = 1.5$, the initial conditions taken at the stable fixed point ($R = R_1 = 0.9193815805$, $dR/d\tau = 0$).

e) Bifurcation responses with the optical lattice shape m as control parameter

As above we use the same set of data, but to V_0 we give the value 10. The threshold function $\rho(V_0, m, \upsilon, g_1, \gamma)$ deriving from eq.(105) and plotted in Fig.45(a) reveals that there are no periodic oscillations around the stable fixed point, because the threshold function ρ is always a positive number for all possible values of the shape parameter m($0 \leq m \leq 1$). That is confirmed in the bifurcation diagram plotted with the same set of data in Fig.(45), and on the Poincaré sections presented in Fig.(46) which always exhibit two closed loops for all value of control parameter m. For this set of parameters, the dynamics of the condensate is always quasi-periodic. This result is also visible on the phase portraits depicted in Fig.(47).

III.3.1.2. Bifurcation responses of heteroclinic trajectories

It is important to mention that the heteroclinic separatrix of the unperturbed system eq.(43) crosses the R axis in the phase space (R,X) at $(-R_2, 0)$ and $(+R_2, 0)$, which represent the maxima of the potential energy. To use these unstable fixed points as initial conditions in numerical simulations characterizes the heteroclinic trajectories.

a) Bifurcation responses with the depth of the optical lattice V_0 as control parameter

We consider the following set of data generally used in experiments: $g_0 = -0.75$, $g_1 = 0.1$, $\upsilon = 1$, $\gamma = 0.5$, $m = 0.5$ and $\epsilon = 0.01$. One observes in Fig.48(a) deriving from the theoretical prediction of the heteroclinic chaos defined in eq.(114) that, the dynamics of the condensate is regular for V_0 between 0 and 2.09, and unstable for V_0 beyond 2.09. Consequently, this control parameter enhances the chaos in the dynamical behaviour of the condensate.
Let's verify the reliability of this result through numerical simulations. Using the saddle point $(+R_2, 0)$ as initial conditions, the bifurcation diagram and the largest Lyapunov exponent plotted respectively in figures 49(a) and 49(c) show that the depth of the optical lattice really enhances

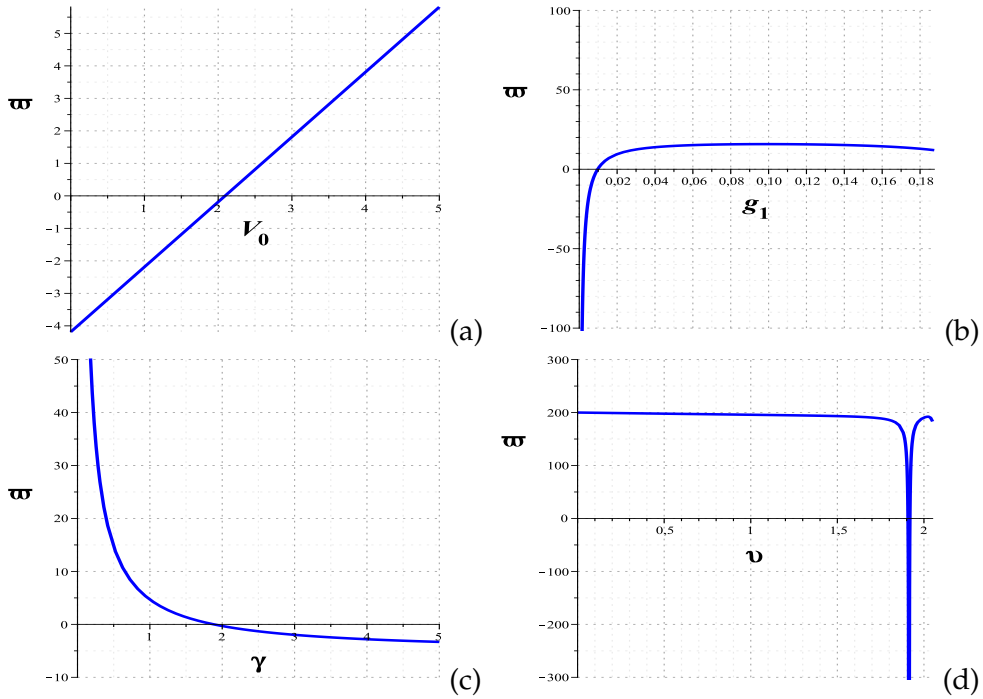

Figure 48: Plot of the heteroclinic threshold function of chaos occurrence versus (a) The optical intensity V_0 (b)The elastic three-body recombination factor g_1 (c) The damping parameter γ, and with $g_1 = 0.05$ (d) The velocity of the optical lattice υ. The other parameters used are: $V_0 = 10$, $\upsilon = 1$, $g_0 = -0.75$, $g_1 = 0.1$, $m = 0.5$, $\gamma = 0.5$.

the chaotic behaviour of the condensate as analytically expected. When the control parameter continue to evolve, in the vicinity of $V_0 = 1.45$, the largest Lyapunov exponent becomes a positive number, and the dynamics of condensed atoms enters suddenly into an aperiodic regime. The Poincaré sections before this bifurcation point always exhibit closed curves, indicating the existence of quasi-periodic oscillations. The depth analysis of Poincaré sections(figures 50(a-b)) and phase portraits(figures 51(a-b)) of the condensate indicates that from two-period quasi periodic oscillations before the bifurcation point, the dynamics of the condensate becomes suddenly chaotic, and the heteroclinic separatrix is particularly affected.

b) Bifurcation responses with the strength of the three-body recombination g_1 as control parameter

As usual, we consider the same set of data as above, and to V_0 we give the value 10. According to Fig.48(b), the dynamics of the condensate is regular for g_1 between 0 and 0.01, and chaotic for g_1 beyond 0.01. Therefore, this control parameter enhances the chaos in the dynamical behaviour of the condensate. The numerical simulations through the bifurcation diagram in Fig.49(b) and the largest Lyapunov exponent in Fig.49(d) confirm really the existence of regular oscillations for very weak values of the control parameter. Once again, the quasi-periodicity characterizes the zone of regularity, and the heteroclinic separatrix is particularly affected in the case of chaotic oscillations.

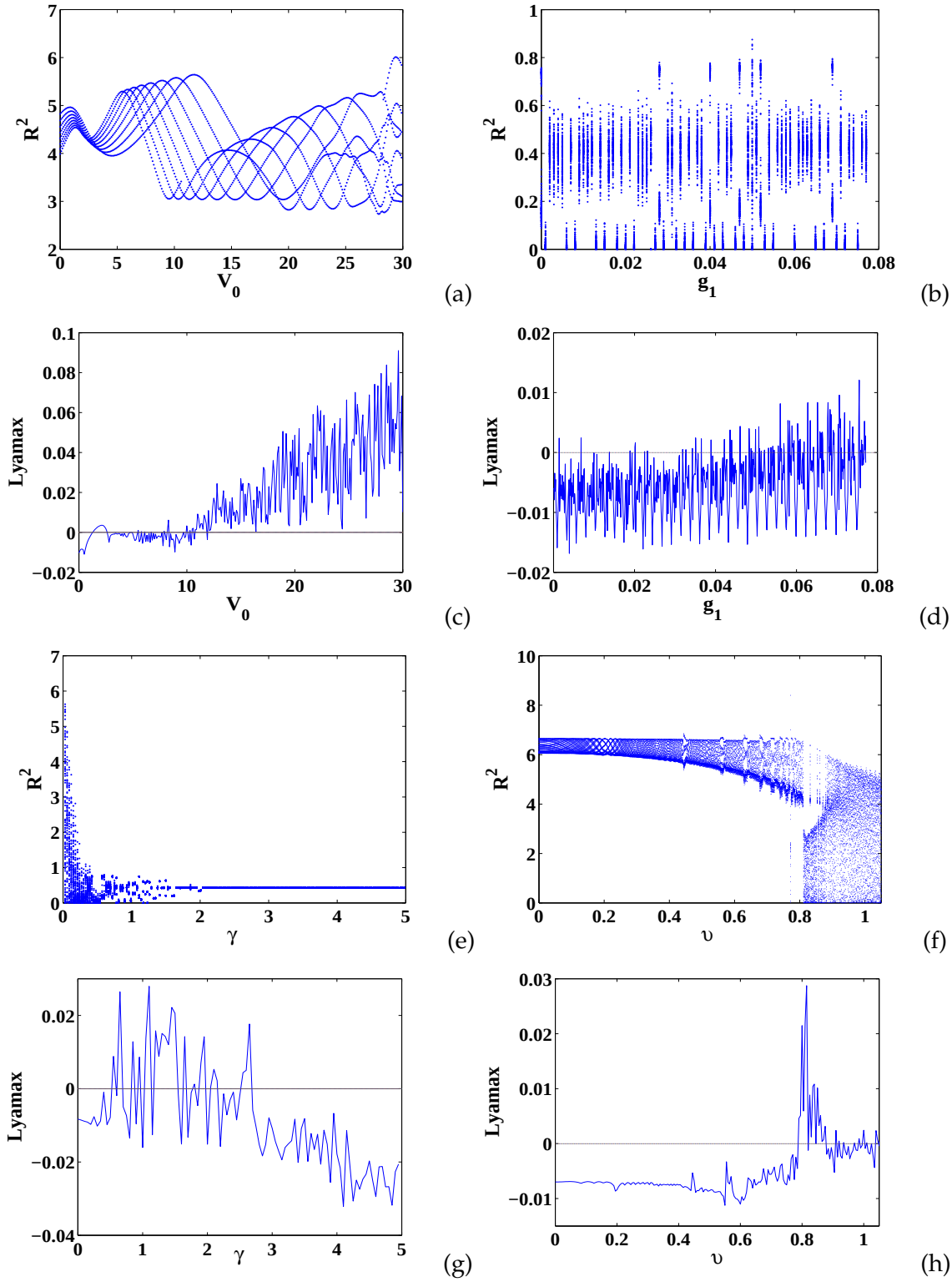

Figure 49: Bifurcation diagrams and corresponding Lyapunov exponents of heteroclinic bifurcations, deduced from eq.(42) (a)-(c) The optical intensity V_0 as control parameter (b)-(d) The elastic three-body recombination factor as control parameter (e)-(g) The damping parameter γ as control parameter (f)-(h) The optical velocity υ as control parameter . The other parameters used are: $\upsilon = 1$, $g_0 = -0.75$, $g_1 = 0.1$, $\epsilon = 0.01$, $m = 0.5$, $\gamma = 0.5$, the initial conditions taken at the unstable fixed point ($R = R_2 = 2.579677792$, $dR/d\tau = 0$).

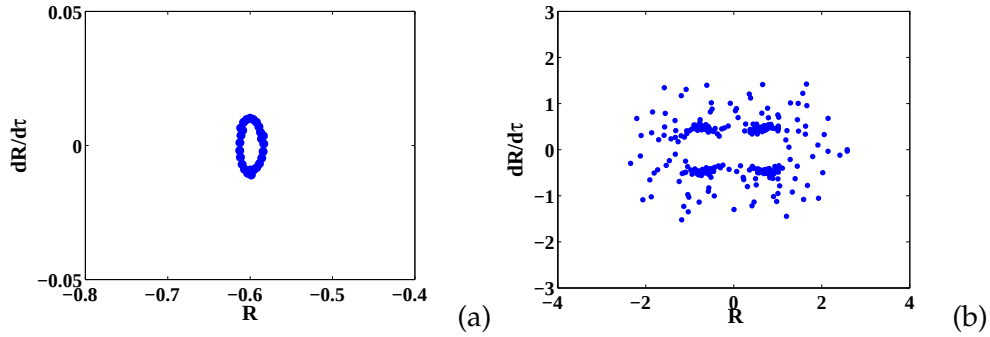

Figure 50: Poincaré sections of heteroclinic bifurcations, deduced from eq.(42) with the optical intensity V_0 as control parameter. (a) $V_0 = 1$ (b) $V_0 = 20$. The other parameters used are: $\upsilon = 1$, $g_0 = -0.75$, $g_1 = 0.1$, $\epsilon = 0.01$, $m = 0.5$, $\gamma = 0.5$, the initial conditions taken at the unstable fixed point ($R = R_2 = 2.579677792$, $dR/d\tau = 0$).

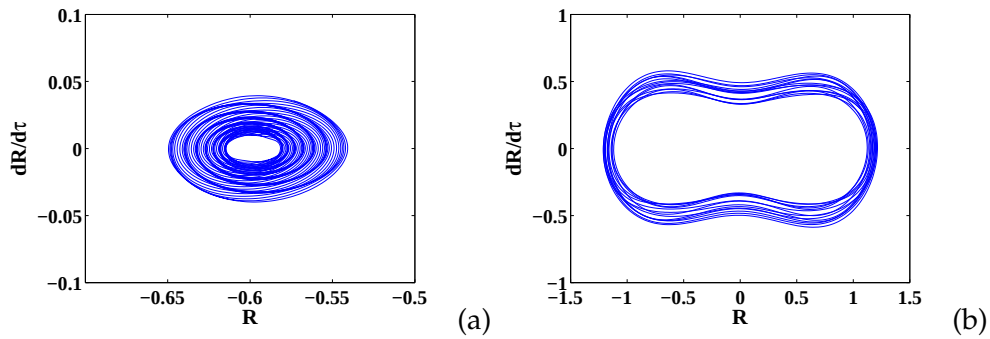

Figure 51: Phase portraits of heteroclinic bifurcations, deduced from eq.(42) with the optical intensity V_0 as control parameter. (a) $V_0 = 1$ (b) $V_0 = 20$. The other parameters used are: $\upsilon = 1$, $g_0 = -0.75$, $g_1 = 0.1$, $\epsilon = 0.01$, $m = 0.5$, $\gamma = 0.5$, the initial conditions taken at the unstable fixed point ($R = R_2 = 2.579677792$, $dR/d\tau = 0$).

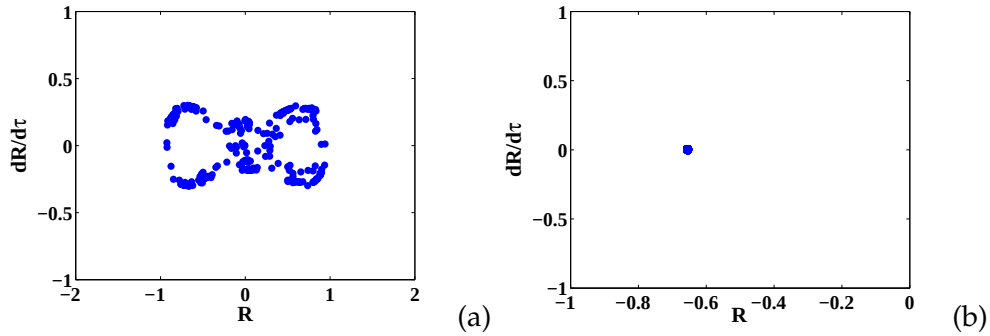

Figure 52: Poincaré sections of heteroclinic bifurcations, deduced from eq.(42) with the dissipation parameter γ as control parameter. (a) $\gamma = 0.5$ (b) $\gamma = 4$. The other parameters used are: $\upsilon = 1$, $g_0 = -0.75$, $g_1 = 0.05$, $V_0 = 10$, $\epsilon = 0.01$, $m = 0.5$, the initial conditions taken at the unstable fixed point ($R = R_2 = 2.579677792$, $dR/d\tau = 0$).

c) Bifurcation responses with the damping coefficient γ as control parameter

As above, we use the same set of data, and to g_1 we give the value 0.05. The theoretical prediction of the heteroclinic chaos depicted in Fig.48(c) reveals that the dissipation parameter reduces the chaotic behaviour of the condensate, and the regular oscillations are obtained for γ beyond 1.88. Through the bifurcation diagram and the largest Lyapunov exponent plotted in figures 49(e) and 49(g)respectively, the critical value of the control parameter leading to a periodic regime is $\gamma = 2.71$. The relative uncertainty of 30.62% between these critical values can seem enough, but that was expected according to the fact that the **MM** is related to transient chaos whereas the bifurcation diagrams and the largest Lyapunov exponent are related to steady chaos. The deep analysis of Poincaré sections reveal that from chaotic oscillations, the dynamics of the condensate becomes suddenly periodic(see Fig.(52)).

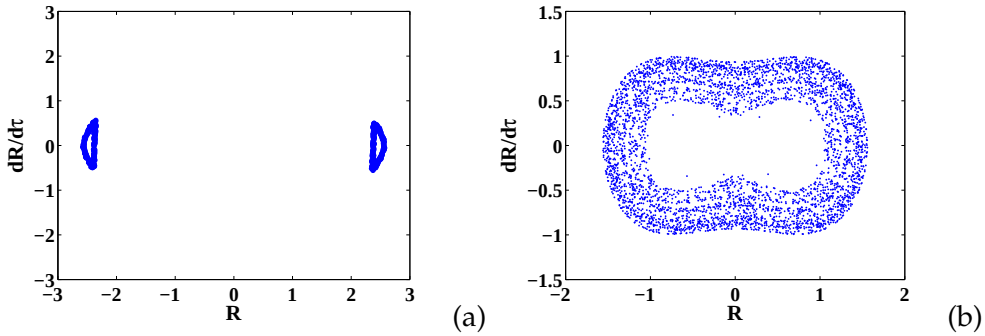

Figure 53: Poincaré sections of heteroclinic bifurcations, deduced from eq.(42) with the velocity of optical lattice υ as control parameter. (a) $\upsilon = 0.5$ (b) $\upsilon = 0.9$. The other parameters used are: $g_0 = -0.75$, $g_1 = 0.1$, $V_0 = 10$, $\epsilon = 0.01$, $m = 0.5$, $\gamma = 0.05$, the initial conditions taken at the stable fixed point ($R = R_2 = 2.579677792$, $dR/d\tau = 0$).

d) Bifurcation responses with the velocity of the optical lattice υ as control parameter

We consider as control parameter the velocity of the optical lattice υ. As above, we use the following experimental set of data: $g_0 = -0.75$, $g_1 = 0.1$, $\gamma = 0.05$, $\epsilon = 0.01$, $V_0 = 10$, and $m = 0.5$. Our work hypothesis characterizing the coexistence of both homoclinic and heteroclinic orbits defined in equations (84) and (85) compels the control parameter to vary between 0 and 2.053. That was already mentioned in the case of homoclinic bifurcations. In Fig.48(d), the boundary threshold function defined in eq.(114) characterizing the theoretical prediction of heteroclinic chaos is always a positive number, except in the vicinity of $\upsilon = 1.905$ where it is not defined. Remembering that the Melnikov method predicts the end or the beginning of the periodic oscillations, one deduces from Fig.48(d) that there is no periodic regime in the dynamics of the condensate.

Taking as initial conditions the unstable fixed point $(R_2, 0)$ to characterize the heteroclinic trajectories, one observes through the bifurcation diagram in Fig.49(f) the non existence of periodic oscillations. The corresponding largest Lyapunov exponent depicted in Fig.49(h) presents a neg-

ative part for υ varying between 0 and 0.77, which can be interpreted as an existence of periodic oscillations. However, the depth analysis of Poincaré sections for this range of the velocity of the optical lattice υ does not exhibit a point attractor, but reveals two distorted closed curves, characteristic of quasi-periodic oscillations as clearly shown on the Poincaré section presented in Fig.53(a) for $\upsilon = 0.5$. Moreover, from two-period quasi-periodic oscillations, in the vicinity of $\upsilon = 0.77$, via a Hopf bifurcation, the dynamics of the condensate culminates suddenly into chaos. Once again, the heteroclinic separatrix is particularly affected.

III.3.2 Case of a BEC of atoms subjected to inelastic collisions

In this subsection, we take into account the inelastic processes in the dynamics of the condensate. Firstly, with Maple software, we analyze thoroughly the theoretical conditions for the occurrence of chaotic oscillations expressed in equations (124) and (133), and some zones of instability in different parameter space are determined, and displayed in figures (12), (13), (14) and (15). Secondly, our theoretical results are verified by numerical simulations (Bifurcation diagrams and Poincaré sections). For each parameter space, we take a point inside the instability zone and then outside the instability zone and we plot the corresponding Poincaré sections to verify the analytical prediction. Thirdly, to verify the reliability of our investigations, we compare our findings with those of references [22, 24, 25, 26] in which the condensed atoms trapped in a harmonic potential were studied by a variational approach. The aim of our study being the impact of inelastic processes on the dynamics of the condensate, we consider particularly the cases in which the regions of instability in parameter space (γ_i, γ_j) have approximately linear boundaries, and we attempt to find the link between parameters related to these inelastic collisions for the occurrence of chaotic oscillations.

III.3.2.1. Bifurcation responses of homoclinic orbits

We begin the analysis with the parameter space (γ_0, δ) presented in Fig.12(a). The point $(\gamma_0 = 0.01, \delta = 2)$ is inside of the instability zone coloured in gray. The Fig.55(a) exhibits a strange attractor as Poincaré section, signature of chaotic oscillations of the condensate. Conversely, the point $(\gamma_0 = 0.4, \delta = 5)$ is outside of the region of instability. The corresponding Poincaré section depicted in Fig.55(b) shows a set of seven points attractor, proof of existence of a period-7 limit cycle in phase space. The deep analysis of Poincaré sections reveals that, when one increases the parameter related to atomic feeding γ_0 while δ is kept constant, the number of points characterizing the Poincaré sections decreases progressively. The periodic oscillations are finally obtained for very large values of γ_0. This result is also visible on the bifurcation diagram plotted in Fig.54(a), and can be useful in the control of chaos in the dynamics of the condensate.

By continuing this reasoning with the parameter space (γ_1, δ) displayed in Fig.12(b), the point of components $(\gamma_1 = 0.0005, \delta = 2)$ is within the instability zone coloured in gray. The corresponding Poincaré section is a strange attractor, characteristic of a chaotic behaviour of the condensate. Conversely, the point of components $(\gamma_1 = 0.1, \delta = 2)$ is outside of the region of instability. The corresponding Poincaré section exhibits once again a set of seven points attractor. The thorough

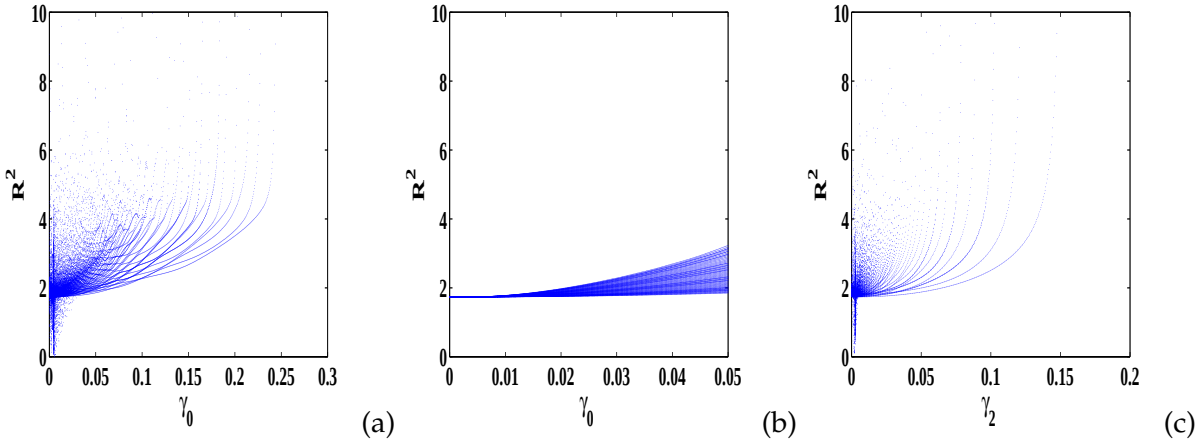

Figure 54: Bifurcation diagrams of homoclinic bifurcation deduced from eq(69). (a)-(b) The feeding rate γ_0 as control parameter, with V_0 respectively 2 for (a) and 0.02 for (b). (c) The three-body inelastic recombination factor γ_2 as control parameter. The other parameters used are $\upsilon = 0.0001$, $\alpha = 0$, $\beta = 1$, $g_0 = -0.75$, $g_1 = 0.1$, $m = 0.5$, $\epsilon = 0.01$, $\gamma_0 = 10^{-2}$, $\gamma_1 = 10^{-5}$, $\gamma_2 = 10^{-3}$, and $V_0 = 2$. The initial conditions taken at the stable fixed point ($R = R_1$=1.316979712, $dR/d\tau = 0$).

analysis of Poincaré sections reveals that when one increases gradually the parameter related to the dipolar relaxation γ_1, the number of points decreases and the Poincaré section is finally restricted to a point attractor when one is far from threshold boundary function.

We pursue the treatment in parameter space (γ_i, γ_j), i=0,1,2 with Fig.13. It comes from eq.(124) that for $\gamma_2 = 10^{-3}$, varying increasingly the atomic feeding parameter γ_0 from 0 to 0.1, the parameter related to the dipolar relaxation γ_1 does not exceed 0.035. The chaotic region coloured in gray in parameter space (γ_1, γ_0) is approximately given by the following expression $-0.0075 \leq \gamma_0 - 3.17\gamma_1 \leq 0.0269$. The point ($\gamma_1 = 0.005$, $\gamma_0 = 0.02$) is inside of the instability zone. The corresponding Poincaré section plotted in Fig.56(a) shows a strange attractor, proof of chaotic oscillations. Conversely, the point $(\gamma_1 = 0.1, \gamma_0 = 0.02)$ is outside of the instability region. The corresponding Poincaré section plotted in Fig.56(b) exhibits a set of seven points attractor, proof of existence of a period-7 attractor. The double inequality expressed above to characterize the zone of instability coloured in gray can be restricted at $\frac{\gamma_0}{\gamma_1} = 3.17$. That is to say that the atomic feeding and the dipolar relaxation parameters must be approximately in the same order for the occurrence of erratic oscillations of the condensate. This result was already obtained in the previous section in the framework of a **BEC** with repulsive two-body and attractive three-body interactions .

In parameter space (γ_2, γ_0) as presented in Fig.13(b) for $\gamma_1 = 10^{-5}$, the analytical condition for the occurrence of the homoclinic chaos reveals that when γ_0 increases between 0 and 0.1, γ_2 increase also between 0 and 0.0104. The region of instability in parameter space (γ_2, γ_0) coloured in gray is approximately given by the following inequalities $-0.0157 \leq \gamma_0 - 11.13\gamma_2 \leq 0.0171$. The point ($\gamma_2 = 0.005$, $\gamma_0 = 0.06$) is inside of the instability region, and the corresponding Poincaré section exhibits a strange attractor, proof of existence of chaotic oscillations. Conversely, the point($\gamma_2 = 0.07$, $\gamma_0 = 0.01$) is outside of the instability zone. The corresponding Poincaré section

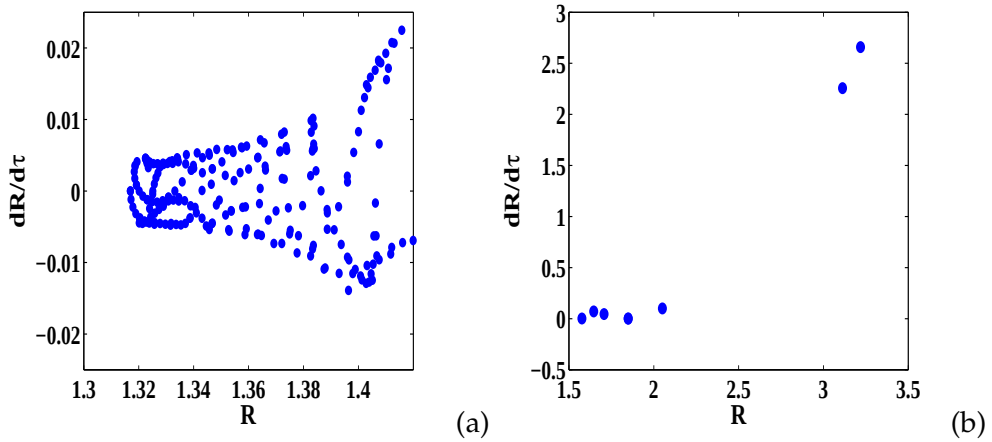

Figure 55: Poincaré sections of homoclinic bifurcations deriving from eq.(69) in parameter space (γ_0, δ) (a) The point with components $(\gamma_0 = 0.01, \delta = 2)$ inside the region of instability (b) The point with components $(\gamma_0 = 0.4, \delta = 5)$ inside the region of stability. The other parameters used are: $\upsilon = 0.0001$, $\alpha = 0$, $\beta = 1$, $m = 0.5$, $\epsilon = 0.01$, $g_0 = -0.75$, $g_1 = 0.1$, $V_0 = 2$, $\gamma_1 = 10^{-5}$, $\gamma_2 = 10^{-3}$, the initial conditions taken at the stable fixed point (R=R_1'=1.316979712, $dR/d\tau = 0$).

exhibits a set of seven points attractor, characterizing a period-7 limit cycle. From the double inequality expressing the zone of instability coloured in gray, the chaotic oscillations of the condensate can be restricted at $\frac{\gamma_0}{\gamma_2} = 11.13$. That is to say that the feeding parameter is about one order of magnitude larger than the thee-body recombination parameter. The deep computational analysis of Poincaré sections shows that in parameter space, the further away one is from the boundary threshold function, progressively the dynamics of the condensate becomes regular. Exploring thoroughly the regions of instability, we observe through numerical simulations that for very weak values of the optical depth V_0 and very weak values of the inelastic three-body collision parameter γ_2, the regions of instability in parameter space (γ_1, γ_0) are discrete and appear as a sequence of an island of points as one can see on the figure 13(c). In other words, the regions of instability appear like a linear alternation of patterns. The centers G_n of these regions of instability in parameter space (γ_1, γ_0) are in arithmetic progression and approximately given by $G_n(\gamma_1 = 0.0005n, \gamma_0 = 0.0016n)$ for the set of parameters used. The outcome of that, is merely the existence of crises and growth-collapse cycles in the dynamics of the condensate.

Now, let's compare our results with those of references [22, 24, 25, 26] in which the study was made by a variational approach on a **BEC** with an attractive two-body and a repulsive three-body recombination and trapped in a magnetic field. As relevant result, their study reveals that quantitatively the chaotic dynamics occurs mainly when the feeding parameter is one or two orders of magnitude larger than the three-body recombination parameter. It comes also from their study that small values of feeding parameter are favourable to regular oscillations whereas large values of feeding parameter are favourable to chaotic behaviour of the condensate. Using the same set of parameters which in fact are those generally used in experiments, we obtain analytically that the homoclinic chaos in the dynamics of the condensate is governed by the ratio $\frac{\gamma_0}{\gamma_2} = 11.13$. That is to say that the chaotic behaviour of the condensate occurs when the feeding

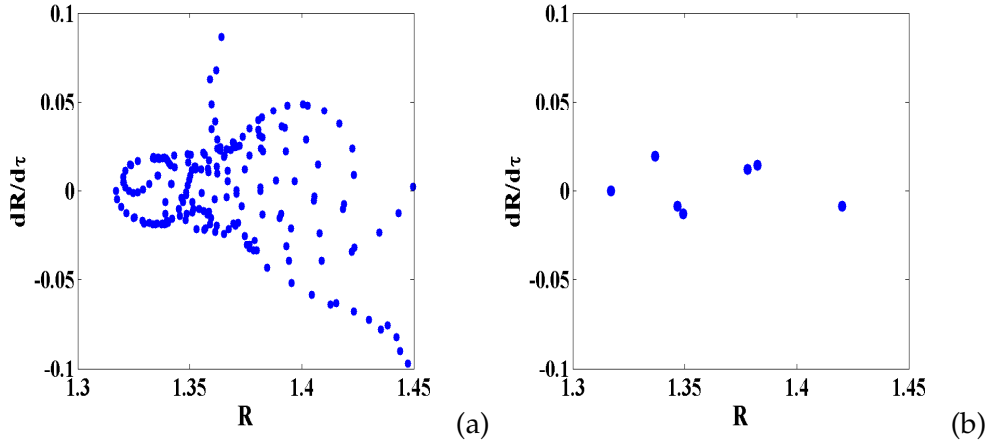

Figure 56: Poincaré sections of homoclinic bifurcations deriving from eq.(69) in parameter space (γ_1, γ_0) (a) The point with components $(\gamma_1 = 0.005, \gamma_0 = 0.02)$ inside the unstable region (b) The point with components $(\gamma_1 = 0.1, \gamma_0 = 0.02)$ inside the stable region. The other parameters used are: $\upsilon = 0.0001$, $\alpha = 0$, $\beta = 1$, $\epsilon = 0.01$, $g_0 = -0.75$, $g_1 = 0.1$, $m = 0.5$, $V_0 = 2$, $\gamma_2 = 10^{-3}$. The initial conditions taken at the stable fixed point ($R = R_1'$=1.316979712, $dR/d\tau = 0$)

.

parameter is about one order of magnitude larger than the thee-body recombination parameter. This result is in perfect accord with their findings. However, our study reveals a certain disagreement with the above-mentioned references. We observe that weak values of the feeding parameter do not necessary imply regular oscillations, and large values of the feeding parameter do not necessary imply erratic oscillations. In the optical lattices potential, the depth of the trap potential plays a key role in the chaotic dynamics of the condensate. That can be viewed on figures 12(a) and 14(a), where for weak values of the feeding parameter, to be inside or outside of the instability region depends of values of the depth and the variable shape of the optical lattice. Numerically that is also verified, as one can see on the bifurcation diagrams plotted in Fig.54. In Fig.54(a) and Fig.54(c), one realizes that for the optical depth V_0 taking the value 2 (per unit of recoil energy), the dynamics of the condensate is chaotic for weak values of parameter related to atomic feeding while in Fig.54(b), one realizes that for weak values of the atomic feeding parameter and for weak values of the optical depth $(V_0 = 0.02)$, the dynamics of the condensate is regular. The depth and the variable shape of the optical lattice play a crucial role in the dynamical behaviour of the condensate. One can understand the choice of the optical lattice on the form of the Jacobi sine function used in this thesis, choice which give the possibility to the experimentalist to change the geometry of the optical lattice, thus allowing the control of chaos.

III.3.2.2. Bifurcation responses of heteroclinic orbits

The theoretical condition for the apparition of the heteroclinic chaos deriving from eq.(133) provides large regions of instability when we are in parameter space (γ_i, δ) with i=0,1,2, as one can see through the figure 14. In fact, this result is not surprising, because the heteroclinic orbits connecting unstable fixed points will be necessarily unstable. Once more, as in the case of homoclinic bifurcations, one observes that the stable dynamics of the condensate is obtained with

the very small values of the optical depth V_0. Taking as initial conditions the unstable fixed point $(-R_2^{'}, 0)$ or $(+R_2^{'}, 0)$, the same program used to plot the homoclinic bifurcation diagrams diverges, probably because the double well ϕ^6 potential is unbounded at these points. Fig.15 exhibits in parameter space (γ_i, γ_j) with $i \neq j$, the regions of instability, which appear sometimes like an island of points when the feeding parameter and the dipolar relaxation parameters vary. This result has been previously observed in Fig.13(c) in the case of homoclinic bifurcations and can be interpreted as crisis, collapse and growth-collapse cycles in the dynamics of the condensate.

III.4 Conclusion

A comparative study between analytical and numerical investigations is made. As relevant results, the depth and the parameter shape of the optical lattice always enhance the instability and chaos in the dynamics of condensed atoms while its velocity annihilates the chaotic behaviour of the condensate with repulsive two-body and attractive three-body interactions, and enhances the dynamical behaviour of a condensate with attractive two-body and repulsive three-body interactions. It comes from this study that the transition route to chaos is the period-doubling scenario in the case of a condensate with repulsive two-body and attractive three-body elastic collisions, and the quasi-periodicity for a condensate with attractive two-body and repulsive three-body elastic collisions. Moreover, the study reveals that the weak values of depth and parameter shape of the optical lattice are favourable to regular oscillations and these parameters are good candidates for chaos control in the dynamical behaviour of condensed atoms. When they are used as control parameters, the bifurcation points which represents the instability points leading to chaos describe the Feigenbaum numbers. This result can help in the control of chaos in the dynamical behaviour of the condensate. It also turn out from this study that, the chaotic behaviour of a condensate with attractive two-body and repulsive three-body interactions between atoms moreover subjected to inelastic collisions in the framework of homoclinic bifurcations occurs when the feeding parameter is about one order of magnitude larger than the parameter related to thee-body inelastic collisions.

GENERAL CONCLUSION AND FUTURES WORKS

Main results

This thesis deals with the study of global bifurcations and transitions routes to chaos in the dynamics of a Bose-Einstein condensate with elastic three-body collisions between atoms taken into account. Moreover, the condensed atoms subjected to inelastic collisions are loaded into a moving optical Fourier-synthesized lattice.
Firstly, we consider the dynamics of such a condensate without inelastic collisions. Seeking the wave function of the condensate on the form of Bloch-like waves, the amplitude equation obtained is a second order nonlinear differential equation. Subsequently, this differential equation is written as a first order system and the Melnikov method applied on it. The Melnikov function(s) is(are) derived, and the condition for the occurrence of horseshoe chaos is determined. The threshold function characterizing the onset of chaos is plotted versus each physical parameter, and the critical value of the control parameter determined. The numerical simulations (Bifurcation diagrams, Poincaré sections, Lyapunov exponents, phase portraits and basins of attraction) are subsequently performed to verify not only the reliability of analytical results, but mainly the transition route to chaos for each physical parameter.
Secondly, taking into account some inelastic processes(linear feeding, dipolar relaxation and three-body recombination) in the dynamics of the condensate, we are interested in finding out how parameters related to these inelastic collisions act on the dynamical behaviour of the condensate, and mainly how they can be used to control the chaos therein. Once again, seeking the wave function of the condensate on the form of Bloch-like waves, the amplitude equation obtained is an integro-differential equation which is subsequently rewritten in the form of a first order system to determine the Melnikov function(s) for homoclinic or both homoclinic and heteroclinic orbits. The condition(s) for the occurrence of chaos is(are) derived, and effects of different physical parameters on the appearance of chaotic oscillations are studied analytically. Different regions of instability are found and plotted in different parameter space.
Let's summarize our analytical and numerical study by answering the five questions underlined in the outline of this thesis.
Concerning the first question, it comes from the study that the depth V_0 and the shape parameter m of the optical lattice always enhance a chaotic behaviour of such condensates. To build an optical lattice with weak values of these parameters is favourable to regular oscillations of condensed atoms. Intuitively this result is surprising, because we expected from optical lattices

with large depths regulars oscillations, due to the fact that bosonic particles need a lot of energy to escape the potential barrier. Undoubtedly, the explanation of that is the existence of the nonlinearity in the equation modeling the dynamics of the condensate.
On the other hand, the velocity of the optical lattice v reduces the chaotic behaviour of the condensate in the case of a positive scattering length and a negative strength of three-body elastic collisions, and enhances the chaotic behaviour of a condensate with a negative scattering length and a positive strength of three-body elastic collisions. Thus, for such a condensate with a positive scattering length, the numerical simulations reveal that a fixed optical lattice or an optical lattice moving very slowly is favourable to a chaotic behaviour of condensed atoms, and the regular oscillations are obtained for an optical lattice moving very rapidly. One can understand the choice of a moving optical lattice used in this thesis. Furthermore, the study reveals that the repulsive three-body interactions always destabilize the dynamics of a condensate with an attractive two-body interaction, while under certain conditions, an attractive three-body interactions can help to stabilize the dynamics of a condensate with a repulsive two-body interaction.
Let's continue with the second question. In the case of such a condensate with inelastic collisions neglected, the numerical simulations through the bifurcation diagrams, Poincaré sections, and phase portraits reveal that the transition route to chaos is the period-doubling scenario for a condensate with repulsive two-body and attractive three-body elastic collisions, and the quasi-periodicity(Torus-doubling, Ruelle-Takens scenario, Torus breakdown, sudden chaos) via Hopf bifurcations for a condensate with attractive two-body and repulsive three-body elastic collisions. Moreover, in the case of period-doubling cascades leading to chaotic oscillations, the bifurcation points obey the Feigenbaum formula about the period-doubling process(Feigenbaum numbers), indicating once again the universality of chaos in this physical system.
The spatiotemporal evolutions of the condensate in the case of stable dynamics(before the chaotic regime characterized by the positive values of largest Lyapunov exponent) allow us to answer the third question. In the case of period-doubling bifurcations leading to chaotic oscillations(a condensate with repulsive two-body and attractive three-body interactions), the spatiotemporal evolutions of the condensate before the bifurcation point leading to homoclinic chaos depicted in figure Fig.(21)(a-b-c) show that the real amplitude of the condensate is virtually constant for a long range of the spatiotemporal variable. The condensate being assumed dissipative, intuitively one understands a certain balance between the dissipation and nonlinearities. It is well known that this property is a signature of solitary waves. Mainly, for weak values of optical depth and optical shape parameter, one has solitonic solutions as bright solitons and black or gray solitons. On the other hand, in the case of quasi-periodicity as transition route to homoclinic chaos(a condensate with attractive two-body and repulsive three-body interactions), the spatiotemporal evolution of condensed atoms before the bifurcation point leading to chaos depicted in figure Fig.(38)(d-e) show the solitonic solutions of eq.(41). One recognizes on these figures, the envelope solitons. In addition, it is interesting to note that bright solitons can be obtained for such a condensate with a scattering length as well positive as negative. That is clearly visible on figures Fig.(5)(a) and Fig.(10)(a) which present bright solitons in the unperturbed system eq.(43) for positive and negative values of the scattering length.

For the fourth question, the analytical study reveals that for a fixed number of atoms in the condensate, the attractive two-body and repulsive three-body elastic collisions tend to increase the density of the traveling wave and increase the spatiotemporal extension of the condensate, while the repulsive two-body and attractive three-body collisions tend to increase the density and decrease the spatiotemporal extension of the condensate. Furthermore, the atomic feeding parameter and parameters related to two-and three-body inelastic collisions must be in the same order for the occurrence of homoclinic chaos in the case of a condensate with repulsive two-body and attractive three-body elastic collisions between atoms. In the case of a condensate with attractive two-body and repulsive three-body elastic collisions between atoms, the homoclinic chaos occurs when the feeding parameter is about one order of magnitude larger than the thee-body recombination factor. This result was obtained in other references in which the condensate was studied by a variational approach, and the condensed atoms trapped by a harmonic potential.

The last question devoted to the control of chaos in the dynamical behaviour of such a condensate finds answer in the different parts of this thesis. Firstly, in the case of a condensate with repulsive two-body and attractive three-body elastic collisions between atoms, the depth and the shape parameter of the optical lattice are good parameters for the control of chaos, because when they are used as control parameters, the different points of instability which represent in fact the bifurcation points gradually obtained, are given by the Feigenbaum formula in the period-doubling phenomenon. That can allow the control of chaos in the dynamics of such a condensate. Here resides the advantage in the use of an optical lattice, and mainly the type of trap potential used in this thesis, the opportunity to the experimentalist to change the geometry of the optical lattice by varying the intensity of Laser beams, or the shape parameter of the optical lattice to control the chaotic behaviour of the condensate.

It is well known today through the Feshbach resonance techniques that one has the ability to control the scattering length, varying it from positive to negative values, as it was shown recently in the Bose-Einstein condensation of ^{85}Rb. Our study reveals that the behaviour of the condensate depends on the sign of the scattering length when the velocity of the optical lattice is used as control parameter. From chaotic oscillations for weak values of velocity of the optical lattice in the case of a condensate with a positive scattering length, the dynamics of the condensate can become regular by reversing the sign of this scattering length through the Feshbach resonance techniques. Coupling thus the velocity of the optical lattice and the Feshbach resonance techniques, can allow the control of chaos in the dynamics of the condensate.

In parameter space $(\gamma_i, \delta = V_0 b_0(m))$, we observe that for a fixed value of depth of the optical lattice taken inside the zone of instability, the regular oscillations of the condensate can be obtained by increasing gradually the parameters related to inelastic collisions. With numerical simulations(bifurcation diagrams) we observe that from chaotic dynamics for large values of optical depth, as the parameters related to losses evolve, the condensate undergoes a cascade of period-doubling bifurcations culminating finally to regular oscillations. Thus, coupling analytical and numerical studies may help to control the homoclinic chaos in the dynamics of the condensate. Moreover, we realize that with optical lattices trap potential, weak values of atomic feeding do

not imply necessary regular oscillations, and large values of this parameter do not imply necessary a chaotic behaviour of the condensate, as it is well known with a harmonic magnetic trap potential. The depth of the optical lattice plays a key role in the control of chaos in the dynamics of the condensate. In addition, we have discovered that in parameter space (γ_i, γ_j), if parameters related to inelastic processes are in the same order then the chaotic behaviour of the condensate is observed. That can be used to control the chaotic behaviour of the condensate.
Secondly, in the framework of the study of a condensate with an attractive two-body and a repulsive three-body interactions between bosonic atoms subjected to some inelastic processes as mentioned above, we obtain theoretically that the chaotic behaviour of the condensate in the case of homoclinic bifurcations occurs when the feeding parameter is about one order of magnitude larger than the thee-body recombination parameter. That can be helpful in controlling chaos in the dynamics of the condensate.

Perspectives

The study has revealed that large values of depth and shape parameter of the optical lattice are favourable to chaotic oscillations of condensed atoms. In the framework of the atom Laser project for example, coherence in the beam of atoms compels the suppression of chaos in the dynamics of condensed atoms. A further work that could be based on this thesis is the suppression of chaos by a periodic force, according to the OGY method.
Moreover, the study has revealed that the behaviour of the condensate depends of the sign of the scattering length when the velocity of the optical lattice is used as control parameter. From chaotic oscillations for weak values of velocity of the optical lattice in the case of a condensate with a positive scattering length, the dynamics of the condensate can become regular by reversing the sign of this scattering length. An-other work based on this thesis which could be made is the control of chaos in the dynamical behaviour of condensed atoms with the Feshbach resonance techniques.

APPENDICES

Appendix A: Integration of T

$$T = \int_{-\tau_c}^{+\tau_c} \frac{X_0(\tau)}{R_0^3(\tau)} \left(\int_{-\tau_c}^{\tau} \left(\gamma_0 R_0^2(\tau) - \gamma_1 R_0^4(\tau) - \gamma_2 R_0^6(\tau) \right) d\tau \right)^2 d\tau. \tag{A.1}$$

Let's evaluate the different terms of T.
Directly via Maple software we obtain

$$\begin{aligned} \chi_1 &= \int_{-\tau_c}^{\tau} R_0^2(\tau) d\tau \\ &= \frac{2a}{g_0\sqrt{\sigma'^2-1}} \left[\arctan\left(\sqrt{\frac{\sigma'+1}{\sigma'-1}} \tanh\left(\frac{a\tau}{2}\right) \right) + \arctan\left(\sqrt{\frac{\sigma'+1}{\sigma'-1}} \tanh\left(\frac{a\tau_c}{2}\right) \right) \right]. \end{aligned} \tag{A.2}$$

$$\begin{aligned} \chi_2 &= \int_{-\tau_c}^{\tau} R_0^4(\tau) d\tau \\ &= \frac{2a^3}{g_0^2(\sigma'^2-1)^{3/2}} \left[\arctan\left(\sqrt{\frac{\sigma'+1}{\sigma'-1}} \tanh\left(\frac{a\tau}{2}\right) \right) + \arctan\left(\sqrt{\frac{\sigma'+1}{\sigma'-1}} \tanh\left(\frac{a\tau_c}{2}\right) \right) \right] \\ &\quad + \frac{a^3\sigma'}{g_0^2(\sigma'^2-1)} \left(\frac{\sinh(a\tau)}{-1+\sigma'\cosh(a\tau)} + \frac{\sinh(a\tau_c)}{-1+\sigma'\cosh(a\tau_c)} \right). \end{aligned} \tag{A.3}$$

$$\begin{aligned} \chi_3 &= \int_{-\tau_c}^{\tau} R_0^6(\tau) d\tau \\ &= \frac{a^5(\sigma'^2+2)}{g_0^3(\sigma'^2-1)^{5/2}} \left[\arctan\left(\sqrt{\frac{\sigma'+1}{\sigma'-1}} \tanh\left(\frac{a\tau}{2}\right) \right) + \arctan\left(\sqrt{\frac{\sigma'+1}{\sigma'-1}} \tanh\left(\frac{a\tau_c}{2}\right) \right) \right] \\ &\quad - \frac{3a^5\sigma'}{2g_0^3(\sigma'^2-1)^2} \left(\frac{\sinh(a\tau)}{-1+\sigma'\cosh(a\tau)} + \frac{\sinh(a\tau_c)}{-1+\sigma'\cosh(a\tau_c)} \right) \\ &\quad + \frac{a^5\sigma'}{2g_0^3(\sigma'^2-1)} \left(\frac{\sinh(a\tau)}{(-1+\sigma'\cosh(a\tau))^2} + \frac{\sinh(a\tau_c)}{(-1+\sigma'\cosh(a\tau_c))^2} \right). \end{aligned} \tag{A.4}$$

$$\int_{-\tau_c}^{\tau}\left(\gamma_0 R_0^2(\tau)-\gamma_1 R_0^4(\tau)-\gamma_2 R_0^6(\tau)\right)d\tau=\gamma_0\chi_1-\gamma_1\chi_2-\gamma_2\chi_3$$
$$=K_1\left[\arctan\left(\sqrt{\frac{\sigma'+1}{\sigma'-1}}\tanh\left(\frac{a\tau}{2}\right)\right)+\arctan\left(\sqrt{\frac{\sigma'+1}{\sigma'-1}}\tanh\left(\frac{a\tau_c}{2}\right)\right)\right]$$
$$+K_2\left(\frac{\sinh(a\tau)}{-1+\sigma'\cosh(a\tau)}+\frac{\sinh(a\tau_c)}{-1+\sigma'\cosh(a\tau_c)}\right)$$
$$+K_3\left(\frac{\sinh(a\tau)}{(-1+\sigma'\cosh(a\tau))^2}+\frac{\sinh(a\tau_c)}{(-1+\sigma'\cosh(a\tau_c))^2}\right) \tag{A.5}$$

Where K_1, K_2, and K_3 are given by

$$\begin{cases} K_1=\dfrac{2\,\gamma_0 a}{g_0\sqrt{\sigma'^2-1}}-\dfrac{2\,\gamma_1 a^3}{{g_0}^2\left(\sigma'^2-1\right)^{3/2}}-\dfrac{\gamma_2 a^5\left(\sigma'^2+2\right)}{{g_0}^3\left(\sigma'^2-1\right)^{5/2}} \\ K_2=-\dfrac{a^3\gamma_1\sigma'}{{g_0}^2\left(\sigma'^2-1\right)}+\dfrac{3a^5\gamma_2\sigma'}{2{g_0}^3\left(\sigma'^2-1\right)^2} \\ K_3=-\dfrac{a^5\gamma_2\sigma'}{2\,{g_0}^3\left(\sigma'^2-1\right)} \end{cases} \tag{A.6}$$

$\dfrac{X_0(\tau)}{R_0^3(\tau)}=-\dfrac{g_0\sigma'}{2a}\sinh(a\tau)$ is an odd function. Hence, let us expand the square of the right-hand side of eq.(A.5). Retaining only the odd part of the expansion, we obtain

$$T=-\frac{g_0\sigma'}{2a}\Big[K_4\int_{-\tau_c}^{+\tau_c}\sinh(a\tau)\arctan\left(\sqrt{\frac{\sigma'+1}{\sigma'-1}}\tanh\left(\frac{a\tau}{2}\right)\right)d\tau+K_5\int_{-\tau_c}^{+\tau_c}\frac{\sinh^2(a\tau)\,d\tau}{-1+\sigma'\cosh(a\tau)}$$
$$+K_6\int_{-\tau_c}^{+\tau_c}\frac{\sinh^2(a\tau)\,d\tau}{(-1+\sigma'\cosh(a\tau))^2}\Big]. \tag{A.7}$$

With K_4, K_5 and K_6 given by

$$\begin{cases} K_4=2\,K_1^2\arctan\left(\sqrt{\dfrac{\sigma'+1}{\sigma'-1}}\tanh\left(\dfrac{a\tau_c}{2}\right)\right)+\dfrac{2\,K_1K_2\sinh(a\tau_c)}{-1+\sigma'\cosh(a\tau_c)}+\dfrac{2\,K_1K_3\sinh(a\tau_c)}{(-1+\sigma'\cosh(a\tau_c))^2} \\ K_5=2\,K_1K_2\arctan\left(\sqrt{\dfrac{\sigma'+1}{\sigma'-1}}\tanh\left(\dfrac{a\tau_c}{2}\right)\right)+\dfrac{2\,K_2^2\sinh(a\tau_c)}{-1+\sigma'\cosh(a\tau_c)}+\dfrac{2\,K_2K_3\sinh(a\tau_c)}{(-1+\sigma'\cosh(a\tau_c))^2} \\ K_6=2\,K_1K_3\arctan\left(\sqrt{\dfrac{\sigma'+1}{\sigma'-1}}\tanh\left(\dfrac{a\tau_c}{2}\right)\right)+\dfrac{2\,K_2K_3\sinh(a\tau_c)}{-1+\sigma'\cosh(a\tau_c)}+\dfrac{2\,K_3^2\sinh(a\tau_c)}{(-1+\sigma'\cosh(a\tau_c))^2}. \end{cases} \tag{A.8}$$

Thus, the expression of T can be rewritten as

$$T=-\frac{g_0\sigma'}{2a}(K_4W_1+K_5W_2+K_6W_3), \tag{A.9}$$

with

$$W_1=\int_{-\tau_c}^{+\tau_c}\sinh(a\tau)\arctan\left(\sqrt{\frac{\sigma'+1}{\sigma'-1}}\tanh\left(\frac{a\tau}{2}\right)\right)d\tau, \tag{A.10}$$

$$W_2 = \int_{-\tau_c}^{+\tau_c} \frac{\sinh^2(a\tau)\, d\tau}{-1+\sigma' \cosh(a\tau)}, \tag{A.11}$$

and

$$W_3 = \int_{-\tau_c}^{+\tau_c} \frac{\sinh^2(a\tau)\, d\tau}{(-1+\sigma' \cosh(a\tau))^2}. \tag{A.12}$$

With the integration by part method through the Maple software, we obtain

$$W_1 = 2\left(\frac{\cosh(a\tau_c)}{a} - \frac{1}{\sigma' a}\right)\arctan\left(\sqrt{\frac{\sigma'+1}{\sigma'-1}}\tanh\left(\frac{a\tau_c}{2}\right)\right) - \frac{\sqrt{\sigma'^2-1}}{\sigma'}\tau_c. \tag{A.13}$$

With the remark that $\dfrac{\sinh^2(a\tau)}{-1+\sigma' \cosh(a\tau)} = \dfrac{1}{\sigma'}\left(\cosh(a\tau) - \dfrac{\sigma'^2-1}{\sigma'(-1+\sigma'\cosh(a\tau))} + \dfrac{1}{\sigma'}\right)$, directly via the Maple software one obtains

$$W_2 = -\frac{4\sqrt{\sigma'^2-1}}{a\sigma'^2}\arctan\left(\sqrt{\frac{\sigma'+1}{\sigma'-1}}\tanh\left(\frac{a\tau_c}{2}\right)\right) + \frac{2\sinh(a\tau_c)}{\sigma' a} + \frac{2\tau_c}{\sigma'^2}. \tag{A.14}$$

With the remark that $\dfrac{\sinh^2(a\tau)}{(-1+\sigma'\cosh(a\tau))^2} = \dfrac{1}{\sigma'^2}\left(1 + \dfrac{2}{-1+\sigma'\cosh(a\tau)} - \dfrac{\sigma'^2-1}{(-1+\sigma'\cosh(a\tau))^2}\right)$, W_3 can be performed directly with the Maple software. Thus, we obtain after some algebraic manipulations

$$W_3 = \frac{4}{a\sigma'^2\sqrt{\sigma'^2-1}}\arctan\left(\sqrt{\frac{\sigma'+1}{\sigma'-1}}\tanh\left(\frac{a\tau_c}{2}\right)\right) - \frac{2\sinh(a\tau_c)}{\sigma' a(-1+\sigma'\cosh(a\tau_c))} + \frac{2\tau_c}{\sigma'^2}. \tag{A.15}$$

Appendix B: Integration of Σ

$$\Sigma = \int_{-\tau_c}^{+\tau_c} \frac{X_{hom}(\tau)}{R_{hom}^3(\tau)}\left(\int_{-\tau_c}^{\tau}\left(\gamma_0 R_{hom}^2(\tau) - \gamma_1 R_{hom}^4(\tau) - \gamma_2 R_{hom}^6(\tau)\right)d\tau\right)^2 d\tau. \tag{B.1}$$

Let's evaluate each term of Σ.

$$\begin{aligned} A_1 &= \int_{-\tau_c}^{\tau} R_{hom}^2(\tau)d\tau \\ &= \frac{-2a}{g_0\sqrt{1-\sigma'^2}}\left[arc\tanh\left(\sqrt{\frac{1-\sigma'}{1+\sigma'}}\tanh\left(\frac{a\tau}{2}\right)\right) + arc\tanh\left(\sqrt{\frac{1-\sigma'}{1+\sigma'}}\tanh\left(\frac{a\tau_c}{2}\right)\right)\right] \end{aligned} \tag{B.2}$$

$$\begin{aligned} A_2 &= \int_{-\tau_c}^{\tau} R_{hom}^4(\tau)d\tau \\ &= -\frac{a^2 A_1}{g_0(1-\sigma'^2)} - \frac{a^3\sigma'}{g_0^2(1-\sigma'^2)}\left(\frac{\sinh(a\tau)}{1+\sigma'\cosh(a\tau)} + \frac{\sinh(a\tau_c)}{1+\sigma'\cosh(a\tau_c)}\right). \end{aligned} \tag{B.3}$$

$$\begin{aligned} A_3 &= \int_{-\tau_c}^{\tau} R_{hom}^6(\tau)d\tau \\ &= \frac{a^4(\sigma'^2+2)A_1}{2g_0^2(1-\sigma'^2)^2} + \frac{3a^5\sigma'}{2g_0^3(1-\sigma'^2)^2}\left(\frac{\sinh(a\tau)}{1+\sigma'\cosh(a\tau)} + \frac{\sinh(a\tau_c)}{1+\sigma'\cosh(a\tau_c)}\right) \\ &\quad + \frac{a^5\sigma'}{2g_0^3(1-\sigma'^2)}\left(\frac{\sinh(a\tau)}{(1+\sigma'\cosh(a\tau))^2} + \frac{\sinh(a\tau_c)}{(1+\sigma'\cosh(a\tau_c))^2}\right). \end{aligned} \tag{B.4}$$

Inserting these integrals into the expression of Σ defined in eq.(B.1), one obtains

$$\begin{aligned} &\int_{-\tau_c}^{\tau}\left(\gamma_0 R_{hom}^2(\tau) - \gamma_1 R_{hom}^4(\tau) - \gamma_2 R_{hom}^6(\tau)\right)d\tau = \gamma_0 A_1 - \gamma_1 A_2 - \gamma_2 A_3 \\ &= \Delta_1\left[arc\tanh\left(\sqrt{\frac{1-\sigma'}{1+\sigma'}}\tanh\left(\frac{a\tau}{2}\right)\right) + arc\tanh\left(\sqrt{\frac{1-\sigma'}{1+\sigma'}}\tanh\left(\frac{a\tau_c}{2}\right)\right)\right] \\ &+\Delta_2\left[\frac{\sinh(a\tau)}{1+\sigma'\cosh(a\tau)} + \frac{\sinh(a\tau_c)}{1+\sigma'\cosh(a\tau_c)}\right] + \Delta_3\left[\frac{\sinh(a\tau)}{(1+\sigma'\cosh(a\tau))^2} + \frac{\sinh(a\tau_c)}{(1+\sigma'\cosh(a\tau_c))^2}\right]. \end{aligned} \tag{B.5}$$

Δ_1, Δ_2 and Δ_3 are given by

$$\begin{cases} \Delta_1 = -\dfrac{2\,\gamma_0 a}{\sqrt{1-\sigma'^2}\,g_0} - \dfrac{2\,\gamma_1 a^3}{\left(1-\sigma'^2\right)^{3/2} g_0^2} + \dfrac{\gamma_2 a^5\left(\sigma'^2+2\right)}{\left(1-\sigma'^2\right)^{5/2} g_0^3} \\ \Delta_2 = \dfrac{\gamma_1 a^3\sigma'}{g_0^2\left(1-\sigma'^2\right)} - \dfrac{3\gamma_2 a^5\sigma'}{2g_0^3\left(1-\sigma'^2\right)^2} \\ \Delta_3 = -\dfrac{\gamma_2 a^5\sigma'}{2g_0^3\left(1-\sigma'^2\right)}. \end{cases} \tag{B.6}$$

$$\frac{X_{hom}(\tau)}{R_{hom}^3(\tau)} = \frac{g_0\sigma'}{2a}\sinh(a\tau). \tag{B.7}$$

It comes from eq.(B.7) that the first part of the integrand of Σ is an odd function. The other part, square of eq.(B.5) must be an odd function also, to avoid Σ being null. Hence, we truncate the square of the right-hand side of eq.(B.5), and we retain only the odd part of the expansion. Thus, one obtains

$$\begin{aligned} &\frac{X_{hom}(\tau)}{R_{hom}^3(\tau)}\left(\int_{-\tau_c}^{\tau}\left(\gamma_0 R_{hom}^2(\tau) - \gamma_1 R_{hom}^4(\tau) - \gamma_2 R_{hom}^6(\tau)\right)d\tau\right)^2 = \\ &\frac{g_0\sigma'}{2a}\left[\Delta_4 arc\tanh\left(\sqrt{\frac{1-\sigma'}{1+\sigma'}}\tanh\left(\frac{a\tau}{2}\right)\right)\sinh(a\tau) + \frac{\Delta_5\sinh^2(a\tau)}{1+\sigma'\cosh(a\tau)} + \frac{\Delta_6\sinh^2(a\tau)}{(1+\sigma'\cosh(a\tau))^2}\right]. \end{aligned} \tag{B.8}$$

$$\begin{cases} \Delta_4 = 2\Delta_1^2 arc\tanh\left(\sqrt{\dfrac{1-\sigma'}{1+\sigma'}}\tanh\left(\dfrac{a\tau_c}{2}\right)\right) + \dfrac{2\Delta_1\Delta_2\sinh(a\tau_c)}{1+\sigma'\cosh(a\tau_c)} + \dfrac{2\Delta_1\Delta_3\sinh(a\tau_c)}{(1+\sigma'\cosh(a\tau_c))^2} \\ \Delta_5 = 2\Delta_1\Delta_2 arc\tanh\left(\sqrt{\dfrac{1-\sigma'}{1+\sigma'}}\tanh\left(\dfrac{a\tau_c}{2}\right)\right) + \dfrac{2\Delta_2^2\sinh(a\tau_c)}{1+\sigma'\cosh(a\tau_c)} + \dfrac{2\Delta_2\Delta_3\sinh(a\tau_c)}{(1+\sigma'\cosh(a\tau_c))^2} \\ \Delta_6 = 2\Delta_1\Delta_3 arc\tanh\left(\sqrt{\dfrac{1-\sigma'}{1+\sigma'}}\tanh\left(\dfrac{a\tau_c}{2}\right)\right) + \dfrac{2\Delta_2\Delta_3\sinh(a\tau_c)}{1+\sigma'\cosh(a\tau_c)} + \dfrac{2\Delta_3^2\sinh(a\tau_c)}{(1+\sigma'\cosh(a\tau_c))^2}. \end{cases} \tag{B.9}$$

The integration of eq.(B.8) between $-\tau_c$ and $+\tau_c$ leads to Σ expressed as

$$\Sigma = \frac{g_0\sigma'}{2a}\left(\Delta_4\Sigma_1 + \Delta_5\Sigma_2 + \Delta_6\Sigma_3\right), \tag{B.10}$$

where Σ_1, Σ_2 and Σ_3 represent the following integrals

$$\begin{cases} \Sigma_1 = \displaystyle\int_{-\tau_c}^{+\tau_c} arc\tanh\left(\sqrt{\frac{1-\sigma'}{1+\sigma'}}\tanh\left(\frac{a\tau}{2}\right)\right)\sinh(a\tau)d\tau \\ \Sigma_2 = \displaystyle\int_{-\tau_c}^{+\tau_c} \frac{\sinh^2(a\tau)d\tau}{1+\sigma'\cosh(a\tau)} \\ \Sigma_3 = \displaystyle\int_{-\tau_c}^{+\tau_c} \frac{\sinh^2(a\tau)d\tau}{(1+\sigma'\cosh(a\tau))^2}. \end{cases} \tag{B.11}$$

These integrals can be carried out with the integration by parts method in the Maple software environment. After some algebraic manipulations, we obtain

$$\begin{cases} \Sigma_1 = \dfrac{2(1+\sigma'\cosh(a\tau_c))}{a\sigma'} arc\tanh\left(\sqrt{\dfrac{1-\sigma'}{1+\sigma'}}\tanh\left(\dfrac{a\tau_c}{2}\right)\right) - \dfrac{\sqrt{1-\sigma'^2}}{\sigma'}\tau_c \\ \Sigma_2 = +\dfrac{4\sqrt{1-\sigma'^2}}{a\sigma'^2} arc\tanh\left(\sqrt{\dfrac{1-\sigma'}{1+\sigma'}}\tanh\left(\dfrac{a\tau_c}{2}\right)\right) + \dfrac{2\sinh(a\tau_c)}{a\sigma'} - \dfrac{2\tau_c}{\sigma'^2} \\ \Sigma_3 = -\dfrac{4}{a\sigma'^2\sqrt{1-\sigma'^2}} arc\tanh\left(\sqrt{\dfrac{1-\sigma'}{1+\sigma'}}\tanh\left(\dfrac{a\tau_c}{2}\right)\right) - \dfrac{2}{a\sigma'}\left(\dfrac{\sinh(a\tau_c)}{1+\sigma'\cosh(a\tau_c)}\right) + \dfrac{2\tau_c}{\sigma'^2} \end{cases} \tag{B.12}$$

Appendix C: Integration of F

$$F = \int_{-\tau_c}^{+\tau_c} \frac{X_{het}(\tau)}{R_{het}^3(\tau)}\left(\int_{-\tau_c}^{\tau}\left(\gamma_0 R_{het}^2(\tau) - \gamma_1 R_{het}^4(\tau) - \gamma_2 R_{het}^6(\tau)\right)d\tau\right)^2 d\tau. \tag{C.1}$$

Let's calculate each term of F.

$$\begin{aligned} B_1 \;=\; & \int_{-\tau_c}^{\tau} R_{het}^2(\tau)d\tau = R_2'^2(\tau+\tau_c) - \frac{2\,R_2'^2\,(1-\Gamma')}{\omega'\sqrt{\Gamma'^2-1}} \times \\ & \left[arc\tanh\left(\sqrt{\frac{\Gamma'+1}{\Gamma'-1}}\tanh\left(\frac{\omega'\tau}{2}\right)\right) + arc\tanh\left(\sqrt{\frac{\Gamma'+1}{\Gamma'-1}}\tanh\left(\frac{\omega'\tau_c}{2}\right)\right)\right]. \end{aligned} \tag{C.2}$$

The symbol $\times$ denotes the multiplication as an arithmetic operation.

$$\begin{aligned} B_2 = \int_{-\tau_c}^{\tau} R_{het}^4(\tau)d\tau = R_2'^4\left[(\tau+\tau_c) + \frac{\Gamma'-1}{\omega'(\Gamma'+1)}\left(\frac{\sinh(\omega'\tau)}{\Gamma'-\cosh(\omega'\tau)} + \frac{\sinh(\omega'\tau_c)}{\Gamma'-\cosh(\omega'\tau_c)}\right)\right] + \\ \frac{2\,R_2'^4\,(\Gamma'-1)\,(\Gamma'+2)}{\omega'(\Gamma'+1)\sqrt{\Gamma'^2-1}}\left[arc\tanh\left(\sqrt{\frac{\Gamma'+1}{\Gamma'-1}}\tanh\left(\frac{\omega'\tau}{2}\right)\right) + arc\tanh\left(\sqrt{\frac{\Gamma'+1}{\Gamma'-1}}\tanh\left(\frac{\omega'\tau_c}{2}.\right)\right)\right] \end{aligned} \tag{C.3}$$

$$B_3 = \int_{-\tau_c}^{\tau} R_{het}^6(\tau)d\tau = R_2'^6(\tau+\tau_c) + \frac{3(\Gamma'-1)(\Gamma'+2)R_2'^6}{2\omega'(\Gamma'+1)^2}\left(\frac{\sinh(\omega'\tau)}{\Gamma'-\cosh(\omega'\tau)} + \frac{\sinh(\omega'\tau_c)}{\Gamma'-\cosh(\omega'\tau_c)}\right)$$
$$-\frac{(\Gamma'-1)^2R_2'^6}{2\omega'(\Gamma'+1)}\left(\frac{\sinh(\omega'\tau)}{(\Gamma'-\cosh(\omega'\tau))^2} + \frac{\sinh(\omega'\tau_c)}{(\Gamma'-\cosh(\omega'\tau_c))^2}\right) + \frac{(2\Gamma'^2+6\Gamma'+7)(\Gamma'-1)R_2'^6}{\omega'(\Gamma'+1)^2\sqrt{\Gamma'^2-1}} \times$$
$$\left[arc\tanh\left(\sqrt{\frac{\Gamma'+1}{\Gamma'-1}}\tanh\left(\frac{\omega'\tau}{2}\right)\right) + arc\tanh\left(\sqrt{\frac{\Gamma'+1}{\Gamma'-1}}\tanh\left(\frac{\omega'\tau_c}{2}\right)\right)\right]. \quad \text{(C.4)}$$

$$\int_{-\tau_c}^{\tau}\left(\gamma_0 R_{het}^2 - \gamma_1 R_{het}^4 - \gamma_2 R_{het}^6\right)d\tau = \gamma_0 B_1 - \gamma_1 B_2 - \gamma_2 B_3$$
$$= Z_1\left[arc\tanh\left(\sqrt{\frac{\Gamma'+1}{\Gamma'-1}}\tanh\left(\frac{\omega'\tau}{2}\right)\right) + arc\tanh\left(\sqrt{\frac{\Gamma'+1}{\Gamma'-1}}\tanh\left(\frac{\omega'\tau_c}{2}\right)\right)\right] + Z_2(\tau+\tau_c)$$
$$+Z_3\left(\frac{\sinh(\omega'\tau)}{\Gamma'-\cosh(\omega'\tau)} + \frac{\sinh(\omega'\tau_c)}{\Gamma'-\cosh(\omega'\tau_c)}\right) + Z_4\left(\frac{\sinh(\omega'\tau)}{(\Gamma'-\cosh(\omega'\tau))^2} + \frac{\sinh(\omega'\tau_c)}{(\Gamma'-\cosh(\omega'\tau_c))^2}\right). \quad \text{(C.5)}$$

The quantities Z_1, Z_2, Z_3, and Z_4 mentioned above are given by

$$\begin{cases} Z_1 = -\dfrac{2\,\gamma_0 R_2'^2\,(1-\Gamma')}{\omega'\sqrt{\Gamma'^2-1}} - \dfrac{2\,\gamma_1 R_2'^4\,(\Gamma'-1)\,(\Gamma'+2)}{\omega'\,(\Gamma'+1)\sqrt{\Gamma'^2-1}} - \dfrac{\gamma_2 R_2'^6\left(2\,\Gamma'^2+6\,\Gamma'+7\right)(\Gamma'-1)}{\omega'\,(\Gamma'+1)^2\sqrt{\Gamma'^2-1}} \\ Z_2 = \gamma_0 R_2'^2 - \gamma_1 R_2'^4 - \gamma_2 R_2'^6 \\ Z_3 = -\dfrac{\gamma_1\,(\Gamma'-1)\,R_2'^4}{\omega'\,(\Gamma'+1)} - \dfrac{3\gamma_2\,(\Gamma'-1)\,(\Gamma'+2)\,R_2'^6}{2\omega'\,(\Gamma'+1)^2} \\ Z_4 = \dfrac{\gamma_2 R_2'^6\,(\Gamma'-1)^2}{2\omega'\,(\Gamma'+1)}. \end{cases} \quad \text{(C.6)}$$

The last term of the integrand of F is given by the following expression

$$\frac{X_{het}(\tau)}{R_{het}^3(\tau)} = \frac{(1-\Gamma')\,\omega'\,\sinh(\omega'\tau)}{2R_2'^2\,(-1+\cosh(\omega'\tau))^2}. \quad \text{(C.7)}$$

It is obvious to see that this quotient of functions is an odd function, and moreover does not exist for $\tau = 0$. Being one part of the integrand of F, the other part given by the square of eq.(C.5) must also be an odd function. Hence, taking the square of the right-hand side of eq.(C.5), and truncating the result only to odd functions of τ, the integrand of F becomes

$$\frac{X_{het}(\tau)}{R_{het}^3(\tau)}\left(\int_{-\tau_c}^{\tau}\left(\gamma_0 R_{het}^2(\tau) - \gamma_1 R_{het}^4(\tau) - \gamma_2 R_{het}^6(\tau)\right)d\tau\right)^2 =$$
$$\frac{(1-\Gamma')\,\omega'}{2R_2'^2}\left[\frac{Z_5\sinh(\omega'\tau)}{(-1+\cosh(\omega'\tau))^2}arc\tanh\left(\sqrt{\frac{\Gamma'+1}{\Gamma'-1}}\tanh\left(\frac{\omega'\tau}{2}\right)\right) + \frac{Z_6\tau\sinh(\omega'\tau)}{(-1+\cosh(\omega'\tau))^2}\right.$$
$$\left.+\frac{Z_7\sinh^2(\omega'\tau)}{(-1+\cosh(\omega'\tau))^2(\Gamma'-\cosh(\omega'\tau))} + \frac{Z_8\sinh^2(\omega'\tau)}{(-1+\cosh(\omega'\tau))^2(\Gamma'-\cosh(\omega'\tau))^2}\right], \quad \text{(C.8)}$$

with the quantities Z_5, Z_6, Z_7, Z_8 given by the following expressions

$$\begin{cases} Z_5 = 2Z_1^2 arc\tanh\left(\sqrt{\dfrac{\Gamma'+1}{\Gamma'-1}}\tanh\left(\dfrac{\omega'\tau_c}{2}\right)\right) + 2Z_1Z_2\tau_c + \dfrac{2Z_1Z_3\sinh(\omega'\tau_c)}{\Gamma'-\cosh(\omega'\tau_c)} + \dfrac{2Z_1Z_4\sinh(\omega'\tau_c)}{(\Gamma'-\cosh(\omega'\tau_c))^2} \\ Z_6 = 2Z_1Z_2 arc\tanh\left(\sqrt{\dfrac{\Gamma'+1}{\Gamma'-1}}\tanh\left(\dfrac{\omega'\tau_c}{2}\right)\right) + 2Z_2^2\tau_c + \dfrac{2Z_2\,Z_3\,\sinh(\omega'\tau_c)}{\Gamma'-\cosh(\omega'\tau_c)} + \dfrac{2Z_2\,Z_4\,\sinh(\omega'\tau_c)}{(\Gamma'-\cosh(\omega'\tau_c))^2} \\ Z_7 = 2Z_1Z_3 arc\tanh\left(\sqrt{\dfrac{\Gamma'+1}{\Gamma'-1}}\tanh\left(\dfrac{\omega'\tau_c}{2}\right)\right) + 2Z_2\,Z_3\,\tau_c + \dfrac{2Z_3^2\sinh(\omega'\tau_c)}{\Gamma'-\cosh(\omega'\tau_c)} + \dfrac{2Z_3Z_4\sinh(\omega'\tau_c)}{(\Gamma'-\cosh(\omega'\tau_c))^2} \\ Z_8 = 2Z_1Z_4 arc\tanh\left(\sqrt{\dfrac{\Gamma'+1}{\Gamma'-1}}\tanh\left(\dfrac{\omega'\tau_c}{2}\right)\right) + 2Z_2Z_4\tau_c + \dfrac{2Z_3\,Z_4\,\sinh(\omega'\tau_c)}{\Gamma'-\cosh(\omega'\tau_c)} + \dfrac{2Z_4^2\sinh(\omega'\tau_c)}{(\Gamma'-\cosh(\omega'\tau_c))^2}. \end{cases} \tag{C.9}$$

It is clearly visible in eq.(C.8) that the integrand of F diverges in the vicinity of $\tau = 0$. But, in terms of area, this integral F can be approximated, by avoiding the vicinity of $\tau = 0$. Thus, the spatiotemporal variable τ will belong to the interval $]-\tau_c, -\tau_i[\cup]\tau_i, \tau_c[$, where the value of τ_i is very close to zero. Hence, carrying out the integration of the right-hand side of eq.(C.8), the approximate expression of F is given by

$$F = \frac{\omega'(1-\Gamma')}{R_2'^2}\left(Z_5F_1 + Z_6F_2 + Z_7F_3 + Z_8F_4\right), \tag{C.10}$$

where F_1, F_2, F_3 and F_4 denote the following integrals

$$\begin{cases} F_1 = \displaystyle\int_{\tau_i}^{\tau_c} \frac{\sinh(\omega'\tau)}{(-1+\cosh(\omega'\tau))^2} arc\tanh\left(\sqrt{\frac{\Gamma'+1}{\Gamma'-1}}\tanh\left(\frac{\omega'\tau}{2}\right)\right) d\tau \\ F_2 = \displaystyle\int_{\tau_i}^{\tau_c} \frac{\tau\sinh(\omega'\tau)d\tau}{(-1+\cosh(\omega'\tau))^2} \\ F_3 = \displaystyle\int_{\tau_i}^{\tau_c} \frac{\sinh^2(\omega'\tau)d\tau}{(-1+\cosh(\omega'\tau))^2(\Gamma'-\cosh(\omega'\tau))} \\ F_4 = \displaystyle\int_{\tau_i}^{\tau_c} \frac{\sinh^2(\omega'\tau)d\tau}{(-1+\cosh(\omega'\tau))^2(\Gamma'-\cosh(\omega'\tau))^2}. \end{cases} \tag{C.11}$$

The integrals F_1 and F_2 are performed by the integration by parts method, which lead to integrals able to be carried out with Maple software. On the contrary, the integrals F_3 and F_4 are directly

obtained by Maple software. The outcome of that is given by

$$
\begin{cases}
F_1 = \dfrac{(\cosh(\omega'\tau_c)-\Gamma')arc\tanh\left(\sqrt{\dfrac{\Gamma'+1}{\Gamma'-1}}\tanh\left(\dfrac{\omega'\tau_c}{2}\right)\right)}{\omega'(-1+\cosh(\omega'\tau_c))(\Gamma'-1)} - \dfrac{(\cosh(\omega'\tau_i)-\Gamma')arc\tanh\left(\sqrt{\dfrac{\Gamma'+1}{\Gamma'-1}}\tanh\left(\dfrac{\omega'\tau_i}{2}\right)\right)}{\omega'(-1+\cosh(\omega'\tau_i))(\Gamma'-1)} \\
+\dfrac{\sqrt{\Gamma'^2-1}}{2\omega'\ (\Gamma'-1)}\left(\dfrac{1}{\tanh\left(\dfrac{\omega'\tau_c}{2}\right)} - \dfrac{1}{\tanh\left(\dfrac{\omega'\tau_i}{2}\right)}\right) \\
F_2 = -\dfrac{\tau_c\omega'\ \tanh\left(\dfrac{\omega'\tau_c}{2}\right) - 1 + \cosh(\omega'\tau_c)}{\omega'^2\left(-1+\cosh(\omega'\tau_c)\right)\tanh\left(\dfrac{\omega'\tau_c}{2}\right)} + \dfrac{\tau_i\omega'\ \tanh\left(\dfrac{\omega'\tau_i}{2}\right) - 1 + \cosh(\omega'\tau_i)}{\omega'^2\left(-1+\cosh(\omega'\tau_i)\right)\tanh\left(\dfrac{\omega'\tau_i}{2}\right)} \\
F_3 = -\dfrac{2(\Gamma'+1)arc\tanh\left(\sqrt{\dfrac{\Gamma'+1}{\Gamma'-1}}\tanh\left(\dfrac{\omega'\tau_c}{2}\right)\right)}{\omega'(\Gamma'-1)\sqrt{\Gamma'^2-1}} + \dfrac{2(\Gamma'+1)arc\tanh\left(\sqrt{\dfrac{\Gamma'+1}{\Gamma'-1}}\tanh\left(\dfrac{\omega'\tau_i}{2}\right)\right)}{\omega'(\Gamma'-1)\sqrt{\Gamma'^2-1}} \\
-\dfrac{2}{\omega'\ (\Gamma'-1)}\left(\dfrac{1}{\tanh\left(\dfrac{\omega'\tau_c}{2}\right)} - \dfrac{1}{\tanh\left(\dfrac{\omega'\tau_i}{2}\right)}\right) \\
F_4 = -\dfrac{2(2+\Gamma')arc\tanh\left(\sqrt{\dfrac{\Gamma'+1}{\Gamma'-1}}\tanh\left(\dfrac{\omega'\tau_c}{2}\right)\right)}{\omega'(\Gamma'-1)^2\sqrt{\Gamma'^2-1}} + \dfrac{2\left(2+\Gamma'\right)arc\tanh\left(\sqrt{\dfrac{\Gamma'+1}{\Gamma'-1}}\tanh\left(\dfrac{\omega'\tau_i}{2}\right)\right)}{\omega'\left(\Gamma'-1\right)^2\sqrt{\Gamma'^2-1}} \\
+\dfrac{1}{\omega'\ (\Gamma'-1)\left(\Gamma'-\cosh(\omega'\tau_c)\right)\tanh\left(\dfrac{\omega'\tau_c}{2}\right)} - \dfrac{1}{\omega'\ (\Gamma'-1)\left(\Gamma'-\cosh(\omega'\tau_i)\right)\tanh\left(\dfrac{\omega'\tau_i}{2}\right)} \\
-\dfrac{3}{\omega'\ (\Gamma'-1)^2\tanh\left(\dfrac{\omega'\tau_c}{2}\right)} + \dfrac{3}{\omega'\ (\Gamma'-1)^2\tanh\left(\dfrac{\omega'\tau_i}{2}\right)}.
\end{cases}
\tag{C.12}
$$

Bibliography

[1] S.N. Bose, Plancks gesetz und lichtquantenhypothese, Zeitschrift f*ü*r Physik, **26**, 178-181 (1924).

[2] A. Einstein, Quantentheorie des einatomingen idealen gases, S.B.Preus.Akad.Wiss, **22**, 261-267 (1924).

[3] A. Einstein, Quantentheorie des einatomingen idealen gases, S.B.Preus.Akad.Wiss, **23**, 3-14 (1925).

[4] A. Einstein, Zur quantentheorie des idealen gases, S.B.Preus.Akad.Wiss, **23**, 18-25 (1925).

[5] P. Kapitza, Viscosity of liquid helium below the λ-point, Nature, **141**, 74-74 (1938).

[6] J.F. Allen and A.D. Misener, Flow of liquid helium II, Nature, **141**, 75-75 (1938).

[7] F. London, On the Bose-Einstein condensation, Phys.Rev, **54**, 947-954 (1938).

[8] F. London, The λ-phenomenon of liquid helium and the Bose-Einstein degeneracy, Nature, **141**, 643-644 (1938).

[9] L.P. Pitaevskii, Vortex lines in an imperfect Bose gas, Sov.Phys.JETP, **13**, 646-651 (1961).

[10] E.P. Gross, Structure of quantized vortex in boson systems, Nuovo Cimento, **20**, 454-477 (1961).

[11] M.R. Andrews, C.G. Townsend, H.J. Miesner, D.S. Durfee, D.M. Kurn, and W. Ketterle, Observation of interference between two Bose condensates, Science, **275** , 637-641 (1997).

[12] Y. Shin, C. Sanner, G.B. Jo, T.A. Pasquini, M. Saba, W. Ketterle, D.E. Pritchard, M. Vengalattore and M. Prentiss, Interference of Bose-Einstein condensates split with an atom chip, Phys.Rev A, **72**, 021604(1-4) (2005).

[13] S. Raghavan, A. Smerzi, S. Fantoni and S.R. Shenoy, Coherent oscillations between two weakly coupled Bose-Einstein condensates: Josephson effects, π oscillations, and macroscopic quantum self-trapping, Phys.Rev A, **59**, 620-633 (1999).

[14] L. Fei, S. Xing, L. Hai-Lu and R. Zhong-Zhou, Atomic population oscillations between two coupled Bose-Einstein condensates with time-dependent nonlinear interaction, Chin.Phys, **16**, 650-659 (2007).

[15] S. Inouye, M.R. Andrews, J. Stenger, H.J. Miesner, D.M. Stamper-Kurn, and W. Ketterle, Observation of Feshbach resonances in a Bose-Einstein condensate, Nature, **392**, 151-154 (1998).

[16] J. Stenger, S. Inouye, M.R. Andrews, H.J. Miesner, D.M. Stamper-Kurn, and W. Ketterle, Strongly enhanced inelastic collisions in a Bose-Einstein condensate near Feshbach resonances, Phys.Rev.Lett, **82**, 2422-2425 (1999).

[17] J.L. Roberts, N.R. Claussen, S.L. Cornish and C.E. Wieman, Magnetic field dependence of ultracold inelastic collisions near a Feshbach resonance, Phys.Rev.Lett, **85**, 728-731 (2000).

[18] J. S*ö*ding, D. Guéry-Odelin, P. Desbiolles, F. Chevy, H. Inamori, J. Dalibard, Three-body decay of a rubidium Bose-Einstein condensate, Appl.Phys B, **69**, 257-261 (1999).

[19] F.Kh. Abdullaev, A. Gammal, Lauro Tomio and T. Frederico, Stability of trapped Bose-Einstein condensates, Phys.Rev A, **63**, 043604(1-14) (2001).

[20] A. Gammal, T. Frederico, Lauro Tomio, F.Kh. Abdullaev, Stability analysis of the D-dimensional nonlinear Schr*ö*dinger equation with trap and two-and three-body interactions, Physics Letters A, **267**, 305-311 (2000).

[21] A. Gammal, T. Frederico, Lauro Tomio and Ph. Chomaz, Atomic Bose-Einstein condensation with three-body interactions and collective excitations, J.Phys.B: At.Mol.Opt.Phys, **33**, 4053-4067 (2000).

[22] L. Tomio, V.S. Filho, A. Gammal and T. Frederico, Stability of atomic condensed systems with attractive two-body interactions, Laser Physics, **13**, 582-586 (2003).

[23] L. Tomio, V.S. Filho, A. Gammal and T. Frederico, Dynamics of Bose-Einstein condensed atoms with attractive two-body interaction and three-body dissipation, Nuclear Physics A, **684**, 681-683 (2001).

[24] V.S. Filho, L. Tomio, A. Gammal, T. Frederico, Dynamical mean-field study of strongly interacting BoseEinstein condensate, Physics Letters A, **325** , 420-425 (2004).

[25] V.S. Filho, T. Frederico, A. Gammal and L. Tomio, Stability of the trapped nonconservative Gross-Pitaevskii equation with attractive two-body interaction, Phys.Rev E, **66**, 036225(1-6) (2002).

[26] V.S. Filho, F.Kh. Abdullaev, A. Gammal and L. Tomio, Autosolitons in trapped Bose-Einstein condensates with two-and three-body inelastic processes, Phy.Rev A, **63**, 053603(1-7), (2001).

[27] R. Chacón, D. Bote and R. Carretero-González, Controlling chaos of a Bose-Einstein condensate loaded into a moving optical Fourier-synthesized lattice, Phys.Rev E, **78**, 036215(1-6) (2008).

[28] G. Chong, W. Hai, and Q. Xie, transient and stationary chaos of a Bose-Einstein condensate loaded into a moving optical lattice potential, Phys.Rev E, **70**, 036213(1-6) (2004).

[29] S. Tchatchueng, M. Siewe Siewe, F.M. Moukam Kakmeni, C. Tchawoua, Bifurcation response and Melnikov chaos in the dynamic of a BoseEinstein condensate loaded into a moving optical lattice, Nonlinear Dyn, **75**, 461-474 (2014).

[30] S. Tchatchueng, M. Siewe Siewe, F.M. Moukam Kakmeni, C. Tchawoua, Impact of inelastic processes on the chaotic dynamics of a Bose-Einstein condensate trapped into a moving optical lattice, Eur.Phys.J.Plus, **132**, 117-133 (2017).

[31] L. Tisza, Transport Phenomena in Helium II, Nature, **141**, 913-913 (1938).

[32] L. Tisza, The theory of liquid helium, Phys.Rev, **72**, 838-854 (1947).

[33] L.D. Landau, The theory of superfluidity of helium II, Phys.Rev, **60**, 356-358 (1941).

[34] N.N. Bogoliubov, On the theory of superfluidity, J.Phys.USSR, **11**, 23-32 (1947).

[35] S.T. Beliaev, Application of the methods of quantum field theory to a system of bosons, Sov.Phys.JETP, **7**, 289-299 (1958).

[36] N.M. Hugenholtz, D. Pines, Ground state energy and excitation spectrum of a system of interacting bosons, Phys.Rev, **116**, 489-506 (1959).

[37] C.E. Hecht, The possible superfluid behaviour of hydrogen atom gases and liquids, Physica, **25**, 1159-1161 (1959).

[38] W.C. Stwalley and L.H. Nosanow, Possible new quantum systems, Phys.Rev.Lett, **36**, 910-913 (1976).

[39] I.F. Silvera and J.T.M. Walraven, Stabilization of atomic hydrogen at low temperature, Phys.Rev.Lett, **44**, 164-168 (1980).

[40] H.F. Hess, D.A. Bell, G.P. Kochanski, R.W. Cline, D. Kleppner, and T.J. Greytak, Observation of 3-body recombination in spin-polarized hydrogen, Phys.Rev.Lett, **51**, 483-486 (1983).

[41] H.F. Hess, Evaporative cooling of magnetically trapped and compressed spin-polarized hydrogen, Phys.Rev B, **34**, 3476-3479 (1986).

[42] J.M. Doyle, J.C. Sandberg, I.A. Yu, C.L. Cesar, D. Kleppner, and T.J. Greytak, Hydrogen in the submillikelvin regime: Sticking probability on superfluid ^{4}He, Phys.Rev.Lett **67**, 603-606 (1991).

[43] D.J. Wineland and H. Dehmelt, Proposed $10^{14}\Delta\nu = \nu$ laser fluorescence spectroscopy on TI^+ mono-ion oscillator III, Bulletin of the Americal Physical Society, **20**, 637-641 (1975).

[44] T.W. Hansch and A.L. Schawlow, Cooling of gases by laser radiation, Opt. Comm, **13**, 68-69 (1975).

[45] V.S. Letokhov, Two quantum amplification of a short light pulse, Pis'ma Zh.Eksp.Teor.Fiz, **7**, 224-227 (1968).

[46] A. Ashkin, Trapping of atoms by resonance radiation pressure, Phys.Rev.Lett, **40**, 729-732 (1978).

[47] J.E. Bjorkholm, J.R. Freeman, A. Ashkin and D. Pearson, Observation of focusing on neutral atoms by the dipole forces of resonance-radiation pressure, Phys.Rev.Lett, **41**, 1361-1364 (1978).

[48] W. Neuhauser, M. Hohenstatt, P. Toschek and H. Dehmelt, Optical-sideband cooling of visible atom cloud confined in parabolic well, Phys.Rev.Lett, **41**, 223-227 (1978).

[49] D.J. Wineland, R.E. Drullinger and F.L. Walls, Radiation-pressure cooling of bound-resonant absorbers, Phys.Rev.Lett, **40**, 1639-1642 (1978).

[50] S.V. Andreev, V.I. Balykin, V.S. Letokhov and V.G. Minogin, Radiative slowing down and monochromatization of a beam of sodium atoms in a counterpropagating laser beam, Sov.Phys.JETP , **55**, 828-834 (1982).

[51] J. Prodan, A. Migdall, W.D. Phillips, I. So, H. Metcalf and J. Dalibard, Stopping atoms with Laser light, Phys.Rev.Lett, **54**, 992-995 (1985).

[52] W. Ertmer, R. Blatt, J.L. Hall and M. Zhu, Laser manipulation of atomic beam velocities: Demonstration of stopped atoms and velocity reversal, Phys.Rev.Lett, **54**, 996-999 (1985).

[53] S. Chu, L. Hollberg, J.E. Bjorkholm, A. Cable and A. Ashkin, Three-dimensional viscous confinement and cooling of atoms by resonance radiation pressure, Phys.Rev.Lett, **55**, 48-53 (1985).

[54] S. Chu, J.E. Bjorkholm, A. Ashkin and A. Cable, Experimental observation of optically trapped atoms, Phys.Rev.Lett, **57**, 314-318 (1986).

[55] E.L. Raab, M. Prentiss, A. Cable, S. Chu, and D.E. Pritchard, Trapping of neutral sodium with radiation pressure, Phys.Rev.Lett, **59**, 2631-2634 (1987).

[56] P.D. Lett, R.N. Watts, C.I. Westbrook, W.D. Phillips, P.L. Gould and H.J. Metcalf, Observation of atoms Laser cooled below the Doppler Limit, Phys.Rev.Lett, **61**, 169-173 (1988).

[57] J. Dalibard et al., in Proceedings, 11th International Conference on Atomic Physics: World Scientific, Singapore (1989).

[58] S. Chu et al., in Proceedings, 11th International Conference on Atomic Physics: World Scientific, Singapore (1989).

[59] R.N. Watts and C.E. Wieman, Manipulating atomic velocities using diode Laser, Opt.Lett, **11**, 291-293 (1986).

[60] D.E. Pritchard, E.L. Raab, V. Bagnato, C.E. Wieman and R.N. Watts, Light traps using spontaneous forces, Phys.Rev.Lett, **57**, 310-313 (1986).

[61] D. Sesko, T. Walker, C. Monroe, A. Gallagher and C. Wieman, Collisional Losses from a Light-Force Atom Trap, Phys.Rev.Lett, **63**, 961-964 (1989).

[62] T. Walker, D. Sesko and C. Wieman, Collective behavior of optically trapped neutral atoms, Phys.Rev.Lett, **64**, 408-412 (1990).

[63] D.W. Sesko, T.G. Walker and C.E. Wieman, Behavior of neutral atoms in a spontaneous force trap, J.Opt.Soc.Am B, **8**, 946-958 (1991).

[64] J. Dalibard and C. Cohen-Tannoudji, Laser cooling below the Doppler limit by polarization gradients: simple theoretical models, J.Opt.Soc.Am B, **6**, 2023-2045 (1989).

[65] S. Chu, Nobel lecture: The manipulation of neutral particles, Rev.Mod.Phys, **70**, 685-706 (1998).

[66] C.N. Cohen-Tannoudji, Nobel lecture: Manipulating atoms with photon, Rev.Mod.Phys, **70**, 707-719 (1998).

[67] W.D. Phillips, Nobel lecture: The manipulation of neutral particles, Rev.Mod.Phys, **70**, 721-741 (1998).

[68] C. Monroe, W. Swann, H. Robinson and C. Wieman, Very cold trapped atoms in a vapor cell, Phys.Rev.Lett, **65**, 1571-1575 (1990).

[69] W. Ketterle, K.B. Davis, M.A. Joffe, A. Martin and D.E. Pritchard, High-densities of cold atoms in a dark spontaneous-force optical trap, Phys.Rev.Lett, **70**, 2253-2256 (1993).

[70] M.O. Mewes, M.R. Andrews, D.M. Kurn, D.S. Durfee, C.G. Townsend, and W. Ketterle, Output coupler for Bose-Einstein condensed atoms, Phys.Rev.Lett, **78**, 582-585 (1997).

[71] S.L. Cornish, N.R. Claussen, J.L. Roberts, E.A. Cornell, and C.E. Wieman, Stable ^{85}Rb Bose-Einstein Condensates with widely tunable interactions, Phys.Rev.Lett, **85**, 1795-1798 (2000).

[72] H. Feshbach, A unified theory of nuclear reactions, Rev.Mod.Phys, **36**, 1076-1078 (1964).

[73] H. Feshbach, A unified theory of nuclear reactions II, Annals of Physics, **19**, 287-313 (1962).

[74] E. Tiesinga, A. Moerdijk, B.J. Verhaar, and H.T.C. Stoof, Conditions for Bose-Einstein condensation in magnetically trapped atomic cesium, Phys.Rev A, **46**, R1167-R1170 (1992).

[75] E. Tiesinga, B.J. Verhaar, and H.T.C. Stoof, Threshold and resonance phenomena in ultracold ground-state collisions, Phys.Rev A, **47**, 4114-4122 (1993).

[76] M.H. Anderson, J.R. Enscher, M.R. Matthews, C.E. Wieman and E.A. Cornell, Observation of Bose-Einstein Condensation in a dilute atomic vapor, Science, **269**, 198-201 (1995).

[77] E. Cornell, very cold indeed: The nanoKelvin physics of Bose-Einstein condensation, J.Res.Natl.Inst.Stand.Technol, **101**, 419-434 (1996).

[78] E.A. Cornell, C.E. Wieman, Nobel lecture: Bose-Einstein condensation in a dilute gas, the first 70 years and some recent experiments, Rev.Mod.Phys, **74**, 875-893 (2001).

[79] W. Ketterle, Nobel lecture: When atoms behave as waves: Bose-Einstein condensation and the atom laser, Rev.Mod.Phys, **74**, 1131-1151 (2002).

[80] Rehman Fazal, Jia-Zhen Li, Zhi-Wen Chen, Yuan Qin, Ya-Yi Lin, Zuan-Xian Zhang, Shan-Chao Zhang, Wei Huang, Hui Yan and Shi-Liang Zhu, Production of ^{87}Rb Bose-Einstein condensate with a simple evaporative cooling method, Chin.Phys.Lett, **37**, 036701(1-5) (2020).

[81] C. Denz, S. Flach, Y.S. Kivshar, Nonlinearities in periodic structures and metamaterials, Springer Series in optical sciences, **150**, 195-203 (2010).

[82] R.P. Feynman, Quantum mechanical computers, Opt.News, **11**, 11-20 (1985).

[83] R.P. Feynman, Quantum mechanical computers, Found.Phys, **16**, 507-531 (1986).

[84] E. Jane, G. Vidal, W. Dür, P. Zoller, and J.I. Cirac, Simulation of quantum dynamics with quantum optical systems, Quantum Inform.Comput, **3**, 15-37 (2003).

[85] B.P. Anderson, M.A. Kasevich, Macroscopic quantum interference from atomic tunnel arrays, Science , **282**, 1686-1689 (1998).

[86] F.S. Cataliotti, S. Burger, C. Fort, P. Maddaloni, F. Minardi, A. Trombettoni, A. Smerzi and M. Inguscio, Josephson junction arrays with Bose-Einstein condensates, Science, **293** , 843-846 (2001).

[87] D. Jaksch, C. Bruder, J.I. Cirac, C. W. Gardiner, P. Zoller, Cold bosonic atoms in optical lattices, Phys.Rev.Lett, **81**, 3108-3111 (1998).

[88] C. Orzel, A.K. Tuchman, M.L. Fenselau, M. Yasuda, M.A. Kasevich, Squeezed states in a Bose-Einstein condensate, Science, **291**, 2386-2389 (2001).

[89] B. Wu, Q. Niu, Landau and dynamical instabilities of the superflow of Bose-Einstein condensates in optical lattices, Phys.Rev A, **64**, 061603(1-4) (2001).

[90] A. Smerzi, A. Trombettoni, P.G. Kevrekidis, A.R. Bishop, Dynamical superfluid-insulator transition in a chain of weakly coupled Bose-Einstein condensates, Phys.Rev.Lett, **89**, 170402(1-4) (2002).

[91] L. Fallani, L. DeSarlo, J.E. Lye, M. Modugno, R. Saers, C. Fort and M. Inguscio, Observation of dynamical instability for a Bose-Einstein condensate in a moving 1D optical lattice, Phys.Rev.Lett, **93**, 140406-140406(1-4) (2004).

[92] C. Fort, F.S. Cataliotti, L. Fallani, F. Ferlaino, P. Maddaloni, and M. Inguscio, Collective excitations of a trapped Bose-Einstein Condensate in the presence of a 1D optical lattice, Phys.Rev.Lett, **90**, 140405(1-4) (2003).

[93] M. Krämer, L. Pitaevskii and S. Stringari, Macroscopic dynamics of a trapped Bose-Einstein condensate in the presence of a 1D and 2D optical lattice, Phys.Rev.Lett, **88**, 180404(1-4) (2002).

[94] F. Ferlaino, P. Maddaloni, S. Burger, F.S. Cataliotti, C. Fort, M. Modugno, and M. Inguscio, Dynamics of a Bose-Einstein condensate at finite temperature in an atom-optical coherence filter, Phys.Rev A, **66**, 011604(1-4) (2002).

[95] C. Menotti, M. Krömer, L. Pitaevskii and S. Stringari, Dynamic structure factor of a Bose-Einstein condensate in a one-dimensional optical lattice, Phys.Rev A, **67**, 053609(1-4) (2003).

[96] T. Stöferle, H. Moritz, C. Schori, M. Köhl, T. Esslinger, Transition from a strongly interacting 1D superfluid to a Mott insulator. Phys.Rev.Lett, **92**, 130403(1-4) (2004).

[97] B. Wu and Q. Niu, Nonlinear Landau-Zener tunneling, Phys.Rev A, **61**, 023402(1-4) (2000).

[98] M. Machholm, C.J. Pethick and H. Smith, Band structure elementary excitations and stability of a Bose-Einstein condensate in a periodic potential, Phys.Rev A, **67**, 053613(1-4) (2003).

[99] N.R. Cooper, J. Dalibard and I.B. Spielman, Topological bands for ultracold atoms, Rev.Mod.Phys, **91**, 015005(1-55) (2019).

[100] J. Mun, P. Medley, G.K. Campbell, L.G. Marcassa, D.E. Pritchard, and W. Ketterle, Phase Diagram for a Bose-Einstein condensate moving in an optical lattice, Phys.Rev.lett, **99**, 150604(1-4) (2007).

[101] Z. Wei Xie, W. Zhang, S.T. Chui and W.M. Liu, Magnetic solitons of spinor Bose-Einstein condensates in an optical lattice, Phys.Rev A, **69**, 053609(1-4) (2004).

[102] H. Poincaré, On the three-body problem and the equations of dynamics, Acta mathematica, **13**, 1-270 (1890).

[103] E.N. Lorenz, Deterministic non-periodic flow, Journal of the Atmospheric Sciences, **20**, 130-141 (1963).

[104] A. Gammal, V.S. Filho, L. Tomio and T. Frederico, Spatio-temporal chaos in time evolution of **BEC** with attractive two-body interactions, NATO Science Series II, **45**, 61-67 (2001).

[105] K. Zhang, W. Chen, M. Bhattacharya and P. Meystre, Hamiltonian chaos in a coupled **BEC**-optomechanical-cavity system, Phys.Rev. A, **81**, 013802(1-6) (2010).

[106] Xu Jun, Hai Wen-Hua and Li Hui, Generation and control of chaos in a Bose-Einstein condensate, Chin.Phys, **16**, 2244-2254 (2007).

[107] E. Ott, C. Grebogi, J.A. Yorke, Controlling chaos, Phys.Rev.Lett, **64**, 1196-1199 (1990).

[108] T. Shinbrot, E. Ott, C. Grebogi, J.A. Yorke, Using chaos to direct trajectories, Phys.Rev.Lett, **65** , 3215-3218 (1990).

[109] T. Shinbrot, E. Ott, C. Grebogi, J.A. Yorke, Using small perturbations to control chaos, Nature, **363**, 411-417 (1993).

[110] S. Hayes, C. Grebogi, E. Ott, Communicating with chaos, Phys.Rev.Lett, **70**, 3031-3034 (1993).

[111] E.R. Hunt, Stabilizing high-period orbits in a chaotic system: The diode resonator, Phys.Rev.Lett, **67**, 1953-1957 (1993).

[112] V. Petrov, V. Gaspar, J. Masere, K. Showalter, Controlling chaos in the Belousov-Zhabotinsky reaction, Nature, **361** 240-243 (1993).

[113] E.A. Jackson, A.W. Huebler, Periodic entrainment of chaotic logistic map dynamics, Physica D, **44**, 407-420 (1990).

[114] K. Pyragas, Continuous control of chaos by self-controlling feedback, Phys.Lett. A, **170**, 421-428 (1992).

[115] R. Lima, M. Pettini, Suppression of chaos by resonant parametric perturbations, Phys.Rev A, **41**, 726-733 (1990)

[116] Y. Braiman, I. Goldhirsch, Taming chaotic dynamics with weak periodic perturbations, Phys.Rev.Lett, **20**, 2545-2548 (1991)

[117] F.Kh. Abdullaev and R.A. Kraenkel, Coherent atomic oscillations and resonances between coupled Bose-Einstein Condensates with time-dependent trapping potential, Phys.Rev A, **62**, 023613(1-9) (2000)

[118] C. Lee, W. Hai, L. Shi, X. Zhu, and K. Gao, Chaotic and frequency-locked atomic population oscillations between two coupled Bose-Einstein condensates, Phys.Rev A, **64**, 053604(1-9) (2001).

[119] V.M. Eguiluz, E. Hernndez-Garca, O. Piro and S. Balle, Frozen spatial chaos induced by boundaries, Phys.Rev E, **60**, 6571-6579 (1999).

[120] G. Chong, W. Hai, and Q. Xie, Controlling chaos in a weakly coupled array of Bose-Einstein condensates, Phys.Rev E, **71**, 016202(1-7) (2005).

[121] A.D. Martin, C.S. Adams and S.A. Gardiner, Bright matter-wave soliton collisions in a harmonic trap: Regular and chaotic dynamics, Phys.Rev.Lett, **98**, 020402(1-4) (2007).

[122] A.K. Pattanayak, A. Gammal, C.A. Sackett and R.G. Hulet, Stabilizing an attractive Bose-Einstein condensate by driving a surface collective mode, Phys.Rev A, **63**, 033604(1-4) (2001).

[123] C. Zhang, J. Liu, M.G. Raizen and Q. Niu, Quantum chaos of Bogoliubov waves for a Bose-Einstein Condensate in stadium billiards, Phys.Rev.lett, **93**, 074101(1-4) (2004).

[124] L. Fei, R. Zhong-Zhou, L. Hai-Lu, S. Wei-Xing and W. Qin, Spatial chaos of Bose-Einstein Condensates in a cigar shaped Trap, Commun.Theor.Phys, **48**, 107-111 (2007).

[125] B.A. Idowu and U.E. Vincent, Synchronization and stabilization of chaotic dynamics in a quasi-1D Bose-Einstein condensate, Journal of Chaos, **2013**, 1-8 (2013).

[126] D.S Petrov, Three-Body interacting bosons in free space, Phys.Rev.Lett, **112**, 103201(1-5) (2014).

[127] A.E. Leanhardt, A.P. Chikkatur, D. Kielpinski, Y.Shin, T.L. Gustavson, W. Ketterle and D.E. Pritchard, Propagation of a Bose-Einstein condensate in a magnetic waveguide, Phys.Rev.Lett, **89**, 040401(1-4) (2002).

[128] P. Ping and L. Guan-Qiang, Effects of three-body interaction on collective excitation and stability of Bose-Einstein condensate, Chin.Phys B, **18**, 3221-3225 (2009).

[129] E. Kengne and A. Lakhssassi, Dynamics of solitary-wave structures in one-dimensional Gross-Pitaevskii equation with distributed coefficients, Eur.Phys.J.Plus, **130**, 197-207 (2015).

[130] P.A. Ruprecht, M.J. Holland, K. Burnett and M. Edwards, Time-dependent solution of the nonlinear Schrödinger equation for Bose-condensed trapped neutral atoms, Phys.Rev A, **51**, 4704-4711 (1995).

[131] P. Coullet and N. Vandenberghe, Chaotic dynamics of a Bose-Einstein condensate in a double-well trap, J.Phys.B: At.Mol.Opt.Phys, **35**, 1593-1612 (2002)

[132] E. Wamba, A. Mohamadou and T.C. Kofané, Modulational instability of a trapped Bose-Einstein condensate with two-and three-body interactions, Phys.Rev E, **77**, 046216(1-4) (2008).

[133] E. Wamba, T.C. Kofané and A. Mohamadou, Matter-wave solutions of BoseEinstein condensates with three-body interaction in linear magnetic and time-dependent laser fields, Chin.Phys B, **21**, 070504(1-7) (2012).

[134] D. Belobo Belobo, G.H. Ben-Bolie, T.C. Kofané, Dynamics of matter-wave condensates with time-dependent two-and three-body interactions trapped by a linear potential in the presence of atom gain or loss, Phys.Rev E, **89**, 042913(1-20) (2014).

[135] D. Belobo Belobo, G.H. Ben-Bolie and T.C. Kofané, Three-body interactions beyond the Gross-Pitaevskii equation and modulational instability of Bose-Einstein condensate, J.Mod.Phys B, **26**, 1250202(1-16) (2012).

[136] D. Belobo Belobo, G.H. Ben-Bolie, T.B. Ekogo, C.G. Latchio Tiofack and T.C. Kofané, Modulational instability of a Bose-Einstein condensate beyond the Fermi pseudopotential with a time-dependent complex potential, J.Mod.Phys B, **26**, 1250164(1-17) (2012).

[137] I. Marino, S. Raghavan, S. Fantoni, S.R. Shenoy, and A. Smerzi, Bose-condensate tunneling dynamics: Momentum-shortened pendulum with damping, Phys.Rev A, **60**, 487-493 (1999).

[138] A. Aftalion, Q. Du, and Y. Pomeau, Dissipative flow and vortex shedding in the Painlev boundary layer of a Bose-Einstein condensate, Phys.Rev.Lett, **91**, 090407(1-4) (2003).

[139] M. Tsubota, K. Kasamatsu, M. Ueda, Vortex lattice formation in a rotating Bose-Einstein condensate, Phys.Rev A, **65**, 023603(1-4) (2002).

[140] K. Kasamatsu, M. Tsubota, M. Ueda, Nonlinear dynamics of vortex lattice formation in a rotating Bose-Einstein condensate, Phys.Rev A, **67**, 033610(1-4) (2003).

[141] F. Bloch, Über die quantenmechanik der elektronen in Kristallgittern, Zeitschrift f*ü*r Physik, **52**, 555-600 (1928).

[142] I. Bloch, Ultracold quantum gases in optical lattices, Nature Physics, **1**, 23-30 (2005).

[143] I. Bloch, Quantum gases in optical lattices, Phys.World, **17**, 2529 (2004).

[144] M. Peyrard et T. Dauxois, Physique des solitons, EDP SCIENCES et CNRS ÉDITIONS (2004).

[145] I.S. Gradshteyn, I.M. Ryzhik, Table of integrals, series and products, Academic Press, New York (1994).

[146] T. Salger, C. Geckeler, S. Kling and M. Weitz, Atomic Landau-Zener tunneling in Fourrier-synthesized optical lattice, Phys.Rev.Lett, **99**, 190405(1-4) (2007).

[147] V. K. Melnikov, On the stability of the centre for time-periodic perturbations, Transactions Moscow Mathematical Society, **12**, 1-57 (1963).

[148] S. Wiggins, Global Bifurcations and Chaos-Analytical Methods, Springer-Verlag New York, Heidelberg Berlin (1988).

[149] S. Wiggins, On the detection and dynamical consequences of orbits homoclinic to hyperbolic periodic orbits and normally hyperbolic invariant tori in a class of crdinary differential equations, SIAM J.Appl.Math, **48**, 262-285 (1988).

[150] M. Siewe Siewe, C. Tchawoua, P. Woafo, Melnikov chaos in a periodically driven Rayleigh-Duffing oscillator, Mechanics Research Communications, **37**, 363-368 (2010).

[151] B.R. Nana Nbendjo, Y. Salissou, P. Woafo, Active control with delay of catastrophic motion and horseshoes chaos in a single well Duffing oscillator, Chaos, Solitons and Fractals, **23** 809-816 (2005).

[152] B.R. Nana Nbendjo, R. Tchoukuegno, P. Woafo, Active control with delay of vibration and chaos in a double-well Duffing oscillator, Chaos, Solitons and Fractals **18** 345-353 (2003).

[153] C. Tchawoua, M. Siewe Siewe, S. Tchatchueng and F.M. Moukam Kakmeni, Nonlinear dynamics of parametrically driven particles in a ϕ^6 potential, Nonlinearity, **21**, 1041-1055 (2008).

[154] J.L. Roberts, N.R. Claussen, S.L. Cornish, E.A. Donley, E.A. Cornell and C.E. Wieman, Controlled collapse of a Bose-Einstein condensate, Phys.Rev.Lett, **86**, 4211(1-4) (2001).

[155] N.R. Claussen, E.A. Donley, S.T. Thomspson and C.E. Wieman, Microscopic dynamics in a strongly interacting Bose-Einstein condensate, Phys.Rev.Lett, **89**, 010401(1-4) (2002).

[156] J. Hecker Denschlag, J. E. Simsarian, H. H$\ddot{a}$ffner, C. M^c Kenzie, A. Browaeys, D. Cho, K. Helmerson, S.L. Rolston, and W.D. Phillips, A Bose-Einstein Condensate in an optical lattice, J.Phys.B, **35**, 3095-3110 (2002).

[157] G. Chong, W. Hai, and Q. Xie, Spatial chaos of trapped Bose-Einstein condensate in one-dimensional weak optical lattice potential, Chaos, **14**, 217-223 (2004).

[158] D. Ruelle and F. Takens, On the Nature of Turbulence, Commun.Math.Phys, **20**, 167-192 (1971).

[159] S.E. Newhouse, D. Ruelle and R. Takens, Occurence of Strange Axiom A attractors near quasi-perioidc flows on T_m (m = 3 or more), Commun.Math.Phys, **64**, 35-40 (1978).

[160] F. Dalfovo, S. Giorgini, Lev P. Pitaevskii and S. Stringari, Theory of Bose-Einstein condensation in trapped gases, Rev.Mod.Phys, **71**, 463-512 (1999).

[161] P.W. Courteille, V.S. Bagnato and V.I. Yukalov, Bose-Einstein condensation of trapped atomic gases, Laser Phys, **11**, 659-800 (2001).

LIST OF PUBLICATIONS IN INTERNATIONAL REFEREED JOURNALS

1- **Sylvin Tchatchueng**, Martin Siewe Siewe, François Marie Moukam Kakmeni and Clément Tchawoua, Impact of inelastic processes on the chaotic dynamics of a Bose-Einstein condensate trapped into a moving optical lattice, Eur.Phys.J.Plus, **132**, 117-133 (2017).

2- **S. Tchatchueng**, M. Siewe Siewe, F.M. Moukam Kakmeni and C. Tchawoua, Bifurcation response and Melnikov chaos in the dynamics of a Bose-Einstein condensate loaded into a moving optical lattice, Nonlinear Dyn, **75**, 461-474 (2014).

EPJ Plus

EPJ.org
your physics journal

Eur. Phys. J. Plus (2017) **132**: 117 DOI 10.1140/epjp/i2017-11368-1

Impact of inelastic processes on the chaotic dynamics of a Bose-Einstein condensate trapped into a moving optical lattice

Sylvin Tchatchueng, Martin Siewe Siewe, François Marie Moukam Kakmeni and Clément Tchawoua

Società Italiana di Fisica

Springer

Eur. Phys. J. Plus (2017) **132**: 117
DOI 10.1140/epjp/i2017-11368-1

THE EUROPEAN PHYSICAL JOURNAL PLUS

Regular Article

Impact of inelastic processes on the chaotic dynamics of a Bose-Einstein condensate trapped into a moving optical lattice

Sylvin Tchatchueng[1,a], Martin Siewe Siewe[1,b], François Marie Moukam Kakmeni[2,c], and Clément Tchawoua[1,d]

[1] Université de Yaoundé I, Faculté des sciences, Département de Physique, Laboratoire de Mécanique, BP: 812 Yaoundé, Cameroon
[2] University of Buea, Faculty of Science P.O. Box 63 Buea, Cameroon

Received: 21 November 2016 / Revised: 27 January 2017
Published online: 8 March 2017 –

Abstract. We investigate the dynamics of a Bose-Einstein condensate with attractive two-body and repulsive three-body interactions between atoms trapped into a moving optical lattice and subjected to some inelastic processes (a linear atomic feeding and two dissipative terms related to dipolar relaxation and three-body recombination). We are interested in finding out how the nonconservative terms mentioned above act on the dynamical behaviour of the condensate, and how they can be used in the control of possible chaotic dynamics. Seeking the wave function of condensate on the form of Bloch waves, we notice that the real amplitude of the condensate is governed by an integro-differential equation. As theoretical tool of prediction of homoclinic and heteroclinic chaos, we use the Melnikov method, which provides two Melnikov functions related to homoclinic and heteroclinic bifurcations. Applying the Melnikov criterion, some regions of instability are plotted in the parameter space and reveal complex dynamics (solitonic stable solutions, weak and strong instabilities leading to collapse, growth-collapse cycles and finally to chaotic oscillations). It comes from some parameter space that coupling the optical intensity and parameters related to atomic feeding and atomic losses (dissipations) as control parameters can help to reduce or annihilate chaotic behaviours of the condensate. Moreover, the theoretical study reveals that there is a certain ratio between the atomic feeding parameter and the parameters related to the dissipation for the occurrence of chaotic oscillations in the dynamics of condensate. The theoretical predictions are verified by numerical simulations (Poincaré sections), and there is a certain reliability of our analytical treatment.

1 Introduction

Based on ideas of Bose about the quantum statistics of photons [1], the Bose-Einstein condensation (BEC) predicted by Einstein in 1925 [2] is a state of matter of a dilute gas of bosons cooled to temperatures very close to absolute zero. After the discovery of the superfluidity of ^{4}He below the transition temperature of 2.17 K by Kapitsa [3], Allen and Misener [4] in 1938, London [5] suggested that this new phase of matter might have some connection with the phenomenon of Bose-Einstein condensation. Thenceforth, to understand the link between those two phenomena, the quest of temperatures very close to absolute zero became a new challenge in modern physics. The achievement of this challenge gave rise to the first observation of the Bose-Einstein condensation of ^{87}Rb atoms around 0.5 nK in 1995 [6]. Later on, at very low temperatures, the Bose-Einstein condensation of following atoms: ^{23}Na, ^{7}Li, ^{1}H, ^{4}He, ^{85}Rb, ^{41}K and ^{133}Cs was achieved. Thus, a BEC can be viewed as the coldest place in the universe. Rewarded by the Nobel prize in 2001 [7], this technological prowess has enabled numerous fascinating experiments in which fundamental quantum mechanics is studied in a macroscopic scale, mainly when the bosonic atoms are trapped in optical lattices, as illustrated in the following references. In [8] the superfluidity of Bose-Einstein condensates in optical lattices is investigated and the authors have shown that apart from the usual Landau instability, which occurs when a BEC flows faster than the speed of sound, the BEC can also suffer a dynamical instability, resulting in period-doubling and

[a] e-mail: stchatchueng@yahoo.fr
[b] e-mail: martinsiewesiewe@yahoo.fr
[c] e-mail: fmoukam@yahoo.com
[d] e-mail: ctchawa@yahoo.fr

other sorts of symmetry breaking of the system. The authors of ref. [9] have shown that BEC in lattices can be used to study nonlinear dynamics of three-dimensional systems. In [10], the stability of superfluid currents in a system of ultracold bosons is studied using a moving optical lattice and the authors have proven that, superfluid currents in a very weak lattice become unstable when their momentum exceeds 0.5 recoil momentum. The authors of [11] have studied the magnetic solitons in spinor Bose-Einstein condensates confined in a one-dimensional optical lattice by the Holstein-Primakoff transformation method. They arrived at the conclusion that, due to the long-range light-induced and static magnetic dipole-dipole interactions, there exist different types of magnetic solitary excitations in different parameter regions.

Recently, the dynamics of a Bose-Einstein condensate subjected to some inelastic processes (linear feeding from thermal cloud and two dissipative terms related to dipolar relaxation and three-body collisions of atoms) has been investigated. The authors of refs. [12–15] have studied the stability of a Bose-Einstein condensate with some inelastic processes which appear in the equation modeling the condensate as an addition of an imaginary part in the Gross-Pitaesvkii formalism, and the condensate is now governed by the complex Ginzburg-Landau equation (GLE). As results, they have obtained through numerical simulations that the small values of feeding parameter or the small values of the ratio between the feeding parameter and the three-body recombination parameter are favourable to stable dynamics of condensate whereas under the large values of ratio between the feeding parameter and dissipative parameters, the system becomes very unstable. In these studies, the authors have considered the bosonic atoms trapped into a harmonic magnetic field, and the variational approach was the tool used in the treatment. Motivated by their results obtained numerically, we are excited to know if the nature of the trap potential don't affects the relevant results of their study. Hence, we consider the same mean-field approximation, but with bosonic atoms trapped into a moving optical lattice. Instead of the variational approach, the Melnikov method, already used in our earlier work [16] in the case of repulsive two-and attractive three-body interactions between atoms is the method used in the theoretical treatment. The advantage of this approach, although it implies complicated and sometimes nonintegrable integrals, is the possibility to express analytically the condition of occurrence of chaotic dynamics of condensate. Thus, the connections between the atomic feeding parameter and parameters related to the dissipation can be deduced analytically, and verified numerically through the bifurcations diagrams and Poincaré sections.

We organize the study as follows: We first present the extended (GP) formalism that we have considered, and we establish the integro-differential equation governing the particle number density of condensate in sect. 2. Section 3 is devoted to fixed points of unperturbed system. The Melnikov analysis is used in sect. 4 to predict theoretically the conditions of occurrence of chaos in the framework of homoclinic and heteroclinic bifurcations. We exhibit our numerical results and discussions in sect. 5, and we conclude the study in sect. 6.

2 Extended nonconservative Gross-Pitaevskii equation

At low enough temperatures, the mean-field approximation usually used to describe the dynamics of a Bose-Einstein condensate (BEC) of dilute bosonic gases is a nonlinear Shrödinger equation (NLSE), the so-called Gross-Piteavskii equation (GPE). In this formalism, the atom-atom interactions are restricted only to the elastic two-body interaction. In ref. [17], the elastic three-body interaction in the dynamics of a BEC has been established theoretically. Although the experimental proof of that elastic three-body interaction remain an open question, the repulsive three-body interaction was introduced in the GP formalism [12–15,18–21] to stabilize the dynamics of condensed atoms with a negative s-wave atom-atom scattering length which is unstable for a large number of atoms. The two kinds of inelastic processes which can contribute significantly to the decay of a Bose-Einstein condensate are the three-body recombination and the two-body dipolar relaxation. These inelastic collisions between atoms, which must be viewed as a dissipation phenomenon in the dynamics of a condensate have been proved experimentally in ref. [22]. The inelastic collisions between atoms (atomic losses) eject the atoms from the confining trap, and to keep constant the number of atoms, a atomic pumping process is necessary, taking atoms from uncondensed state and injecting them into the condensate (atomic feeding). In what follows, we consider a thin cigar-shaped condensate resulting from a 3D BEC with a strong radial confinement, so that the transversal dynamics can be neglected. Moreover, we take into account the irreversible terms related to losses and to the atomic feeding mentioned above. The bosonic atoms are trapped into a particular moving optical lattice with the possibility to control its depth. Thus, the thin cigar-shaped condensate is governed by the following quasi-one-dimensional (1D) time-dependent Gross-Pitaevskii-Ginzburg equation (GPGE),

$$i\hbar\frac{\partial\psi}{\partial t} = -\frac{\hbar^2}{2m_a}\frac{\partial^2\psi}{\partial x^2} + \left(\tilde{V}_{\text{trap}} + \tilde{g_0}|\psi|^2 + \tilde{g_1}|\psi|^4\right)\psi + i\left(\tilde{\gamma_0} - \tilde{\gamma_1}|\psi|^2 - \tilde{\gamma_2}|\psi|^4\right)\psi, \tag{1}$$

where $\psi(x;t)$ is the wave function of condensate, $\xi = x+\upsilon_L t$ is the space-time variable, $\upsilon_L = \frac{\Delta f}{2k}$ the velocity of traveling lattice, with Δf the frequency difference between the two Fourier-synthesized counter-propagating laser beams. $k = \frac{2\pi}{\lambda}$ is the laser wave vector, m_a is the atomic mass. The negative real number $\tilde{g_0} = \frac{4\pi\hbar^2 a_s}{m_a}$ is the interatomic two-body

interaction strength, with a_s the s-wave scattering length. The positive real number $\tilde{g_1}$ is the strength of the effective three-body interactions. $\eta = \frac{2K(m)k}{\pi}$, with $K(m)$ the complete elliptic integral of first kind. $\tilde{V}_{\text{trap}} = \tilde{V_0} sn^2(\eta\xi; m)$ is the periodic moving optical lattice. The function $sn(\cdot; m)$ is the Jacobian sine elliptic function of parameter m ($0 \leq m \leq 1$). The choice of this form of trap potential compared with the classical form generally used is that it will be very helpful in experiments, due to the possibility to change (with the variable shape m) the depth of the optical lattice.

$\tilde{\gamma_0}$ represents the rate of pumping process. $\tilde{\gamma_1}$ and $\tilde{\gamma_2}$ are parameters related to atomic losses. In fact, $\tilde{\gamma_1}$ and $\tilde{\gamma_2}$ are, respectively, related to dipolar relaxation and to the three-body recombination. The signs $(-)$ in front of dissipation parameters displayed in eq. (1) imply that $\tilde{\gamma_0}$, $\tilde{\gamma_1}$ and $\tilde{\gamma_2}$ will be positive real numbers.

Due to fact that generally the optical lattices are periodic functions, that compels to seek the solutions of eq. (1) on the form of Bloch waves [23,24],

$$\psi(x;t) = \varphi(\xi) \exp[i(\tilde{\alpha}x + \tilde{\beta}t)], \tag{2}$$

where $\varphi(\xi)$ is a complex function modeling the amplitude of the traveling wave. The parameters $\tilde{\alpha}$ and $\tilde{\beta}$ are two real constants to be determined with boundary conditions on the wave function. Considering the case where the traveling wave $\varphi(\xi)$ has the same velocity with the elliptic optical lattice, let us insert eq. (2) into eq. (1). Rescaling φ by $k^{\frac{3}{2}}$ and normalizing the space-time variable ξ by $\frac{2K(m)}{\pi}$, we obtain the dimensionless ordinary differential equation, describing the dynamic of the complex traveling wave amplitude $\varphi(\xi)$ given by

$$\frac{\mathrm{d}^2\varphi}{\mathrm{d}\tau^2} - \left[\alpha^2 + \beta + V_0 sn^2\left(\frac{2K(m)\tau}{\pi}, m\right)\right]\varphi - g_0|\varphi|^2\varphi - g_1|\varphi|^4\varphi = i\left[-(\upsilon + 2\alpha)\frac{\mathrm{d}\varphi}{\mathrm{d}\tau} + \left(\gamma_0 - \gamma_1|\varphi|^2 - \gamma_2|\varphi|^4\right)\varphi\right], \tag{3}$$

with $\tau = \eta\xi$, $\alpha = \frac{\tilde{\alpha}}{k}$, $\beta = \frac{\hbar\tilde{\beta}}{E_r}$, $g_0 = \frac{\tilde{g_0}k^3}{E_r} = 8\pi a_s k$, $g_1 = \frac{\tilde{g_1}k^6}{E_r}$, $\gamma_0 = \frac{\tilde{\gamma_0}}{E_r}$, $\gamma_1 = \frac{\tilde{\gamma_1}k^3}{E_r}$, $\gamma_2 = \frac{\tilde{\gamma_2}k^6}{E_r}$, $V_0 = \frac{\tilde{V_0}}{E_r}$, $\upsilon = \frac{2m_a v_L}{\hbar k}$ and $E_r = \frac{\hbar^2 k^2}{2m_a}$ the recoil energy, which is a natural energy scale for neutral atoms in periodic light fields.

Considering $R(\tau)$ and $\theta(\tau)$, respectively, as the real amplitude and the phase of the traveling wave $\varphi(\xi)$, eq. (3) can be rewritten in the form of a nonintegrable system as

$$\begin{cases} \dfrac{\mathrm{d}^2R}{\mathrm{d}\tau^2} - R\left(\dfrac{\mathrm{d}\theta}{\mathrm{d}\tau}\right)^2 - (\alpha^2+\beta)R - g_0R^3 - g_1R^5 = \left[(\upsilon+2\alpha)\dfrac{\mathrm{d}\theta}{\mathrm{d}\tau} + V_0 sn^2\left(\dfrac{2K(m)\tau}{\pi}; m\right)\right]R \\ 2\dfrac{\mathrm{d}R}{\mathrm{d}\tau}\dfrac{\mathrm{d}\theta}{\mathrm{d}\tau} + R\dfrac{\mathrm{d}^2\theta}{\mathrm{d}\tau^2} = -(\upsilon+2\alpha)\dfrac{\mathrm{d}R}{\mathrm{d}\tau} + \gamma_0 R - \gamma_1 R^3 - \gamma_2 R^5. \end{cases} \tag{4}$$

Before applying the Melnikov method, it is worthwhile to uncouple the two variables of system (4). Hence, we multiply the second equation of system (4) by $R(\tau)$. Integrating the result between $-\infty$ and τ yields

$$\frac{\mathrm{d}\theta}{\mathrm{d}\tau} = \frac{1}{R^2}\int_{-\infty}^{\tau}\left(\gamma_0R^2(\tau) - \gamma_1R^4(\tau) - \gamma_2R^6(\tau)\right)\mathrm{d}\tau - \left(\frac{\upsilon+2\alpha}{2}\right). \tag{5}$$

The boundary conditions on the wave function due to fact that the wave amplitude must be null at $\tau = \pm\infty$ leads to

$$\int_{-\infty}^{+\infty}\left(\gamma_0R^2(\tau) - \gamma_1R^4(\tau) - \gamma_2R^6(\tau)\right)\mathrm{d}\tau = 0. \tag{6}$$

Equation (6) represents one constraint relation between parameters modeling nonconservative terms. Inserting eq. (5) in the first equation of system (4), one obtains the following integro-differential equation governing the real amplitude of the traveling wave:

$$\frac{\mathrm{d}^2R}{\mathrm{d}\tau^2} - \left[\frac{a^2}{4} + V_0 p\left(\frac{\tau}{2\pi}; m\right)\right]R - g_0R^3 - g_1R^5 = \frac{1}{R^3(\tau)}\left[\int_{-\infty}^{\tau}\left(\gamma_0R^2(\tau) - \gamma_1R^4(\tau) - \gamma_2R^6(\tau)\right)\mathrm{d}\tau\right]^2, \tag{7}$$

where the constant a is given by $a^2 = 4\beta - \upsilon^2 - 4\alpha\upsilon$ and $p(x;m) = sn^2(4K(m)x; m)$ the optical trap potential.

A periodic potential can be formed simply by overlapping two counter-propagating laser beams. The interference between the two laser beams forms an optical standing wave which can trap the atoms. It is clearly shown in ref. [25] that this Jacobian elliptic trap potential $p(x;m)$ can be expanded in Fourier series to obtain a trigonometric form more easy to use in calculations. The advantage of this trigonometric form is that its amplitude (the depth of optical lattice) can be modified during possible experiments, by acting on the shape parameter m. Furthermore in this reference, it is proven that there is not large difference between the full trap potential $p(x;m)$ and its truncated Fourier expansion of order n defined as

$$p^{(n)}\left(\frac{\tau}{2\pi}; m\right) = \sum_{j=1}^{n} b_{j-1}\sin^2(j\tau), \tag{8}$$

where the three first Fourier coefficients of this trap potential are given by

$$\begin{cases} b_0(m) = \dfrac{4\pi^2 q(1-q+q^2-q^3+q^4)}{m(K(m))^2(1-q-q^5+q^6)} \\ b_1(m) = \dfrac{8\pi^2 q^2(1+q^4)}{m(K(m))^2(1-q^3-q^5+q^8)} \\ b_2(m) = \dfrac{4\pi^2 q^3}{m(K(m))^2(1-q^3)^2}\left(1+\dfrac{2(1-q^3)^2}{(1-q)(1-q^5)}\right). \end{cases} \tag{9}$$

$q(m) = \exp(-\frac{\pi K(1-m)}{K(m)})$ and $0 \leq m \leq 1$.

3 Fixed points and phase portrait for unperturbed system

We assume that the optical lattice potential is small amplitude. Hence, we introduce the following scale transformations: $V_0 \to \epsilon V_0$. The nonconservative terms are smaller than the optical lattice depth. To bring the two terms of perturbation closer (V_0 and γ_i) with $i = 0, 1, 2$, we assume for parameters related to inelastic processes the following scale transformations: $\gamma_0 \to \sqrt{\epsilon}\gamma_0$, $\gamma_1 \to \sqrt{\epsilon}\gamma_1$ and $\gamma_2 \to \sqrt{\epsilon}\gamma_2$. Thus, the integro-differential equation (7) can be written as a first-order system:

$$\begin{cases} \dot{R} = X \\ \dot{X} = \dfrac{a^2}{4}R + g_0R^3 + g_1R^5 + \epsilon\Big[\dfrac{V_0}{2}(b_0+b_1+b_2-b_0\cos(2\tau)-b_1\cos(4\tau)-b_2\cos(6\tau))R \\ \qquad +\dfrac{1}{R^3(\tau)}\left(\displaystyle\int_{-\infty}^{\tau}\left(\gamma_0R^2(\tau)-\gamma_1R^4(\tau)-\gamma_2R^6(\tau)\right)\mathrm{d}\tau\right)^2\Big]. \end{cases} \tag{10}$$

The parameter ϵ ($\epsilon \ll 1$) characterizes the smallness of the lattice potential depth and nonconservative terms. One can straightforwardly see that when $\epsilon \ll 1$, then $\sqrt{\epsilon}$ is bigger than ϵ. Thus, to multiply the small values of parameters modeling the atomic feeding and dissipations with $\sqrt{\epsilon}$ will bring nearer the two terms of perturbations, that to avoid the inelastic processes to be negligible.

For the unperturbed system, *i.e.*, when $\epsilon = 0$, eq. (10) is an integrable Hamiltonian system and can be rewritten as

$$\begin{cases} \dot{R} = X \\ \dot{X} = -\dfrac{\mathrm{d}V(R)}{\mathrm{d}R}, \end{cases} \tag{11}$$

where $V(R)$ represents the potential energy of system and can be straightforwardly deduced from eq. (10). In this study, we work on the hypothesis $g_0 < 0$ and $g_1 > 0$. Under such conditions, the potential energy $V(R)$ is an unbounded two-well ϕ^6 potential, and the integrable system eq. (11) exhibits five equilibrium points (see fig. 1). This unperturbed system can exhibit homoclinc orbits only or both homoclinic and heteroclinics orbits. In our previous work [16], we have studied the case of homoclinic orbits only, and now we focus our attention on the case of the coexistence of homoclinic and heteroclinic orbits, to see how the presence of heteroclinic orbits act on the dynamic of condensate. In other words, we reverse the signs of the interatomic two-and three-body interaction strength. It is well known, today, through Feshbach resonance techniques, that the *s*-wave scattering length can vary from positive to negative values, as shown in the Bose-Einstein condensation of ^{85}Rb [26–28]. To fulfill the two conditions (five equilibrium points and simultaneous existence of homoclinic and heteroclinic orbits) of potential energy, the parameters related to elastic two- and three-body interactions must be linked as follows:

$$0 < \frac{g_1a^2}{g_0^2} < \frac{3}{4}. \tag{12}$$

From the condition (12), deriving from the fact that the potential energy $V(R)$ must intersect the R-axis five times, the system (11) possesses three unstable hyperbolic fixed points at $(0,0)$, $(-R_2,0)$ and $(+R_2,0)$, and two stable nonhyperbolic fixed points at $(-R_1,0)$ and $(+R_1,0)$. The three hyperbolic fixed points are saddle points whereas the two nonhyperbolic fixed points are centres. R_1 and R_2 mentioned above, solution of $\frac{\mathrm{d}V(R)}{\mathrm{d}R} = 0$ are given by the

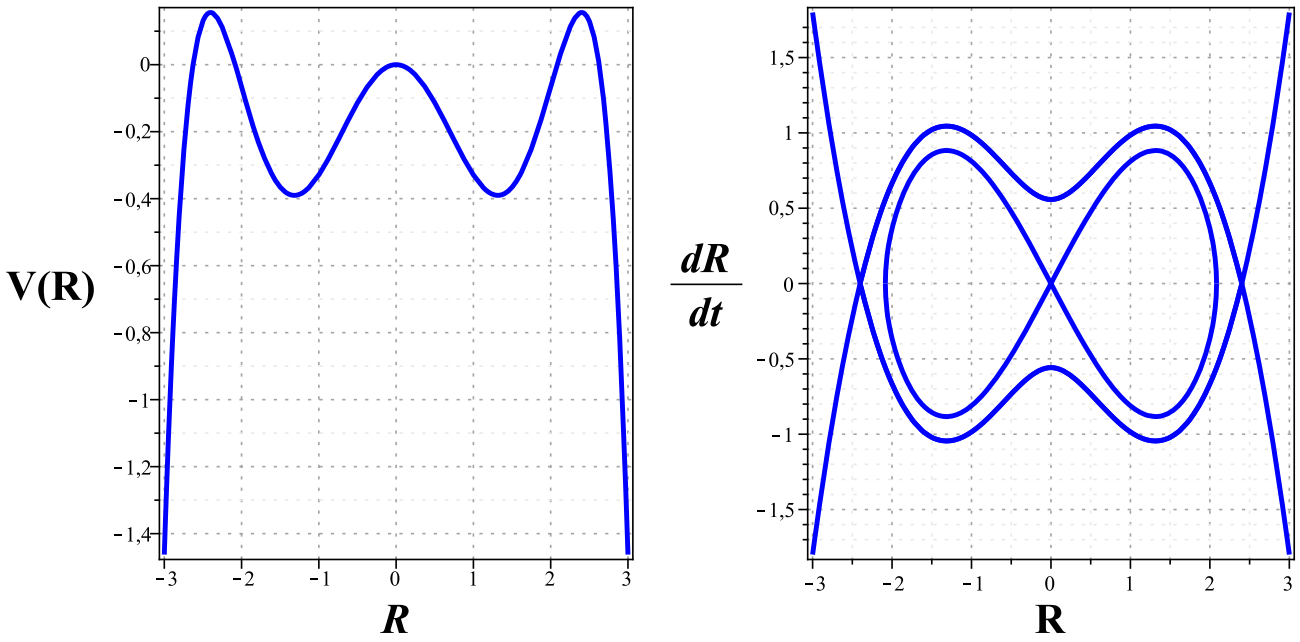

Fig. 1. (a) A configuration of the unbounded ϕ^6 potential with two wells. (b) Local bifurcation near the fixed points of the corresponding potential. The other parameters used are: $a = 2$, $g_0 = -0.75$, $g_1 = 0.1$.

following expressions:

$$\begin{cases} R_1 = \sqrt{-\dfrac{g_0}{2g_1}\left(1 - \sqrt{1 - \dfrac{g_1 a^2}{g_0^2}}\right)} \\ R_2 = \sqrt{-\dfrac{g_0}{2g_1}\left(1 + \sqrt{1 - \dfrac{g_1 a^2}{g_0^2}}\right)}. \end{cases} \tag{13}$$

4 Theoretical predictions of chaos: The Melnikov analysis

This section is devoted to theoretical predictions of occurrence of homoclinic and heteroclinic Smale's horseshoe chaos. The generalized Melnikov method (MM), first introduced by Melnikov [29] and developed by Wiggins [30–34], consists in studying a system in which the unperturbed problem is an integrable Hamiltonian system having a normally hyperbolic invariant set whose stable and unstable manifold intersect nontransversally. The Smale-Birkhoff theorem states that a necessary condition for the occurrence of chaos is that the Melnikov function induced by the perturbation should have simple zeros, *i.e.*, $M(\tau_0) = 0$ and $\frac{\mathrm{d}M(\tau_0)}{\mathrm{d}\tau_0} \neq 0$ at $\tau = \tau_0$. τ_0 represents the cross-section time of the Poincaré map.

According to the MM, the Melnikov function deriving from eq. (10) is given by

$$\begin{aligned} M^{\pm}(\tau_0) = {} & \frac{V_0}{2}(b_0 + b_1 + b_2)\int_{-\infty}^{+\infty} R_0(\tau)X_0(\tau)\mathrm{d}\tau - \frac{V_0}{2}b_0\int_{-\infty}^{+\infty}\cos(2\tau + 2\tau_0)R_0(\tau)X_0(\tau)\mathrm{d}\tau \\ & - \frac{V_0}{2}b_1\int_{-\infty}^{+\infty}\cos(4\tau + 4\tau_0)R_0(\tau)X_0(\tau)\mathrm{d}\tau - \frac{V_0}{2}b_2\int_{-\infty}^{+\infty}\cos(6\tau + 6\tau_0)R_0(\tau)X_0(\tau)\mathrm{d}\tau \\ & + \int_{-\infty}^{+\infty}\left[\frac{X_0}{R_0^3}\left(\int_{-\infty}^{\tau}\left(\gamma_0 R_0^2 - \gamma_1 R_0^4 - \gamma_2 R_0^6\right)\mathrm{d}\tau\right)^2\right]\mathrm{d}\tau, \end{aligned} \tag{14}$$

where $R_0(\tau)$ and $X_0(\tau)$ represent the components of state vector in phase space and are solutions of eq. (11).

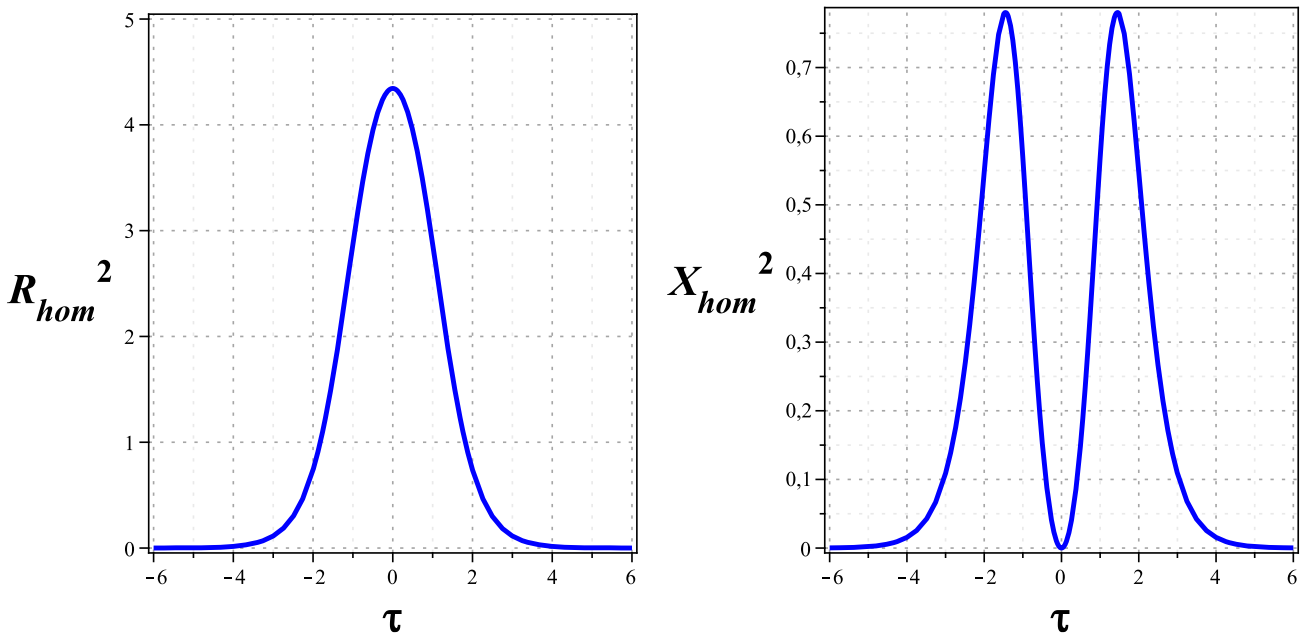

Fig. 2. (a) The spatiotemporal evolution of the particle number density. (b) The first excited state of condensate, deduced from unperturbed system eq. (11). The other parameters used are: $a = 2$, $g_0 = -0.75$, $g_1 = 0.1$.

4.1 Global homoclinic bifurcations

In this subsection, we investigate global bifurcations in the case of homoclinic orbits. The Hamiltonian system (11) possesses a symmetric pair of homoclinic trajectories connecting the unstable point ($R = 0$, $X = 0$) of the potential to itself. Recalling that the Hamiltonian of system (11) is constant on the homoclinic separatrix, and furthermore observing that ($R = 0$, $X = 0$) belongs to this orbit, the components of state vector generating this separatrix are given by

$$\begin{cases} R^{\pm}_{\mathrm{hom}}(\tau) = \pm \dfrac{a}{\sqrt{-g_0[1+\sigma\cosh(a\tau)]}} \\ X^{\pm}_{\mathrm{hom}}(\tau) = \pm \dfrac{a^2\sigma\sinh(a\tau)}{2\sqrt{-g_0[1+\sigma\cosh(a\tau)]^3}}, \end{cases} \tag{15}$$

with $\sigma = \sqrt{1 - \frac{4g_1a^2}{3g_0^2}}$. It comes from eq. (12) that $0 < \sigma < 1$.

In eq. (15), the signs $\pm$ must be understood as follows: X^{-}_{hom} corresponds to R^{+}_{hom} and X^{+}_{hom} corresponds to R^{-}_{hom}.

Replacing, into eq. (14), $R_0(\tau)$ by $R_{\mathrm{hom}}(\tau)$ and $X_0(\tau)$ by $X_{\mathrm{hom}}(\tau)$, and carrying out the integration of the right-hand side with the use of Maple software and the integrals table [35], we obtain after some calculations the following homoclinic Melnikov function:

$$M^{\pm}(\tau_0) = \left[\frac{b_0(m)\sin(2\tau_0)\sin\left(\frac{2}{a}\operatorname{arc\,cosh}\left(\frac{1}{\sigma}\right)\right)}{\sinh\left(\frac{2\pi}{a}\right)} + \frac{2b_1(m)\sin(4\tau_0)\sin\left(\frac{4}{a}\operatorname{arc\,cosh}\left(\frac{1}{\sigma}\right)\right)}{\sinh\left(\frac{4\pi}{a}\right)} + \frac{3b_2(m)\sin(6\tau_0)\sin\left(\frac{6}{a}\operatorname{arc\,cosh}\left(\frac{1}{\sigma}\right)\right)}{\sinh\left(\frac{6\pi}{a}\right)} \right] \times \left(\frac{\pi a V_0}{g_0\sqrt{1-\sigma^2}} \right) + \Sigma. \tag{16}$$

The quantity Σ defined as

$$\Sigma = \int_{-\infty}^{+\infty} \frac{X_{\mathrm{hom}}}{R^3_{\mathrm{hom}}} \left[\int_{-\infty}^{\tau} \left(\gamma_0 R^2_{\mathrm{hom}} - \gamma_1 R^4_{\mathrm{hom}} - \gamma_2 R^6_{\mathrm{hom}} \right) \mathrm{d}\tau \right]^2 \mathrm{d}\tau, \tag{17}$$

denoting the last integral of eq. (14) is evaluated with the remark that $R_{\mathrm{hom}}(\tau)$ is practically null for $]-\infty; \tau_c[\cup]\tau_c; +\infty[$ (see fig. 2), where the symbol $\cup$ stands for the union operator. Therefore, Σ is evaluated taking the spatiotemporal variable τ between $-\tau_c$ and τ_c. In fact, τ_c represents the value of τ for which $R^2_{\mathrm{hom}}(\tau)$, $R^4_{\mathrm{hom}}(\tau)$ and $R^6_{\mathrm{hom}}(\tau)$ can be

assumed close to zero, and its value depends on the set of parameters used. As example, taking the set of parameters as those used to plot the particle number density of condensate for unperturbed system (11), when we solve $R^2_{\rm hom} = 0.0001$ we have as solution $\tau = 6.52$. $R^4_{\rm hom} = 0.0001$ leads to $\tau = 4.22$ and $R^6_{\rm hom} = 0.0001$ gives as solution $\tau = 3.45$. Hence, we give to τ_c the value 4 to our numerical simulations. After a rigorous calculations, the expression of Σ is given by

$$\Sigma = \frac{g_0\sigma}{2a}\left(\Delta_4\Sigma_1 + \Delta_5\Sigma_2 + \Delta_6\Sigma_3\right). \tag{18}$$

The expressions of unknown quantities appearing in eq. (18) are given by

$$\begin{cases} \Sigma_1 = \dfrac{2(\sigma\cosh(a\tau_c)+1)}{a\sigma}\operatorname{arc\,tanh}\left(\sqrt{\dfrac{1-\sigma}{1+\sigma}}\tanh\left(\dfrac{a\tau_c}{2}\right)\right) - \dfrac{\sqrt{1-\sigma^2}}{\sigma}\tau_c \\ \Sigma_2 = +\dfrac{4\sqrt{1-\sigma^2}}{a\sigma^2}\operatorname{arc\,tanh}\left(\sqrt{\dfrac{1-\sigma}{1+\sigma}}\tanh\left(\dfrac{a\tau_c}{2}\right)\right) + \dfrac{2\sinh(a\tau_c)}{a\sigma} - \dfrac{2\tau_c}{\sigma^2} \\ \Sigma_3 = -\dfrac{4}{a\sigma^2\sqrt{1-\sigma^2}}\operatorname{arc\,tanh}\left(\sqrt{\dfrac{1-\sigma}{1+\sigma}}\tanh\left(\dfrac{a\tau_c}{2}\right)\right) - \dfrac{2}{a\sigma}\left(\dfrac{\sinh(a\tau_c)}{1+\sigma\cosh(a\tau_c)}\right) + \dfrac{2\tau_c}{\sigma^2} \end{cases} \tag{19}$$

and

$$\begin{cases} \Delta_4 = 2\Delta_1^2\operatorname{arc\,tanh}\left(\sqrt{\dfrac{1-\sigma}{1+\sigma}}\tanh\left(\dfrac{a\tau_c}{2}\right)\right) + \dfrac{2\Delta_1\Delta_2\sinh(a\tau_c)}{1+\sigma\cosh(a\tau_c)} + \dfrac{2\Delta_1\Delta_3\sinh(a\tau_c)}{(1+\sigma\cosh(a\tau_c))^2} \\ \Delta_5 = 2\Delta_1\Delta_2\operatorname{arc\,tanh}\left(\sqrt{\dfrac{1-\sigma}{1+\sigma}}\tanh\left(\dfrac{a\tau_c}{2}\right)\right) + \dfrac{2\Delta_2^2\sinh(a\tau_c)}{1+\sigma\cosh(a\tau_c)} + \dfrac{2\Delta_2\Delta_3\sinh(a\tau_c)}{(1+\sigma\cosh(a\tau_c))^2} \\ \Delta_6 = 2\Delta_1\Delta_3\operatorname{arc\,tanh}\left(\sqrt{\dfrac{1-\sigma}{1+\sigma}}\tanh\left(\dfrac{a\tau_c}{2}\right)\right) + \dfrac{2\Delta_3^2\sinh(a\tau_c)}{(1+\sigma\cosh(a\tau_c))^2} + \dfrac{2\Delta_2\Delta_3\sinh(a\tau_c)}{1+\sigma\cosh(a\tau_c)}. \end{cases} \tag{20}$$

The expressions of Δ_1, Δ_2 and Δ_3 of eq. (20) are given by

$$\begin{cases} \Delta_1 = -\dfrac{2\,\gamma_0 a}{\sqrt{1-\sigma^2}g_0} - \dfrac{2\,\gamma_1 a^3}{(1-\sigma^2)^{3/2}g_0^2} + \dfrac{\gamma_2 a^5(\sigma^2+2)}{(1-\sigma^2)^{5/2}g_0^3} \\ \Delta_2 = \dfrac{\gamma_1 a^3\sigma}{g_0^2(1-\sigma^2)} - \dfrac{3a^5\gamma_2\sigma}{2g_0^3(1-\sigma^2)^2} \\ \Delta_3 = -\dfrac{\gamma_2 a^5\sigma}{2g_0^3(1-\sigma^2)}. \end{cases} \tag{21}$$

The study of Fourier coefficients of our Jacobian elliptic potential *versus* the shape parameter m reveals that $b_1(m) \ll b_0(m)$ and $b_2(m) \ll b_0(m)$. That was already known through ref. [25]. Hence, we neglect $b_1(m)$ and $b_2(m)$ in the Melnikov function expressed in eq. (16). Applying the Melnikov criterion on the homoclinic Melnikov function for the apparition of homoclinic chaos leads to the following inequality:

$$\delta \geq \left|\frac{g_0\sqrt{1-\sigma^2}\Sigma\sinh\left(\frac{2\pi}{a}\right)}{a\pi\sin\left(\frac{2}{a}\operatorname{arc\,cosh}\left(\sigma^{-1}\right)\right)}\right|. \tag{22}$$

$\delta = V_0 b_0(m)$ represents in fact the amplitude of our trap potential. The advantage to gather together V_0 and $b_0(m)$ in δ is the possibility to change gradually the depth of trap potential by acting on the shape parameter m. That will be very helpful in experiments. The case of equality provides the boundary threshold function in parameter space.

The stable and unstable regions in parameter space deriving from eq. (22) are plotted in figs. 4 and 5.

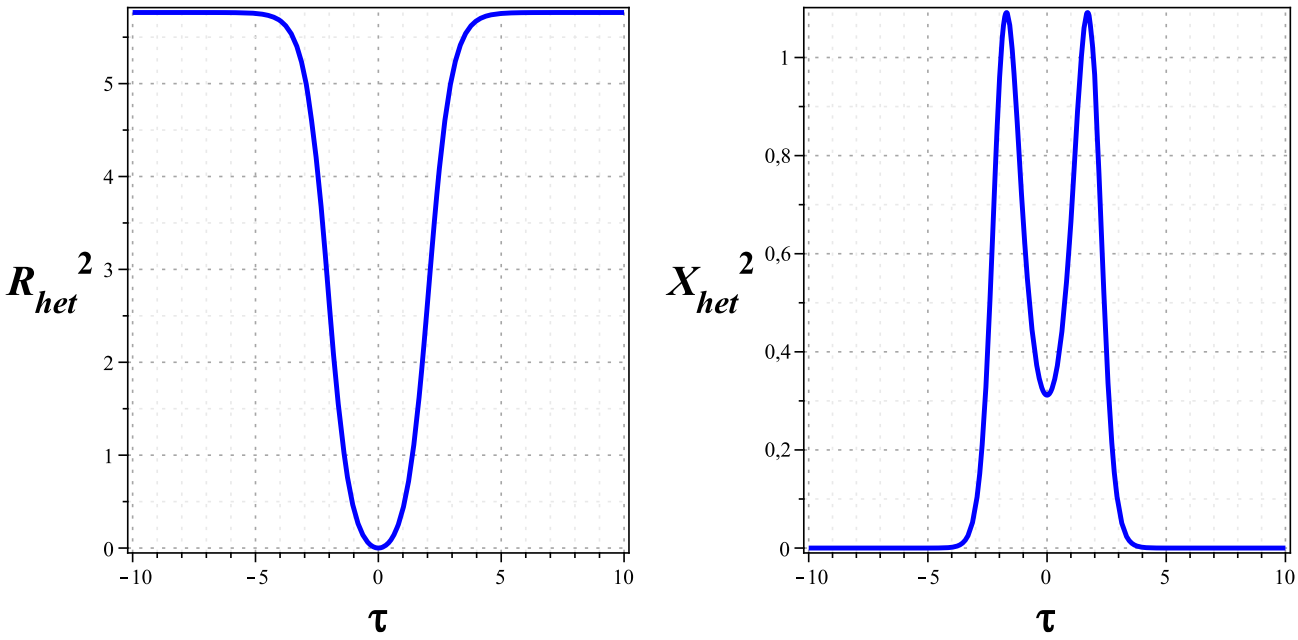

Fig. 3. (a) The spatiotemporal evolution of the particle number density. (b) The first excited state of condensate for heteroclinic orbits, deduced from the unperturbed system (11). The other parameters used are: $a = 2$, $g_0 = -0.75$, $g_1 = 0.1$.

4.2 Global heteroclinic bifurcations

The two unstable fixed points $(-R_2, 0)$ and $(+R_2, 0)$ of potential are connected by two trajectories (heteroclinic separatrix). The state vector generating these orbits has the following components:

$$\begin{cases} R_{\text{het}}^{\pm} = \pm R_2 \sqrt{\dfrac{1-\cosh(\omega\tau)}{\Gamma-\cosh(\omega\tau)}} \\ X_{\text{het}}^{\pm} = \pm \dfrac{\frac{R_2\omega(1-\Gamma)\sinh(\omega\tau)}{(\Gamma-\cosh(\omega\tau))^2}}{2\sqrt{\frac{1-\cosh(\omega\tau)}{\Gamma-\cosh(\omega\tau)}}}, \end{cases} \tag{23}$$

where $\omega = -g_0\sqrt{\frac{\mu(1+\mu)}{g_1}}$, $\mu = \sqrt{1-\frac{g_1 a^2}{g_0^2}}$ and $\Gamma = \frac{1+4\mu}{1-2\mu}$.

Working on the hypothesis of the simultaneous existence of homoclinic and heteroclinic orbits defined in eq. (12) μ and Γ must fulfill the following inequalities: $\frac{1}{2} < \mu < 1$ and $\Gamma < -5$.

In eq. (23), the signs $\pm$ must be understood as: $X_{\text{het}}^{+}(\tau)$ corresponds to $R_{\text{het}}^{+}(\tau)$ and $X_{\text{het}}^{-}(\tau)$ corresponds to $R_{\text{het}}^{-}(\tau)$. Next, we inject $R_{\text{het}}(\tau)$ and $X_{\text{het}}(\tau)$ in the expression of the Melnikov function defined in eq. (14). Using the integrals table [35] and verifying the results directly by Maple Software we obtain the following heteroclinic Melnikov function:

$$\begin{aligned} M^{\pm}(\tau_0) = \Bigg[& \frac{b_0(m)\sin(2\tau_0)\sin\left(\frac{2}{\omega}\operatorname{arc\,cosh}(-\Gamma)\right)}{\sinh\left(\frac{2\pi}{\omega}\right)} + \frac{2b_1(m)\sin(4\tau_0)\sin\left(\frac{4}{\omega}\operatorname{arc\,cosh}(-\Gamma)\right)}{\sinh\left(\frac{4\pi}{\omega}\right)} \\ & + \frac{3b_2(m)\sin(6\tau_0)\sin\left(\frac{6}{\omega}\operatorname{arc\,cosh}(-\Gamma)\right)}{\sinh\left(\frac{6\pi}{\omega}\right)} \Bigg] \times \left(\frac{\pi V_0 R_2^2}{\omega}\sqrt{\frac{-\Gamma+1}{-\Gamma-1}} \right) + H, \end{aligned} \tag{24}$$

with H the last integral of eq. (14) expressed as

$$H = \int_{-\infty}^{+\infty} \frac{X_{\text{het}}}{R_{\text{het}}^3} \left[\int_{-\infty}^{\tau} \left(\gamma_0 R_{\text{het}}^2 - \gamma_1 R_{\text{het}}^4 - \gamma_2 R_{\text{het}}^6 \right) \mathrm{d}\tau \right]^2 \mathrm{d}\tau. \tag{25}$$

This integral diverges at the vicinity of $\tau = 0$. In fact, for $\tau = 0$, $R_{\text{het}} = 0$ (see fig. 3) and one can straightforwardly see the divergence of this integral. But, in terms of area, this integral can be approximated. We avoid the value $\tau = 0$

and the variable τ is taken between τ_i and τ_c, where the value of τ_i is very close to zero. Hence, the approximation of H is given by

$$H = \frac{\omega\,(1-\Gamma)}{R_2^2}\left(Z_5 H_1 + Z_6 H_2 + Z_7 H_3 + Z_8 H_4\right). \tag{26}$$

The unknown quantities appearing in this expression are given by

$$\begin{cases} H_1 = \dfrac{(\cosh(\omega\,\tau_c)-\Gamma)\,\mathrm{arc\,tanh}\left(\frac{(\Gamma+1)\tanh\left(\frac{\omega\,\tau_c}{2}\right)}{\sqrt{\Gamma^2-1}}\right)}{\omega(-1+\cosh(\omega\,\tau_c))(\Gamma-1)} - \dfrac{(\cosh(\omega\,\tau_i)-\Gamma)\,\mathrm{arc\,tanh}\left(\frac{(\Gamma+1)\tanh\left(\frac{\omega\,\tau_i}{2}\right)}{\sqrt{\Gamma^2-1}}\right)}{\omega(-1+\cosh(\omega\,\tau_i))(\Gamma-1)} \\ \quad -\dfrac{\sqrt{\Gamma^2-1}}{2\omega\,(\Gamma-1)}\left(\dfrac{1}{\tanh\left(\frac{\omega\,\tau_c}{2}\right)} - \dfrac{1}{\tanh\left(\frac{\omega\,\tau_i}{2}\right)}\right) \\ H_2 = -\dfrac{\tau_c\omega\tanh\left(\frac{\omega\,\tau_c}{2}\right)-1+\cosh(\omega\,\tau_c)}{\omega^2(-1+\cosh(\omega\,\tau_c))\tanh\left(\frac{\omega\,\tau_c}{2}\right)} + \dfrac{\tau_i\omega\,\tanh\left(\frac{\omega\,\tau_i}{2}\right)-1+\cosh(\omega\,\tau_i)}{\omega^2(-1+\cosh(\omega\,\tau_i))\tanh\left(\frac{\omega\,\tau_i}{2}\right)} \\ H_3 = \dfrac{2(\Gamma+1)\,\mathrm{arc\,tanh}\left(\frac{(\Gamma+1)\tanh\left(\frac{\omega\,\tau_c}{2}\right)}{\sqrt{\Gamma^2-1}}\right)}{\omega(\Gamma-1)\sqrt{\Gamma^2-1}} - \dfrac{2(\Gamma+1)\,\mathrm{arc\,tanh}\left(\frac{(\Gamma+1)\tanh\left(\frac{\omega\,\tau_i}{2}\right)}{\sqrt{\Gamma^2-1}}\right)}{\omega(\Gamma-1)\sqrt{\Gamma^2-1}} \\ \quad -\dfrac{2}{\omega\,(\Gamma-1)}\left(\dfrac{1}{\tanh\left(\frac{\omega\,\tau_c}{2}\right)} - \dfrac{1}{\tanh\left(\frac{\omega\,\tau_i}{2}\right)}\right) \\ H_4 = \dfrac{2(2+\Gamma)\,\mathrm{arc\,tanh}\left(\frac{(\Gamma+1)\tanh\left(\frac{\omega\,\tau_c}{2}\right)}{\sqrt{\Gamma^2-1}}\right)}{\omega(\Gamma-1)^2\sqrt{\Gamma^2-1}} - \dfrac{2(2+\Gamma)\,\mathrm{arc\,tanh}\left(\frac{(\Gamma+1)\tanh\left(\frac{\omega\,\tau_i}{2}\right)}{\sqrt{\Gamma^2-1}}\right)}{\omega(\Gamma-1)^2\sqrt{\Gamma^2-1}} \\ \quad +\dfrac{1}{\omega\,(\Gamma-1)(\Gamma-\cosh(\omega\,\tau_c))\tanh\left(\frac{\omega\,\tau_c}{2}\right)} - \dfrac{1}{\omega\,(\Gamma-1)(\Gamma-\cosh(\omega\,\tau_i))\tanh\left(\frac{\omega\,\tau_i}{2}\right)} \\ \quad -\dfrac{3}{\omega\,(\Gamma-1)^2\tanh\left(\frac{\omega\,\tau_c}{2}\right)} + \dfrac{3}{\omega\,(\Gamma-1)^2\tanh\left(\frac{\omega\,\tau_i}{2}\right)} \end{cases} \tag{27}$$

and

$$\begin{cases} Z_5 = 2Z_1^2\,\mathrm{arc\,tanh}\left(\dfrac{\Gamma+1}{\sqrt{\Gamma^2-1}}\tanh\left(\dfrac{\omega\tau_c}{2}\right)\right) + 2Z_1Z_2\tau_c + \dfrac{2Z_1Z_3\sinh(\omega\tau_c)}{\Gamma-\cosh(\omega\tau_c)} + \dfrac{2Z_1Z_4\sinh(\omega\tau_c)}{(\Gamma-\cosh(\omega\tau_c))^2} \\ Z_6 = 2Z_1Z_2\,\mathrm{arc\,tanh}\left(\dfrac{\Gamma+1}{\sqrt{\Gamma^2-1}}\tanh\left(\dfrac{\omega\tau_c}{2}\right)\right) + 2Z_2^2\tau_c + \dfrac{2Z_2\,Z_3\sinh(\omega\,\tau_c)}{\Gamma-\cosh(\omega\,\tau_c)} + \dfrac{2Z_2\,Z_4\,\sinh(\omega\,\tau_c)}{(\Gamma-\cosh(\omega\,\tau_c))^2} \\ Z_7 = 2Z_1Z_3\,\mathrm{arc\,tanh}\left(\dfrac{\Gamma+1}{\sqrt{\Gamma^2-1}}\tanh\left(\dfrac{\omega\tau_c}{2}\right)\right) + 2Z_2\,Z_3\,\tau_c + \dfrac{2Z_3^2\sinh(\omega\tau_c)}{\Gamma-\cosh(\omega\tau_c)} + \dfrac{2Z_3Z_4\sinh(\omega\tau_c)}{(\Gamma-\cosh(\omega\,\tau_c))^2} \\ Z_8 = 2Z_1Z_4\,\mathrm{arc\,tanh}\left(\dfrac{\Gamma+1}{\sqrt{\Gamma^2-1}}\tanh\left(\dfrac{\omega\tau_c}{2}\right)\right) + 2Z_2Z_4\tau_c + \dfrac{2Z_3\,Z_4\sinh(\omega\,\tau_c)}{\Gamma-\cosh(\omega\,\tau_c)} + \dfrac{2Z_4^2\sinh(\omega\,\tau_c)}{(\Gamma-\cosh(\omega\,\tau_c))^2}. \end{cases} \tag{28}$$

The expressions of quantities Z_1, Z_2, Z_3 and Z_4 of eq. (28) are given by

$$\begin{cases} Z_1 = \dfrac{2\,\gamma_0R_2^2(1-\Gamma)}{\omega\,\sqrt{\Gamma^2-1}} + \dfrac{2\,\gamma_1R_2^4(\Gamma-1)(\Gamma+2)}{\omega\,(\Gamma+1)\sqrt{\Gamma^2-1}} + \dfrac{\gamma_2R_2^6(2\,\Gamma^2+6\,\Gamma+7)(\Gamma-1)}{\omega\,(\Gamma+1)^2\sqrt{\Gamma^2-1}} \\ Z_2 = \gamma_0R_2^2 - \gamma_1R_2^4 - \gamma_2R_2^6 \\ Z_3 = -\dfrac{R_2^4(\Gamma-1)(2\,\gamma_1\Gamma+2\,\gamma_1+3\,\gamma_2R_2^2\Gamma+6\,\gamma_2R_2^2)}{2\omega\,(\Gamma+1)^2} \\ Z_4 = \dfrac{\gamma_2R_2^6(\Gamma-1)^2}{2\omega\,(\Gamma+1)}. \end{cases} \tag{29}$$

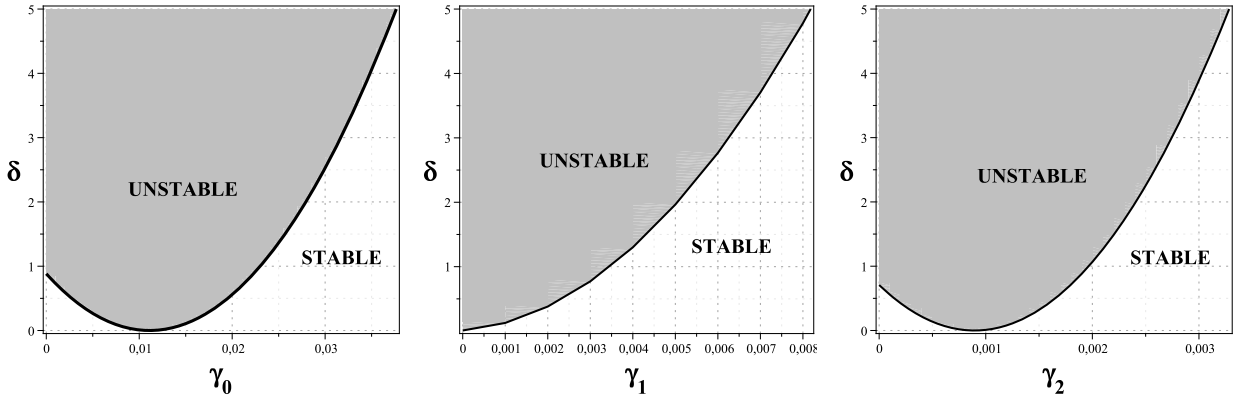

Fig. 4. Stable and unstable zones in parameter space (γ_i, δ), $i = 0, 1, 2$ for homoclinic bifurcations. Modulated lattice potential depth δ *versus* (a) the feeding parameter γ_0; (b) the dipolar relaxation parameter γ_1; (c) the three-body recombination factor γ_2. The other parameters used are: $a = 2$, $g_0 = -0.75$, $g_1 = 0.1$, $\gamma_0 = 10^{-2}$, $\gamma_1 = 10^{-5}$, $\gamma_2 = 10^{-3}$, $\tau_c = 4$.

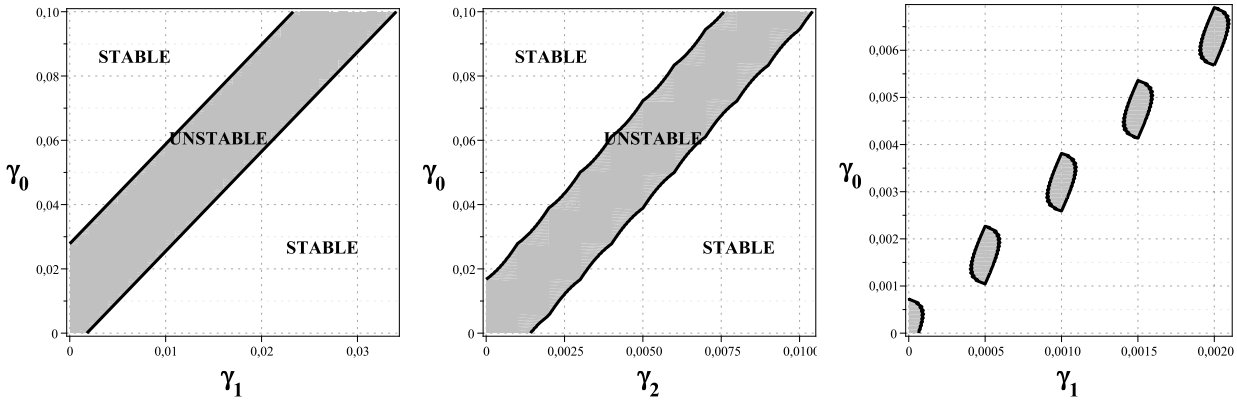

Fig. 5. Stable and unstable zones in parameter space (γ_i, γ_j), $i = 0, 1, 2$ for homoclinic bifurcations. (a) Feeding parameter *versus* the dipolar relaxation parameter for $\gamma_2 = 10^{-3}$. (b) Feeding parameter *versus* the three-body inelastic recombination factor for $\gamma_1 = 10^{-5}$. (c) Discrete unstable regions in parameter space (γ_1, γ_0) for $\gamma_2 = 10^{-5}$, $V_0 = 0.02$, $\tau_c = 5$. The other parameters used are: $a = 2$, $g_0 = -0.75$, $g_1 = 0.1$, $m = 0.5$, $V_0 = 2$, $\tau_c = 4$.

Theoretically, the condition to obtain the heteroclinic Melnikov chaos of perturbed system (10) is expressed as follows:

$$\delta \geq \left| \frac{\omega \sqrt{\frac{-\Gamma-1}{-\Gamma+1}} H \sinh\left(\frac{2\pi}{\omega}\right)}{\pi R_2^2 \sin\left(\frac{2}{\omega} \operatorname{arc\,cosh}(-\Gamma)\right)} \right|. \tag{30}$$

5 Numerical simulations and discussions

In this section, we first analyze thoroughly the theoretical conditions of apparition of chaotic oscillations in the dynamics of condensed atoms obtained in eqs. (22) and (30). Next, our theoretical results are verified by the corresponding numerical simulations. In the end, to verify the reliability of our investigations, we compare our findings with those of refs. [12–15], in which the condensate was studied with variational approach. From eq. (22) and eq. (30), via Maple software the regions of stable and unstable behaviours of condensate are obtained and shown in figs. 4, 5, 6 and 7. For each parameter space, we take a point inside the unstable and stable zones and we plot the corresponding Poincaré sections to verify the analytical predictions. The aim of our study being the impact of inelastic processes (nonconservative terms) on the dynamics of condensate, we focus our attention on the cases for which the unstable regions in parameter space (γ_i, γ_j) have linear boundaries, and we attempt to find the link between parameters related to losses and atomic feeding to the occurrence of chaotic oscillations.

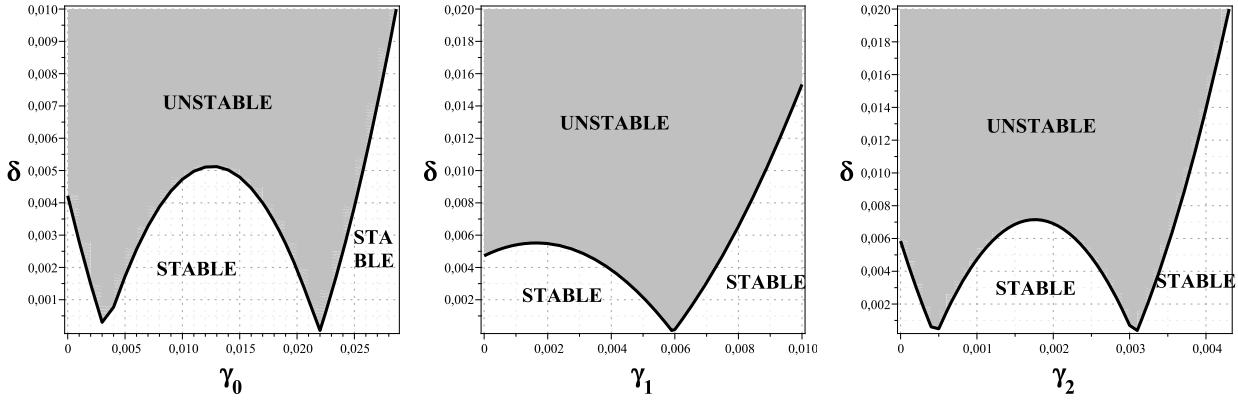

Fig. 6. Unstable and stable zones in parameter space (γ_i, δ), $i = 0, 1, 2$ for heteroclinic bifurcations. Modulated lattice potential depth δ *versus*: (a) feeding parameter γ_0; (b) the dipolar relation parameter γ_1; (c) the three-body inelastic recombination factor γ_2. The other parameters used are: $a = 2$, $g_0 = -0.75$, $g_1 = 0.1$, $\gamma_0 = 10^{-2}$, $\gamma_1 = 10^{-5}$, $\gamma_2 = 10^{-3}$, $\tau_c = 4$, $\tau_i = 0.005$, $V_0 = 2$.

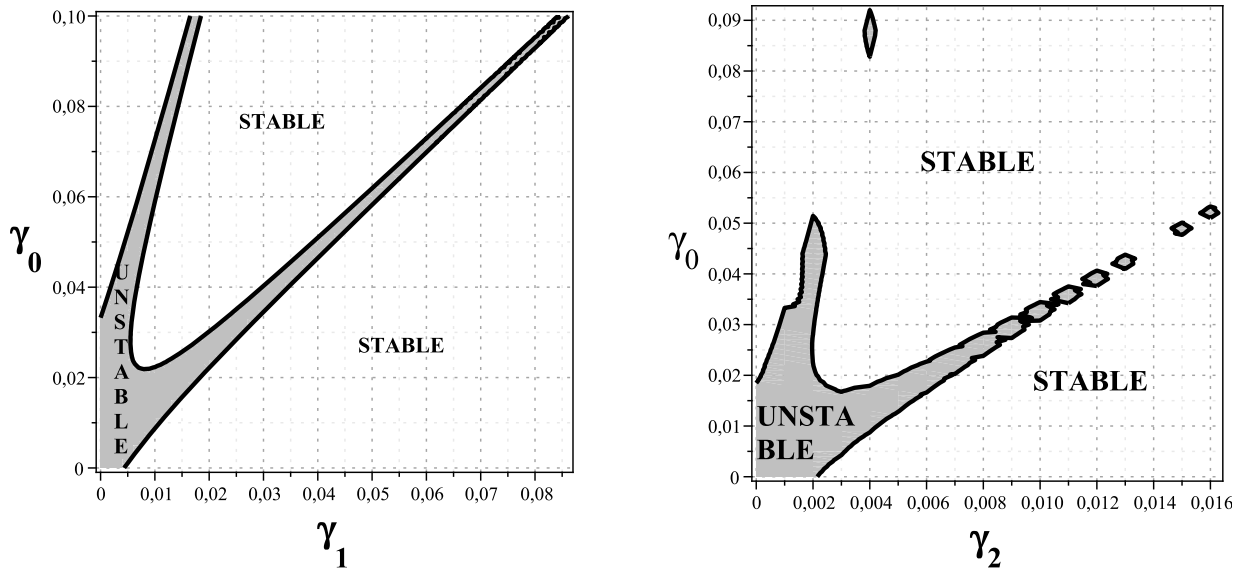

Fig. 7. Unstable and stable zones in parameter space (γ_i, γ_j), $i = 0, 1, 2$ for heteroclinic bifurcations: (a) feeding parameter *versus* the dipolar relation parameter for $\gamma_2 = 10^{-3}$; (b) feeding parameter *versus* the three-body inelastic recombination factor for $\gamma_1 = 10^{-5}$. The other parameters used are: $a = 2$, $g_0 = -0.75$, $g_1 = 0.1$, $m = 0.5$, $\tau_c = 4$, $\tau_i = 0.005$, $V_0 = 2$.

5.1 Case of homoclinic bifurcations

We begin the analysis with the plot of fig. 4(a) in parameter space (γ_0, δ). The point with the components $(\gamma_0 = 0.01, \delta = 2)$ is inside the unstable zone coloured in gray. The fig. 8(a) exhibits a strange attractor as Poincaré section, hallmark of chaotic oscillations of condensate. On the contrary, the point $(\gamma_0 = 0.4, \delta = 5)$ is outside the unstable region. The corresponding Poincaré section depicted in fig. 8(b) shows a set of seven points, characterizing the period-7 limit cycle in phase space. The deep analysis of Poincaré sections reveals that, when one increases the parameter related to atomic feeding γ_0 while δ is keeping constant, the number of points characterizing the Poincaré sections decreases progressively. The periodic oscillations are finally obtained for very large values of γ_0. This result is also visible on the bifurcation diagram plotted in fig. 9(a).

Continuing this reasoning with fig. 4(b) in parameter space (γ_1, δ) and proceeding as above, the point with components $(\gamma_1 = 0.0005, \delta = 2)$ is inside the unstable region. One realize that the corresponding Poincaré section is a strange attractor, characteristic of chaotic behaviour of condensate. Conversely, the point $(\gamma_1 = 0.1, \delta = 2)$ in parameter space is outside the unstable region. The corresponding Poincaré section exhibits also a set of seven points. The thorough analysis of Poincaré sections reveals that when one increases gradually the parameter related to the dipolar relaxation γ_1, the number of points decreases and the system leads finally to a point attractor when we are far from threshold boundary function.

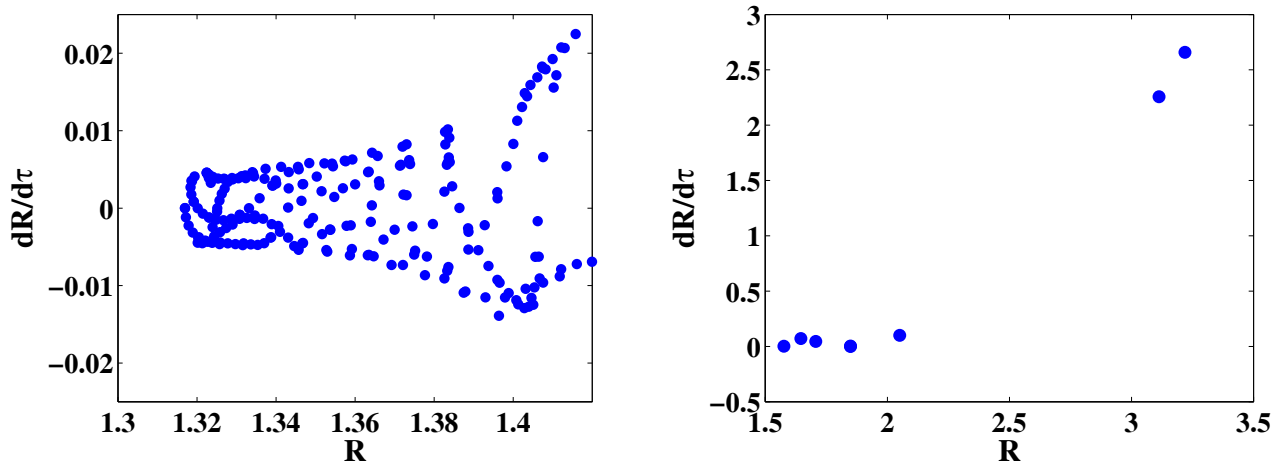

Fig. 8. Poincaré sections deriving from fig. 4 in parameter space (γ_0, δ) for $\gamma_1 = 10^{-5}$, $\gamma_2 = 10^{-3}$. (a) Point with components $(\gamma_0 = 0.01, \delta = 2)$ inside the unstable region. (b) Point with components $(\gamma_0 = 0.4, \delta = 5)$ inside the stable region. The other parameters used are: $\upsilon = 0.0001$, $\alpha = 0$, $\beta = 1$, $m = 0.5$, $\epsilon = 0.01$, $g_0 = -0.75$, $g_1 = 0.1$, $V_0 = 2$, the initial conditions are taken at the stable fixed point $R = R_1 = 1.316979712$ and $\frac{\mathrm{d}R}{\mathrm{d}\tau} = 0$.

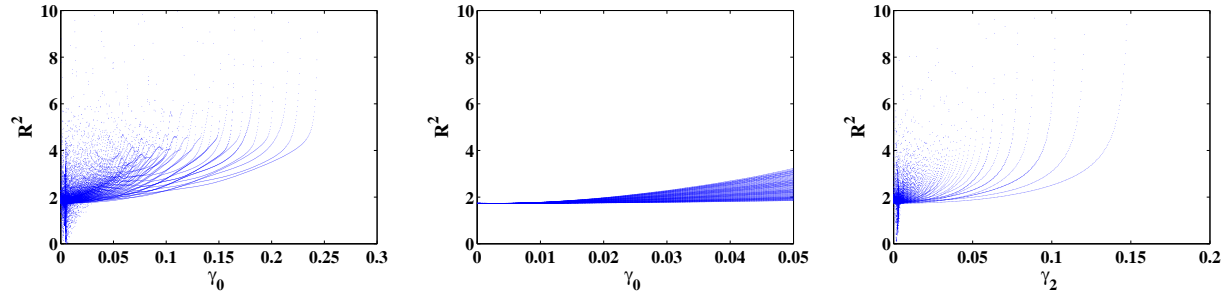

Fig. 9. Bifurcation diagrams deduced from eq. (4). (a)-(b) The feeding rate γ_0 as control parameter with $\gamma_1 = 10^{-5}$, $\gamma_2 = 10^{-3}$ and V_0, respectively, 2 for (a) and 0.02 for (b). (c) The three-body inelastic recombination factor γ_2 as control parameter and $\gamma_0 = 10^{-2}$, $\gamma_1 = 10^{-5}$ and $V_0 = 2$. The other parameters used are $\upsilon = 0.0001$, $\alpha = 0$, $\beta = 1$, $g_0 = -0.75$, $g_1 = 0.1$, $m = 0.5$, $\epsilon = 0.01$, the initial conditions are taken at the stable fixed point $R = R_1 = 1.316979712$ and $\frac{\mathrm{d}R}{\mathrm{d}\tau} = 0$.

We pursue the investigations in parameter space (γ_i, γ_j), $i = 0, 1, 2$ with fig. 5. It comes from eq. (22) that, for $\gamma_2 = 10^{-3}$, varying increasingly the atomic feeding parameter γ_0 from 0 to 0.1, the corresponding parameter related to the dipolar relaxation γ_1 not exceed 0.035. The chaotic region coloured in gray in the parameter space (γ_1, γ_0) is given by the following approximate expression: $-0.0075 \leq \gamma_0 - 3.17\gamma_1 \leq 0.0269$. The point with coordinates $(\gamma_1 = 0.005, \gamma_0 = 0.02)$ is inside the unstable zone. The corresponding Poincaré section plotted in fig. 10(a) shows a strange attractor, proof of chaotic oscillations. The point with components $(\gamma_1 = 0.1, \gamma_0 = 0.02)$ is outside the unstable region. The corresponding Poincaré section plotted in fig. 10(b) exhibits a set of seven points. The atomic feeding and the dipolar relaxation parameters are approximately linked as $\frac{\gamma_0}{\gamma_1} = 3.17$ for the occurrence of erratic oscillations of condensate.

With the fig. 5(b), for $\gamma_1 = 10^{-5}$, the theoretical condition of apparition of homoclinic chaos reveals that when γ_0 increases between 0 and 0.1, γ_2 varies between 0 and 0.0104. The unstable region in parameter space (γ_2, γ_0) coloured in gray is given approximately by the following inequalities $-0.0157 \leq \gamma_0 - 11.13\gamma_2 \leq 0.0171$. The point $(\gamma_2 = 0.005, \gamma_0 = 0.06)$ is inside the unstable region and the corresponding Poincaré section exhibits a strange attractor, hallmark of chaotic oscillations of condensate. Conversely, the point $(\gamma_2 = 0.07, \gamma_0 = 0.01)$ is outside the unstable zone. The corresponding Poincaré section exhibits a set of points. The chaotic oscillations of condensate are approximately governed by the ratio $\frac{\gamma_0}{\gamma_2} = 11.13$. The deep computational analysis of Poincaré sections shows that the more we are far from the boundary threshold function in parameter space, the dynamics of condensate is regular.

Exploring thoroughly the chaotic regions, we observe through our computational simulations that for very small values of optical intensity V_0 and very weak value of the inelastic three-body recombination parameter γ_2, the regions of instability in parameter space (γ_1, γ_0) are discrete and appear as a sequence of an island of points as one sees through fig. 5(c). In other words, the unstable regions appear like a linear alternation of patterns. The centres G_n of these

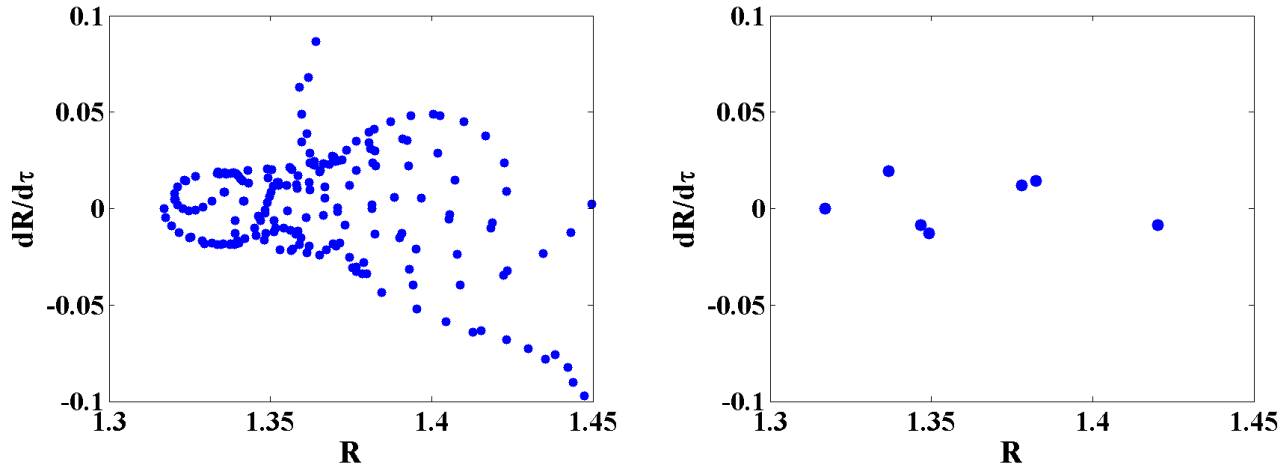

Fig. 10. Poincaré sections deriving from fig. 5 in parameter space (γ_1, γ_0) for $\gamma_2 = 10^{-3}$. (a) Point with components ($\gamma_1 = 0.005, \gamma_0 = 0.02$) inside the unstable. (b) Point with components ($\gamma_1 = 0.1, \gamma_0 = 0.02$) inside the stable region. The other parameters used are: $\upsilon = 0.0001$, $\alpha = 0$, $\beta = 1$, $\epsilon = 0.01$, $g_0 = -0.75$, $g_1 = 0.1$, $m = 0.5$, $V_0 = 2$, the initial conditions are taken at the stable fixed point $R = R_1 = 1.316979712$ and $\frac{\mathrm{d}R}{\mathrm{d}\tau} = 0$.

unstable regions in parameter space (γ_1, γ_0) are in arithmetic progression and given by $G_n(\gamma_1 = 0.0005n, \gamma_0 = 0.0016n)$ for the set of other parameters used. The outcome of that, is simply the existence of growth-collapse cycles in the dynamics of condensate.

Let's compare now our results with those of refs. [12–15], in which the study was made by a variational approach. The relevant result from their numerical studies, verified by experiments is that the small values of feeding parameter or the small values of the ratio between the feeding parameter and the three-body recombination parameter are favourable to stable dynamics of condensate, whereas under the large values of ratio between the feeding parameter and dissipation parameters, the system becomes very unstable (quantitatively, the chaotic dynamics occur mainly when the feeding parameter is one or two orders of magnitude larger than the three-body recombination parameter). Using the same set of parameters which in fact are those used in experiments, we obtain analytically that the homoclinic chaotic dynamics of condensate are governed by the ratio $\frac{\gamma_0}{\gamma_2} = 11.13$. *I.e.* the chaotic behaviours of condensate occur when the feeding parameter is about one order of magnitude larger than the thee-body recombination parameter. This result is in perfect accord with their findings. Our study reveals a certain disaccord with the above-mentioned references. We observe that weak values of feeding parameter not imply necessary regular oscillations. In optical lattices the depth of the trap potential plays an important role on the chaotic dynamics of condensate. That can be viewed on the figs. 4(a) and 6(a), where for weak values of feeding parameter, to be inside or outside of unstable region depends of the value of the modulated optical depth δ. Numerically that is also verified, as one can see through the bifurcation diagrams plotted in fig. 9. In fig. 9(a) and (c), one realize that for the optical intensity V_0 taking the value 2 (per unit of recoil energy), the dynamics of condensate is chaotic for small values of parameters related to atomic feeding. In fig. 9(b), one realizes that for weak values of atomic feeding parameter and very small values of the optical intensity ($V_0 = 0.02$), the dynamics of condensate is regular.

5.2 Case of heteroclinic bifurcations

The theoretical condition of heteroclinic chaos deriving from eq. (30) provides large regions of instability when we are in parameter space (γ_i, δ) with $i = 0, 1, 2$, as one sees through fig. 6. In fact, this result is not surprising because the heteroclinic orbits connecting unstable fixed points will be necessary unstable. Taking as initial conditions a fixed point $(-R_2, 0)$ or $(+R_2, 0)$, the same program used to plot the homoclinic bifurcation diagrams diverges, probably because the double-well ϕ^6 potential is unbounded at these points. Figure 7 exhibits in parameter space (γ_i, γ_j) with $i \neq j$, the stable and unstable regions. One observes the discontinuity of the unstable regions, which appear like the island of points when the feeding parameter and the dipolar relaxation parameters vary. This remark has been previously observed in fig. 5(c) in the case of homoclinic bifurcations and can be interpreted as collapses and growth-collapse cycles in the dynamics of condensate. It comes from fig. 7 that very small values of nonconservative terms are favourable to the heteroclinic chaos, as one can see through the unstable regions coloured in gray.

6 Conclusion

We have studied the dynamics of a Bose-Einstein condensate with bosonic atoms trapped into a moving optical lattice, and subjected to some nonconservative terms neglected in the (GP) formalism. Let us summarize our theoretical and numerical investigations. Firstly, we prove that the real amplitude of condensate is governed by an integro-differential equation which thereafter is used to provide through the Melnikov method the appearance conditions of the chaotic behaviours of condensate. From these analytical conditions, we realize that for a fixed values of the optical intensity taken inside the unstable zone in parameter space $(\gamma_i, \delta = V_0 b_0(m))$, the regular dynamics of condensate can be obtained by increasing gradually the parameters related to inelastic processes (nonconservative terms). Through numerical investigations (bifurcation diagrams) we observe that from chaotic dynamics for large values of the optical intensity, the condensate undergoes a cascade of period-doubling bifurcations culminating finally to regular oscillations. Moreover, we realize that with optical lattices trap, weak values of atomic feeding and dissipation parameters not imply necessary regular oscillations, and large values of these parameters not imply necessary chaotic behaviours, as it is well known with harmonic magnetic trap potential. The depth of optical lattices plays an important role in the dynamic of condensate, and its large values are favourable to chaotic oscillations.

Secondly, in the framework of homoclinic bifurcations, unstable regions in parameter space (γ_i, γ_j) reveals that homoclinic chaotic behaviours of condensate occur when the feeding parameter is about one order of magnitude larger than the thee-body recombination parameter. That is in agreement with numerical results of previous works. Moreover for small values of the optical intensity and the inelastic three-body interactions parameter, the unstable regions appear like a linear alternation of islands of points. That justifies theoretically the existence of collapses and growth-collapses cycles in the dynamics of condensate. These phenomena (collapses, growth-collapse cycles and chaos) are also obtained in the case of heteroclinic bifurcations for large values of the three-body recombination parameter.

Thirdly, the computational simulations reveal that the route leading to chaotic oscillations when the optical intensity and the strength of elastic three-body interactions are used as control parameters is the quasi-periodicity, mainly the torus-doubling bifurcations. In these cases, eq. (1) provides solitonic solutions as envelope solitons and bright solitons in the case of stable dynamics and that can be explained as a balance between the dispersion and the nonlinearity.

Appendix A. Integration of Σ

$$\Sigma = \int_{-\infty}^{+\infty} \left[\frac{X_0}{R_0^3} \left(\int_{-\infty}^{\tau} \left(\gamma_0 R_0^2 - \gamma_1 R_0^4 - \gamma_2 R_0^6 \right) \mathrm{d}\tau \right)^2 \right] \mathrm{d}\tau. \tag{A.1}$$

In this expression, we replace R_0 and X_0, respectively, by R_{hom} and X_{hom} as defined in eq. (15). For a set of parameters obeying the condition eq. (14), R_{hom} and X_{hom} can be considered as zero functions for $]-\infty; \tau_c[\cup]\tau_c; +\infty[$. For this reason, Σ can be expressed as

$$\Sigma = \int_{-\tau_c}^{+\tau_c} \frac{X_{\mathrm{hom}}}{R_{\mathrm{hom}}^3} \left(\int_{-\tau_c}^{\tau} \left(\gamma_0 R_{\mathrm{hom}}^2 - \gamma_1 R_{\mathrm{hom}}^4 - \gamma_2 R_{\mathrm{hom}}^6 \right) \mathrm{d}\tau \right)^2 \mathrm{d}\tau, \tag{A.2}$$

$$A_1 = \int_{-\tau_c}^{\tau} R_{\mathrm{hom}}^2(\tau)\mathrm{d}\tau$$

$$= \frac{-2a}{g_0\sqrt{1-\sigma^2}} \left[\operatorname{arc\,tanh}\left(\sqrt{\frac{1-\sigma}{1+\sigma}} \tanh\left(\frac{a\tau}{2} \right) \right) + \operatorname{arc\,tanh}\left(\sqrt{\frac{1-\sigma}{1+\sigma}} \tanh\left(\frac{a\tau_c}{2} \right) \right) \right], \tag{A.3}$$

$$A_2 = \int_{-\tau_c}^{\tau} R_{\mathrm{hom}}^4(\tau)\mathrm{d}\tau = \frac{-a^2 A_1}{g_0(1-\sigma^2)} - \frac{\frac{a^3\sigma\sinh(a\tau)}{1+\sigma\cosh(a\tau)} + \frac{a^3\sigma\sinh(a\tau_c)}{1+\sigma\cosh(a\tau_c)}}{g_0^2(1-\sigma^2)}, \tag{A.4}$$

$$A_3 = \int_{-\tau_c}^{\tau} R_{\mathrm{hom}}^6(\tau)\mathrm{d}\tau$$

$$= \frac{a^4(\sigma^2+2)A_1}{2g_0^2(1-\sigma^2)^2} + \frac{\frac{3a^5\sigma\sinh(a\tau)}{1+\sigma\cosh(a\tau)} + \frac{3a^5\sigma\sinh(a\tau_c)}{1+\sigma\cosh(a\tau_c)}}{2g_0^3(1-\sigma^2)^2} + \frac{\frac{a^5\sigma\sinh(a\tau)}{(1+\sigma\cosh(a\tau))^2} + \frac{a^5\sigma\sinh(a\tau_c)}{(1+\sigma\cosh(a\tau_c))^2}}{2g_0^3(1-\sigma^2)}, \tag{A.5}$$

$$\int_{-\tau_c}^{\tau} \left(\gamma_0 R_{\rm hom}^2 - \gamma_1 R_{\rm hom}^4 - \gamma_2 R_{\rm hom}^6\right) \mathrm{d}\tau = \gamma_0 A_1 - \gamma_1 A_2 - \gamma_2 A_3 =$$
$$\Delta_1 \left[\operatorname{arc\,tanh}\left(\sqrt{\frac{1-\sigma}{1+\sigma}}\tanh\left(\frac{a\tau}{2}\right)\right) + \operatorname{arc\,tanh}\left(\sqrt{\frac{1-\sigma}{1+\sigma}}\tanh\left(\frac{a\tau_c}{2}\right)\right)\right]$$
$$+ \Delta_2 \left[\frac{\sinh(a\tau)}{1+\sigma\cosh(a\tau)} + \frac{\sinh(a\tau_c)}{1+\sigma\cosh(a\tau_c)}\right] + \Delta_3 \left[\frac{\sinh(a\tau)}{(1+\sigma\cosh(a\tau))^2} + \frac{\sinh(a\tau_c)}{(1+\sigma\cosh(a\tau_c))^2}\right], \tag{A.6}$$

with Δ_1, Δ_2 and Δ_3 defined in eq. (21)

$$\frac{X_{\rm hom}(\tau)}{R_{\rm hom}^3(\tau)} = \frac{g_0\sigma\sinh(a\tau)}{2a}. \tag{A.7}$$

Taking the square of the right-hand side of eq. (A.6) and neglecting all even functions of τ, we obtain

$$\frac{X_{\rm hom}(\tau)}{R_{\rm hom}^3(\tau)} \left(\int_{-\tau_c}^{\tau} \left(\gamma_0 R_{\rm hom}^2(\tau) - \gamma_1 R_{\rm hom}^4(\tau) - \gamma_2 R_{\rm hom}^6(\tau)\right) \mathrm{d}\tau\right)^2 =$$
$$\frac{g_0\sigma}{2a}\left[\Delta_4 \operatorname{arc\,tanh}\left(\sqrt{\frac{1-\sigma}{1+\sigma}}\tanh\left(\frac{a\tau}{2}\right)\right)\sinh(a\tau) + \frac{\Delta_5\sinh^2(a\tau)}{1+\sigma\cosh(a\tau)} + \frac{\Delta_6\sinh^2(a\tau)}{(1+\sigma\cosh(a\tau))^2}\right], \tag{A.8}$$

with Δ_4, Δ_5 and Δ_6 defined in eq. (20). Integrating eq. (A.8) between $-\tau_c$ and $+\tau_c$ leads to Σ defined in eq. (17), where Σ_1, Σ_2 and Σ_3 appearing in eq. (18) obtained by the integration by part method, represent the following integrals:

$$\begin{cases} \displaystyle\int_{-\tau_c}^{+\tau_c} \operatorname{arc\,tanh}\left(\sqrt{\frac{1-\sigma}{1+\sigma}}\tanh\left(\frac{a\tau}{2}\right)\right)\sinh(a\tau)\mathrm{d}\tau = \Sigma_1 \\ \displaystyle\int_{-\tau_c}^{+\tau_c} \frac{\sinh^2(a\tau)\mathrm{d}\tau}{1+\sigma\cosh(a\tau)} = \Sigma_2 \\ \displaystyle\int_{-\tau_c}^{+\tau_c} \frac{\sinh^2(a\tau)\mathrm{d}\tau}{(1+\sigma\cosh(a\tau))^2} = \Sigma_3. \end{cases} \tag{A.9}$$

Appendix B. Integration of H

$$H = \int_{-\infty}^{+\infty} \frac{X_{\rm het}}{R_{\rm het}^3} \left(\int_{-\infty}^{\tau} \left(\gamma_0 R_{\rm het}^2 - \gamma_1 R_{\rm het}^4 - \gamma_2 R_{\rm het}^6\right) \mathrm{d}\tau\right)^2 \mathrm{d}\tau. \tag{B.1}$$

It comes from fig. 3 that $X_{\rm het}(\tau)$ is practically null for $]-\infty;\tau_c[\cup]\tau_c;+\infty[$, where the value of τ_c depends on the set of parameters used. Another remark is that H cannot be evaluated for $\tau = 0$. But in terms of area, we approximate the value of H by avoiding the vicinity of $\tau = 0$. With this remark, H can be rewritten as

$$H = \int_{-\tau_c}^{+\tau_c} \frac{X_{\rm het}}{R_{\rm het}^3} \left(\int_{-\tau_c}^{\tau} \left(\gamma_0 R_{\rm het}^2 - \gamma_1 R_{\rm het}^4 - \gamma_2 R_{\rm het}^6\right) \mathrm{d}\tau\right)^2 \mathrm{d}\tau, \tag{B.2}$$

$$B_1 = \int_{-\tau_c}^{\tau} R_{\rm het}^2(\tau)\mathrm{d}\tau$$
$$= R_2^2 \left[\frac{2\,(1-\Gamma)}{\omega\sqrt{\Gamma^2-1}}\left(\operatorname{arc\,tanh}\left(\frac{(\Gamma+1)\tanh\left(\frac{\omega\tau}{2}\right)}{\sqrt{\Gamma^2-1}}\right) + \operatorname{arc\,tanh}\left(\frac{(\Gamma+1)\tanh\left(\frac{\omega\tau_c}{2}\right)}{\sqrt{\Gamma^2-1}}\right)\right) + \tau + \tau_c\right], \tag{B.3}$$

$$
\begin{aligned}
B_2 &= \int_{-\tau_c}^{\tau} R_{\rm het}^4(\tau)\mathrm{d}\tau \\
&= R_2^4\Bigg[-\frac{2\,(\Gamma-1)(\Gamma+2)}{\omega(\Gamma+1)\sqrt{\Gamma^2-1}}\left(\operatorname{arc\,tanh}\left(\frac{(\Gamma+1)\tanh\left(\frac{\omega\,\tau}{2}\right)}{\sqrt{\Gamma^2-1}}\right)+\operatorname{arc\,tanh}\left(\frac{(\Gamma+1)\tanh\left(\frac{\omega\,\tau_c}{2}\right)}{\sqrt{\Gamma^2-1}}\right)\right) \\
&\quad +(\tau+\tau_c)+\frac{\Gamma-1}{\omega(\Gamma+1)}\left(\frac{\sinh(\omega\tau)}{\Gamma-\cosh(\omega\tau)}+\frac{\sinh(\omega\tau_c)}{\Gamma-\cosh(\omega\tau_c)}\right)\Bigg], \qquad \text{(B.4)}\\
B_3 &= \int_{-\tau_c}^{\tau} R_{\rm het}^6(\tau)\mathrm{d}\tau \\
&= R_2^6\Bigg[-\frac{(2\Gamma^2+6\Gamma+7)(\Gamma-1)}{\omega(\Gamma+1)^2\sqrt{\Gamma^2-1}}\left(\operatorname{arc\,tanh}\left(\frac{(\Gamma+1)\tanh\left(\frac{\omega\,\tau}{2}\right)}{\sqrt{\Gamma^2-1}}\right)+\operatorname{arc\,tanh}\left(\frac{(\Gamma+1)\tanh\left(\frac{\omega\,\tau_c}{2}\right)}{\sqrt{\Gamma^2-1}}\right)\right) \\
&\quad +(\tau+\tau_c)+\frac{3(\Gamma-1)(\Gamma+2)}{2\omega(\Gamma+1)^2}\left(\frac{\sinh(\omega\tau)}{\Gamma-\cosh(\omega\tau)}+\frac{\sinh(\omega\tau_c)}{\Gamma-\cosh(\omega\tau_c)}\right) \\
&\quad -\frac{(\Gamma-1)^2}{2\omega(\Gamma+1)}\left(\frac{\sinh(\omega\tau)}{(\Gamma-\cosh(\omega\tau))^2}+\frac{\sinh(\omega\tau_c)}{(\Gamma-\cosh(\omega\tau_c))^2}\right)\Bigg] \qquad \text{(B.5)}\\
&\int_{-\tau_c}^{\tau}\left(\gamma_0 R_{\rm het}^2-\gamma_1 R_{\rm het}^4-\gamma_2 R_{\rm het}^6\right)\mathrm{d}\tau=\gamma_0 B_1-\gamma_1 B_2-\gamma_2 B_3 \\
&= Z_1\left[\operatorname{arc\,tanh}\left(\frac{(\Gamma+1)\tanh\left(\frac{\omega\,\tau}{2}\right)}{\sqrt{\Gamma^2-1}}\right)+\operatorname{arc\,tanh}\left(\frac{(\Gamma+1)\tanh\left(\frac{\omega\,\tau_c}{2}\right)}{\sqrt{\Gamma^2-1}}\right)\right]+Z_2(\tau+\tau_c) \\
&\quad +Z_3\left(\frac{\sinh(\omega\tau)}{\Gamma-\cosh(\omega\tau)}+\frac{\sinh(\omega\tau_c)}{\Gamma-\cosh(\omega\tau_c)}\right)+Z_4\left(\frac{\sinh(\omega\tau)}{(\Gamma-\cosh(\omega\tau))^2}+\frac{\sinh(\omega\tau_c)}{(\Gamma-\cosh(\omega\tau_c))^2}\right), \qquad \text{(B.6)}
\end{aligned}
$$

with Z_1, Z_2, Z_3 and Z_4 defined in eq. (29),

$$
\frac{X_{\rm het}(\tau)}{R_{\rm het}^3(\tau)}=\frac{(1-\Gamma)\omega\sinh(\omega\,\tau)}{2R_2^2(-1+\cosh(\omega\,\tau))^2}\,. \qquad \text{(B.7)}
$$

Taking the square of the right-hand side of eq. (B.6) and neglecting all even functions of τ, we obtain

$$
\begin{aligned}
&\frac{X_{\rm het}(\tau)}{R_{\rm het}^3(\tau)}\left(\int_{-\tau_c}^{\tau}\left(\gamma_0 R_{\rm het}^2(\tau)-\gamma_1 R_{\rm het}^4(\tau)-\gamma_2 R_{\rm het}^6(\tau)\right)\mathrm{d}\tau\right)^2= \\
&\frac{(1-\Gamma)\omega}{2R_2^2}\Bigg[\frac{Z_5\sinh(\omega\tau)}{(-1+\cosh(\omega\,\tau))^2}\operatorname{arc\,tanh}\left(\frac{(\Gamma+1)\tanh\left(\frac{\omega\,\tau}{2}\right)}{\sqrt{\Gamma^2-1}}\right)+\frac{Z_6\tau\sinh(\omega\tau)}{(-1+\cosh(\omega\,\tau))^2} \\
&\quad +\frac{Z_7\sinh^2(\omega\tau)}{(-1+\cosh(\omega\,\tau))^2(\Gamma-\cosh(\omega\tau))}+\frac{Z_8\sinh^2(\omega\tau)}{(-1+\cosh(\omega\,\tau))^2(\Gamma-\cosh(\omega\tau))^2}\Bigg]. \qquad \text{(B.8)}
\end{aligned}
$$

The expressions of Z_5, Z_6, Z_7, and Z_8 are defined in eq. (28). Integrating eq. (B.8) between $-\tau_c$ and $+\tau_c$ leads to H defined in eq. (25), where H_1, H_2, H_3 and H_4 appearing in eq. (26) are the following integrals:

$$
\begin{cases}
\displaystyle\int_{-\tau_c}^{+\tau_c}\frac{\sinh(\omega\tau)}{(-1+\cosh(\omega\,\tau))^2}\operatorname{arc\,tanh}\left(\frac{(\Gamma+1)\tanh\left(\frac{\omega\,\tau}{2}\right)}{\sqrt{\Gamma^2-1}}\right)\mathrm{d}\tau=2H_1 \\
\displaystyle\int_{-\tau_c}^{+\tau_c}\frac{\tau\sinh(\omega\tau)\mathrm{d}\tau}{(-1+\cosh(\omega\,\tau))^2}=2H_2 \\
\displaystyle\int_{-\tau_c}^{+\tau_c}\frac{\sinh^2(\omega\tau)\mathrm{d}\tau}{(-1+\cosh(\omega\,\tau))^2(\Gamma-\cosh(\omega\tau))}=2H_3 \\
\displaystyle\int_{-\tau_c}^{+\tau_c}\frac{\sinh^2(\omega\tau)\mathrm{d}\tau}{(-1+\cosh(\omega\,\tau))^2(\Gamma-\cosh(\omega\tau))^2}=2H_4.
\end{cases} \qquad \text{(B.9)}
$$

These integrals diverge at $\tau = 0$. In terms of area, we have the approximate values of H_1, H_2, H_3 and H_4 by avoiding the vicinity of $\tau = 0$. Thus, the integrals of eq. (B.9) are calculated for τ belonging to $[-\tau_c, -\tau_i] \cup [\tau_i, \tau_c]$, where τ_i is a value very close to zero. Hence, H_i with $i = 1, 2, 3, 4$ are finally given by the following integrals:

$$\begin{cases} \displaystyle\int_{\tau_i}^{+\tau_c} \frac{\sinh(\omega\tau)}{(-1+\cosh(\omega\,\tau))^2} \operatorname{arc\,tanh}\left(\frac{(\Gamma+1)\tanh\left(\frac{\omega\,\tau}{2}\right)}{\sqrt{\Gamma^2-1}}\right) \mathrm{d}\tau = H_1 \\ \displaystyle\int_{\tau_i}^{+\tau_c} \frac{\tau\sinh(\omega\tau)\mathrm{d}\tau}{(-1+\cosh(\omega\,\tau))^2} = H_2 \\ \displaystyle\int_{\tau_i}^{+\tau_c} \frac{\sinh^2(\omega\tau)\mathrm{d}\tau}{(-1+\cosh(\omega\,\tau))^2(\Gamma-\cosh(\omega\tau))} = H_3 \\ \displaystyle\int_{\tau_i}^{+\tau_c} \frac{\sinh^2(\omega\tau)\mathrm{d}\tau}{(-1+\cosh(\omega\,\tau))^2(\Gamma-\cosh(\omega\tau))^2} = H_4. \end{cases} \tag{B.10}$$

The expressions of these integrals are given in eq. (27).

References

1. S.N. Bose, Z. Phys. **26**, 178 (1924).
2. A. Einstein, S. B. Preuss. Akad. Wiss **22**, 261 (1924).
3. P. Kapitza, Nature **141**, 74 (1938).
4. J.F. Allen, A.D. Misener, Nature **141**, 75 (1938).
5. F. London, Phys. Rev. **54**, 947 (1938).
6. Eric Cornell, J. Res. Natl. Instr. Stand. Technol. **101**, 419 (1996).
7. M.H. Anderson, J.R. Enscher, M.R. Matthews, C.E. Wieman, E.A. Cornell, Science **269**, 198 (1995).
8. Biao Wu, Qian Niu, Phys. Rev. A **64**, 061603 (2001).
9. Oliver Morsch, Markus Oberthaler, Rev. Mod. Phys. **78**, 179 (2006).
10. Jongchul Mun, Patrick Medley, Gretchen K. Campbell, Luis G. Marcassa, David E. Pritchard, Wolfgang Ketterle, Phys. Rev. Lett. **99**, 150604 (2007).
11. Zheng-Wei Xie, Weiping Zhang, S.T. Chui, W.M. Liu, Phys. Rev. A **69**, 053609 (2004).
12. L. Tomio, V.S. Filho, A. Gammal, T. Frederico, Laser Physics **13**, 582 (2003).
13. Victo S. Filho, Lauro Tomio, A. Gammal, T. Frederico, Phys. Lett. A **325**, 420 (2004).
14. Victo S. Filho, T. Frederico, Arnaldo Gammal, Lauro Tomio, Phys. Rev. E **66**, 036225 (2002).
15. Victo S. Filho, F.Kh. Abdullaev, A. Gammal, Lauro Tomio, Phys. Rev. A **63**, 053603 (2001).
16. S. Tchatchueng, M. Siewe Siewe, F.M. Moukam Kakmeni, C. Tchawoua, Nonlinear Dyn. **75**, 461 (2014).
17. A. Gammal, T. Frederico, Lauro Tomio, Ph. Chomaz, J. Phys. B: At. Mol. Opt. Phys. **33**, 4053 (2000).
18. D.S. Petrov, Phys. Rev. Lett. **112**, 103201 (2014).
19. A.E. Leanhardt, A.P. Chikkatur, D. Kielpinski, Y. Shin, T.L. Gustavson, W. Ketterle, D.E. Pritchard, Phys. Rev. Lett. **89**, 040401 (2002).
20. Peng Ping, Li Guan-Qiang, Chin. Phys. B **18**, 3221 (2009).
21. Emmanuel Kengne, Ahmed Lakhssassi, Eur. Phys. J. Plus **130**, 197 (2015).
22. J. Söding, D. Guéry-Odelin, P. Desbiolles, F. Chevy, H. Inamori, J. Dalibard, Appl. Phys. B **69**, 257 (1999).
23. F. Bloch, Z. Phys. **52**, 555 (1928).
24. Immanuel Bloch, Nat. Phys. **1**, 23 (2005).
25. R. Chacón, D. Bote, R. Carretero-González, Phys. Rev. E **78**, 036215 (2008).
26. J.L. Roberts, N.R. Claussen, S.L. Cornish, E.A. Donley, E.A. Cornell, C.E. Wieman, Phys. Rev. Lett. **86**, 4211 (2001).
27. E.A. Donley, N.R. Claussen, S.L. Cornish, J.L. Roberts, E.A. Cornell, C.E. Wieman, Nat. London **412**, 295 (2001).
28. N.R. Claussen, E.A. Donley, S.T. Thomspson, C.E. Wieman, Phys. Rev. Lett. **89**, 010401 (2002).
29. V.K. Melnikov, Trans. Moscow Math. Soc. **12**, 1 (1963).
30. S. Wiggins, *Global Bifurcations and Chaos Analytical Methods* (Springer-Verlag, New York, Heidelberg, Berlin, 1988).
31. S. Wiggins, J. Appl. Math. **48**, 262 (1988).
32. S. Wiggins, *Introduction to Applied Nonlinear Dynamical Systems and Chaos* (Springer-Verlag, New York, Heidelberg, Berlin, 1990).
33. S. Wiggins, Physica D **40**, 471 (1990).
34. W. Show, S. Wiggins, Physica D **31**, 190 (1988).
35. I.S. Gradshteyn, I.M. Ryzhik, *Table of Integrals, Series and Products* (Academic Press, New York, 1994).

Nonlinear Dyn
DOI 10.1007/s11071-013-1078-2

ORIGINAL PAPER

Bifurcation response and Melnikov chaos in the dynamic of a Bose–Einstein condensate loaded into a moving optical lattice

S. Tchatchueng · M. Siewe Siewe · F.M. Moukam Kakmeni · C. Tchawoua

Received: 30 December 2012 / Accepted: 11 September 2013

Abstract We investigate global bifurcation of a Bose–Einstein condensate with both repulsive two-body interaction between atoms and attractive three-body interaction loaded into a traveling optical lattice. Slow-flow equations of the traveling wave function are the first to derive and the reduced amplitude equation is obtained. The Melnikov method is applied on the reduced parametrically driven system and the Melnikov function is subsequently established. Effects of different physical parameters on the global bifurcation are studied analytically and numerically, and different chaotic regions of the parameter space are found. The results suggest that optical intensity may help to enhance chaos while the strength of the effective three-body interaction, the velocity of the optical lattice, and the damping coefficients annihilate or reduce chaotic behavior of the steady-state traveling wave solution of the particle number density of a Bose–Einstein condensate.

Keywords Bose–Einstein condensate · Optical lattice · Chaos · Melnikov's theory · Bifurcation

S. Tchatchueng (✉) · M. Siewe Siewe · C. Tchawoua
Faculté des sciences, Département de Physique, Laboratoire de Mécanique, Université de Yaoundé I, BP. 812, Yaoundé, Cameroon
e-mail: stchatchueng@yahoo.fr

M. Siewe Siewe
e-mail: martinsiewesiewe@yahoo.fr

C. Tchawoua
e-mail: ctchawa@yahoo.fr

F.M. Moukam Kakmeni
Laboratory of Research on Advanced Materials and Nonlinear Science (LARAMANS), Department of Physics, Faculty of Science, University of Buea, P.O. Box 63, Buea, SW-Province, Cameroon
e-mail: moukamkakmeni@gmail.com

1 Introduction

After the experimental achievement of the Bose–Einstein condensation back in 1995 [1], there has been a surge of papers [2–8] focused on nonlinear phenomena specific to Bose–Einstein-condensed gases. The authors of [9] created the Faraday waves in a cigar-shaped Bose–Einstein condensate. Further, the authors in [10] have investigated analytically the dynamics of a trapped, quasi-one-dimensional Bose–Einstein condensate subject to resonant and nonresonant periodic modulation of the transverse confinement. In [11], it is shown by extensive numerical simulations and analytical variational calculations that elongated binary nonmiscible Bose–Einstein condensates subject to periodic modulations of the radial confinement exhibit a Faraday instability similar to that seen in one-component condensates. In [12], the statics and dynamics of single and multiple matter-wave dark solitons in the quasi one-dimensional setting in atomic Bose–Einstein condensates, in higher dimensional settings, as well as in the dimensionality crossover regime is discussed. The authors of [13] have studied

Published online: 10 October 2013

the resonant energy transfer in Bose–Einstein condensates. The fractional and period-states of BECs loaded into optical lattices have been considered in [14, 15], as well as linear and nonlinear resonances (see [16, 17]).

In recent years, significant progress in the manipulation of ultra-cold atoms have been achieved leading to the possibility of trapping ultra-cold bosonic atoms in optical lattice [18–20]. Taking into account the two-body interactions between atoms in the Schrödinger equation to describe the dynamic of the Bose–Einstein condensate can be considered as the necessary condition for possible appearance of temporal [21, 22], spatial [23, 24], and spatiotemporal [25, 26] chaos in the dynamic of the condensate.

Another important topic in scientific research today is the control of chaos. Broadly speaking, there are two kinds of chaos control. One is the so-called OGY method, first introduced in 1990 by Ott et al. [27–29], which uses some weak feedback control to make the chaotic trajectory approach and settle down finally to a desired stabilized periodic orbit, formerly unstably embedded in the chaotic manifold. The OGY method is a kind of feedback control. The other kind of chaos control belongs to nonfeedback control, which usually uses given external or parametric excitations to control system behavior [30–32]. Both kinds of chaos control are still developing. As a matter of fact, chaos control may have a dual function: to generate chaos or to suppress it. Numerous qualitative analysis demonstrated the existence and characteristics of chaotic motions in deterministic non-linear systems. It is interesting to know the parameter values below, which no periodic motion would occur in the forced nonlinear oscillator. The authors of [33] use a variation of Melnikov's method developed for a slowly varying oscillator. The original Melnikov method [34] is applicable to a one degree-of-freedom system with a time period perturbation only. When the system is perturbed by external excitations and dissipative forces, the Homoclinic motions can break into Homoclinic tangles providing the conditions for chaotic motions. Although the Melnikov method is merely approximative, it is one of a few methods allowing analytical prediction of chaos occurrence. Moreover, it can be applied to a relatively large class of dynamical systems. The Melnikov integral has been generalized by [35–37] to high-dimensional conservative Hamiltonian systems.

The possible existence of chaos in the dynamic of condensate compelled it control, for a probable use in technology. Recently in [38], the control of chaos in BECs loaded into a moving optical lattice have been investigated. They focused their attention on the control of chaos using as control parameter the traveling optical lattice shape and they arrived to the conclusion that the chaos could be control with a small change of this control parameter. It is proved in [39–41] that atomic traps are effectively described by the Gross–Pitaevskii–Ginzburg (GPG) formulation of the nonlinear Schrödinger (NLSE) equation, which includes two-body and three-body interactions. In this respect, it has been used by [42, 43] the time-dependent (GPG) equation to describe the dynamic of the condensate. They investigated the case where the effects of inelastic two-body and three-body collisions on the dynamics of BEC's are neglected, i.e., the two-body and three-body interactions coefficients are real numbers.

In this paper, our attention is focused on the combination of a Bose–Einstein condensate and a moving optical lattice. Through our analysis, we attempt to study how the optical intensity, the strength of the effective three-body interaction, the velocity of the optical lattice, and the damping coefficient affect the dynamic of condensate. We use the (GPG) formalism to investigate the dynamic of condensate in the hypothesis where the two-body and three-body interactions coefficients are real numbers. Furthermore, using the fact that in [44–48], it is shown that condensates, as observed experimentally, are weakly dissipative and decay over time, we introduce a dissipative term in (GPG). We analyze respectively the effects of the above mentioned parameters in the occurrence of homoclinic chaos, using the Melnikov method and numerical simulations (bifurcation diagrams, basin of attraction, and phase portraits).

The plan of the paper is as follows: In Sect. 2, we present the general formalism that we have considered, and we establish the differential equation involving the real amplitude of condensate. In Sect. 3, the Melnikov analysis is used to determine the condition of appearance of homoclinic chaos, and some chaotic threshold functions are depicted. We exhibit our numerical results in Sect. 4, and our study is concluded in Sect. 5.

2 Derivation of the slow-flow equations

In the present paper, we consider a thin cigar-shaped condensate with a strong radial confinement. Hence,

we can neglect the transversal dynamic, and the condensate can be described by the quasi-one-dimensional (1D) time-dependent Gross–Pitaevskii–Ginzburg (GPG) [39–43] equation

$$(\gamma+i)\hbar\frac{\partial\psi}{\partial t} = -\frac{\hbar^2}{2m_a}\frac{\partial^2\psi}{\partial x^2} + \left(\tilde{V}_0 sn^2(\eta\xi,m)+\tilde{g}_0|\psi|^2+\tilde{g}_1|\psi|^4\right)\psi \quad (1)$$

where $\psi(x;t)$ is the wave function of condensate, $\tilde{V}_0 sn^2(\eta\xi,m)$ is the periodic moving optical lattice. $\xi = x+\upsilon_L t$ is the space time variable, $\upsilon_L = \frac{\delta}{2k}$ the velocity of traveling lattice, with δ the frequency difference between the two Fourier-synthesized counter-propagating laser beams. $k = \frac{2\pi}{\lambda}$ is the laser wave vector, m_a is the atomic mass. $\tilde{g_0} = \frac{4\pi\hbar^2 a}{m_a}$ is the interatomic two-body interaction strength, with a the s-wave scattering length, $\tilde{g_1}$ is the strength of the effective three-body interaction. $\eta = \frac{2K(m)k}{\pi}$, with $K(m)$ the complete elliptic integral of the first kind. The function $sn(.;m)$ is the Jacobian sine elliptic function of parameter m $(0\le m\le 1)$, γ is the damping parameter. The parameters of nonlinearity $\tilde{g_0}$ and $\tilde{g_1}$ in general are the complex quantities. The imaginary parts of $\tilde{g_0}$ and $\tilde{g_1}$ describe the effects of inelastic two-and three-body collisions on the dynamics of BEC's, respectively. In this work, we assume that the cubic and quintic parameters are real numbers. Furthermore, $\tilde{g_0}$ is a positive number and $\tilde{g_1}$ a negative number. A condensate which is initially in the ground state of the nonperiodic moving lattice trap will evolve according to Eq. (1). To understand for what value of the amplitude of the traveling wave solution the system will start responding to the periodic excitation, it is useful to study small perturbation of the wave function of the ground state in a static point. Linearizing the GPG equation in the small perturbation $\varepsilon\psi$, we can determine the conditions under which the system becomes unstable when the periodic moving lattice trap is switched on. This analysis is done by looking the solutions of the form [38, 49]

$$\psi(x;t) = \varphi(\xi)\exp\left[i(\tilde{\alpha}x+\tilde{\beta}t)\right] \quad (2)$$

where $\varphi(\xi)$ is a complex function, and $\tilde{\alpha}$ and $\tilde{\beta}$ are real constants to be determined. It is important to note that the traveling wave $\varphi(\xi)$ has the same velocity as the elliptic optical lattice. Let us insert Eq. (2) into Eq. (1), rescaling φ by $k^{\frac{3}{2}}$ and the space time variable ξ by $\frac{2K(m)}{\pi}$; we obtain the following ordinary differential equation, describing the dynamic of the complex traveling wave amplitude $\varphi(\xi)$:

$$\frac{d^2\varphi}{d\tau^2}+\gamma\upsilon\frac{d\varphi}{d\tau}-\left(\beta+\alpha^2\right)\varphi-g_0|\varphi|^2\varphi-g_1|\varphi|^4\varphi = -i\left[(\upsilon+2\alpha)\frac{d\varphi}{d\tau}+\gamma\beta\varphi\right] + V_0\left[sn^2\left(\frac{2K(m)\tau}{\pi};m\right)\right]\varphi \quad (3)$$

with: $\tau=\eta\xi$, $\alpha=\frac{\tilde{\alpha}}{k}$, $\beta=\frac{\hbar\tilde{\beta}}{E_r}$, $g_0=\frac{\tilde{g_0}k^3}{E_r}=8\pi ak$, $g_1=\frac{\tilde{g_1}k^6}{E_r}$, $V_0=\frac{\tilde{V_0}}{E_r}$, $\upsilon=\frac{2m_a\upsilon_L}{\hbar k}$ and $E_r=\frac{\hbar^2k^2}{2m_a}$ the recoil energy. Furthermore, according to [26], we can express the complex traveling wave amplitude $\varphi(\tau)$ in the form

$$\varphi(\tau) = R(\tau)e^{i\theta(\tau)} \quad (4)$$

where $R(\tau)$ and $\theta(\tau)$ are respectively the real amplitude and the phase of the traveling wave. Inserting Eq. (4) into Eq. (3), we obtain the following differential system:

$$\begin{cases} \dfrac{d^2R}{d\tau^2}+\gamma\upsilon\dfrac{dR}{d\tau}-R\left(\dfrac{d\theta}{d\tau}\right)^2-\left(\beta+\alpha^2\right)R \\ \qquad -g_0R^3-g_1R^5 \\ \qquad =\left((\upsilon+2\alpha)\dfrac{d\theta}{d\tau}+V_0sn^2\left(\dfrac{2K(m)\tau}{\pi};m\right)\right)R \\ 2\dfrac{dR}{d\tau}\dfrac{d\theta}{d\tau}+R\dfrac{d^2\theta}{d\tau^2}+\gamma\upsilon R\dfrac{d\theta}{d\tau} \\ \qquad =-(\upsilon+2\alpha)\dfrac{dR}{d\tau}-\gamma\beta R \end{cases} \quad (5)$$

Considering the simple case where the phase $\theta(\tau)$ varies linearly as $\frac{d\theta}{d\tau}=-(\frac{\upsilon}{2}+\alpha)=-\frac{\beta}{\upsilon}$ (see [38]), Eq. (5) can be summarized by the following ordinary differential equation:

$$\frac{d^2R}{d\tau^2}+\gamma\upsilon\frac{dR}{d\tau}-\left[\frac{\upsilon^2}{4}+V_0p\left(\frac{\tau}{2\pi};m\right)\right]R - g_0R^3-g_1R^5=0 \quad (6)$$

where $p(x;m)=sn^2(4K(m)x;m)$ is the optical lattice trap potential. The case $m=0$, i.e., $p(\frac{\tau}{2\pi};0)=\sin^2(\tau)$, corresponding to a pure trigonometric potential, has been recently studied in [26]. When the parameter m is close to 1, the optical trap potential $p(x;m)$ is virtually constant except on a set of points

of Lebesgue measure zero. The optical lattice in this case is static and the spatiotemporal chaotic steady-state is not possible. In the following of our theoretical analysis, let us expand the optical trap potential in Fourier series as

$$p(x;m)=\sum_{j=1}^{\infty} b_{j-1}\sin^2(2\pi jx) \tag{7}$$

The three first Fourier coefficients after some calculations are given by

$$\begin{cases} b_0(m)=\dfrac{4\pi^2 q(1-q+q^2-q^3+q^4)}{m(K(m))^2(1-q-q^5+q^6)} \\ b_1(m)=\dfrac{8\pi^2 q^2(1+q^4)}{m(K(m))^2(1-q^3-q^5+q^8)} \\ b_2(m)=\dfrac{4\pi^2 q^3}{m(K(m))^2(1-q^3)^2}\left(1+\dfrac{2(1-q^3)^2}{(1-q)(1-q^5)}\right) \end{cases} \tag{8}$$

with $q(m)=\exp(-\frac{\pi K(1-m)}{K(m)})$ the nome, and $0\le m\le 0.99$. It is proved in [38] that there is not large difference between the full trap potential $sn^2(\frac{4K(m)x}{\pi};m)$ and its truncated Fourier expansion of order n define as

$$p^{(n)}(x;m)=\sum_{j=1}^{n} b_{j-1}\sin^2(2\pi jx) \tag{9}$$

In this new form of trap potential $p(x;m)$, we straightforwardly obtain:

$$p^{(n)}\left(\frac{\tau}{2\pi};m\right)=\sum_{j=1}^{n} b_{j-1}\sin^2(j\tau) \tag{10}$$

3 Melnikov's approach to chaos

The aim of this section is to determine the condition of occurrence of homoclinic Smale's horseshoe chaos. We use as mathematical tools for the analytical prediction of chaos, the Melnikov method (MM) proposed in [34, 50–56]. The Melnikov method consists of studying a system in which the unperturbed problem is an integrable Hamiltonian system having a normally hyperbolic invariant set whose stable and unstable manifold intersect non-transversally. For the sake of simplicity, we assume that the dissipation term and the optical lattice potential are small amplitude. Thus, we introduce the following scale transformations: $\gamma\to\epsilon\gamma$, $V_0\to\epsilon V_0$. The differential equation (6) can be expressed as a first-order system in the form

$$\begin{cases} \dot{R}=X \\ \dot{X}=\dfrac{\upsilon^2}{4}R+g_0R^3+g_1R^5 \\ \qquad +\epsilon\Big[-\gamma\upsilon X+\dfrac{V_0}{2}\big(b_0+b_1+b_2 \\ \qquad -b_0\cos(2\tau)-b_1\cos(4\tau)-b_2\cos(6\tau)\big)R\Big] \end{cases} \tag{11}$$

ϵ is a small parameter($\epsilon\ll 1$) characterizing the smallness of dissipation and trap potential amplitude. For the unperturbed system, i.e., when $\epsilon=0$, Eq. (11) is an Hamiltonian system, and can be expressed as

$$\begin{cases} \dot{R}=X \\ \dot{X}=\dfrac{\upsilon^2}{4}R+g_0R^3+g_1R^5 \end{cases} \tag{12}$$

We can straightforwardly deduce from Eq. (12) that the potential energy of the system is given by

$$V(R)=-\frac{\upsilon^2}{8}R^2-\frac{g_0}{4}R^4-\frac{g_1}{6}R^6 \tag{13}$$

Depending on the set of the parameters, finally three physically interesting situations can be considered where the potential is: (i) single-well, (ii) double-well, or (iii) triple-well. The unperturbed system has a homoclinic or heteroclinic orbit or both of them depending of the type of potential well. In this paper, we work in the hypothesis $g_0>0$ and $g_1<0$. This situation leads to a bounded double well trap potential, and the system of Eq. (12) exhibits only homoclinic orbits. Equation (12) has three equilibrium points (see Fig. 1(a)), solutions of the algebraic equation

$$\frac{\upsilon^2}{4}R+g_0R^3+g_1R^5=0 \tag{14}$$

Among these three equilibrium points. there are two stable fixed points at $(\pm R_1,0)$ and one unstable fixed point at $(0,0)$, with $R_1^2=-\frac{g_0}{2g_1}(1+\sqrt{1-\frac{g_1\upsilon^2}{g_0^2}})$.

The Hamiltonian system Eq. (12) possesses two homoclinic orbits connecting the unstable point $(0,0)$ of the potential to itself. These orbits are given by the following components:

$$\begin{cases} R_0^{\pm}(\tau)=\pm\dfrac{\upsilon}{\sqrt{g_0[-1+\sigma\cosh(\upsilon\tau)]}} \\ X_0^{\pm}(\tau)=\pm\dfrac{\upsilon^2\sigma\sinh(\upsilon\tau)}{2\sqrt{g_0}[-1+\sigma\cosh(\upsilon\tau)]^{\frac{3}{2}}} \end{cases} \tag{15}$$

with $\sigma=\sqrt{1-\frac{4g_1\upsilon^2}{3g_0^2}}$.

The maximum value $R_{0\max}^2$ of the particle number density of condensate deduced from unperturbed system

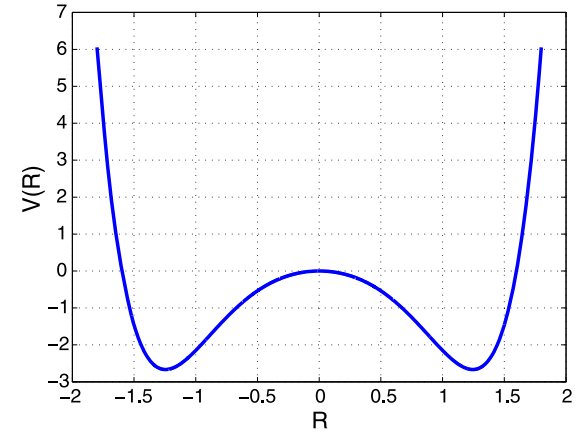

(a)

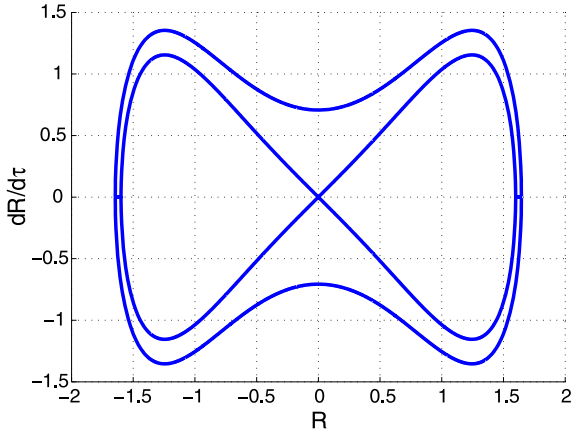

(b)

Fig. 1 (**a**) A configuration of the ϕ^6 potential with two wells. (**b**) Local bifurcation near the fixed points of the corresponding potential. The other parameters used are: $\upsilon = 2$, $g_0 = 0.75$, $g_1 = -0.9$

Eq. (12), is obtained for $\tau = 0$ in the expression of $R_0(\tau)$ as defined in Eq. (15). $R^2_{0\max}$ is straightforwardly given by the expression

$$R^2_{0\max} = \frac{\upsilon^2}{g_0(-1+\sigma)} \tag{16}$$

The width of condensate at the mid-height $\Delta\tau$ for the unperturbed system Eq. (12) is obtained by solving the equation $R_0^2(\tau) = \frac{R^2_{0\max}}{2}$. This value of $\Delta\tau$ characterizing the spatiotemporal extension of condensate is given by the expression

$$\Delta\tau = \frac{2}{\upsilon}\operatorname{arccosh}\left(2 - \frac{1}{\sigma}\right) \tag{17}$$

It comes from Figs. 2(d) and (e) that, by regulating increasingly each interaction coefficient g_0 and g_1 tends to increase the number of atoms in the condensate, and to decrease the spatiotemporal extension of condensate. According to the MM, the Melnikov function is defined as

$$\begin{aligned} M(\tau_0) &= -\gamma\upsilon\int_{-\infty}^{+\infty} X_0^2(\tau)\,d\tau \\ &\quad + \frac{V_0}{2}(b_0+b_1+b_2)\int_{-\infty}^{+\infty} R_0(\tau)X_0(\tau)\,d\tau \\ &\quad - \frac{V_0}{2}b_0\int_{-\infty}^{+\infty} \cos(2\tau+2\tau_0)R_0(\tau)X_0(\tau)\,d\tau \\ &\quad - \frac{V_0}{2}b_1\int_{-\infty}^{+\infty} \cos(4\tau+4\tau_0)R_0(\tau)X_0(\tau)\,d\tau \\ &\quad - \frac{V_0}{2}b_2\int_{-\infty}^{+\infty} \cos(6\tau+6\tau_0)R_0(\tau)X_0(\tau)\,d\tau \end{aligned} \tag{18}$$

where τ_0 is the cross-section time of the Poincaré map and can be interpreted as the initial time of the forcing term. Carrying out the integration of the right-hand side of Eq. (18) with the use of [57], we find after some algebraic manipulations that

$$\begin{aligned} M^{\pm}(\tau_0) &= \frac{3\gamma g_0\upsilon^2}{16g_1}\left[1+2\sqrt{2-\left(\frac{4g_1\upsilon^2}{3g_0^2}+\frac{3g_0^2}{4g_1\upsilon^2}\right)}\right. \\ &\quad \left.\times\arctan\left(\sqrt{\frac{1+\sigma}{-1+\sigma}}\right)\right] - \sqrt{-\frac{3\pi^2}{4g_1}}V_0 \\ &\quad \times\left[b_0(m)\operatorname{csch}\left(\frac{2\pi}{\upsilon}\right)\sinh\left(\frac{2}{\upsilon}\arccos\left(-\frac{1}{\sigma}\right)\right)\sin(2\tau_0)\right. \\ &\quad + 2b_1(m)\operatorname{csch}\left(\frac{4\pi}{\upsilon}\right)\sinh\left(\frac{4}{\upsilon}\arccos\left(-\frac{1}{\sigma}\right)\right)\sin(4\tau_0) \\ &\quad + 3b_2(m)\operatorname{csch}\left(\frac{6\pi}{\upsilon}\right)\sinh\left(\frac{6}{\upsilon}\arccos\left(-\frac{1}{\sigma}\right)\right) \\ &\quad \left.\times\sin(6\tau_0)\right] \end{aligned} \tag{19}$$

We begin our analysis by the determination of the condition of appearance of homoclinic chaos at $m = 0$. From Eq. (8), $b_0(0) = 1$, $b_1(0) \simeq 0$ and $b_2(0) = 0$. Thus, the theoretical condition for the occurrence of horseshoe chaos for the homoclinic bifurcation solved from Eq. (19) can be expressed as

$$\frac{V_0}{\gamma} \geq U_0(m=0,\upsilon,g_1) \tag{20}$$

where

$$\begin{aligned} U_0(m=0,\upsilon,g_1) &= \frac{g_0\upsilon^2}{8\pi}\sqrt{\frac{-3}{g_1}}\sinh\left(\frac{2\pi}{\upsilon}\right) \\ &\quad \times\operatorname{csch}\left(\frac{2}{\upsilon}\arccos\left(-\frac{1}{\sigma}\right)\right) \\ &\quad \times\left[1+2\sqrt{2-\left(\frac{4g_1\upsilon^2}{3g_0^2}+\frac{3g_0^2}{4g_1\upsilon^2}\right)}\right. \\ &\quad \left.\times\arctan\left(\sqrt{\frac{1+\sigma}{-1+\sigma}}\right)\right] \end{aligned} \tag{21}$$

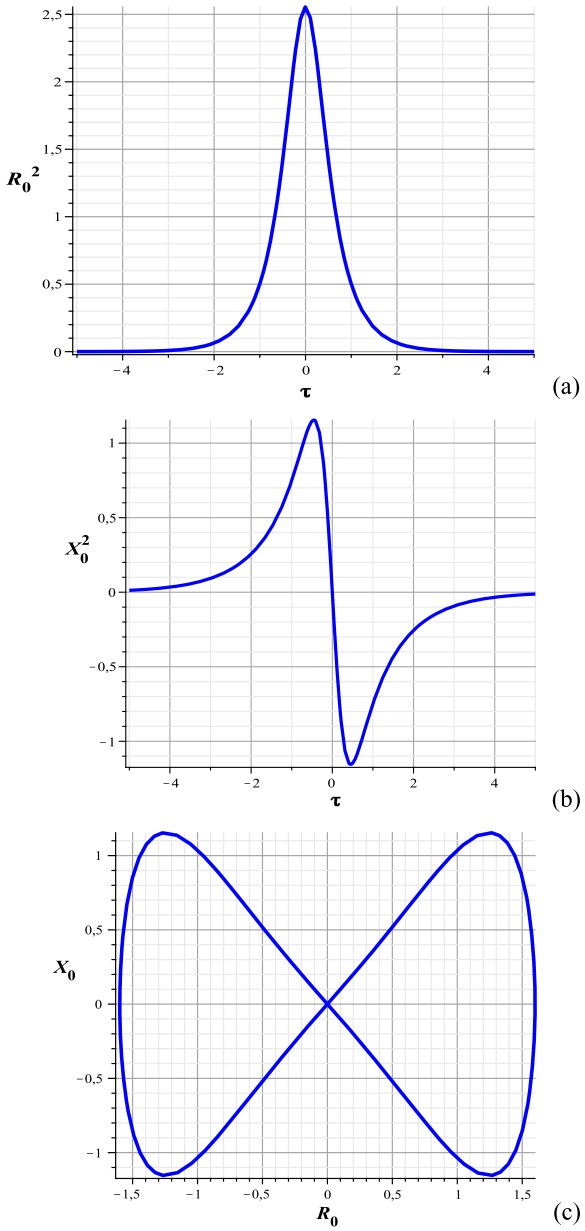

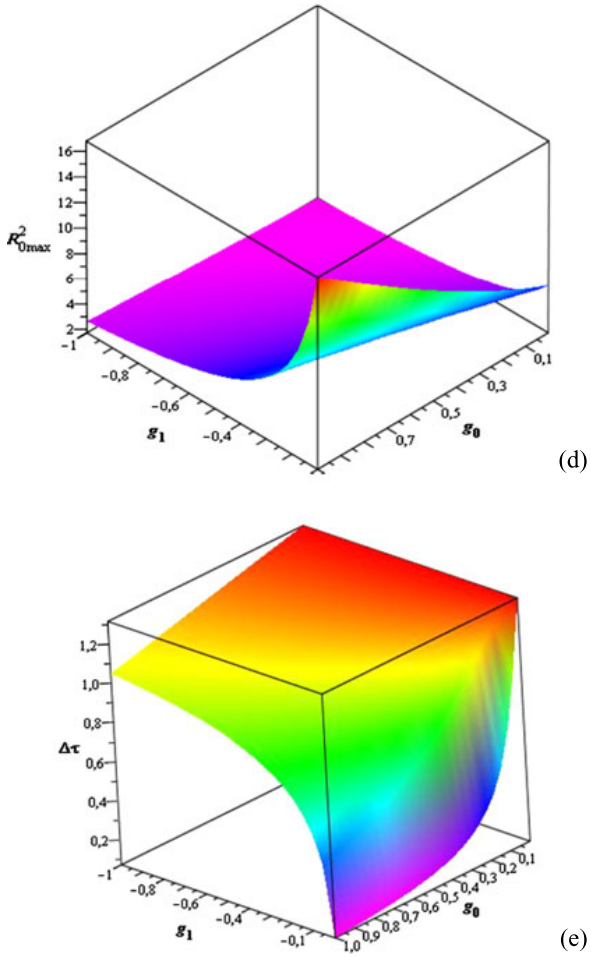

Fig. 2 (**a**)–(**b**) The spatiotemporal evolution of the particle number density and first excited state of condensate, deduced from unperturbed system Eq. (12). (**c**) Separatrix of unperturbed system Eq. (12). The other parameters used are: $\upsilon = 2$, $g_0 = 0.75$, $g_1 = -0.9$. (**d**)–(**e**) Maximum value and spatiotemporal extension of particle number density of condensate as function of the strength of two-body and three-body interactions for $\upsilon = 2$

is the chaotic threshold function associated with a pure trigonometric optical lattice. Next, we focus our attention on the condition of occurrence of homoclinic chaos in the case $m > 0$. The simple zeros of $M(\tau_0)$ are not analytically easy to find. To achieve our aim, we will attempt to do some approximations. From Eq. (8), the calculations show that, at the range $0 \leq m \leq 0.9$, the maximum value of $\frac{b_2(m)}{b_0(m)}$ is 0.04 and the higher value of $\frac{b_1(m)}{b_0(m)}$ is 0.27. Hence, we can neglect $b_2(m)$ and $b_1(m)$ in Eq. (19). Thus, the approximate necessary condition of Eq. (11) to exhibit the horseshoe homoclinic chaos can be expressed as

$$\frac{V_0}{\gamma} \geq U(m, \upsilon, g_1) \tag{22}$$

with

$$U(m, \upsilon, g_1) = \frac{U_0(m = 0, \upsilon, g_1)}{b_0(m)} \tag{23}$$

the chaotic threshold function for the parameter shape over the range $0 \leq m \leq 0.9$. Figures 3(a) and (b) exhibit respec-

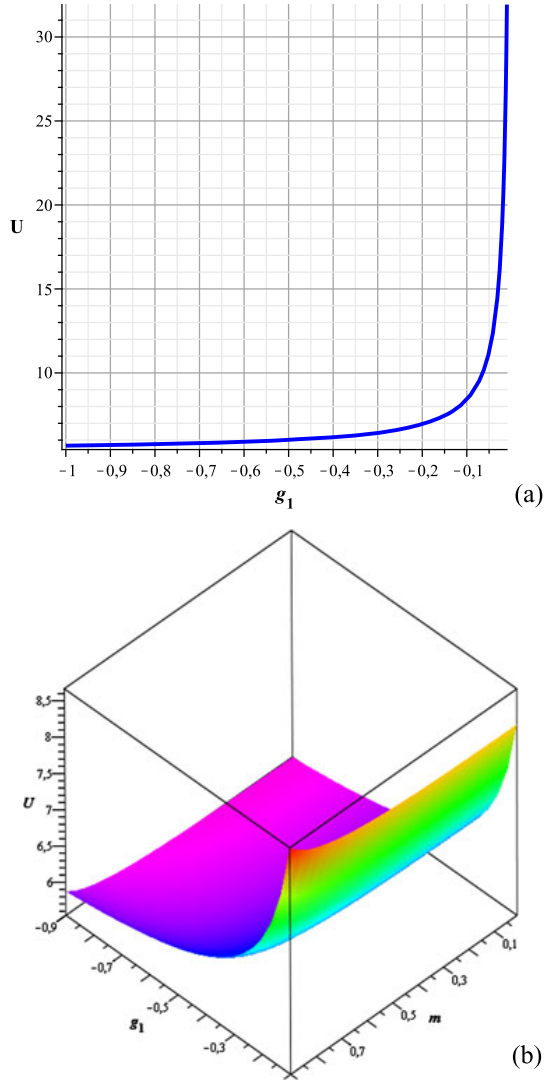

Fig. 3 Threshold function U: (**a**) as function of the strength of the three-body interaction g_1 for $m = 0.8$. (**b**) as function of the strength of the three-body interaction g_1 and lattice variable shape m. The other parameters used are: $g_0 = 0.75$, $\upsilon = 2$

tively the monotonically increasing behavior of the chaotic boundary curve as function of the effective three-body interaction between atoms, then as a function of the effective three-body interaction and optical lattice variable shape.

4 Numerical simulations

4.1 Bifurcations diagrams and phase portraits

After the theoretical prediction of chaos summarized by Eq. (22), we continue our investigations numerically with the following method. We begin by choosing a set of parameters following [38, 58, 59], except the control parameter. Solving Eq. (22) via MAPLE in the parameters space, i.e., plotting $\frac{V_0}{\gamma} - U$ versus the control parameter, we determine not only the critical value of control parameter, but also the range of control parameter corresponding to the homoclinic chaos. Next, we depict with the same parameters, the bifurcation diagram, taking as initial conditions the values of real amplitude around the maximum value of R ($R_{0\max} \simeq 1.6$) of unperturbed system Eq. (12). This corresponds to $\frac{dR}{d\tau} \simeq 0$. The bifurcation diagram is used to determine the numerical critical value, which is compared with the theoretical one, to see if there is concordance between the Melnikov prediction and the numerical results. In fact, we do not expect a perfect coincidence between these values because the MM is a perturbative method generally related to transient chaos, while bifurcation diagram provide information solely concerning steady chaos. Furthermore, we plot some phase portraits to verify the period-doubling bifurcations exhibited by the bifurcation diagrams. Combining these two studies can help the control of chaos in the dynamic of (BEC), for a choice of a set of parameters.

4.1.1 Global bifurcations with the optical intensity V_0 as control parameter

We take as values of parameters, the following data: $m = 0.8$, $g_0 = 0.75$, $g_1 = -0.9$, $\upsilon = 2$, $\gamma = 5$, $\epsilon = 0.03$. The theoretical prediction defined in Eq. (22) gives as critical value of optical intensity for the occurrence of homoclinic chaos $V_{0c} = 28.5$. Numerically, according to Fig. 4(a), we obtain as a critical value of V_0 at the first bifurcation 49.5. To have the real gap between this values, we will not forget that we have done a scale transformation $V_0 \to \epsilon V_0$ in Sect. 2. The gap 0.63 between these values is probably due to the fact that we have neglected $b_1(m)$ and $b_2(m)$ in the Melnikov function to solve the problem analytically. This difference can also be explained by the fact that the MM is approximate. Next, we increase gradually the optical intensity in the phase space, to verify the period-doubling bifurcations route leading to the homoclinic chaos, as it is well seen on the bifurcation diagram.

For $V_0 = 20$, this situation leads analytically to the periodic oscillations. Figure 6(a) exhibits a limit cycle as phase portrait and the regular dynamic of the condensate is shown in Fig. 6(b). Now, let us give V_0 the value 80. According to Eq. (22), the dynamic of the condensate will be chaotic. To verify that, we plot in Fig. 6(c) the phase portrait and we obtain a period-2 attractor. The quasiperiodic oscillations of condensate is shown in Fig. 6(d). When $V_0 = 135$, we see in Fig. 6(e) the period-4 attractor as a phase portrait and the quasiperiodic oscillations of condensate in Fig. 6(f). Finally, when $V_0 = 180$, we observe in Fig. 6(g) that the phase orbit evolves in a finite region and exhibits confusion, which is the chaotic feature. The phase portrait in this case is a strange attractor. Figure 6(h) presents the erratic spatiotemporal evolution of condensate. In addition, the bifurcation

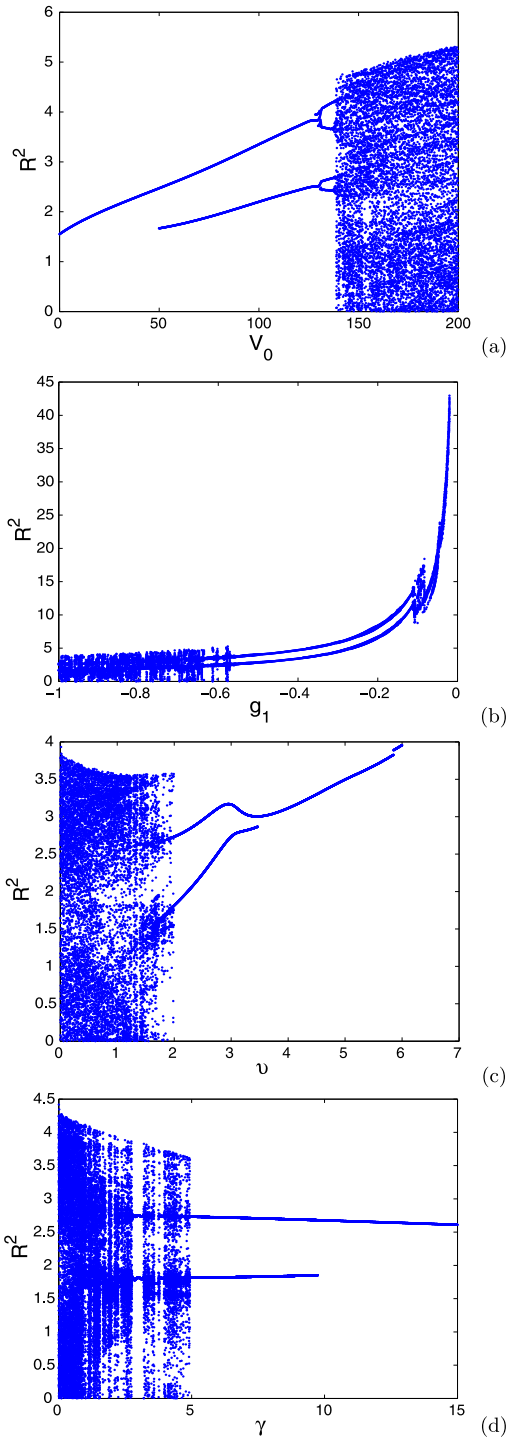

Fig. 4 Bifurcation diagram of particle number density R^2: (**a**) as a function of optical intensity V_0 for $g_1 = -0.9$, $\gamma = 5$, $\upsilon = 2$, and $\epsilon = 0.03$. Initial conditions: $R(0) = 1.45$, $\frac{dR}{d\tau}(0) = 0$. (**b**) as function of the strength of the effective three--body interaction g_1 for $V_0 = 200$, $\gamma = 5$, $\upsilon = 2$, and $\epsilon = 0.01$. Initial conditions: $R(0) = 1.7$, $\frac{dR}{d\tau}(0) = 0$. (**c**) as a function of lattice velocity υ for $V_0 = 50$, $\gamma = 5$, $g_1 = -0.9$, and $\epsilon = 0.04$. Initial conditions: $R(0) = 1.7$, $\frac{dR}{d\tau}(0) = -0.3$. (**d**) as a function of damping coefficient γ for $V_0 = 50$, $g_1 = -0.9$, $\upsilon = 2$ and $\epsilon = 0.04$. Initial conditions: $R(0) = 1.7$, $\frac{dR}{d\tau}(0) = -0.3$. The other parameters used are: $g_0 = 0.75$, $m = 0.8$

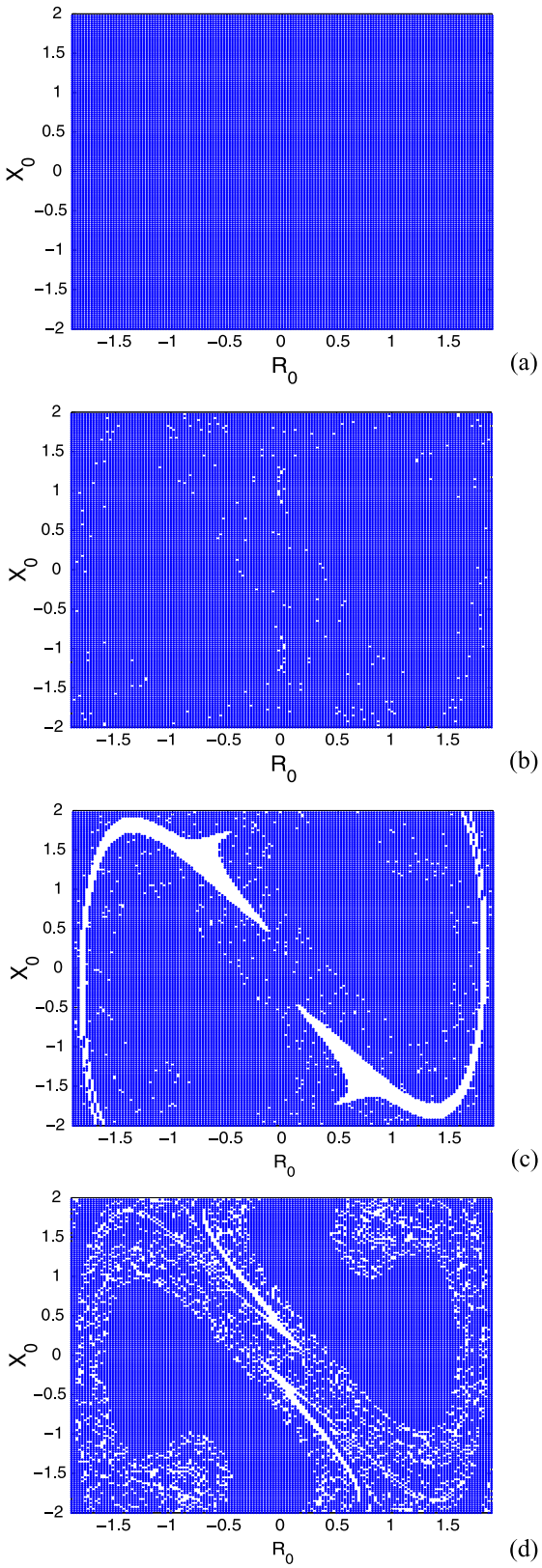

Fig. 5 The effect of V_0 on the basins of attraction. (**a**) $V_0 = 28$, (**b**) $V_0 = 30$, (**c**) $V_0 = 45$, (**d**) $V_0 = 70$. The others parameters used are: $g_0 = 0.75$, $m = 0.8$, $g_1 = -0.9$, $\gamma = 5$, $\upsilon = 2$, and $\epsilon = 0.02$

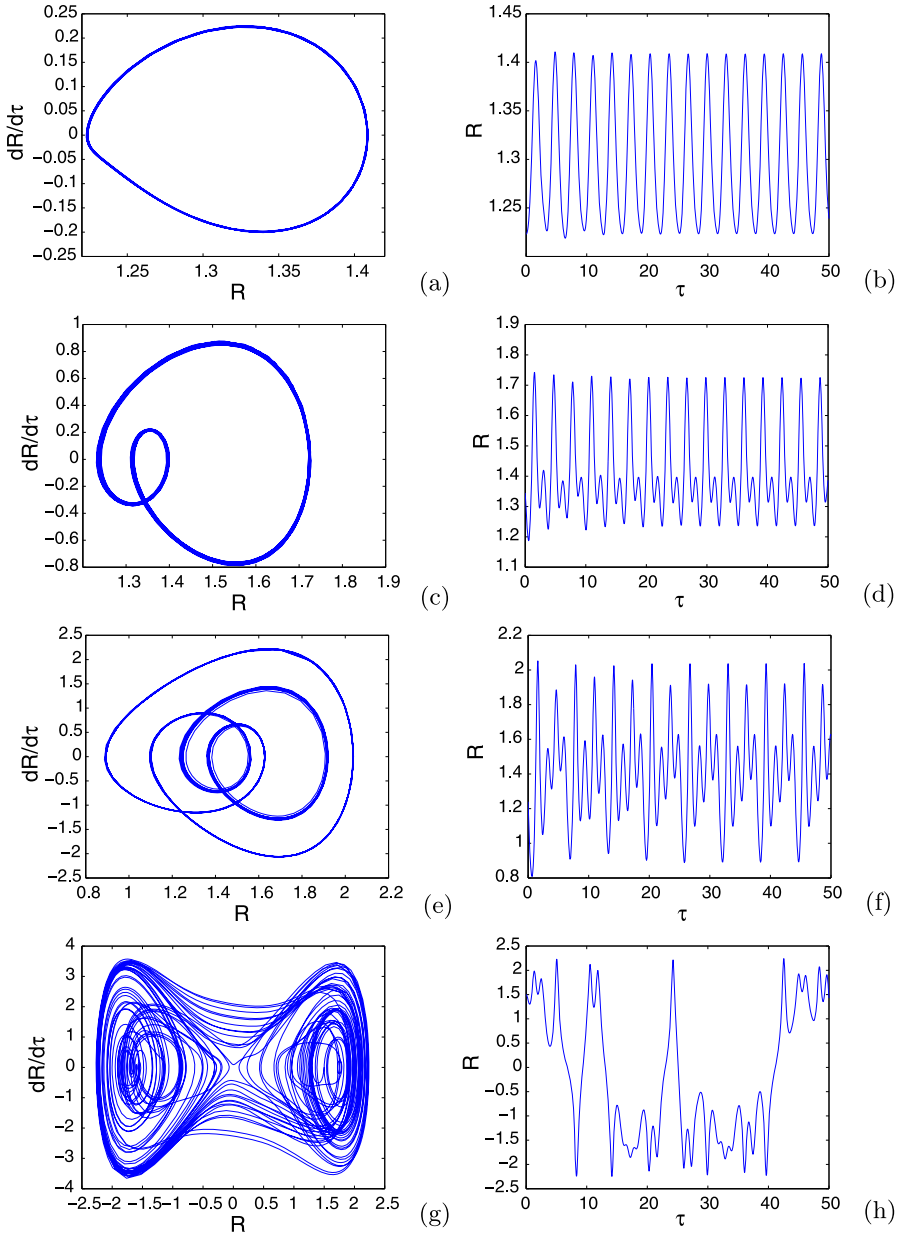

Fig. 6 (**a**)–(**b**) Regularized oscillations for $V_0 = 20$. (**c**)–(**d**) Period-2 attractor and quasiperiodic oscillations for $V_0 = 80$. (**e**)–(**f**) Period-4 attractor and quasiperiodic oscillations for $V_0 = 135$. (**g**)–(**h**) Strange attractor and irregular oscillations for $V_0 = 180$. The other parameters used are: $\upsilon = 2$, $m = 0.8$, $\gamma = 5$, $\epsilon = 0.03$, $g_0 = 0.75$, $g_1 = -0.9$

diagram depicted in Fig. 4(a) summarizes the influence of the potential well depth of the lattice V_0 on the dynamic of the particle number density. There is concordance between this bifurcation diagram and our phase portraits.

4.1.2 Global bifurcations with the strength of the effective three-body interaction g_1 as control parameter

In this paragraph, we take into consideration the set of the following parameters: $m = 0.8$, $g_0 = 0.75$, $\upsilon = 2$, $\gamma = 5$, $\epsilon = 0.01$, and $V_0 = 200$. According to the Melnikov prediction, the critical value is $g_c = -0.0075$. The critical value of g_1 obtained by the numerical calculations is -0.0105. The gap 0.003 between these values can be explained as mentioned above. Let us depict some phase portraits to verify the period-doubling bifurcations. We begin with $g_1 = -0.8$. Theoretically, we expect the chaotic dynamic of condensate. The numerical simulations present in Fig. 7(a) a strange attractor as a phase portrait and the irregular spatiotemporal evolutions of the condensate in Fig. 7(b). Increasing the control parameter at -0.05, theoretically the chaotic dynamic of the condensate is expected. But we observe in Fig. 7(c) a period-3 attractor as a phase portrait and the quasiperiodic oscillations of the condensate in Fig. 7(d). Now, when $g_1 = -0.035$, we expect analytically a chaotic dynamic of the condensate. The numerical simulations present in Fig. 7(e) a period-2 attractor as the phase portrait and quasiperiodic oscillations of condensate in Fig. 7(f). Lastly, when $g_1 = -0.01$, according to our the-

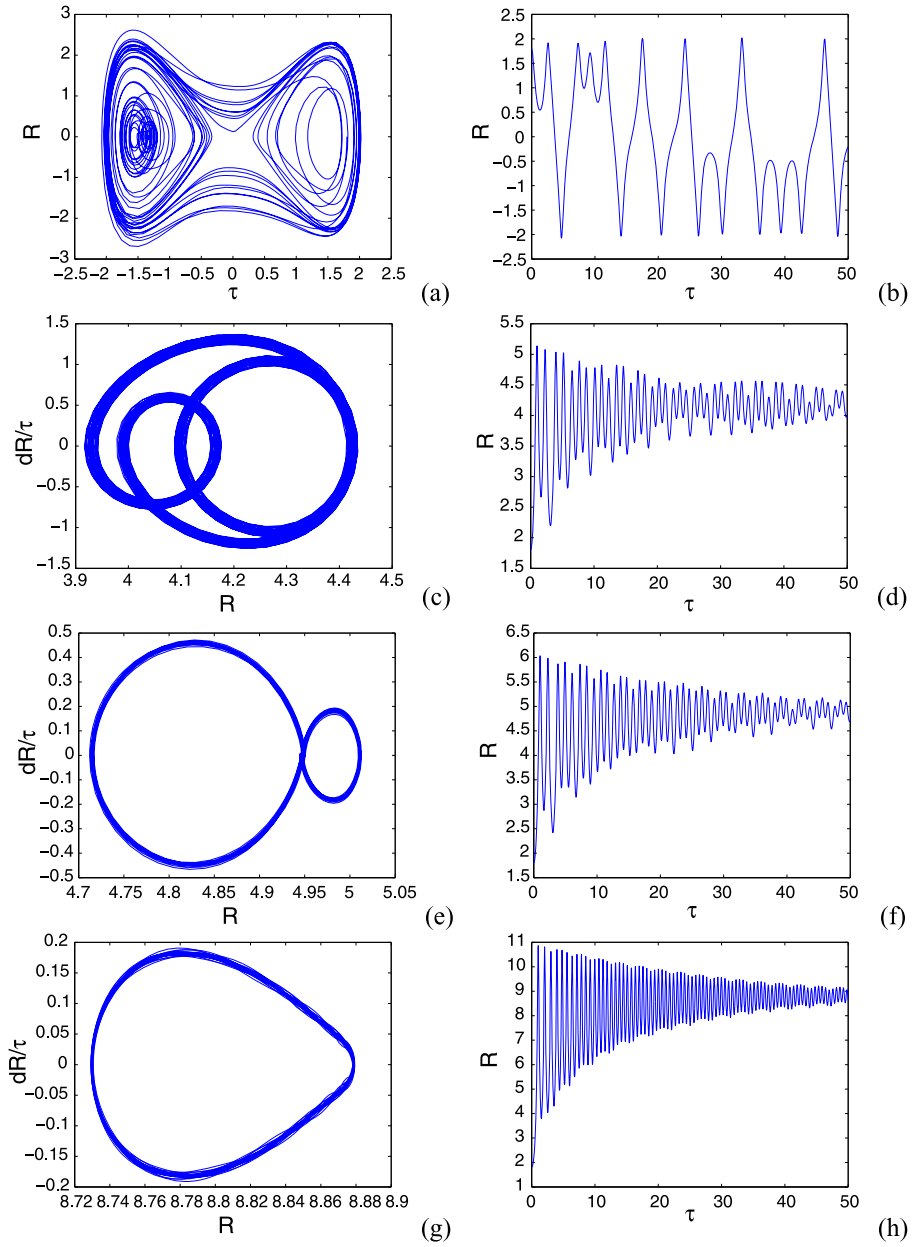

Fig. 7 (**a**)–(**b**) Chaotic oscillations for $g_1 = -0.8$. (**c**)–(**d**) Period-3 attractor and quasiperiodic oscillations for $g_1 = -0.05$. (**e**)–(**f**) Period-2 attractor and quasiperiodic oscillations for $g_1 = -0.035$. (**g**)–(**h**) Regularized oscillations for $g_1 = -0.01$. The other parameters used are: $\upsilon = 2$, $m = 0.8$, $\gamma = 5$, $\epsilon = 0.01$, $g_0 = 0.75$, and $V_0 = 200$

oretical prediction, the regular behavior of the condensate is expected. The phase portrait depicted in Fig. 7(g) shows a limit cycle, proof of regular spatiotemporal evolution of the condensate.

4.1.3 Global bifurcations with the velocity of optical lattice υ as control parameter

In this paragraph, we use as a control parameter, the lattice velocity υ. We give to the other parameters the values: $m = 0.8$, $g_0 = 0.75$, $g_1 = -0.9$, $\gamma = 5$, $\epsilon = 0.04$, and $V_0 = 50$. The theoretical prediction defined in Eq. (22) indicates that the homoclinic chaos will appear for $0 \leq \upsilon \leq 2.70$. Numerically, the bifurcation diagram depicted in Fig. 4(c) shows that from chaotic oscillations for υ close to 0, as υ increases, the bifurcation leading to the regular dynamic of condensate appears at $\upsilon_c = 3.46$. Once more, one sees that these two values are close, and the difference 0.76 can be explained as mentioned above. To verify the process of period-doubling bifurcations leading to the homoclinic chaos as summarized in Fig. 4(c), we vary the control parameter as follows. We begin with $\upsilon = 1$. Analytically, a chaotic dynamic of condensate is expected. Through the phase portrait plotted in Fig. 8(a), we observe a strange attractor, proof of chaotic oscillations, as we can see in Fig. 8(b), with the irregular evolution of the condensate. Carrying on with $\upsilon = 2.5$, according to our theoretical calculations, the dynamic of the condensate will be chaotic.

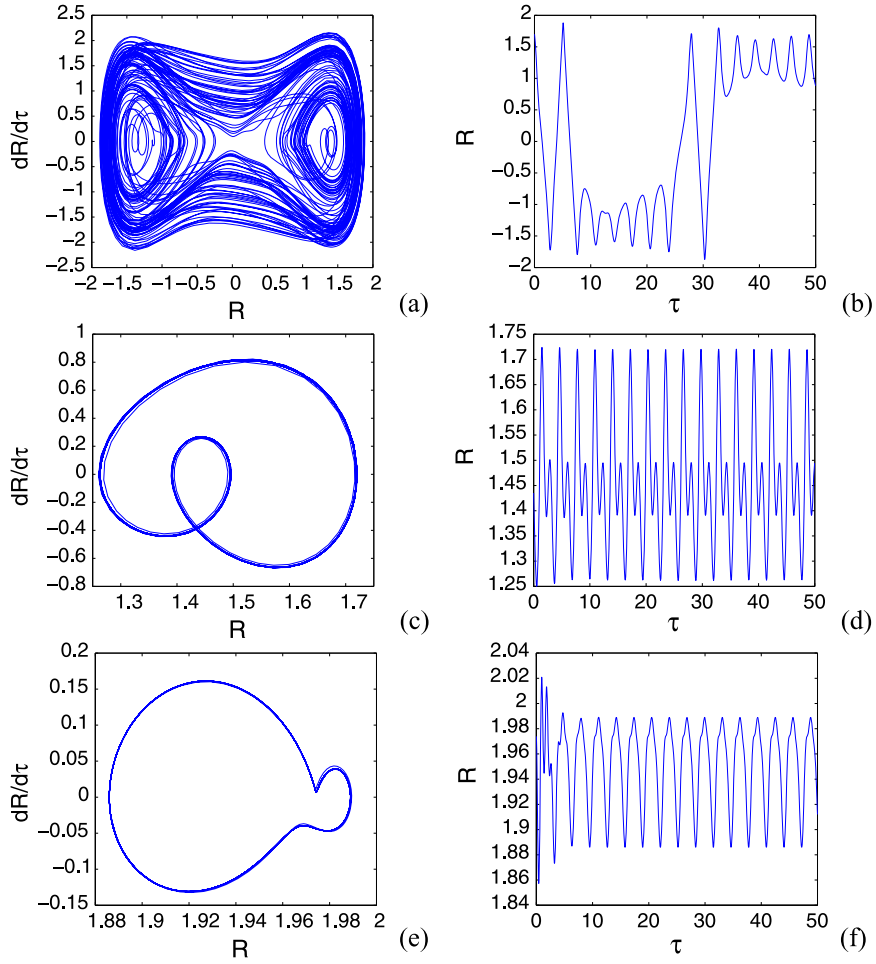

Fig. 8 (**a**)–(**b**) Chaotic oscillations for $\upsilon = 1$. (**c**)–(**d**) Period-2 attractor and quasiperiodic oscillations for $\upsilon = 2.5$ (**e**)–(**f**) Regularized oscillations for $\upsilon = 6$. The other parameters used are: $g_1 = -0.9$, $m = 0.8$, $\gamma = 5$, $\epsilon = 0.04$, $g_0 = 0.75$, and $V_0 = 50$

The phase portrait exhibits in Fig. 8(c) a period-2 attractor, and we can see the quasiperiodic oscillations of condensate in Fig. 8(d). We end with $\upsilon = 6$. The theoretical prediction indicates a regular behavior of condensate. The numerical simulations exhibit in Fig. 8(e) a limit cycle as a phase portrait, and the periodic oscillations of condensate in Fig. 8(f).

4.1.4 Global bifurcations with the damping coefficient γ as control parameter

The damping parameter γ is used as a control parameter, and the other parameters used are given by the following set of data: $m = 0.8$, $g_0 = 0.75$, $g_1 = -0.9$, $\upsilon = 2$, $\epsilon = 0.04$, and $V_0 = 50$. According to the bifurcation diagram plotted in Fig. 4(d), one sees that the periodic oscillations appear at $\gamma_c = 9.7$, while the critical value of γ obtained theoretically is 8.76. Recalling the scale transformation $\gamma \to \epsilon\gamma$, the gap 0.0376 between these values can be explained as indicated above. To confirm the period-doubling bifurcations process leading to the homoclinic chaos, we depict some phase portraits as follows. For $\gamma = 0.5$, according to our theoretical prediction, the chaotic oscillations are expected. Figure 9(a) presents a strange attractor as phase portrait and the aperiodic oscillations of condensate can be seen in Fig. 9(b). Let us continue with $\gamma = 6$. Expecting analytically a chaotic dynamics of condensate, we obtain in Fig. 9(c) a period-2 attractor as the phase portrait, and the quasiperiodic oscillations of the condensate are observed in Fig. 9(d). Finally, when $\gamma = 11$, theoretically, the regular dynamic of the condensate is expected. Figure 9(e) presents a limit cycle as the phase portrait, proof of periodic oscillations of the condensate as we can see in Fig. 9(f).

4.2 Basin erosion pattern

A basin of attraction is defined as the set of points taken as initial conditions, which are attracted to a fixed point or an invariant set. In this section, we choose the same set of parameters as in Sect. 4.1, i.e., $m = 0.8$, $g_0 = 0.75$, $g_1 = -0.9$, $\upsilon = 2$, $\gamma = 5$. When the optical intensity V_0 is taken as the control parameter as shown in the bifurcation diagram (see Fig. 4(a)) of R^2 versus V_0 with $\epsilon = 0.02$, by performing a scan of the initial conditions in the (R_0, X_0) plane for various values of V_0, we find that when V_0 is less than the homoclinic critical value, the basins of attraction are regular (see

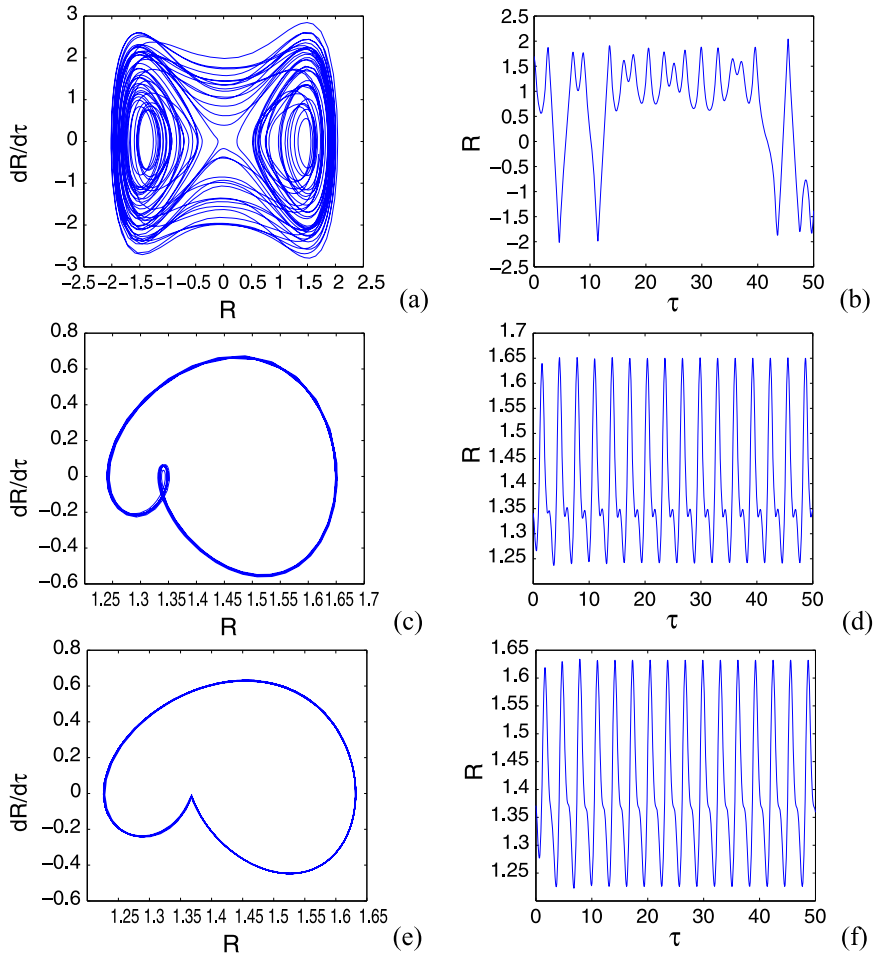

Fig. 9 (**a**)–(**b**) Chaotic oscillations for $\gamma = 0.5$. (**c**)–(**d**) Period-2 attractor and quasiperiodic oscillations for $\gamma = 6$. (**e**)–(**f**) Regularized oscillations for $\gamma = 11$. The other parameters used are: $g_1 = -0.9$, $m = 0.8$, $\upsilon = 2$, $\epsilon = 0.04$, $g_0 = 0.75$ and $V_0 = 50$

Fig. 5(a)). As V_0 increases above the analytical threshold (i.e., $V_{0c} = 28.5$), the regular shape of the basin of attraction is destroyed and the fractal behavior becomes more and more visible (see Figs. 5(b) to 5(d)). Note that the results of Fig. 5 represent the basins of attraction of the motion around the two fixed points $(\pm R_1, 0)$ of potential as in Fig. 1(a).

5 Conclusion

The goal of this paper was the study of the nonlinear dynamic of a (BEC) with a repulsive two-body interaction and attractive three-body interaction loaded into a moving optical lattice. Our investigations reveal that the very small values of the optical intensity V_0, i.e., the very small values of the potential well depth of the lattice are favorable to the regular oscillations. On the contrary, the very small values of the strength of the effective three-body interaction g_1, the velocity of optical lattice υ, and the damping coefficient γ are favorable to the chaotic oscillations of the condensate. This study reveals also that the MM for the prediction of homoclinic chaos in the dynamic of condensate with both repulsive two-body interaction and attractive three-body interaction predicts sure enough the appearance or the disappearance of period-2-attractor in the phase space. Focusing our attention on some control parameters as V_0, g_1, υ, γ, we observe numerically that, when these parameters evolve, the process of period-doubling bifurcations is the route leading to a chaotic dynamic or to a periodic oscillations of condensate. It comes from our investigations that regulating increasingly these control parameters when others are fixed may be helpful in regulating transient chaos in the dynamic of particle number density of condensate $|\psi|^2$.

Acknowledgements The authors are grateful to the anonymous referees for their valuable comments. M. Siewe Siewe is indebted to the International Centre for Theoretical Physics (ICTP) for its financial support to do research work as a research visitor and also indebted to the Mathematics Group of ICTP for hosting him to undertake part of this work.

References

1. Pethick, C.J., Smith, H.: Bose–Einstein Condensation in Dilute Gases. Cambridge University Press, Cambridge (2002)

2. Dalfovo, F., Giorgini, S., Pitaevskii, L.P., Stringari, S.: Theory of Bose–Einstein condensation in trapped gases. Rev. Mod. Phys. **71**, 463 (1999)
3. Filho, V.S., Gammal, A., Frederico, T., Tomio, L.: Chaos in collapsing Bose-condensed gas. Phys. Rev. A **62**, 033605 (2000)
4. Sun, K., Tian, B., Wen-Jun, L., Jiang, Y., Qi-Xing, Q., Wan, P.: Soliton dynamics and interaction in the Bose–Einstein condensates with harmonic trapping potential and time varying interatomic interaction. Nonlinear Dyn. **67**, 165–175 (2012)
5. Wang, M., Tian, B., Wen-Rui, S., Lü, X., Yu-Shan, X.: Soliton and their collisions in the spinor Bose–Einstein condensates. Nonlinear Dyn. **69**, 1137–1148 (2012)
6. Raghavan, S., Smerzi, A., Fantoni, S., Shenoy, S.R.: Coherent oscillations between two weakly coupled Bose–Einstein condensate. Phys. Rev. A **59**, 620–633 (1999)
7. Hong-Wei, Y., Wei, Z.: Josephson dynamics of a Bose–Einstein. Chin. Phys. Lett. **24**, 620–623 (2007)
8. Liu, H., Yan, F., Xu, C.: The bifurcation and exact traveling wave solution of $(1+2)$ dimensional nonlinear Schrödinger equation with dual-power law nonlinearity. Nonlinear Dyn. **67**, 465–473 (2012)
9. Engels, P., Atherton, C., Hoefer, M.A.: Observation of Faraday waves in a Bose–Einstein condensate. Phys. Rev. Lett. **98**(98), 095301 (2007)
10. Nicolin, A.I.: Resonant wave formation in Bose–Einstein condensates. Phys. Rev. E **84**(84), 056202 (2011)
11. Balaz, A., Nicolin, A.I.: Faraday waves in binary nonmiscible Bose–Einstein condensates. Phys. Rev. A **85**, 023613 (2012)
12. Frantzeskakis, D.J.: Dark solitons in atomic Bose–Einstein condensates: from theory to experiments. J. Phys. A, Math. Theor. **43**, 213001 (2010)
13. Nicolin, A.I., Jensen, M.H., Thomsen, J.W., Carretero, G.R.: Resonant energy transfer in Bose–Einstein condensates. Physica D **237**, 2476–2481 (2008)
14. Machholm, M., Nicolin, A., Pethick, C.J., Smith, H.: Spatial period doubling in Bose–Einstein condensates in an optical lattice. Phys. Rev. A **69**, 043604 (2004)
15. Nistazakis, H.E., Porter, M.A., Kevrekidis, P.G., Frantzeskakis, D.J., Nicolin, A., Chin, J.K.: Fractional-period excitations in continuum periodic systems. Phys. Rev. A **74**, 063617 (2006)
16. Pollack, S.E., Dries, D., Hulet, R.G.: Collective excitation of a Bose–Einstein condensate by modulation of the atomic scattering length. Phys. Rev. A **81**, 053627 (2010)
17. Vidanovic, I., Balaz, A., Hamid, A.J., Axel, P.: Nonlinear Bose–Einstein-condensate dynamics induced by a harmonic modulation of the s-wave scattering length. Phys. Rev. A **84**, 013618 (2011)
18. Bing, L.X., Wen, X.X., Fei, Z.X.: Suppression of chaos in a Bose–Einstein condensate loaded into a moving optical superlattice potential. Chin. Phys. Lett. **27**, 040302 (2010)
19. Cong, F., Wang, Z., Hua, H., Pang, S., Tong, S.: Controlling chaos in the Bose–Einstein condensate. J. Exp. Theor. Phys. **114**, 377–381 (2012)
20. Peil, S., Porto, J.V., Laburthe Tolra, B., Obrecht, J.M., King, B.E., Subbotin, M., Rolston, S.L., Phillips, W.D.: Patterned loading of a Bose–Einstein condensate into an optical lattice. Phys. Rev. A **67**, 051603 (2003)
21. Abdullaev, F.Kh., Kraenkel, R.A.: Coherent atomic oscillations and resonances between coupled Bose–Einstein condensates with time-dependent trapping potential. Phys. Rev. A **62**, 023613 (2000)
22. Lee, C., Hai, W., Shi, L., Zhu, X., Gao, K.: Chaotic and frequency-locked atomic population oscillations between two coupled Bose–Einstein condensates. Phys. Rev. A **64**, 053604 (2001)
23. Eguiluz, V.M., Hernández-García, E., Piro, O., Balle, S.: Frozen spatial chaos induced by boundaries. Phys. Rev. E **60**, 6571–6579 (1999)
24. Chong, G., Hai, W., Xie, Q.: Controlling chaos in a weakly coupled array of Bose–Einstein condensates. Phys. Rev. E **71**, 016202 (2005)
25. Martin, A.D., Adams, C.S., Gardiner, S.A.: Bright matter-wave soliton collisions in a harmonic trap: regular and chaotic dynamics. Phys. Rev. Lett. **98**, 020402 (2007)
26. Chong, G., Hai, W., Xie transient, Q.: Transient and stationary chaos of a Bose–Einstein condensate loaded into a moving optical lattice potential. Phys. Rev. E **70**, 036213 (2004)
27. Ott, E., Grebogi, C., Yorke, J.A.: Controlling chaos. Phys. Rev. Lett. **64**, 1196–1199 (1990)
28. Shinbrot, T., Ott, E., Grebogi, C., Yorke, J.A.: Using small perturbations to control chaos. Nature **363**, 411–417 (1993)
29. Shinbrot, T., Ott, E., Grebogi, C., Yorke, J.A.: Using chaos to direct trajectories. Phys. Rev. Lett. **65**, 3215–3218 (1990)
30. Lima, R., Pettini, M.: Suppression of chaos by resonant parametric perturbations. Phys. Rev. A **41**, 726–733 (1990)
31. Ramesh, M., Narayanan, S.: Chaos control by non-feedback methods in the presence of noise. Chaos Solitons Fractals **10**, 1473–1489 (1990)
32. Braiman, Y., Goldhirsch, I.: Taming chaotic dynamics with weak periodic perturbations. Phys. Rev. Lett. **20**, 2545–2548 (1991)
33. Show, W., Wiggins, S.: Chaotic dynamics of a whirling pendulum. Physica D **31**, 190–211 (1988)
34. Melnikov, V.K.: On the stability of the centre for time-periodic perturbations. Trans. Mosc. Math. Soc. **12**, 1–57 (1963)
35. Holmes, P.J., Marsden, J.E.: Horseshoe and Arnold diffusion for Hamiltonian system on Lie groups. Indiana Univ. Math. J. **32**, 273–309 (1983)
36. Holmes, P.J., Marsden, J.E.: Horseshoes in perturbations of Hamiltonian systems with two degrees of freedom. Commun. Math. Phys. **82**, 523–544 (1982)
37. Holmes, P.J., Marsden, J.E.: Melnikov's method and Arnold diffusion for perturbations of integrable Hamiltonian systems. J. Math. Phys. **23**, 669–675 (1982)
38. Chacón, R., Bote, D., Carretero-González, R.: Controlling chaos of a Bose–Einstein condensate loaded into a moving optical Fourier-synthesized lattice. Phys. Rev. E **78**, 036215 (2008)
39. Ginzburg, V.L., Pitaevskii, L.P.: On the theory of superfluidity. Zh. Èksp. Teor. Fiz. **34**, 1240–1245 (1958)
40. Pitaevskii, L.P.: Vortex lines in an imperfect Bose gas. Sov. Phys. JETP **13**, 451–454 (1961)
41. Gross, E.P.: Hydrodynamics of a superfluid condensate. J. Math. Phys. **4**, 195–207 (1963)

42. Abdullaev, F.Kh., Gammal, A., Tomio, L., Frederico, T.: Stability of trapped Bose–Einstein condensates. Phys. Rev. A **63**, 043604 (2001)
43. Gammal, A., Frederico, T., Tomio, L., Abdullaev, F.Kh.: Stability analysis of the D-dimensional nonlinear Schrödinger equation with trap and two- and three-body interactions. Phys. Lett. A **267**, 305–311 (2000)
44. Stamper-Kurn, D., Miesner, H.-J., Inouye, S., Andrews, M., Ketterle, W.: Collisionless and hydrodynamic excitations of a Bose–Einstein condensate. Phys. Rev. Lett. **81**, 500–503 (1998)
45. Marino, I., Raghavan, S., Fantoni, S., Shenoy, S.R., Smerzi, A.: Bose-condensate tunneling dynamics: momentum-shortened pendulum with damping. Phys. Rev. A **60**, 487–493 (1999)
46. Aftalion, A., Du, Q., Pomeau, Y.: Dissipative flow and vortex shedding in the Painlevé boundary layer of a Bose–Einstein condensate. Phys. Rev. Lett. **91**, 090407 (2003)
47. Tsubota, M., Kasamatsu, K., Ueda, M.: Vortex lattice formation in a rotating Bose–Einstein condensate. Phys. Rev. A **65**, 023603 (2002)
48. Kasamatsu, K., Tsubota, M., Ueda, M.: Nonlinear dynamics of vortex lattice formation in a rotating Bose–Einstein condensate. Phys. Rev. A **67**, 033610 (2003)
49. Bloch, F.: Über die Quantenmechanik der Elektronen in Kristallgittern. Z. Phys. **52**, 555–600 (1928)
50. Sun, Z., Xu, W., Yang, X., Fang, T.: Inducing or suppressing chaos in a double-well Duffing oscillator by time delay feedback. Chaos Solitons Fractals **27**, 705–714 (2006)
51. Tchawoua, C., Siewe Siewe, M., Tchatchueng, S., Moukam, F.M.: Kakmeni, nonlinear dynamics of parametrically driven particles in a ϕ^6 potential. Nonlinearity **21**, 1041–1055 (2008)
52. Siewe Siewe, M., Moukam Kakmeni, F.M., Tchawoua, C., Woafo, P.: Bifurcation and chaos in the triple-well ϕ^6 Van der Pol oscillator driven by external and parametric excitations. Physica A **357**, 383–396 (2005)
53. Siewe Siewe, M., Yamgoué, S.B., Moukam Kakmeni, F.M., Tchawoua, C.: Chaos controlling self-sustained electromechanical seismograph system based on the Melnikov theory. Nonlinear Dyn. **62**, 379–389 (2010)
54. Chacón, R.: Comparison between parametric excitation and additional forcing terms as chaos-suppressing perturbations. Phys. Lett. A **247**, 431–436 (1998)
55. Wang, C.-N., Ma, J., Liu, Y., Huang, L.: Chaos control, spiral wave formation, and the emergence of spatiotemporal chaos in networked Chua circuits. Nonlinear Dyn. **67**, 139–146 (2012)
56. Liu, D., Yamaura, H.: Chaos control of a ϕ^6 Van der Pol oscillator driven by external excitation. Nonlinear Dyn. **68**, 95–105 (2012)
57. Gradshteyn, I.S., Ryzhik, I.M.: Table of Integrals, Series and Products. Academic Press, New York (1994)
58. Denschlag, J.H., Simsarian, J.E., Häffner, H., McKenzie, C., Browaeys, A., Cho, D., Helmerson, K., Rolston, S.L., Phillips, W.D.: A Bose–Einstein condensate in an optical lattice. J. Phys. B **35**, 3095–3110 (2002)
59. Chong, G., Hai, W., Xie, Q.: Spatial chaos of trapped Bose–Einstein condensate in one-dimensional weak optical lattice potential. Chaos **14**, 217–223 (2004)